

Lewis Structures Technology—1988

**Volume 3—Structural Integrity
Fatigue and Fracture
Wind Turbines
HOST**

SPRINT REPORT
CONFERENCE REPORT
CONFERENCE REPORT
CONFERENCE REPORT

*Proceedings of an exposition and
symposium of structures technology
developed under the auspices of
NASA Lewis Research Center's
Structures Division
Cleveland, Ohio
May 24-25, 1988*

NASA

NASA Conference Publication 3003—Vol. 3

Lewis Structures Technology—1988

**Volume 3—Structural Integrity
Fatigue and Fracture
Wind Turbines
HOST**

*Proceedings of an exposition and
symposium of structures technology
developed under the auspices of
NASA Lewis Research Center's
Structures Division
Cleveland, Ohio
May 24–25, 1988*



National Aeronautics and
Space Administration

**Scientific and Technical
Information Branch**

1988

PREFACE

Aeronautical and space propulsion systems structures technology has been the mission of the Structures Division at the NASA Lewis Research Center for many years. We have carried out both fundamental and applied research projects in pursuit of that mission. We have worked cooperatively with members of the industrial and academic communities in order to strengthen our ties to both the discipline rigors found in university research and the needs of industrial design engineers. It is from this perspective that we have prepared the material for this symposium. And we hope to transfer our technology beyond our usual industrial partners.

The technology required for the reliable, high-performance, lightweight structures needed for aerospace propulsion is among the most complex and challenging facing the design engineer. We provide a comprehensive review of the status of the technology, a review of our recent contributions, and a flavor of the directions for the future. The symposium is meant to be as informative as possible, with the intent to establish new and broader lines for technology transfer. We encourage continued interaction and the chance to exchange information, ideas, and problems with the intention of improving the capability of aerospace propulsion systems.

Our two-day symposium and exposition, LST '88, is expected to attract 300 technologists from all walks of structurally related engineering. The 83 technical contributions have been created by over 100 authors who are respected authorities in their fields. Fifty percent of these are NASA civil servants, and twenty-five percent are on-site contractors and grantees, National Research Council associates, Institute for Computational Mechanics in Propulsion (ICOMP) associates, and U.S. Army Aviation Research and Technology Activity (AVSCOM) personnel. The balance are from industry and academia.

It is a well-rounded symposium, and the proceedings should be a valuable resource for several years to come. The format is easy to access and extract information from. Each topic within a presentation is self-contained on a single page. The topic title appears at the top of the page followed by an extended figure caption, and the figure is located at the bottom of the page. Considerable effort has been expended in streamlining the presentations and freeing them of extraneous information so as to make them clear to the potential user - YOU. References are cited for more detailed followup of a particular topic. On-site personnel are also willing to lend assistance in answering questions and resolving problems that need clarification.

Lester D. Nichols
Chief, Structures Division
NASA Lewis Research Center

PRECEDING PAGE BLANK NOT FILMED

CONTENTS TO VOLUME 3

CERAMIC COMPONENT RELIABILITY

Session Overview	3-1
John P. Gyekenyesi, NASA Lewis Research Center	
Monolithic Ceramic Analysis Using the SCARE Program	3-5
Jane M. Manderscheid, NASA Lewis Research Center	
Whisker-Reinforced Ceramic Composites for Heat Engine Components	3-21
Stephen F. Duffy, Cleveland State University	
Continuous Fiber Ceramic Matrix Composites for Heat Engine Components	3-41
David E. Tripp, Cleveland State University	

NONDESTRUCTIVE EVALUATION

Session Overview	3-63
Alex Vary, NASA Lewis Research Center	
Nondestructive Evaluation by Acousto-Ultrasonics	3-67
Harold E. Kautz, NASA Lewis Research Center	
Characterization of Sintered SiC by Using NDE	3-79
George Y. Baaklini, NASA Lewis Research Center	
Systems for Ultrasonic Scanning, Analysis, and Imagery	3-93
David B. Stang, Sverdrup Technology, Inc., Lewis Research Center Group, Edward R. Generazio, NASA Lewis Research Center, and Steve Abe, Cleveland State University	
Flaw Characterization in Structural Ceramics Using Scanning Laser Acoustic Microscopy	3-107
Don J. Roth, NASA Lewis Research Center	
Nondestructive Evaluation of Sintered Ceramics	3-123
George Y. Baaklini, Stanley J. Klima, and William A. Sanders, NASA Lewis Research Center	

FRACTURE MECHANICS

Session Overview	3-135
John L. Shannon, Jr., NASA Lewis Research Center	
Fracture Technology for Brittle Materials	3-141
Jonathan A. Salem, NASA Lewis Research Center	
Mode II Fracture Mechanics	3-149
Robert J. Buzzard, NASA Lewis Research Center, and Louis Ghosn, Cleveland State University	
In Situ Fatigue Loading Stage Inside Scanning Electron Microscope . . .	3-161
Jack A. Telesman, NASA Lewis Research Center, Peter Kantzos, Case Western Reserve University, and David N. Brewer, U.S. Army Aviation Research and Technology Activity - AVSCOM	

Grain Boundary Oxidation and Low-Cycle Fatigue at Elevated Temperatures	3-173
H.W. Liu and Y. Oshida, Syracuse University	
Elevated Temperature Crack Growth	3-187
K.S. Kim, R.H. Van Stone, S.N. Malik, and J.H. Laflen, General Electric Co.	

FATIGUE AND DAMAGE

Session Overview	3-199
Marvin H. Hirschberg, NASA Lewis Research Center	
Cumulative Fatigue Damage Models	3-201
Michael A. McGaw, NASA Lewis Research Center	
Fatigue Damage Mapping	3-213
Darrell Socie, University of Illinois at Urbana-Champaign	
Bithermal Fatigue: A Simplified Alternative to Thermomechanical Fatigue	3-221
Michael J. Verrilli, NASA Lewis Research Center	
Life Prediction Modeling Based on Strainrange Partitioning	3-231
Gary R. Halford, NASA Lewis Research Center	
Life Prediction Modeling Based on Cyclic Damage Accumulation	3-245
Richard S. Nelson, Pratt & Whitney	
Fatigue Damage Modeling for Coated Single Crystal Superalloys	3-259
David M. Nissley, Pratt & Whitney	
Life and Reliability of Rotating Disks	3-271
Erwin V. Zaretsky, NASA Lewis Research Center, and Todd E. Smith and Richard August, Sverdrup Technology, Inc., Lewis Research Center Group	

WIND TURBINES

Large-Scale Wind Turbine Structures	3-285
David A. Spera, NASA Lewis Research Center	

HOST

Aircraft Engine Hot Section Technology - An Overview of the HOST Project	3-301
Daniel E. Sokolowski, NASA Lewis Research Center	
Research Sensors	3-323
David R. Englund, NASA Lewis Research Center	
HOST Combustion R&T Overview	3-337
Raymond E. Gaugler and James D. Holdeman, NASA Lewis Research Center	
Review and Assessment of the HOST Turbine Heat Transfer Program	3-349
Herbert J. Gladden, NASA Lewis Research Center	

APPENDIX

Contents to Volume 1	3-370
Contents to Volume 2	3-373

CERAMIC COMPONENT RELIABILITY

SESSION OVERVIEW

John P. Gyekenyesi
Structural Integrity Branch
NASA Lewis Research Center

Ceramics and ceramic matrix composites (CMC) offer significant potential for raising the thrust-to-weight ratio of gas turbine engines by enabling higher cycle temperatures with the use of refractory, high specific strength material systems. Silicon based ceramics, such as silicon carbide (SiC) and silicon nitride (Si_3N_4), offer the most high-temperature strength, thermal stability, and resistance to thermal shock and oxidation. The structural promise of these materials in monolithic form is being evaluated in engine demonstration programs such as the DOE-sponsored Advanced Gas Turbine (AGT) Project. The objective is to develop a competitive fuel-efficient gas turbine automobile engine having an all ceramic hot section.

Monolithic ceramics have yet to be applied in aircraft engines, chiefly because of their poor structural reliability and reproducibility. Because they lack fracture toughness, these materials are very sensitive to microscopic cracks or flaws. Since conventional ceramic processing will unavoidably lead to both intrinsic and external surface imperfections, ceramics vary widely in strength, and their load carrying capability depends greatly on their geometric size.

There are several approaches to make ceramics stronger, tougher, and more reliable. Strength can be improved and its scatter reduced by improved processing. Adding a reinforcing or toughening phase can improve fracture toughness and decrease the sensitivity of the matrix to flaws. The reinforcing ceramic second phase can have a variety of shapes, ranging from nearly spherical particles, through whiskers and chopped fibers with various length-to-diameter (L/D) ratios, to continuous fibers. Compact particles and whiskers lend themselves to traditional ceramic processing methods, with a high-volume production potential and a material that can range from fully isotropic to that displaying anisotropic thermoelastic properties. Continuous small diameter fibers, however, reinforce ceramics more efficiently since their orientation in the direction of the principal load significantly enhances the matrix cracking strain, as well as the ultimate load carrying capability of the composite. In addition, through optimized volume fraction and fiber-matrix interface behavior, the effective composite fracture toughness can be greatly increased, whereby the composite displays metal-like, graceful failure response before ultimate fracture.

In the past, most components using structural ceramics and CMC were designed by "trial and error", since the emphasis was on feasibility demonstration rather than on fully understanding the parameters controlling structural response. In

addition, the continuous change and development of these material systems and the lack of standardized design data minimized the emphasis on mathematical modeling, both for analysis of deformation (micromechanics) and of failure (macromechanics). Fast fracture, durability, environmental response, impact tolerance, and life prediction are presently being addressed for monolithics, but very little has been done for the toughened and continuous fiber reinforced CMC's. The objective of our fracture analysis and brittle material design program is to investigate appropriate structural models and implement them in general purpose analysis codes for use by industry in designing heat engine components. The use of computers, linear elastic fracture mechanics (LEFM), and statistics are key ingredients to any deformation and failure studies of these brittle systems, since it is important to have a mechanistic rather than a phenomenological understanding of the material's behavior. It is the use of these disciplines, which are not usually a part of the mechanical engineer's curriculum, that makes brittle-material design unique and different from that used with traditional, forgiving materials like metals and plastics. At the Lewis Research Center our emphasis is on fast fracture behavior of isotropic monolithics, of toughened isotropic and anisotropic ceramics, and of the fully anisotropic laminated and woven composites. Our progress for fast fracture of monolithics has been extensive, so that issues of fatigue (subcritical crack growth) will also be addressed at Lewis in the near future. Our program with the other material systems, however, is less than a year old, and progress with them is difficult to forecast.

In this session, you will hear three presentations, each describing the fast fracture problem in monolithics, whisker toughened ceramics, and laminated CMC's. In addition, the prediction of thermoelastic properties of toughened ceramics will be emphasized since the micromechanics of isotropic ceramics and laminated composites, at least in the linear regime, will be identical to those previously developed for other materials. Work for woven composites, both in micromechanics and macromechanics, is only in the planning stage, although the importance of these engineered materials is evident from the successes of the world's most mature CMC, the French Societe Europeenne de Propulsion's (SEP's) SiC/SiC cerasep.

STRUCTURAL CERAMICS IN REVIEW (UP TO 3000 °F)

A. MONOLITHICS

- HIGH-TEMPERATURE STRENGTH, LOW DENSITY, ISOTROPIC BEHAVIOR
- GOOD RESISTANCE TO THERMAL SHOCK, OXIDATION, CORROSION
- TRADITIONAL, NET SHAPE, HIGH-VOLUME PROCESSING
- LOW FRACTURE TOUGHNESS, CATASTROPHIC FAILURE, LOW RELIABILITY

B. PARTICULATE AND WHISKER TOUGHENED CERAMICS ($L/D < 30$)

- SAME AS ABOVE EXCEPT FOR MODERATE IMPROVEMENTS IN FRACTURE TOUGHNESS AND RELIABILITY (UP TO 100% INCREASE IN K_{Ic})
- VARIES FROM ISOTROPIC TO FULLY ANISOTROPIC BEHAVIOR

C. CONTINUOUS FIBER REINFORCED CERAMICS

- ANISOTROPIC RESPONSE WITH FULL TAILORING POTENTIAL
- GREATLY IMPROVED TOUGHNESS WITH INCREASED TOLERANCE TO FLAWS, IMPROVED RELIABILITY, AND GRACEFUL FAILURE
- MUCH MORE DIFFICULT TO PROCESS, REQUIRES OPTIMUM INTERFACE AND IMPROVEMENTS IN PERFORMANCE OF FIBERS

CD-88-31726

CERAMIC COMPONENTS RELIABILITY ANALYSIS

A. MONOLITHICS

- MICROMECHANICS AND STRUCTURAL ANALYSIS—WELL IN HAND
- FAST FRACTURE—REASONABLY UNDERSTOOD, LIMITED DESIGN CODES
- LIFE PREDICTION (FATIGUE, CREEP, OXIDATION, IMPACT)—SOME MODELS EXIST BUT NEED TO BE STUDIED AND PROGRAMMED

B. PARTICULATE AND WHISKER TOUGHENED CERAMICS

- MICROMECHANICS AND STRUCTURAL ANALYSIS—SOME MODELS EXIST
- FAST FRACTURE—MOSTLY PHENOMENOLOGICAL
- LIFE PREDICTION—MOSTLY EMPIRICAL

C. CONTINUOUS FIBER REINFORCED CERAMICS

1. LAMINATED COMPOSITES

- MICROMECHANICS AND STRUCTURAL ANALYSIS—WELL IN HAND (LINEAR REGIME)
- FAST FRACTURE—SOME MODELS EXIST BUT NEED TO BE STUDIED
- LIFE PREDICTION—MOSTLY EMPIRICAL

2. WOVEN COMPOSITES

- MICROMECHANICS AND STRUCTURAL ANALYSIS—SOME MODELS EXIST
- FAST FRACTURE—MOSTLY PHENOMENOLOGICAL
- LIFE PREDICTION—MOSTLY EMPIRICAL

CD-88-31727

MONOLITHIC CERAMIC ANALYSIS USING THE SCARE PROGRAM

Jane M. Manderscheid
Structural Integrity Branch
NASA Lewis Research Center

ABSTRACT

The SCARE (Structural Ceramics Analysis and Reliability Evaluation) computer program calculates the fast fracture reliability of monolithic ceramic components. The code is a post-processor to the MSC/NASTRAN general purpose finite element program. SCARE automatically accepts the MSC/NASTRAN output necessary to compute reliability. This includes element stresses, temperatures, volumes, and areas. The SCARE program computes two-parameter Weibull strength distributions from input fracture data for both volume and surface flaws. The distributions can then be used to calculate the reliability of geometrically complex components subjected to multiaxial stress states. Several fracture criteria and flaw types are available for selection by the user, including out-of-plane crack extension theories. The theoretical basis for the reliability calculations was proposed by Batdorf. These models combine linear elastic fracture mechanics (LEFM) with Weibull statistics to provide a mechanistic failure criterion. Other fracture theories included in SCARE are the normal stress averaging technique and the principle of independent action. The objective of this presentation is to summarize these theories, including their limitations and advantages, and to provide a general description of the SCARE program, along with example problems.

OUTLINE

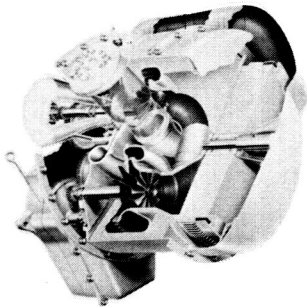
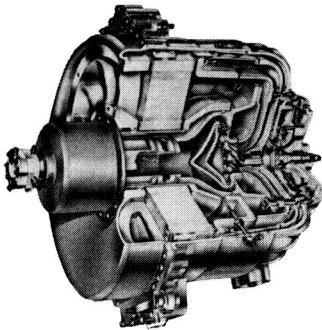
Designing with ceramics requires a new approach involving statistics. Inherent to this method is the realization that any component will have a finite failure probability; that is, no design is fail-safe. Methods of quantifying this failure probability have been investigated and refined. These theories have been programmed into SCARE. The accuracy of the FORTRAN coding and the mathematical modeling has been verified by analytical and experimental methods. Using SCARE a design engineer can easily calculate the change in reliability due to a design change. This can lead to more efficient material utilization and system efficiency.

- BASIC CONCEPTS OF BRITTLE MATERIAL DESIGN
- STATISTICAL FRACTURE THEORIES:
 - 1. BASED ON STATISTICS AND OBSERVATIONS:
UNIAXIAL WEIBULL, NORMAL STRESS AVERAGING, PIA
 - 2. BASED ON STATISTICS AND FRACTURE MECHANICS: BATDORF
- THE SCARE PROGRAM
- VERIFICATION AND APPLICATION OF SCARE
- SUMMARY

CD-88-32561

CERAMICS FOR ENGINES

Structural ceramics have been utilized for various test engine components since the early 1970's. This work has been sustained by the unique properties that ceramics offer in the areas of high-temperature strength, environmental resistance, and low density. These characteristics can result in large benefits in system efficiency and performance. However, the brittle nature of ceramics causes a high sensitivity to microscopic flaws and catastrophic fracture. The subsequent low reliability of ceramic components has limited their application in large scale engine production.



CERAMIC PROPERTIES

- HIGH-TEMPERATURE STRENGTH
- ENVIRONMENTAL RESISTANCE
- LOW DENSITY



IMPROVED EFFICIENCY AND
PERFORMANCE

BUT

- HIGH CERAMIC SENSITIVITY TO FLAWS
- BRITTLE CATASTROPHIC FAILURE



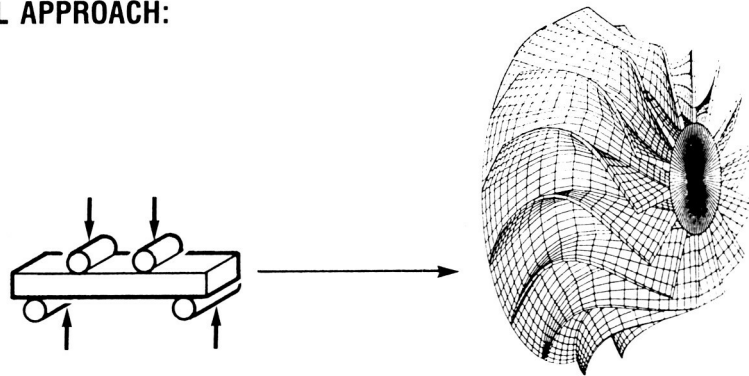
- LOW RELIABILITY
- LIMITED APPLICATION

CD-88-32562

BRITTLE MATERIAL DESIGN

The design of ceramics differs from that of ductile metals in that ceramic materials are unable to redistribute high local stresses induced by inherent flaws. Random flaw size and orientation require a probabilistic analysis. The first step of a probabilistic design methodology is the determination of a temperature-dependent fracture strength distribution from flexural or tensile test specimens. From this data, the reliability for a given component geometry and loading is then computed. An important characteristic of probabilistic design is that the stress distribution over the entire volume is needed. The design is not necessarily governed by the most highly stressed location, but by the entire stress field.

- CERAMICS ARE BRITTLE AND HAVE MANY FLAWS
- RANDOM FLAW SIZE AND ORIENTATION REQUIRE PROBABILISTIC METHOD
- GENERAL APPROACH:



SIMPLE TESTS

COMPLEX PREDICTIONS

- REQUIRES ENTIRE STRESS FIELD, NOT MAXIMUM STRESS POINT

STATISTICAL FRACTURE THEORIES

A common aspect of any weakest link theory is that the component volume and/or surface area of a stressed material will affect its strength, whereby larger components result in lower average strengths. This observation led Weibull (1939) to propose a phenomenological model to describe the scatter in brittle material fracture strengths. To predict material response under multiaxial stresses Weibull suggested averaging the tensile normal stress in all directions. As this approach is arbitrary and involves tedious numerical integration, other approaches have been subsequently introduced. The most simplistic is the principle of independent action (PIA) model (Barnett, 1967, and Freudenthal, 1968). The PIA theory assumes that each tensile principal stress contributes to the failure probability as if no other stress were present. Finally, Batdorf and Crose (1974) incorporated LEFM with the weakest link theory to predict failure on a mechanistic basis. The model was extended to account for mixed-mode fracture by Batdorf and Heinisch (1978). All of these models are available in the SCARE program.

WEAKEST LINK FRACTURE MODEL	SIZE EFFECT	STRESS STATE EFFECTS	COMPUTATIONAL SIMPLICITY	THEORETICAL BASIS
WEIBULL (1939)	YES	UNIAXIAL	SIMPLE	PHENOMENOLOGICAL
NORMAL STRESS AVERAGING (1939)	YES	MULTIAXIAL	COMPLEX	PHENOMENOLOGICAL
PRINCIPLE OF INDEPENDENT ACTION (1967)	YES	MULTIAXIAL	SIMPLE	MAXIMUM PRINCIPAL STRESS THEORY
BATDORF (SHEAR-INSENSITIVE, 1974) (SHEAR-SENSITIVE, 1978)	YES	MULTIAXIAL	COMPLEX	LINEAR ELASTIC FRACTURE MECHANICS

WEIBULL DISTRIBUTION

The Weibull distribution is a key ingredient for weakest link fracture theories. As the number of flaws present in a structure is proportional to its volume, the failure probability increases with both the applied stress and the material volume. The Weibull failure probability is dependent on three statistical parameters; the Weibull modulus m , the scale parameter σ_0 , and the threshold strength σ_u . The Weibull modulus is indicative of strength variability, with smaller values representing a larger variation. The scale parameter, or normalizing stress, is related to the mean strength. The threshold strength is usually taken as zero because of limited experimental data and the mathematical simplicity of the resultant equation. A similar form of the Weibull distribution has been developed for surface flaw induced fracture, with corresponding surface material parameters.

FAILURE PROBABILITY FOR VOLUMETRIC FLAWS IN UNIAXIAL TENSION

$$P_f = 1 - \exp \left[- \int_V \left(\frac{\sigma - \sigma_u}{\sigma_0} \right)^m dV \right] \quad (\sigma > \sigma_u)$$
$$P_f = 0 \quad (\sigma \leq \sigma_u)$$

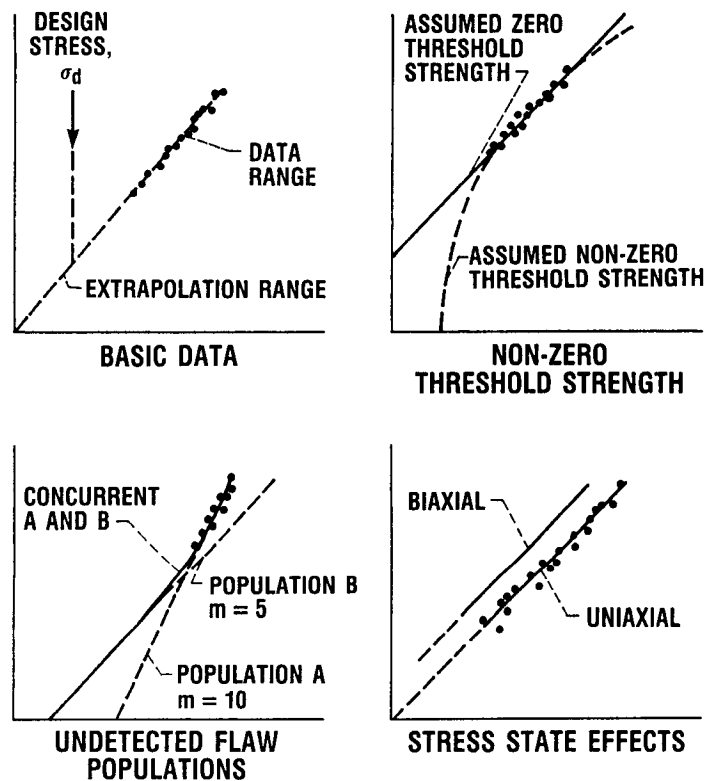
WHERE

- σ APPLIED TENSILE STRESS
- σ_0 SCALE PARAMETER
- σ_u THRESHOLD STRENGTH
- m WEIBULL MODULUS
- V VOLUME OF STRESSED MATERIAL

CD-88-32565

LIMITATIONS OF THE DIRECT STATISTICAL APPROACH

Several limitations are inherent to a purely statistical approach. One problem occurs when the design stress is below the range of experimental data. Extrapolation of the Weibull distribution into this regime may yield erroneous results if other phenomena are present. When two flaw populations exist concurrently, but only one is active in the strength regime tested, the predicted failure probability may be low (Johnson, 1983). Further, if the threshold strength is not zero, the strength may be underestimated (Shih, 1980). Finally, an approach based only on statistics can account for stress state effects only in an empirical fashion.



CD-88-32566

BATDORF FRACTURE THEORY

Recognizing that brittle fracture is governed by LEFM, Batdorf proposed that reliability predictions should be based on a combination of the weakest link theory and fracture mechanics. Conventional fracture mechanics dictates that both the size of the critical crack and its orientation relative to the applied loads determine the fracture stress. However, with ceramics the small critical flaw size and the large number of flaws prevent determination of the critical flaw, let alone its size and orientation. Instead, the combined probability of the critical flaw being within a certain size range and being oriented so that it may cause fracture is calculated. As flaw sizes correspond to strength levels and since strength is easier to measure than size for these microscopic flaws, the probability of a crack existing within a critical strength range is determined. This involves the derivative of the Batdorf crack density function which is expressed using the Weibull parameters obtained in uniaxial testing.

$$P_f = 1 - \exp \left[- \int_V dV \int_0^{\sigma_1} \left(\frac{\Omega}{4\pi} \right) \frac{dN}{d\sigma_{cr}} d\sigma_{cr} \right]$$

INVOLVES TWO PROBABILITIES:

(1) P [EXISTENCE OF A CRACK IN A GIVEN CRITICAL STRENGTH RANGE] = $dV \frac{dN}{d\sigma_{cr}} d\sigma_{cr}$

$N(m, \sigma_0, \sigma_{cr})$ BATDORF CRACK DENSITY FUNCTION (MATERIAL PROPERTY)

σ_{cr} REMOTE, NORMALLY APPLIED, FRACTURE STRESS OF A CRACK

(2) P [ORIENTATION OF A CRACK SUCH THAT $\sigma_e \geq \sigma_{cr}$] = $\frac{\Omega}{4\pi}$

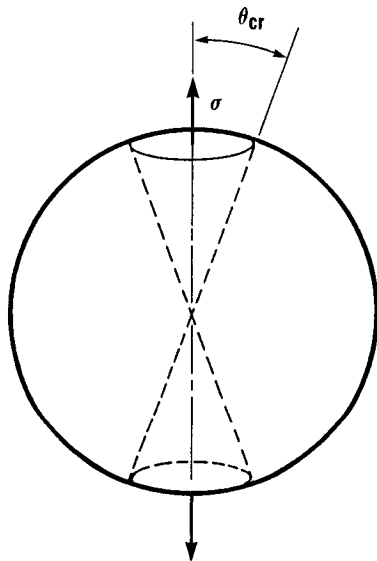
σ_e CRACK EFFECTIVE STRESS (FUNCTION OF CRACK GEOMETRY AND ORIENTATION, STRESS STATE, FRACTURE CRITERION)

Ω SOLID ANGLE IN STRESS SPACE WHICH INCLUDES ALL CRACK NORMALS FOR WHICH $\sigma_e \geq \sigma_{cr}$

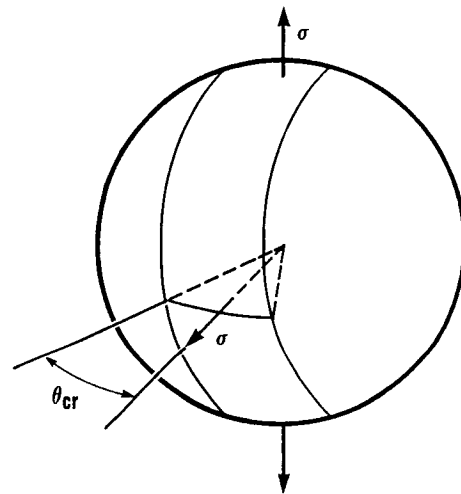
CD-88-32567

REPRESENTATIVE SOLID ANGLES

Fracture depends not only on the existence of a crack with a certain critical strength, but also on the crack orientation, the far-field stress state, and the crack shape. A collection of crack orientations can be described by a solid angle. A solid angle is measured by its subtended surface area on a sphere of unit radius. Therefore, the measure of the solid angle containing all possible crack orientations is 4π . The other solid angle of interest, Ω , is defined as that angle which includes all crack normals for which $\sigma_e \geq \sigma_{cr}$ (Batdorf and Crose, 1974). This assumes that fracture depends on an effective stress producing a singularity at the crack tip and that crack propagation occurs when the effective stress is greater than or equal to the critical stress. For uniaxial tension the effective stress is highest on cracks normal to the applied load. Therefore, the solid angle can be measured by the surface area of "polar caps" around the loading axis. The caps will decrease in size as the critical stress is increased, until $\sigma_{cr} = \sigma_1$ and $\Omega = 0$. A solid angle representative of equibiaxial tension is also shown.



**UNIAXIAL TENSION—
TWO CONES**



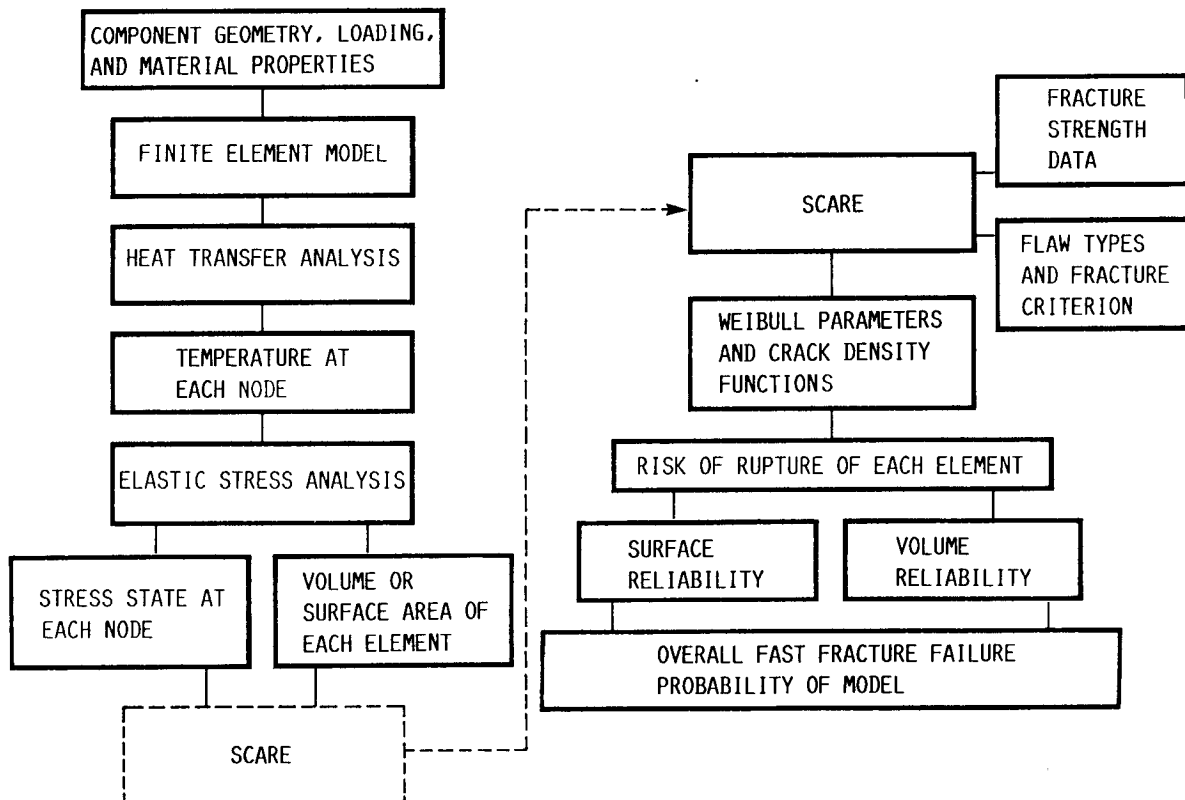
**EQUAL BIAxIAL TENSION—
EQUATORIAL BELT BETWEEN
TWO CONES**

AS THE CRITICAL STRESS INCREASES, THE SOLID ANGLE DECREASES

CD-88-32568

SCARE PROCEDURAL DIAGRAM

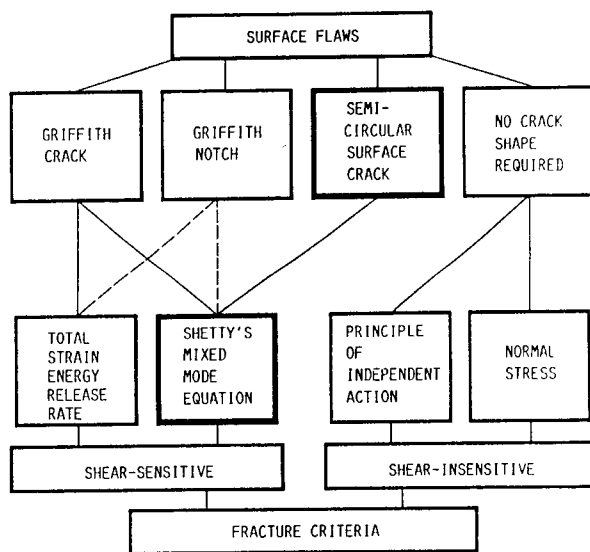
The previously noted fracture theories have all been implemented in SCARE (Gyekenyesi, 1986, and Gyekenyesi and Nemeth, 1987). The bulk of the input data for SCARE comes from a finite element stress analysis and, if necessary, heat transfer analysis of the component. MSC/NASTRAN was chosen as the primary finite element package because of its extensive capabilities and widespread usage. The SCARE program can be readily modified to accept input from other methods of stress analysis. Input specifying fracture strength data from test specimens, usually MOR (modulus of rupture) bars, is also required. These specimens must be separated into two categories, those which failed because of surface flaws and those which fractured because of volume flaws. In addition, a flaw geometry and fracture criterion must be selected. The SCARE program then calculates the statistical parameters for both the Weibull and Batdorf fracture models. The survival probability is calculated for both volume and surface flaws for each element or subelement. Since the reliability of each subelement is independent, the failure probability for a given component under the specified load is computed.



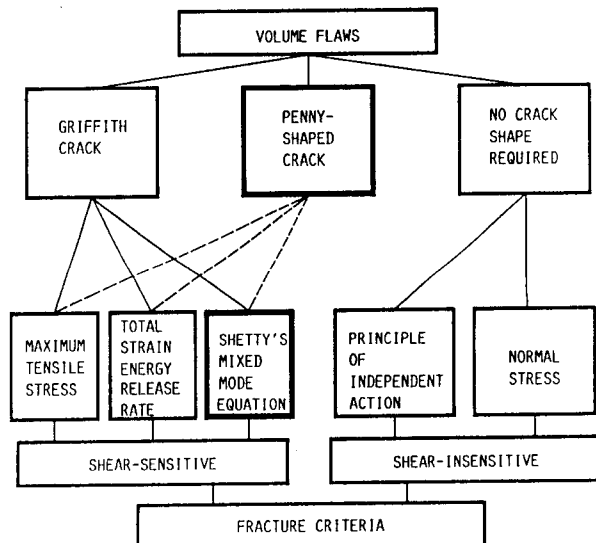
CD-88-32569

AVAILABLE FLAW TYPES AND FRACTURE CRITERIA

The diagrams below depict the flaw types and fracture criteria available in the SCARE program. The simple statistical fracture theories, PIA and normal stress averaging, do not require a specific crack geometry since they are not based on fracture mechanics. On the other hand, Batdorf's fracture theory can be used with several different mixed-mode fracture criterion and crack geometries. The combination of a particular flaw shape and fracture criterion results in an effective stress equation involving far-field normal and shear stresses. Coplanar crack extension theories include the maximum tensile stress theory and the total strain energy release rate theory. In reality, a crack is not confined to grow within its plane, and out-of-plane crack extension criteria are more accurate. In SCARE, these criteria are approximated by a simple equation (Shetty, 1987). The approach involves a semi-empirical constant which is varied to model the maximum tangential stress theory, the maximum strain energy release rate theory, or experimental results. Because of the flexibility of this equation, it is the preferred model for both volume and surface flaws. Finally, with regard to crack geometry, semi-circular cracks are preferred for surface imperfections, whereas penny-shaped cracks best reflect the geometry of volume imperfections.



CD-88-32570

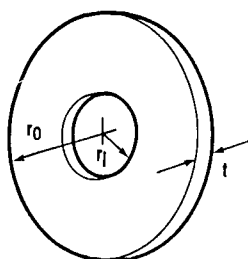


CD-88-32571

CODE VALIDATION

Several sample problems have been selected from the open literature to validate the SCARE program. For example, a silicon nitride disk was spun to fracture (Swank and Williams, 1981). The disk geometry is shown in the first figure, as well as the Weibull parameters from MOR bar testing. Reliability calculations from the SCARE code are compared to experimental results in the second figure. The predictions from a shear-sensitive Batdorf fracture criterion are closest to the experimental results. However, it should be noted that only seven disks were tested, compared to 85 MOR specimens. This leads to a large degree of statistical uncertainty in the disk data and may account for the greater difference between experimental and predicted P_f at lower failure probabilities. Rigorous testing is being conducted in an in-house program to gather more data for code validation purposes. Furthermore, the shear-insensitive fracture models have been favorably tested against proprietary codes with these capabilities.

ROTATING ANNULAR DISK VOLUME FLAW ANALYSIS



DATA:

NC - 132 HOT PRESSED Si_3N_4

m 7.65

σ_0 74.82 MPa METER (0.3922)

$N(\sigma_{cr})$ 16.30 $\left(\frac{\sigma_{cr}}{74.82 \text{ MPa}} \right)^{7.65}$ PER CUBIC METER

SHEAR-INSENSITIVE CALCULATION OF N

r_i 6.35 mm (.25 in.)

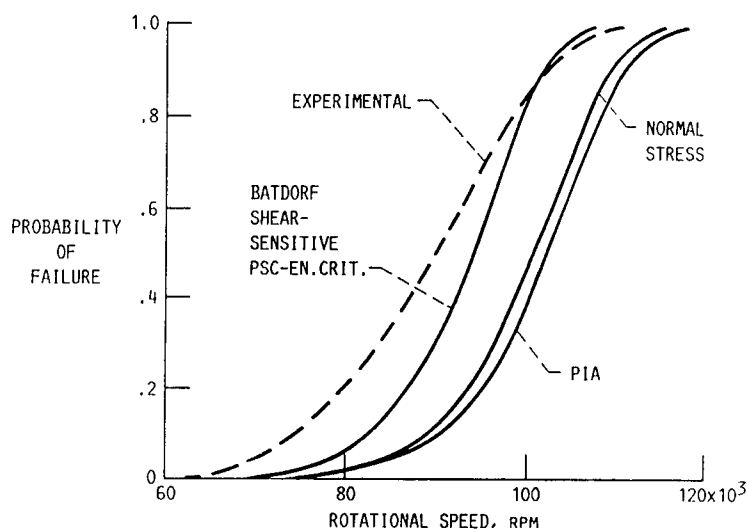
r_o 41.275 mm (1.625 in.)

t 3.80 mm (.15 in.)

RPM 70 000 TO 114 000

CD-88-32572

PROBABILITY OF FAILURE VERSUS DISK ROTATIONAL SPEED

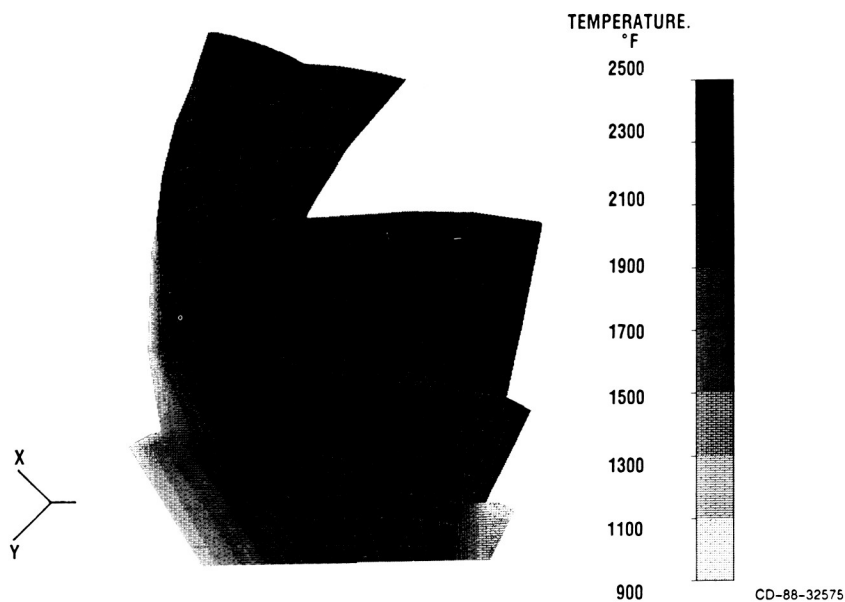


CD-88-32573

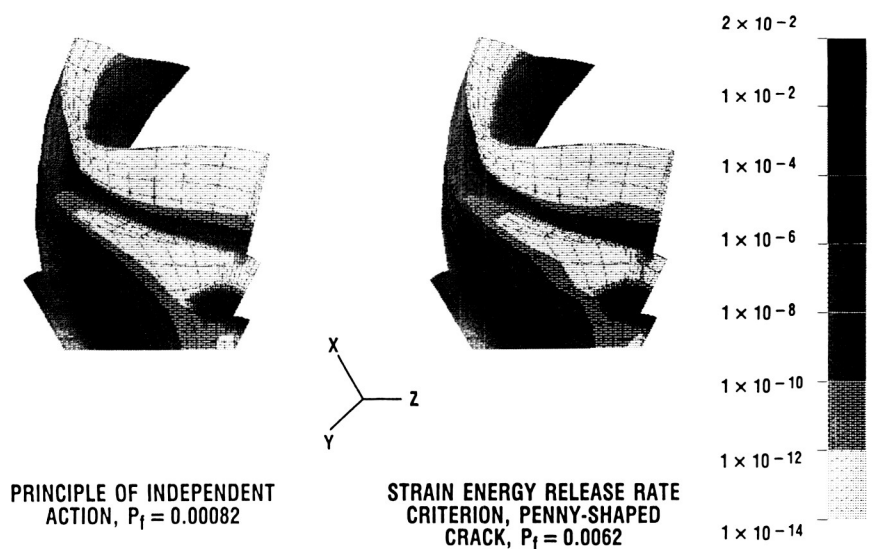
DESIGN APPLICATION

SCARE has been used for the preliminary design of a silicon nitride mixed-flow rotor for application in small, high temperature engines. A single blade and a section of the rotor hub were analyzed using the cyclic symmetry option of MSC/NASTRAN. The results from the heat transfer and reliability analyses are shown below. Again, the shear-sensitive criterion yields a higher probability of failure for the same applied load. However, the regions of low reliability are the same for both models.

SILICON NITRIDE MIXED-FLOW ROTOR TEMPERATURE DISTRIBUTION



COMPARISON OF RISK OF RUPTURE INTENSITIES PER UNIT VOLUME



CURRENT USAGE OF SCARE

SCARE is a unique public-domain program which has been requested by numerous companies in various industries.

INITIAL VERSION OF SCARE RELEASED TO (FEBRUARY 1, 1988)

GENERAL MOTORS CORPORATION
DETROIT DIESEL ALLISON
FORD MOTOR COMPANY
CHRYSLER CORPORATION
TRW VALVE DIVISION
NORTON-TRW CORPORATION
EATON CORPORATION
PDA ENGINEERING
NASA/COSMIC SOFTWARE CENTER
SPARTA
WLT CORPORATION

BOEING AEROSPACE COMPANY
GENERAL ELECTRIC COMPANY
BABCOCK AND WILCOX
AVCO LYCOMING DIVISION
DOW CHEMICAL
TRW SPACE & TECHNOLOGY GROUP
GARRETT TURBINE ENGINE COMPANY
ALLISON GAS TURBINE DIVISION
OAK RIDGE NATIONAL LABORATORY
SUNSTRAND-TURBOMACH CORPORATION
STRUCTURAL INTEGRITY ASSOCIATES

INDUSTRIES INVOLVED—AUTOMOBILE, AEROSPACE, NUCLEAR, & COMPUTER SOFTWARE

CD-88-32576

SUMMARY

A statistical design methodology must be used with ceramics to account for not only the average strength but, also, the scatter in strength. However, statistics must be supplemented with LEFM to provide a mechanistic understanding of the pertinent phenomenon. The improvement in failure predictions when using a shear-sensitive fracture mechanics based failure criterion was shown in the rotating disk example. The fracture mechanics/statistics combination allows for sound predictions when considering multiaxial stress states or concurrent flaw populations. This has been accomplished in the public domain finite element post-processor SCARE. This framework will be built on as we begin research on ceramic fatigue due to slow crack growth.

- **PROBABILISTIC DESIGN APPROACH MUST BE USED FOR CERAMICS**
- **FRACTURE MECHANICS IS NEEDED TO ACCURATELY ACCOUNT FOR:**
 - **MULTIAXIAL EFFECTS**
 - **CONCURRENT VOLUME AND SURFACE FLAW POPULATIONS**
 - **SLOW CRACK GROWTH**
- **SHEAR-SENSITIVE FRACTURE CRITERIA GIVE BETTER RESULTS**
- **FAST FRACTURE PREDICTION CAPABILITIES ARE READILY ACCESSIBLE**

CD-88-32577

REFERENCES

- Barnett, R.L., Connors, C.L., Hermann, P.C., and Wingfield, J., 1967, "Fracture of Brittle Materials Under Transient Mechanical and Thermal Loading," U.S. Air Force Flight Dynamics Laboratory, AFFDL-TR-66-220.
- Batdorf, S.B., and Crose, J.G., 1974, "A Statistical Theory for the Fracture of Brittle Structures Subjected to Nonuniform Polyaxial Stresses," Journal of Applied Mechanics, Vol. 41, No. 2, pp. 459-464.
- Batdorf, S.B., and Heinisch, H.L. Jr., 1978, "Weakest Link Theory Reformulated for Arbitrary Fracture Criterion," Journal of the American Ceramic Society, Vol. 61, Nos. 7-8, pp. 355-358.
- Freudenthal, A.M., 1968, "Statistical Approach to Brittle Fracture," Fracture An Advanced Treatise, Vol. 2, Mathematical Fundamentals, Edited by Liebowitz, H., Academic Press, New York, pp. 591-619.
- Gyekenyesi, J.P., 1986, "SCARE - A Post-Processor Program to MSC/NASTRAN for Reliability Analysis of Structural Ceramic Components," Journal of Engineering for Gas Turbines and Power, Vol. 108, No. 3, pp. 540-546.
- Gyekenyesi, J.P., and Nemeth, N.N., 1987, "Surface Flaw Reliability Analysis of Ceramic Components with SCARE Finite Element Post-Processor Program," Journal of Engineering for Gas Turbines and Power, Vol. 109, No. 3, pp. 274-281.
- Johnson, C.A., 1983, "Fracture Statistics of Multiple Flaw Distributions," Fracture Mechanics of Ceramics, Vol. 5, Surface Flaws, Statistics, and Microcracking, Edited by Bradt, R.C., Evans, A.G., Hasselman, D.P.H., and Lange, F.F., Plenum Press, New York, pp. 365-386.
- Shetty, D.K., 1987, "Mixed-Mode Fracture Criteria for Reliability Analysis and Design with Structural Ceramics," Journal of Engineering for Gas Turbines and Power, Vol. 109, No. 3, pp. 282-289.
- Shih, T.T., 1980, "An Evaluation of the Probabilistic Approach to Brittle Design," Eng. Fract. Mech., Vol. 13, No. 2, pp. 257-271.
- Swank, L.R., and Williams, R.M., 1981, "Correlation of Static Strengths and Speeds of Rotational Failure of Structural Ceramics," American Ceramic Society Bulletin, Vol. 60, No. 8, pp. 830-834.
- Weibull, W., 1939, "A Statistical Theory of the Strength of Materials," Ingeniors Vetenskaps Akademien Handlinger, No. 151.

**WHISKER-REINFORCED CERAMIC COMPOSITES FOR
HEAT ENGINE COMPONENTS***

Stephen F. Duffy
Cleveland State University
Cleveland, Ohio

ABSTRACT

Much work has been undertaken to develop techniques of incorporating SiC whiskers into either a Si_3N_4 or SiC matrix. The result has been the fabrication of ceramic composites with ever-increasing fracture toughness and strength. To complement this research effort, the fracture behavior of whisker-reinforced ceramics is studied so as to develop methodologies for the analysis of structural components fabricated from this toughened material. The results, outlined herein, focus on the following areas: the use of micromechanics to predict thermoelastic properties, theoretical aspects of fracture behavior, and reliability analysis.

*Work performed on-site at NASA Lewis for the Structural Integrity Branch under grant NCC3-81.

SCOPE

Current research activities are being focused on upgrading the performance of heat engines by increasing operating temperatures. With this goal in mind, whisker reinforced ceramics with improved strength and fracture toughness are being investigated for use as structural components in engine hot sections. Even though the fracture toughness of these composites is improved relative to unreinforced ceramics, they remain brittle in nature. Work has been initiated to identify and develop probabilistic methods required in the analysis of whisker-reinforced ceramic components. In addition, approaches using micro-mechanics to predict thermoelastic properties are under review.

- OBJECTIVES
- TOUGHENING MECHANISMS
- CRACK GROWTH MITIGATION PROCESSES IN WHISKER-REINFORCED CERAMICS
- IMPROVEMENTS IN STRENGTH AND TOUGHNESS
- MICROMECHANICS AND WHISKER ORIENTATION
- ELASTIC MATERIAL PROPERTIES
- WEIBULL DATA
- RELIABILITY ANALYSIS
- SUMMARY

CD-88-32512

OBJECTIVE

The objective of this effort includes the identification of whisker reinforced ceramics for use in engine hot sections. Further, the technical thrust is directed towards developing and/or refining analytical methods and computer codes that adequately predict fast fracture and life. The effort complements concurrent research by other organizational groups within NASA, the federal government, academia, and industry.

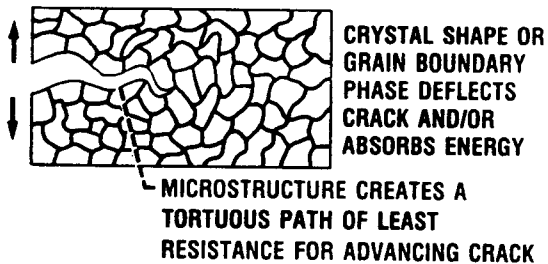
- IDENTIFY WHISKER REINFORCED CERAMICS FOR USE IN
ENGINE HOT SECTIONS
- DEVELOP AND REFINE ANALYTICAL METHODS AND
COMPUTER CODES FOR PREDICTING
 - FAST FRACTURE
 - LIFE

CD-88-32513

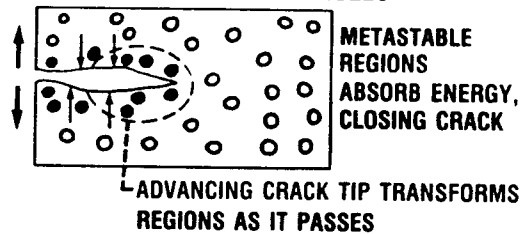
TYPICAL TOUGHENING MECHANISMS FOR CERAMICS

Historically, three approaches have been taken to improve fracture toughness. One approach is to engineer the grain size and shape to provide a tortuous microstructure such that the path of the crack tip is deflected from the optimum orientation for crack growth. The second approach creates microstructures containing second-phase particles resulting in transformation toughening. Here, a zone surrounding the crack tip absorbs energy and shields the tip by reducing the near field stress. The third approach, including whiskers in the matrix, increases toughness by pinning, deflecting, and/or bridging the crack tip.

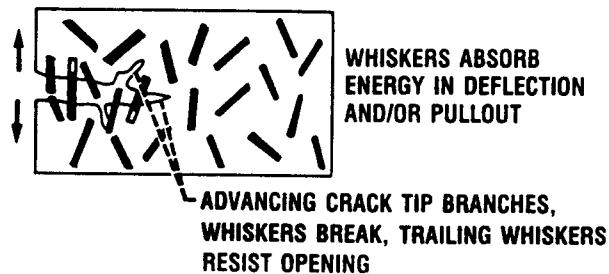
• ENGINEERING GRAIN SIZE AND SHAPE



• CREATING MICROSTRUCTURES WITH SECOND-PHASE PARTICLES



• ADDING HIGH-STRENGTH WHISKERS



CD-88-32514

CRACK GROWTH MITIGATION PROCESSES - WHISKER REINFORCED CERAMICS

It has been demonstrated experimentally that dispersing whiskers in a brittle matrix will mitigate crack growth. The presence of whiskers at the crack tip modifies fracture behavior by effectively increasing the required crack driving force through several mechanisms. As noted previously, these mechanisms include crack deflection, crack pinning, and whisker bridging. Faber and Evans (1983) have studied crack deflection and provide a lucid discussion. Lange (1971) discussed the process of crack pinning, and Wetherhold (1987) provides a probabilistic treatment of the crack bridging phenomenon.

THREE PROCESSES INCREASE FRACTURE TOUGHNESS

- **CRACK DEFLECTION**
 - **TILTING**
 - **TWISTING**
- **CRACK PINNING**
- **WHISKER BRIDGING**

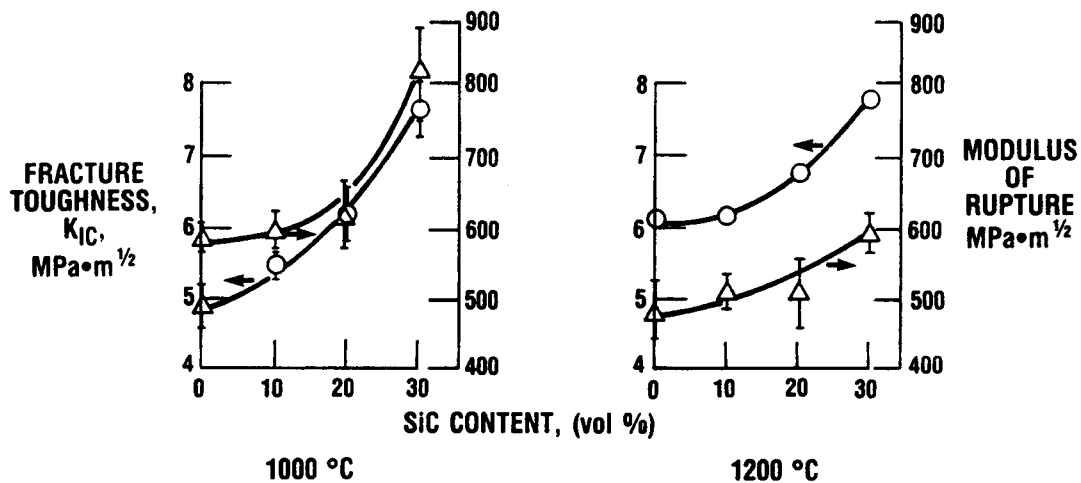
SEVERAL PROCESSES MAY OPERATE SIMULTANEOUSLY

CD-88-32515

IMPROVEMENTS IN STRENGTH AND TOUGHNESS

The addition of SiC whiskers in a Si_3N_4 matrix offers potential for considerable improvement in fracture toughness and strength. Note that the raw materials necessary for fabricating these composites are nonstrategic and are inherently lightweight. Initial attempts to develop whisker composites with these materials met with varying degrees of success (e.g., increased fracture toughness and decreased strength). Recently, Buljan et al. (1987) at GTE Laboratories, Inc., reported improvements in both toughness and strength over the entire range of whisker contents tested.

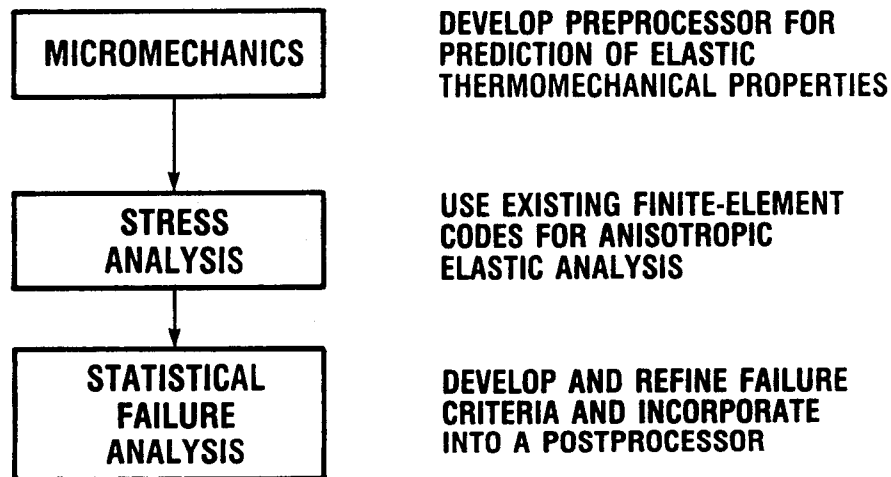
HOT PRESSED Si_3N_4 —SiC WHISKER COMPOSITES



CD-88-32516

ANALYTICAL APPROACH

The analytical approach taken involves the development of an integrated computer algorithm. The algorithm consists of (1) a micromechanics preprocessor, (2) a finite element code capable of incorporating material anisotropy, and (3) a statistical failure postprocessor. Proposed use of MSC/Nastran as the finite element code is based on its anisotropic analysis capability and widespread user base. The preprocessors and postprocessors are currently under development.



CD-88-32517

MICROMECHANICS AND WHISKER ORIENTATION

The thermoelastic properties of ceramic whisker composites are determined by process-induced whisker orientation and the constituent properties. Possible material symmetries resulting from fabrication include isotropy, transverse isotropy, and orthotropy. To characterize the internal structure, a whisker orientation distribution function is adopted. This approach was suggested by Pipes et al. (1982). The function quantifies all states of orientation, from random to perfectly aligned.

MATERIAL SYMMETRIES

- ISOTROPIC
- TRANSVERSELY ISOTROPIC
- ORTHOTROPIC

DEFINE WHISKER ORIENTATION PROBABILITY FUNCTION $n(\phi)$ SUBJECT TO

$$\int_{-\pi}^{\pi} n(\phi) d\phi = 1$$

WHEN

$n(\phi) = \text{CONSTANT}$

RANDOM WHISKER ORIENTATION

$n(\phi) = \delta(\eta - \phi)$

ALIGNED WHISKER ORIENTATION

HERE δ IS THE DIRAC DELTA FUNCTION AND η IS THE PRINCIPAL MATERIAL DIRECTION

CD-88-32518

MICROMECHANICS THEORY

The micromechanics theory proposed by Wu and McCullough (1977) for short fiber polymer composites is being considered for adaptation to whisker-reinforced ceramics. The theory was developed using variational techniques and incorporates the degree of whisker orientation, constituent properties, and volume fractions. The method requires the properties of a reference orientation, usually taken as the random orientation state. The parameters f and g define the orientation distribution and are included in the calculation of volume averaged properties.

EXPRESSING THE EFFECTIVE ELASTIC MATERIAL CONSTANTS AS

$$\langle C_{ijkl} \rangle = C_{ijkl}^{\circ} + F(C_{ijkl}^{\circ}, \bar{C}_{ijkl}) f + G(C_{ijkl}^{\circ}, \bar{C}_{ijkl}) g$$

WHERE

$\langle C_{ijkl} \rangle$ PREDICTED ELASTIC CONSTANTS OF THE COMPOSITE

C_{ijkl}° ELASTIC CONSTANTS FOR RANDOM WHISKER ORIENTATION

\bar{C}_{ijkl} LINEAR COMBINATION OF THE CONSTITUENT ELASTIC CONSTANTS

THE PARAMETERS f AND g ARE FUNCTIONALLY DEPENDENT UPON $n(\phi)$ AND DESCRIBE THE ORIENTATION STATE. WHEN

$f=g=0$ RANDOM WHISKER ORIENTATION

$f=g=1$ ALIGNED WHISKER ORIENTATION

CD-88-32519

PLANAR WHISKER ORIENTATION

The planar orientation of whiskers is often encountered in hot pressed composites. This special case was considered by Pipes et al. (1982). The orientation descriptors f_p and g_p along with the distribution function are defined below. Bozarth, et al. (1987) developed a Monte Carlo simulation that depicts the whisker orientation for specified values f_p .

APPLYING THE CONCEPT TO A PLANAR ORIENTATION OF WHISKERS

$$n(\phi) = K \cos(\lambda \phi)$$

$$f_p = 2\langle \cos^2 \phi \rangle - 1$$

$$g_p = \frac{2f_p(7 - 2f_p)}{5(4 - 2f_p)}$$

WHERE

$$\langle \cos^2 \phi \rangle = \int_{-\pi/2}^{\pi/2} n(\phi) \cos^2 \phi \, d\phi$$

THEN

$$f_p = 0, 1 \quad \text{TRANSVERSE ISOTROPY}$$

$$0 < f_p < 1 \quad \text{ORTHOTROPY}$$

A MONTE CARLO SIMULATION ILLUSTRATES GRAPHICALLY VARIOUS f_p VALUES



$$f_p = 0.0$$



$$f_p = 0.3$$



$$f_p = 0.6$$



$$f_p = 0.9$$

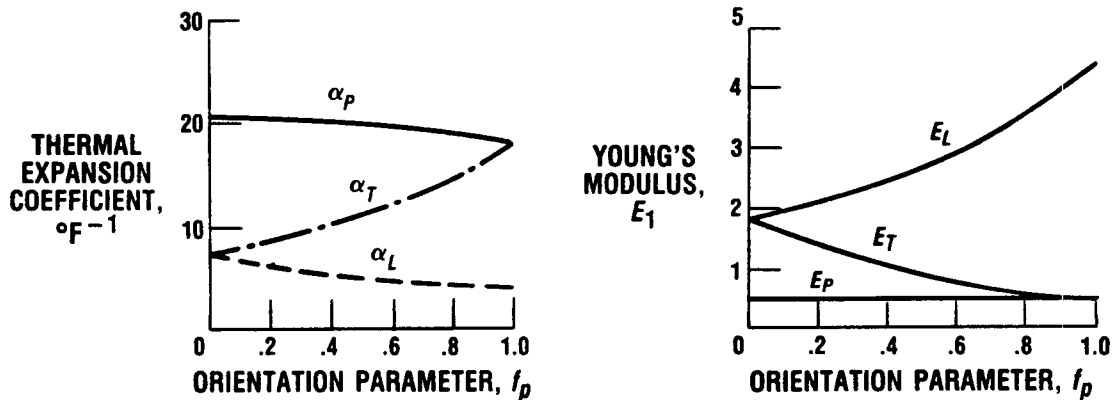
CD-88-32520

INFLUENCE OF WHISKER ORIENTATION ON MATERIAL PROPERTIES

The influence of orientation on material properties is shown below (from Pipes et al., 1982). Both the elastic moduli and the coefficients of thermal expansion are plotted for a short glass fiber phenolic resin matrix composite. The constants are plotted over the full range of f_p . Note that for $f_p = 1$ and $f_p = 0$, the material is transversely isotropic. For all other values, the material is orthotropic.

PREDICTIONS USING THE APPROACH FOR A SHORT FIBER POLYMER COMPOSITE

FIBER ASPECT RATIO $\approx 40-100$; FIBER CONTENT BY WEIGHT = 58%

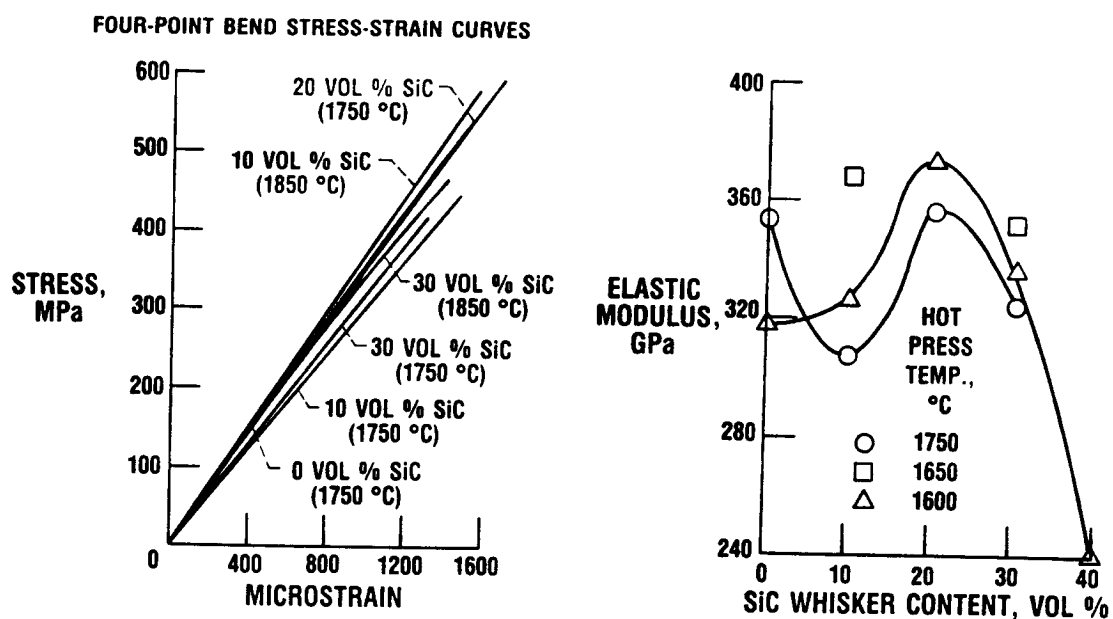


CD-88-32521

ELASTIC MATERIAL PROPERTIES

The examples shown below of stress-strain curves corresponding to various whisker contents were reported by Shalek et al. (1986). Note that the curves exhibit a linear stress-strain response up to the point of fracture. This indicates that crack growth involves only brittle fracture and allows for the application of linear elastic fracture mechanics (LEFM).

SiC WISKER-HOT-PRESSED Si_3N_4



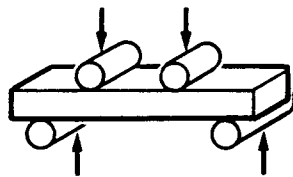
CD-88-32522

WEIBULL MODULUS

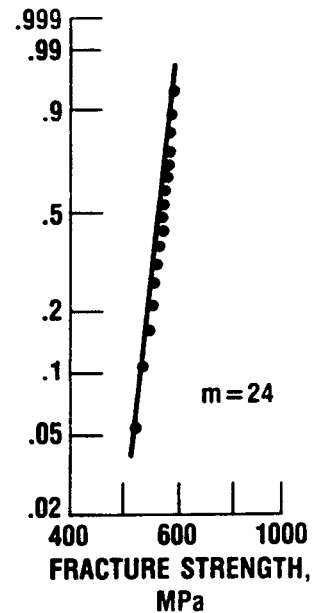
Greatly improved reliability has been cited by a number of authors, including Claussen and Petzow (1985), who have reported the highest Weibull modulus ($m = 24$) in the open literature. Improved processing techniques have resulted in the reduction of inhomogeneities, uniform whisker distribution, and a dense matrix. However, the variability of strength is still too high for the application of deterministic fracture theories.

30% SiC-WHISKER-Si₃N₄-MATRIX COMPOSITE

WHISKER REINFORCED CERAMICS EXHIBIT A VARIABILITY IN STRENGTH; HENCE, PROBABILISTIC METHODS OF ANALYSIS MUST BE APPLIED



PROBABILITY
OF
FAILURE

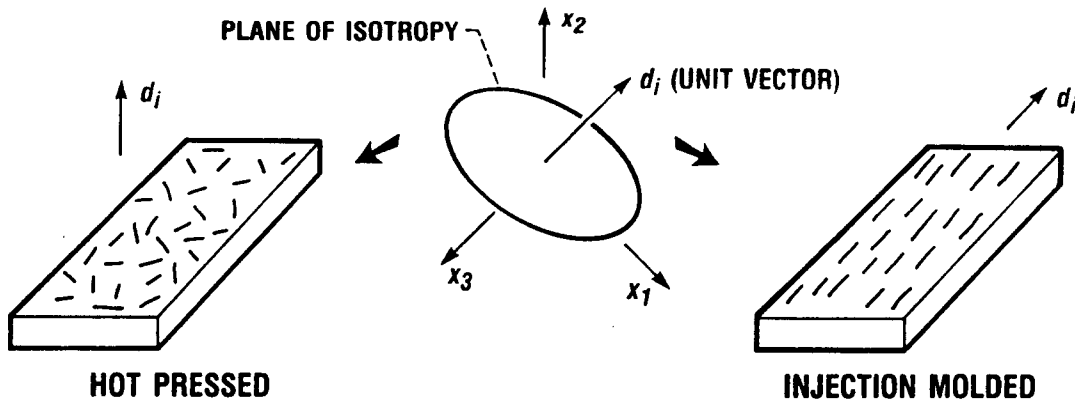


CD-88-32523

TRANSVERSE ISOTROPY

As noted previously, depending on fabrication, a whisker composite may have isotropic, transversely isotropic, or orthotropic material symmetry. It is anticipated that the probabilistic methods used in the analysis of monolithic ceramics will be appropriate for isotropic whisker composites. However, for transversely isotropic whisker composites, the probability of failure P_f must also reflect the preferred direction of the material d_i . This direction is defined as the normal to the plane of isotropy. A simple but rigorous method of including material symmetry in the functional dependence of P_f for transverse isotropy is presented. A similar approach can be developed for orthotropy.

TRANSVERSELY ISOTROPIC WHISKER COMPOSITES



DEPENDENCE OF P_f MUST REFLECT σ_{ij} , d_i , VOLUME AS WELL AS THE WEIBULL PARAMETERS

$$P_f = P_f(\sigma_{ij}, d_i d_j, V, \dots)$$

ASSUMING WEAKEST LINK THEORY IS APPROPRIATE, FORMULATE P_f IN A WAY THAT ACCOUNTS FOR THE ABOVE DEPENDENCE

CD-88-32524

TENSORIAL INVARIANTS

As P_f is a scalar function, it must remain form invariant under arbitrary proper orthogonal transformations. Form invariance is ensured if dependence is taken on invariants that constitute an integrity basis or any subset thereof. Tensorial invariant theory (see Spencer (1971)) serves as the basic mathematical tool in the development of the integrity basis. A subsequent geometric argument is made in constructing a slightly different set of invariants that corresponds to physical mechanisms related to fracture.

ADOPT THE FOLLOWING INTEGRITY BASIS:

$$I_1 = \sigma_{ij}$$

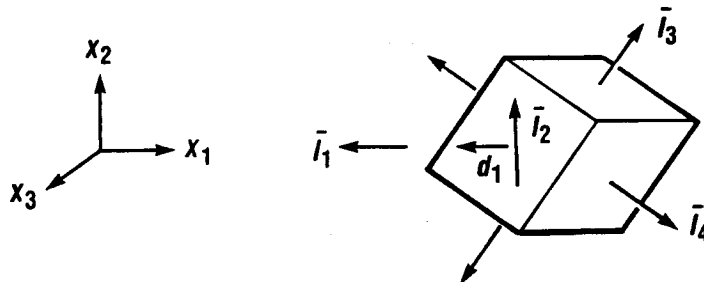
$$I_4 = d_i d_j \sigma_{ij}$$

$$I_2 = \sigma_{ij} \sigma_{ji}$$

$$I_5 = d_i \sigma_{ij} \sigma_{jk} d_k$$

$$I_3 = \sigma_{ij} \sigma_{jk} \sigma_{ki}$$

IDENTIFY DAMAGING STRESS TRACTION VECTORS:



\bar{I}_3, \bar{I}_4 MAXIMUM AND MINIMUM
NORMAL STRESSES IN
PLANE OF ISOTROPY

\bar{I}_1 NORMAL STRESS IN DIRECTION
OF d_i

\bar{I}_2 SHEAR STRESS ACTING ACROSS d_i

CD-88-32525

FAILURE PROBABILITY AS A FUNCTION OF INVARIANTS

The dependence of P_f is subsequently taken on the invariants $\bar{I}_1, \bar{I}_2, \bar{I}_3$, and \bar{I}_4 . This new set of invariants corresponds to the magnitudes of the stress traction vectors assumed to be the primary causes of fracture. These invariants incorporate both the stress tensor σ_{ij} and the direction vector d_i . Adopting the simplest of probabilistic failure theories, that is, a noninteractive theory, results in the form of P_f shown in the figure.

FROM THE INTEGRITY BASIS CONSTRUCT INVARIANTS WITH PHYSICAL INTERPRETATIONS CORRESPONDING TO THE MAGNITUDES OF THE DAMAGING STRESS TRACTION VECTORS

$\bar{I}_1 = I_4$
= COMPONENT OF S_i
PROJECTED ON
DIRECTION d_i

$\bar{I}_3 = \frac{1}{2}(I_1 - I_4) + [(\frac{1}{2})I_2 - I_5 + \frac{1}{4}(I_4^2 - I_1^2) + (\frac{1}{2})I_1 I_4]^{\frac{1}{2}}$
= MAXIMUM NORMAL STRESS IN
PLANE OF ISOTROPY

$S_i = \sigma_{ij} d_j$

$\bar{I}_2 = (I_5 - I_4^2)^{\frac{1}{2}}$
= COMPONENT OF S_i
PROJECTED ON THE
PLANE OF ISOTROPY

$\bar{I}_4 = \frac{1}{2}(I_1 - I_4) - [\frac{1}{2}I_2 - I_5 + \frac{1}{4}(I_4^2 - I_1^2) + \frac{1}{2}I_1 I_4]^{\frac{1}{2}}$
= MAXIMUM NORMAL STRESS IN
PLANE OF ISOTROPY

TAKING

$$P_f = P_f(\bar{I}_1, \bar{I}_2, \bar{I}_3, \bar{I}_4, V, \dots)$$

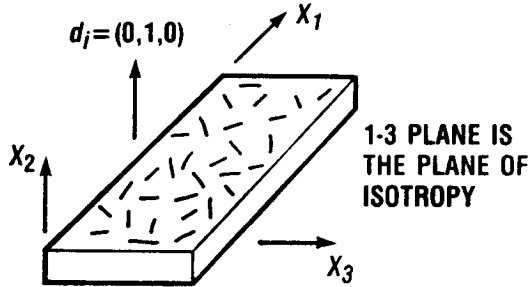
ENSURES P_f IS FORM INVARIANT. ASSUMING THE INVARIANTS ACT SEPARATELY IN PRODUCING FAILURE

$$P_f = 1 - \exp \left\{ - \int_V \left[\left(\frac{\bar{I}_1}{\beta_1} \right)^{\alpha_1} + \left(\frac{\bar{I}_2}{\beta_2} \right)^{\alpha_2} + \left(\frac{\bar{I}_3}{\beta_3} \right)^{\alpha_3} + \left(\frac{\bar{I}_4}{\beta_4} \right)^{\alpha_4} \right] dV \right\}$$

CD-88-32526

PLANE STRESS PROBABILISTIC ANALYSIS

The form of P_f is simplified for plane stress conditions considering two planar orientations of the whiskers. In both cases it is assumed that the whiskers are confined to the 1-3 plane due to fabrication. A random orientation of whiskers in the 1-3 plane reduces P_f to the isotropic formulation. Alternatively, perfect alignment of the whiskers in the 1-3 plane reduces P_f to a formulation proposed by Sun and Yamada (1978), Wetherhold and Pipes (1984), and Cassenti (1984).

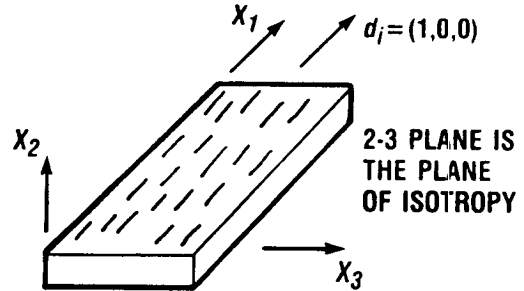


ASSUMING PLANE STRESS
 $\sigma_{12} = \sigma_{22} = \sigma_{23} = 0$

THEN

$$P_f = 1 - \exp \left\{ - \int_V \left[\left(\frac{\sigma_1}{\beta_3} \right)^{\alpha_3} + \left(\frac{\sigma_2}{\beta_3} \right)^{\alpha_3} \right] dV \right\}$$

WHERE σ_1 AND σ_2 ARE THE PRINCIPLE STRESSES IN THE PLANE OF ISOTROPY



ASSUMING PLANE STRESS
 $\sigma_{13} = \sigma_{23} = \sigma_{33} = 0$

THEN

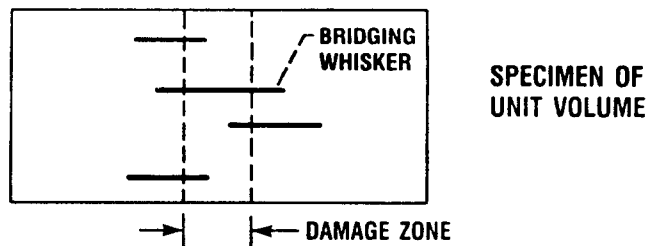
$$P_f = 1 - \exp \left\{ - \int_V \left[\left(\frac{\sigma_{11}}{\beta_1} \right)^{\alpha_1} + \left(\frac{\sigma_{12}}{\beta_2} \right)^{\alpha_2} + \left(\frac{\sigma_{22}}{\beta_3} \right)^{\alpha_3} \right] dV \right\}$$

CD-86-32527

WHISKER BRIDGING

Attempts have been made to develop statistical models that account for the microstructural events leading to crack propagation. Wetherhold (1987) derived a model assuming that fracture behavior is dominated by whiskers bridging a critical damage zone. The damage zone is analogous to a microcrack which is expected to grow and coalesce with other microcracks during progressive fracture. A distribution function for composite strength is developed based on the incorporation of random whisker strength into a bundle fracture theory.

THE FOLLOWING STATISTICAL APPROACH ACCOUNTS FOR THE WHISKER BRIDGING MECHANISM



DEFINE

**[A] = THE EVENT WHERE ULTIMATE COMPOSITE STRENGTH
IS GREATER THAN THE APPLIED LOAD**

THEN

$$P_s = P[A]$$

$$= \sum_{i=0}^N P[A|n=i] P[n=i]$$

WHERE

n NUMBER OF WHISKERS BRIDGING THE DAMAGE ZONE
 N NUMBER OF FIBERS PER UNIT VOLUME

CD-88-32528

SUMMARY

Enough experimental data exist that strongly suggests whisker-reinforced ceramics have promise, especially in the automotive industry where low-cost, high-volume fabrication is a necessity. The Structural Integrity Branch is identifying and refining existing design methodologies and, where necessary, assisting the research community in developing new methodologies. At present, there exists a need for analytical methods that capture the microstructural events that lead to increased fracture toughness and strength. Finally, work has begun on an integrated computer program capable of predicting elastic material properties through the application of micromechanics, the state of stress within a structural component, and the reliability of the component given the state of stress.

- **EXPERIMENTAL DATA SHOW SIGNIFICANT INCREASES OF STRENGTH AND FRACTURE TOUGHNESS DUE TO THE ADDITION OF CERAMIC WHISKERS IN A CERAMIC MATRIX**
- **WHISKER COMPOSITES HAVE THE ATTRACTIVE FEATURE OF USING CONVENTIONAL POWDER PROCESSING TECHNIQUES IN HIGH-VOLUME, LOW-COST FABRICATION**
- **AN INTEGRATED STRUCTURAL ANALYSIS CODE IS BEING DEVELOPED WITH THE FOLLOWING COMPONENTS:**
 - **MICROMECHANICS PREPROCESSOR**
 - **FINITE-ELEMENT PROGRAM**
 - **STATISTICAL FAILURE ANALYSIS POSTPROCESSOR**
- **RESEARCH IS UNDERWAY TO DEVELOP AND REFINE STATISTICAL FAILURE THEORIES TO ACCOUNT FOR MATERIAL ANISOTROPY ALONG WITH THE MICROSTRUCTURAL EVENTS LEADING TO FAILURE (I.E., CRACK DEFLECTION AND WHISKER BRIDGING)**

CD-88-32529

REFERENCES

- Bozarth, M.J., Gillespie, J.W., and McCullough, R.L., 1987, "Fiber Orientation and Its Effect Upon Thermoelastic Properties of Short Carbon Fiber Reinforced Poly (etheretherketone) (PEEK), Polymer Composites, Vol. 8, pp. 74-81.
- Buljan, S.T., Baldoni, J.G., and Huckabee, M.L., 1987, " Si_3N_4 -SiC Composites," Ceramic Bulletin, Vol. 66, pp. 347-352.
- Cassenti, B.N., 1984, "Probabilistic Static Failure of Composite Material," AIAA Journal, Vol. 22, pp. 113-111.
- Claussen, H., and Petzow, G., 1985, "Whisker-reinforced Zirconia Toughened Ceramics," Tailoring Multiphase and Composite Ceramics; Proceedings of the 21st University Conference on Ceramic Science, Plenum Press, New York, pp. 649-662.
- Faber, K.T., and Evans, A.G., 1983, "Crack Deflection Processes - I. Theory," Acta Metallurgica, Vol. 31, pp. 565-576,
- Lange, F.F., 1971, "The Interaction of a Crack Front with a Second-phase Dispersion," Philosophy Magazine, Vol. 22, pp. 983-992.
- Pipes, R.B., McCullough, R.L., and Taggart, D.G., 1982, "Behavior of Discontinuous Fiber Composites: Fiber Orientation," Polymer Composites, Vol. 3, pp. 34-39.
- Shalek, P.D., Petrovic, J.J., Hurley, G.F., and Gac, F.D., 1986, "Hot-Pressed SiC/ Si_3N_4 Matrix Composites," Ceramic Bulletin, Vol. 65, pp. 351-356.
- Spencer, A.J.M., 1971, "Theory of Invariants," Continuum Physics, Vol. I, Eringen, A.C., ed., Academic Press, London, 1971.
- Sun, C.T., and Yamada, S.E., 1978, "Strength Distribution of a Unidirectional Fiber Composite," Journal of Composite Materials, Vol. 12, pp. 169-176.
- Wetherhold, R.C., 1987, "Probabilistic Aspects of the Strength of Fiber-dominated Short-fiber Composites I: Aligned Fibers," Materials Science and Engineering, Vol. 97, pp. 7-12.
- Wetherhold, R.C., and Pipes, R.B., 1984, "Statistics of Fracture of Composite Materials Under Multiaxial Loading," Material Science and Engineering, Vol. 68, pp. 113-118.
- Wu, C.T.D., and McCullough, R.L., 1977, "Constitutive Relationships for Heterogeneous Materials," Developments in Composite Materials. Hollister, G.S., ed., Applied Science Publishers, Ltd., London, U. K., pp. 119-188.

**CONTINUOUS FIBER CERAMIC MATRIX COMPOSITES
FOR HEAT ENGINE COMPONENTS***

David E. Tripp
Cleveland State University
NASA Lewis Research Center

ABSTRACT

High strength at elevated temperatures, low density, resistance to wear, and abundance of nonstrategic raw materials make structural ceramics attractive for advanced heat engine applications. Unfortunately, ceramics have a low fracture toughness and fail catastrophically because of overload, impact, and contact stresses. Ceramic matrix composites provide the means to achieve improved fracture toughness while retaining desirable characteristics, such as high strength and low density.

Unlike polymer matrix composites, where a strong fiber is added to a weak matrix to provide increased strength and stiffness, ceramic matrix composites add fibers to an already strong matrix to achieve improved toughness. The toughening mechanisms in ceramic matrix composites are crack bridging, debonding, fiber friction, and fiber pullout. The factors that increase toughness, such as large fiber diameter and low interfacial bond strength, decrease composite strength. Thus, ceramic matrix composites are very different from polymer matrix composites.

Materials scientists and engineers are trying to develop the ideal fibers and matrices to achieve the optimum ceramic matrix composite properties. A need, however, also exists for the development of failure models for the design of ceramic matrix composite heat engine components. Phenomenological failure models such as maximum stress, maximum strain, Tsai-Hill, and Tsai-Wu are currently the most frequently used in industry, but they are deterministic and do not adequately describe ceramic matrix composite behavior. Semi-empirical models have been proposed, such as Whitney and Nuismer (1974), which relate the failure of notched composite laminates to the stress a characteristic distance away from the notch. Shear lag models such as that proposed by Eringen and Kim (1974) describe composite failure modes at the micromechanics level. The enhanced matrix cracking stress predicted by Aveston, Cooper, and Kelly (1971) occurs at the same applied stress level as predicted by the two models of steady state cracking by Budiansky, Hutchinson, and Evans (1986), and Marshall, Cox, and Evans (1985). Finally, statistical models, such as

*Work performed on-site at the Lewis Research Center for the Structural Integrity Branch under NASA grant NCC-3-81.

Wetherhold and Pipes (1984), take into consideration the distribution in composite failure strength.

The intent at the NASA Lewis Research Center is to develop these models into computer algorithms for the failure analysis of ceramic matrix composites under monotonically increasing loads. These algorithms will be included in a postprocessor to general purpose finite element programs.

SCOPE AND OBJECTIVES

Further developments in advanced heat engines are limited by the metallic materials currently available. For future applications (such as the National Aerospace Plane and automotive gas turbine engines) to become a reality, new materials capable of surviving the required stresses and temperatures for the life of the structure must become available. Not only, however, must those advanced materials systems be identified, but the necessary tools to design a structure with them must also be developed. The Structural Integrity Branch at NASA Lewis Research Center is identifying those ceramic matrix composite (CMC) systems currently being developed which are suitable for high-temperature applications and the failure models available to describe their behavior under monotonic loads. The results will be published in a survey later this year. Those models will then be selectively incorporated into a postprocessor for general purpose finite element programs, comparable to the SCARE postprocessor.

- IDENTIFY CERAMIC MATRIX COMPOSITE SYSTEMS SUITABLE FOR ADVANCED HEAT ENGINE COMPONENTS
- IDENTIFY MODELS FOR THE FAST FRACTURE ANALYSIS OF CERAMIC MATRIX COMPOSITE LAMINATES
- INCORPORATE THOSE MODELS INTO A POSTPROCESSOR FOR GENERAL PURPOSE FINITE ELEMENT PROGRAMS SUCH AS MSC/NASTRAN

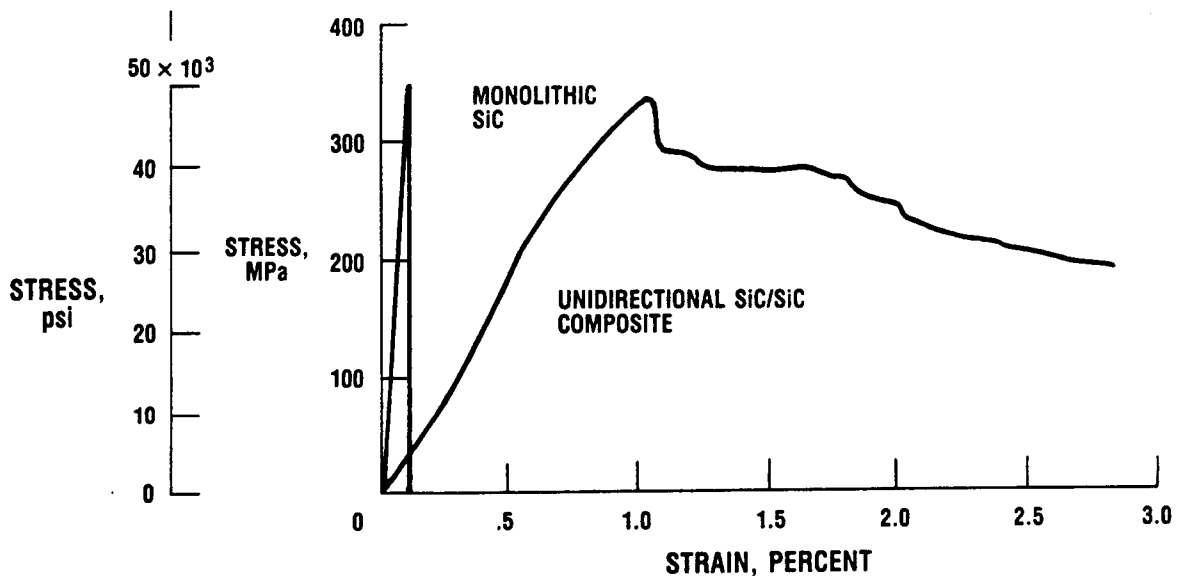
ADVANTAGES OF CERAMIC MATRIX COMPOSITES

Strong ceramic fibers have been added to reinforce low strength, typically glass-ceramic matrices, such as SiC/LAS, to achieve improved strength as in polymer matrix composites. These composites will not satisfy the high-temperature requirements of the applications we are interested in, but they may have other applications. The ceramic matrices attractive for advanced heat engine applications, such as SiC and Si₃N₄, already have adequate strength at elevated temperatures. Unfortunately, monolithic ceramics also have a low fracture toughness and fail catastrophically because of overload, impact, and contact stresses. Continuing improvements are being made in monolithic ceramics, and further reduction in critical flaw size could result in stronger ceramics. But in the past this has only resulted in increased strength without any appreciable increase in fracture toughness, and at a steadily increasing cost. Whisker reinforced composites provide improved fracture toughness and increased tolerance to flaws but still fail in a brittle manner. Continuous-fiber reinforced composites also have improved fracture toughness and increased tolerance to flaws but, in contrast to whisker reinforced composites, fail gracefully and are the answer to improved reliability.

- THERE ARE LIMITED FUTURE IMPROVEMENTS IN MONOLITHIC PROCESSING AND POWDERS. ECONOMIC CONSTRAINTS HAVE BEEN REACHED ON IMPURITIES, DENSITIES, AND FLAW SIZES
- MONOLITHIC TOUGHNESS REMAINS VERY LOW. MONOLITHIC CERAMICS ARE INTRINSICALLY FLAW INTOLERANT AND FAIL CATASTROPHICALLY BECAUSE OF OVERLOAD, IMPACT, AND CONTACT STRESSES
- WHISKER REINFORCED COMPOSITES PROVIDE IMPROVED TOUGHNESS AND INCREASED FLAW TOLERANCE BUT REMAIN BRITTLE
- CONTINUOUS FIBER REINFORCED COMPOSITES PROVIDE INCREASED FLAW TOLERANCE, IMPROVED TOUGHNESS, AND GRACEFUL FAILURE—ANSWER TO IMPROVED RELIABILITY

GRACEFUL FAILURE OF SiC/SiC

A typical stress-strain curve (Caputo et al., 1985) for a SiC/SiC composite at room temperature demonstrates graceful failure. This specimen contained 58 vol % SiC fibers. The maximum flexural strength of 330 MPa was achieved at a strain of 1.05 percent in a four-point flexure test. More significant, however, was the achievement of graceful failure. Unlike the monolithic SiC, which failed catastrophically at a very low strain, the unidirectional SiC/SiC composite is strain tolerant and sustained load after matrix crack initiation. At a strain of 2.8 percent, the specimen maintained a stress of 188 MPa - 57 percent of its maximum strength. This gradual loss of strength as strain increases, in contrast to the catastrophic failure of monolithic ceramics, makes the use of advanced ceramic matrix composites attractive in heat engine applications where catastrophic failure is unacceptable.

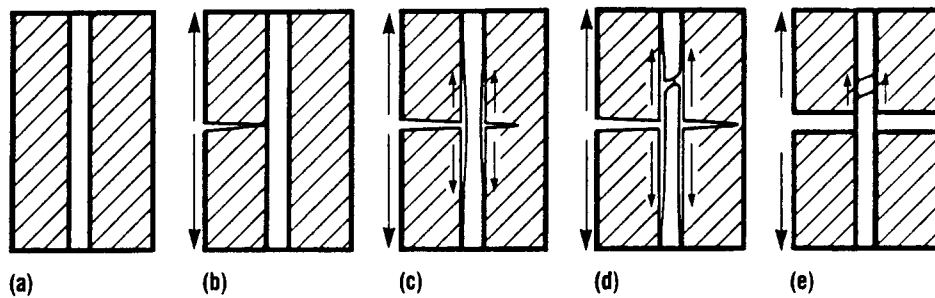


*ADAPTED FROM CAPUTO ET AL. (1984)

CD-88-33072

TOUGHENING MECHANISMS IN CERAMIC MATRIX COMPOSITES

The toughening mechanisms (Harris, 1986) in ceramic matrix composites are described by considering an isolated fiber. A crack initiates in the matrix (fig. (b)) and starts to propagate normal to the load. The higher stiffness and strength of the fiber inhibits further extension of the crack when it reaches the fiber. As the load is increased (fig. (c)), local stress concentrations and Poisson contractions cause the fiber to debond from the matrix, provided the interfacial bond strength is weak enough. Outwater and Murphy (1970) gave an upper limit to the energy of debonding W_{db} . After debonding, the crack will open further as the load is increased. The term W_{fr} is an estimate of the work against frictional resistance as the fiber moves relative to the matrix. Upon further loading of the composite (fig. (e)), the fiber will break at some weak point. As the broken fibers are pulled out against the frictional resistance, they contribute to the work of pullout W_p .



$$W_{db} = \frac{N \pi d_f^2 \sigma_f^2 y}{8 E_f}$$

$$W_{fr} = \frac{N \tau_f \pi d_f y^2 \epsilon_f}{2}$$

$$W_p = \frac{N \tau_f \pi d_f \ell_{cr}}{12}$$

*ADAPTED FROM HARRIS (1986)

CD-86-33073

TOUGHNESS VERSUS STRENGTH

Aveston et al. (1971) showed that first matrix cracking for a brittle matrix composite will occur not at the nominal failure strain of the matrix but at an enhanced matrix cracking strain. According to their analysis, the strength of a brittle matrix composite is enhanced by a small fiber radius, a strong fiber-matrix interfacial shear strength, and a high matrix fracture surface energy. Conversely, fiber pullout increases fracture toughness. Cottrell (1964) and Kelly (1970) show that the pullout work of fracture is increased by a weak interfacial frictional shear stress, a large fiber diameter, and a large fiber failure strain. Toughness is gained at the expense of strength since large fiber diameter contributes to increased toughness but results in decreased strength. A similar relation holds for interfacial properties. Thus, optimal fiber diameters and interfacial properties exist for the desired combination of strength and toughness.

- AVESTON, COOPER, AND KELLY (1971)—THEORY FOR ENHANCED MATRIX CRACKING

$$\epsilon_{mu} = \left(\frac{12\tau\gamma_mE_fV_f^2}{E_cE_m^2r_fV_m} \right)^{1/3}$$

- COTTRELL (1964) AND KELLY (1970)—PULLOUT WORK OF FRACTURE

$$\gamma_{fp} = \frac{\ell_{cr}}{\ell} \left(\frac{V_f^2 \sigma_{fu} r_f}{12\tau_f} \right)$$

- CONCLUSION: FACTORS INCREASING TOUGHNESS MAY DECREASE STRENGTH

DESIRED FEATURES FOR ADVANCED CERAMIC MATRIX COMPOSITES

Ceramic matrix composites fracture by the low-strain propagation of cracks in the brittle matrix (DiCarlo, 1985). High composite fracture strain is achieved by a high volume fraction of fibers bridging the matrix cracks. The bridging fibers reduce crack openings under loading, requiring greater applied strains for matrix crack propagation than those needed in the unreinforced matrix. If the fiber-matrix interfacial bond is strong, the stress concentration on fibers at the crack tip generally will be high enough to fracture the fiber, resulting in a brittle composite fracture. However, if the interfacial bond is weak and the strength of the fibers is high enough to support the applied load, the matrix cracks will propagate around the fibers and not through them. The composite will not fracture catastrophically but will have a series of evenly spaced matrix cracks bridged by reinforcing fibers. Thus, ceramic matrix composites should contain a high volume fraction of fibers that are continuous, are stiffer than the matrix, and possess a small diameter. The high volume fraction and small diameter ensure that a sufficient number of fibers bridge the matrix crack to prevent crack propagation until higher strain levels are reached. The matrix and fibers should also be oxidation resistant to retain their strength at high temperatures. Compatible fiber and matrix thermal expansion coefficients prevent the formation of residual stresses that enhance matrix cracking.

- FIBER SPACING SMALLER THAN CONTROLLING FLAWS IN MATRIX—TYPICALLY LESS THAN 100 μm
- FIBER DIAMETER MUCH SMALLER THAN MATRIX FLAW—TYPICALLY LESS THAN 20 μm
- FIBER YOUNG'S MODULUS GREATER THAN MATRIX YOUNG'S MODULUS FOR GREATER COMPOSITE STRENGTH
- OPTIMUM INTERFACIAL BONDING FOR TOUGHNESS AND STRENGTH
- DENSE, HIGH STRENGTH, HIGH TOUGHNESS, OXIDATION RESISTANT, REFRACTORY MATRIX
- COMPATIBLE FIBER AND MATRIX THERMAL EXPANSION COEFFICIENTS

MATRICES OF CURRENT INTEREST

A requirement of any composite system is compatibility of the matrix and fiber with each other and the environment. Fiber and matrix compatibility must result in optimal interfacial properties, but degradation by reaction or inter-diffusion must be avoided. To achieve a compromise, it may be necessary to coat the fibers to restrict interaction. Matrix materials include sintered powders, organometallic precursors, and materials deposited from the vapor phase (Phillips, 1983). The use of glass-ceramic matrices presents several advantages. The hot-pressing of viscous glass minimizes fiber damage which may occur with crystalline ceramics. The main disadvantage of glass-ceramics is that their temperature is limited compared to other ceramics. Silicon carbide and silicon nitride are regarded as the high-temperature materials of choice for most applications, but alumina and other oxides are also highly refractory. Fabrication from powders has the advantage of using materials which are inexpensive and available, but the formation of matrix agglomerates, inadequate infiltration of the reinforcement, and damage to the fibers by abrasion is a problem. Organometallic precursors can be used for oxide and non-oxide matrices and fiber coatings. A major advantage of this method is that damage to the fibers is less likely since the precursors used are in a fluid state, but densification is difficult to achieve.

	TENSILE MODULUS, GPa	TENSILE STRENGTH, MPa	DENSITY, g/cm ³
BOROSILICATE GLASS	60	100	2.3
LAS	100	100-150	2.0
Si ₃ N ₄	310	410	3.2
Al ₂ O ₃	360-400	250-300	3.9-4.0
SiC	400-440	310	3.2

CD-88-33076

FIBERS OF CURRENT INTEREST

Extensive research is being done in developing high-strength, oxidation resistant, thermally stable small-diameter fibers. As mentioned, fiber-matrix compatibility is critical in composite behavior. A weak fiber-matrix interface causes noncatastrophic failure; whereas a strong interface causes catastrophic failure. The fiber Nicalon, derived from a polymer precursor, is a β -SiC fiber containing excess carbon that forms a weak carbon-rich interface with many matrices (Mah et al., 1987). Nicalon, however, has limited thermal stability and loses significant strength above 1000 °C. The fiber-matrix strength increases, possibly because of oxidation of the fibers, resulting in catastrophic failure of the composite. The AVCO monofilament fiber is produced by chemical vapor deposition of SiC onto a carbon fiber core. A carbon-rich layer is then applied to the fiber, which provides weak interfacial bonding and promotes debonding and fiber pullout. AVCO fibers also experience significant strength degradation. The AVCO fiber is a large diameter fiber. The oxide fibers, Nextel 312 and FP, chemically bond to many matrices causing the composites to fail catastrophically. Fiber coatings, however, may provide optimal interfacial characteristics. None of these fibers are thermally stable above 1200 °C, and work continues on developing new fibers. The Tyranno fiber is produced from a polymer and is similar to Nicalon except for the addition of Ti, which is said to retard grain growth and is expected to preserve high-temperature strength. Nextel 440 and 480 are similar to Nextel 312, except for the reduction in B₂O₃, which is also expected to improve high-temperature properties.

DESIGNATION	COMPOSITION, wt %	TENSILE STRENGTH, MPa	MODULUS, GPa	DENSITY, g/cm	DIAMETER, μm
NICALON	59 Si, 31 C, 10 O	2520-3290	182-210	2.55	10-20
SCS-6	SiC ON CARBON CORE	3920	406	3.0	143
NEXTEL 312	62 Al ₂ O ₃ , 14 B ₂ O ₃ , SiO ₂	1750	154	2.7	11
FP	> 99 α-Al ₂ O ₃	> 1400	385	3.9	20
TYRANNO	Si, Ti, C, O	> 2970	> 200	2.3-2.5	8-10
NEXTEL 440	70 Al ₂ O ₃ , 28 SiO ₂ , 2 B ₂ O ₃	2100	189	3.05	10-12
NEXTEL 480	70 Al ₂ O ₃ , 28 SiO ₂ , 2 B ₂ O ₃	2275	224	3.05	10-12

PHENOMENOLOGICAL FAILURE MODELS

There are five characteristic values of strength for a unidirectional composite: (1) longitudinal tensile strength, (2) longitudinal compressive strength, (3) transverse tensile strength, (4) transverse compressive strength, and (5) in-plane shear. The maximum stress theory states that failure will occur in a lamina if any of the stresses in the principal material axes exceeds the corresponding allowable stress as determined from simple unidirectional stress tests (Nahas, 1986). Failure will occur in the maximum strain theory if any of the strains in the principal axes exceeds the corresponding allowable strain. The maximum strain theory is similar to the maximum stress theory and allowable strains can be directly related to the allowable strengths. Predictions of the two theories are quite close to each other. The differences are due to the Poisson ratio. The Tsai-Hill criteria (Azzi and Tsai, 1985) provides a single function to predict failure and takes into consideration the interaction between strengths. The Tsai-Hill criterion remains applicable for materials with properties different in tension and compression. Tsai and Wu (1971) have proposed a tensor polynomial failure criteria. Wu (1974) has shown the previous criteria are limit cases of this theory. A failure surface in stress space exists where F_i and F_{ij} are second- and fourth-order strength tensors. The noninteraction F terms are related to the engineering strengths. The interaction F terms are determined from biaxial tests and are constrained by the inequality $F_{ii}F_{jj} - F_{ij}^2 > 0$. According to Burk (1983), the maximum stress, maximum strain, Tsai-Hill, and Tsai-Wu failure criteria are the most widely used in industry. These failure criteria, however, are deterministic and do not describe the failure mechanisms. They also do not consider the scatter in ceramic composite strengths and are simply fail/no-fail criteria.

• MAXIMUM STRESS

$$\sigma_1 = \sigma_{1u} \quad \sigma_2 = \sigma_{2u} \quad \tau_{12} = \tau_{12u}$$

• MAXIMUM STRAIN

$$\epsilon_1 = \epsilon_{1u} \quad \epsilon_2 = \epsilon_{2u} \quad \gamma_{12} = \gamma_{12u}$$

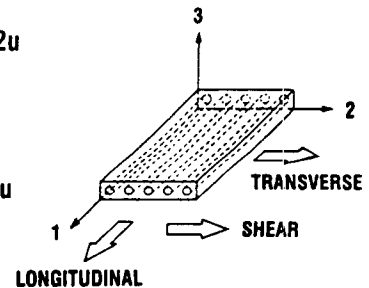
• TSAI-HILL

$$\frac{1}{\sigma_{1u}^2} \sigma_1^2 - \left(\frac{1}{\sigma_{1u}^2} + \frac{1}{\sigma_{2u}^2} - \frac{1}{\sigma_{3u}^2} \right) \sigma_1 \sigma_2 + \frac{1}{\sigma_{2u}^2} \sigma_2^2 + \frac{1}{\gamma_{12}^2} \tau_{12}^2 = 1$$

• TSAI-WU

$$F(\sigma) = F_i \sigma_i + F_{ij} \sigma_i \sigma_j = 1$$

*NAHAS (1986)

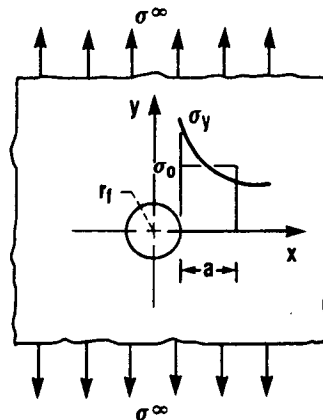


SEMI-EMPIRICAL FAILURE MODELS

Two stress criteria for predicting the tensile strength of notched composite laminates have been proposed by Whitney and Nuismer (1974). The point stress criteria and the average stress criteria assume that fracture occurs when the stress at some characteristic distance away from the discontinuity reaches the unnotched strength. The Whitney-Nuismer failure criteria were motivated by the hole size effect in which larger holes cause greater strength reduction than do smaller holes (Awerbuch and Madhukar, 1985). Although the stress concentration factor is independent of hole size, the normal stress σ_y is concentrated near the hole boundary for a smaller hole. It has been suggested that a larger area is subjected to high stress for a larger hole and, thus, has a higher probability of encountering inherent flaws, resulting in a lower strength. The point stress criteria assumes that failure occurs when the stress σ_y at a distance b away from the discontinuity is equal to the strength of the unnotched laminate. The average stress criteria assumes that failure occurs when the average stress σ_y over some distance a equals the unnotched laminate strength. Interest in the models is based on the assumption that the characteristic distance, b or a , is a material property of a particular laminate design. Experimental evidence suggests this may be true for epoxy systems. The applicability of these models to CMC is not known. Similar models have been proposed by Waddoups et al. (1971), Poe and Sova (1980), and Mar and Lin (1977).

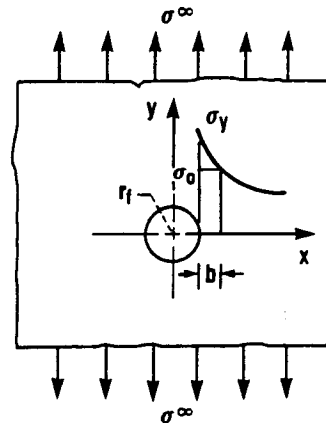
• WHITNEY-NUISMER MODELS

AVERAGE STRESS CRITERION



$$\sigma_0 = \frac{1}{a} \int_{r_f}^{r_f+a} \sigma_y(x,0) dx$$

POINT STRESS CRITERION



$$\sigma_0 = \sigma_y(x,0) \big|_{x=r_f+b}$$

*AWERBUCH AND MADHUKAR (1985)

CD-88-33079

SHEAR LAG FAILURE MODELS

Shear lag failure models examine failure modes at the micromechanics level of ceramic matrix composites. Cox (1952) introduced shear lag models and Hedgepeth (1961) applied them to filamentary structures. Hedgepeth's model considered filaments separated by a constant distance. The displacement of the n th filament is given by $u_n(x,t)$ and the force in the n th filament is given by $P_n(x,t)$. The fibers carry all the tensile load while the matrix carries only shear. Equilibrium of an element of the n th filament results in the partial differential difference equations shown. By applying the appropriate boundary conditions, we can solve the equations for the stress concentrations in the filamentary structure. Eringen and Kim (1974) generalized the model to include transverse loads in the matrix. Neither of these models can accurately describe ceramic matrix composites because they neglect the tensile load carrying capability of the matrix, but further generalizations may make these models applicable. Once such models are available they may be used to consider failure mechanisms, such as longitudinal yielding and matrix splitting, as did Goree and Gross (1979). They generalized Hedgepeth's model to include longitudinal yielding and matrix splitting and arrived at three partial differential difference equations to describe the stresses and displacements in a unidirectional-fiber-reinforced composite.

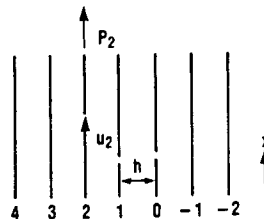
• **HEDGEPETH (1961)**
FORCE IN n th FILAMENT

$$P_n = EA_f \frac{\partial U_n}{\partial x}$$

$$EA_f \frac{\partial^2 U_n}{\partial x^2} + \frac{G}{h} (U_{n+1} - 2U_n + U_{n-1}) = m \frac{\partial^2 U_n}{\partial t^2}$$

SHEAR FORCE

$$\frac{G(U_{n+1} - U_n)}{h}$$



• **ERINGEN AND KIM (1974)**

$$\frac{E_m}{h} (U_{n+1} - 2U_n + U_{n-1}) + \frac{G_m}{2} \left[\frac{1}{2} \frac{d^2}{dy^2} (U_{n+1} + 2U_n + U_{n-1}) + \frac{1}{h} \frac{d}{dy} (v_{n+1} - v_{n-1}) \right] = 0$$

$$GE_f \frac{d^2 v_n}{dy^2} + G_m \left[\frac{1}{2} \frac{d}{dy} (U_{n+1} - U_{n-1}) + \frac{1}{h} (v_{n+1} - 2v_n + v_{n-1}) \right] = 0$$

CD-86-33080

• **GOREE AND GROSS (1979)**
ALL FIBERS EXCEPT n AND $n + 1$

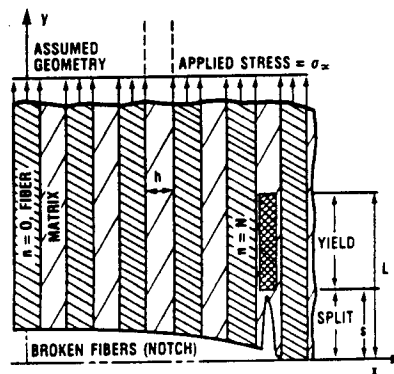
$$\frac{E_f A_f h}{G_m l} \left(\frac{d^2 U_n}{dy^2} \right) + U_{n+1} - 2U_n + U_{n-1} = 0$$

FIBER n

$$\frac{E_f A_f h}{G_m l} \left(\frac{d^2 U_n}{dy^2} \right) + U_{n+1} - U_n - \frac{h}{G_m} \tau (y - s) = 0$$

FIBER $n + 1$

$$\frac{E_f A_f h}{G_m l} \left(\frac{d^2 U_{n+1}}{dy^2} \right) + U_{n+2} - U_{n+1} + \frac{h}{G_m} \tau (y - s) = 0$$



CD-86-33081

FRACTURE MECHANICS MODELS

The first matrix crack marks the beginning of permanent damage and permits oxidation of the fibers through loss of protection by the matrix. As we have seen, Aveston et al. (1971) have shown that first matrix cracking occurs in a ceramic matrix composite at a higher strain than it does for the monolithic ceramic. For a crack to form, the stress in the matrix must be equal to its breaking stress. In addition, the energy condition shown by the inequality below must be satisfied. The inequality consists of energy terms for various failure mechanisms under tensile loads. The fracture surface work in forming a matrix crack is γ_m . The work in breaking the fiber-matrix bond, given by Outwater and Murphy (1969), is γ_{db} . Work as the matrix slides over the fibers against a frictional force is U_{fr} . The decrease in the elastic strain energy in the matrix as the matrix cracks is given by ΔU_m . Conversely, the elastic strain energy in the fibers increases and is given by ΔU_f . Finally, the work done by the applied stresses is ΔW . Substituting these terms into the inequality and assuming a frictional bond between the fiber and matrix yields the formula for the enhanced matrix cracking strain.

• AVESTON, COOPER, AND KELLY (1971) A CRACK WILL FORM PROVIDED

$$2\gamma_m V_m + \gamma_{db} + U_{fr} + \Delta U_f \leq \Delta W + \Delta U_m \quad c = \frac{E_m V_m}{E_f V_f}$$

$$\text{WORK OF APPLIED STRESS} \quad \Delta W = \frac{E_f E_m V_m}{2\tau} \epsilon_{mu}^3 c r_f (1 + c)$$

$$\text{REDUCTION IN MATRIX STRAIN ENERGY} \quad \Delta U_m = \frac{E_f E_m V_m}{3\tau} \epsilon_{mu}^3 c r_f$$

$$\text{INCREASE IN FIBER STRAIN ENERGY} \quad \Delta U_f = \frac{E_f E_m V_m}{2\tau} \epsilon_{mu}^3 c r_f \left(1 + \frac{c}{3}\right)$$

$$\text{WORK OF FRICTION} \quad \Delta U_{fr} = \frac{E_f E_m V_m}{6\tau} \epsilon_{mu}^3 c r_f (1 + c)$$

$$\text{WORK OF DEBONDING} \quad \gamma_{db} = \frac{2\sigma_{mu} V_m G_{II}}{\tau_0}$$

FOR A PURELY FRICTIONAL FIBER-MATRIX BOND, $G_{II} = 0$

$$\text{ENHANCED MATRIX CRACKING STRAIN} \quad \epsilon_{mu} = \left(\frac{12\tau \gamma_m E_f V_f^2}{E_c E_m^2 r_f V_m} \right)^{1/3}$$

CD-88-33082

FRACTURE MECHANICS MODELS CONTINUED

Aveston et al. (1971) looked at the energy states in a crack before and after crack propagation. Budiansky et al. (1986) assumed that if a crack engulfs more than a few fibers the applied stress necessary for propagation is constant and steady state cracking occurs. The assumption of steady state cracking implies that the stresses at the crack front remain unchanged during crack growth and also that the upstream and downstream states, far ahead of and behind the crack, do not change. Equation (1) governs matrix cracking for the fiber slip and no-slip cases. A shear lag analysis is used to determine the upstream and downstream stresses. The matrix cracking stress predicted is essentially the same as that of predicted by Aveston et al. (1971) except for the initial stress term σ'_m . Another model for steady state cracking was proposed by Marshall et al. (1985). The analysis is of unbonded unidirectional lamina in which the sliding of the matrix over fibers is resisted only by frictional forces. The energy solution is derived from the earlier analysis by Aveston et al. (1971) but is expressed in terms of incremental crack extension. For an incremental crack extension work dU is done against frictional forces, the strain energy in the matrix decreases by dU_m , the strain energy in the fibers increases by dU_f , and the potential energy of the loading system decreases by dU_1 . Again, the predicted first cracking stress agrees with the results of Aveston et al. (1971).

• BUDIANSKY, HUTCHINSON, AND EVANS (1986)

$$(1) \frac{1}{2A_c} \int_{-L}^L \int_{A_c} (\sigma^u - \sigma^d) : (\epsilon^u - \epsilon^d) dA_1 dz = V_m G_m$$

$$(2) \frac{1}{2} \int_{-\infty}^{\infty} \left[\frac{V_f}{E_f} (\sigma_f^u - \sigma_f^d)^2 + \frac{V_m}{E_m} (\sigma_m^u - \sigma_m^d)^2 \right] dz + \frac{1}{2\pi r^2 G} \int_{-\infty}^{\infty} \int_a^F (\tau_{rz}^d) 2\pi r_1 dr_1 dz = V_m G_m$$

$$(3) \frac{\sigma_{cr}}{E_c} + \frac{\sigma'_m}{E_m} = \frac{\sigma_1}{E} \quad \sigma = \left(\frac{6V_f^2 E_f \tau_{fr}}{V_m E_m E} \right)^{1/3} \left(\frac{G_m}{a E_m} \right)^{1/3}$$

WHERE σ'_m IS INITIAL MATRIX STRESS

CD-86-33083

• MARSHALL, COX, AND EVANS (1985)

$$dU = 2\gamma_m V_m dc + dU_{fr} + dU_f - dU_m - dU_1$$

$$dU_{fr} = \left[\frac{\sigma_{\infty}^3 l_1}{6\tau E_f V_f^2 (1+c)^2} \right] dc$$

$$dU_m = \left[\frac{\sigma_{\infty}^3 l_1 c}{3\tau E_f V_f (1+c)^3} \right] dc$$

$$dU_f = \left[\frac{\sigma_{\infty}^3 l_1 (3c+1)}{6\tau E_f V_f^2 (1+c)^3} \right] dc$$

$$dU_1 = \left[\frac{\sigma_{\infty}^3 l_1}{2\tau E_f V_f^2 (1+c)^2} \right] dc$$

WHERE

$$\sigma_{\infty} = \left[\frac{6(1-\nu^2) K_{cr}^2 \tau E_f V_f^2 V_m (1+c)^2}{E_m l} \right]^{1/3}$$

AND

$$c = \frac{E_f V_f}{E_m V_m}$$

CD-86-33084

STATISTICAL MODELS

The previous models have ignored the statistical aspects of failure. Average strengths have been employed resulting in fail/no-fail decisions. The models considered here are weakest-link models where the failure of an element of the volume results in the failure of the volume. The principle of independent action considers the stress components to act separately in producing failure. The Weibull shape parameter is β , the Weibull scale parameter is α , and σ is the stress component in the principal material coordinate system. The parameters α and β are obtained from uniaxial strength tests. In not allowing the stresses to interact, the principle of independent action should give nonconservative results. Wetherhold and Pipes (1984) allow for interaction of stresses by incorporating the maximum distortional energy failure function into the probability of failure function. The probability density functions for the strengths X_1 , X_2 , and X (the strengths in the principal material directions) are substituted into the maximum distortional energy failure function. The reliability then is the probability that K is less than one. The resulting integral is analytically intractable. A Monte Carlo simulation is used to evaluate the reliability. Other models have been proposed by Batdorf (1982) and Harlow and Phoenix (1978). Macroscopic models were used in these failure criteria and the micromechanics of failure were not considered. The linking of micromechanics models and macromechanics models could result in better probabilistic models.

• PRINCIPLE OF INDEPENDENT ACTION

$$R = \exp \left\{ - \int_V \left[\left(\frac{\sigma_1}{\beta_1} \right)^{\alpha_1} + \left(\frac{\sigma_2}{\beta_2} \right)^{\alpha_2} + \left(\frac{\sigma_3}{\beta_3} \right)^{\alpha_3} \right] dv \right\}$$

• WETHERHOLD AND PIPES (1984)

$$K = \left(\frac{\sigma_1}{X_1} \right)^2 - \left(\frac{\sigma_1 \sigma_2}{X_1^2} \right) + \left(\frac{\sigma_2}{X_2} \right)^2 + \left(\frac{\sigma_3}{X_3} \right)^2$$

WHERE $K < 1$ = NO FAILURE AND $R = P\{K < 1\}$

$$R = \int_0^{i(1)} \int_0^{h(1,X_3)} \int_0^{g(1,X_2,X_3)} F_{X_1}(X_1) F_{X_2}(X_2) F_{X_3}(X_3) dX_1 dX_2 dX_3$$

WHERE F_{X_1} , F_{X_2} , F_{X_3} = PROBABILITY DENSITY FUNCTIONS FOR X_1 , X_2 , AND X_3

AND

$$i(1) = \frac{\sigma_3}{1} \quad h(1,X_3) = \sqrt{\frac{\sigma_2^2}{1^2 - (\sigma_3/X_3)^2}} \quad g(1,X_2,X_3) = \sqrt{\frac{\sigma_1^2 - \sigma_1 \sigma_2}{1^2 - (\sigma_2/X_2)^2 - (\sigma_3/X_3)^2}}$$

CD-88-33085

SUMMARY AND CONCLUSIONS

Monolithic ceramics have high strength at high temperatures but are very sensitive to flaws. Whisker composites have increased flaw tolerance but still fail in a brittle manner. Ceramic matrix composites have improved fracture toughness and fail noncatastrophically. In ceramic matrix composites, fibers are added to a matrix to improve fracture toughness; whereas in polymer matrix composites, a strong fiber is added to a weak matrix to improve strength. Consequently, designing with ceramic matrix composites is different from designing with polymer matrix composites, and different design criteria are needed. The four most commonly used failure criteria in industry - maximum stress, maximum strain, Tsai-Hill, and Tsai-Wu - do not consider the scatter in ceramic matrix composite strengths but describe phenomenologically the failure mechanisms. Shear lag models describe failure mechanisms at a micromechanics level but are currently not capable of describing ceramic matrix composites. Semi-empirical models fit equations to existing data and are applicable only to tensile loaded composites. Statistical models, such as Wetherhold, consider the scatter in ceramic composite strength but do not model failure mechanisms and are difficult to use. A survey of these failure models will be published later. Future work will involve selectively incorporating portions of these models into a postprocessor for reliability analysis.

- CERAMIC MATRIX COMPOSITES PROVIDE THE MEANS TO ACHIEVE IMPROVED FRACTURE TOUGHNESS AND GRACEFUL FAILURE WHILE RETAINING OTHER DESIRABLE PROPERTIES SUCH AS HIGH-TEMPERATURE STRENGTH AND LOW DENSITY.
- DESIRED FEATURES FOR ADVANCED CERAMIC MATRIX COMPOSITES ARE DIFFERENT FROM THOSE FOR POLYMER MATRIX COMPOSITES.
- VARIOUS FAILURE MODELS FOR MONOTONICALLY LOADED CERAMIC MATRIX COMPOSITES WERE REVIEWED.
- FUTURE WORK WILL INVOLVE SELECTIVELY INCORPORATING THESE MODELS INTO A POSTPROCESSOR FOR RELIABILITY ANALYSIS.

APPENDIX - SYMBOLS

A	area
a	characteristic material distance
b	characteristic material distance
d	diameter
E	Young's modulus
F	strength tensor
G	matrix shear modulus
G_m	critical mode I matrix energy release ratio
G_{II}	debonding energy of fiber matrix interface
g	thickness of filament
h	distance between filaments
K	stress intensity factor
L	composite length
l	fiber load transfer length
m	mass
N	number of fibers bridging crack
P	force
R	reliability
r	radius
s	length of matrix split
t	thickness, time
U	energy
u	displacement of filament
V	volume fraction
v	displacement of matrix
W	work

x, y, z axes

y mean debond length

α Weibull scale parameter

β Weibull shape parameter

γ work of fracture

ϵ strain

ν Poisson's ratio

σ stress

τ interfacial shear

Subscripts:

c composite

cr critical

db debonding

f fiber

fr frictional force

L potential energy

m matrix

n nth filament

o unnotched strength

p pullout

u ultimate strength

x, y, z axes

$1, 2, 3$ principal material axes

Superscripts:

d downstream

m matrix

u upstream

$'$ initial stress

REFERENCES

- Aveston, J., Cooper, G.A., and Kelly, A., 1971, "Single and Multiple Fracture," The Properties of Fiber Composites Conference Proceedings, National Physical Laboratory, pp. 15-26.
- Awerbuch, J., and Madhukar, M.S., 1985, "Notched Strength of Composite Laminates, Predictions and Experiments - A Review," J. Reinforced Plastics and Composites, Vol. 4, pp. 3-159.
- Azzi, A.D., and Tsai, S.W., 1965, "Anisotropic Strength of Composites," Experimental Mechanics, Vol. 5, pp. 283-288.
- Batdorf, S.B., 1982, "Tensile Strength of Unidirectionally Reinforced Composites," J. Reinforced Plastics and Composites, Vol. 1, No. 2., pp. 153-176.
- Budiansky, B., Hutchinson, J.W., and Evans, A.G., 1986, "Matrix Fracture in Fiber-Reinforced Ceramics," J. Mech. Phys. Solids, Vol. 34, pp. 167-189.
- Burk, R.C., 1983, "Standard Failure Criteria Needed for Advanced Composites," Astronautics and Aeronautics, Vol. 21, pp. 58-62.
- Caputo, A.J., Lackey, W.J., and Stinton, D.P., 1985, "Development of a New, Faster Process for the Fabrication of Ceramic Fiber-Reinforced Ceramic Composites by Chemical Vapor Infiltration," Ceram. Eng. Soc. Proc., Vol. 6, No. 7-8, pp. 694-706.
- Cottrell, A.H., 1964, "Strong Solids," Proc. R. Soc. London A, Vol. 282, pp. 2-5.
- Cox, H.L., 1952, "The Elasticity and Strength of Paper and other Fibrous Materials," British J. Appl. Phys., Vol. 3, pp. 72-79.
- DiCarlo, J.A., 1985, "Fibers for Structurally Reliable Metal and Ceramic Composites," Journal of Metals, Vol. 37, pp. 44-49.
- Eringen, A.C., and Kim, B.S., 1974 "Stress Concentrations in Filamentary Composites with Broken Fibers," Letters in Applied and Engr. Sci., Vol. 2, pp. 69-89.
- Goree, J.G., and Gross, R.S., 1979, "Analysis of Unidirectional Composite Containing Broken Fibers and Matrix Damage," Eng. Frac. Mech., Vol. 13, pp. 563-578.
- Harlow, D.G., and Phoenix, S.L, 1978, "The Chain-of-Bundles Probability Model for the Strength of Fibrous Materials." J. Composite Materials, Vol. 12, pp. 195-215.
- Harris, B., 1986, Engineering Composite Materials, The Institute of Metals, Brookfield, Vermont.

- Hedgepeth, J.M., 1961, "Stress Concentrations for Filamentary Structures," NASA TN D-882.
- Kelly, A., 1970, "Interface Effects and the Work of Fracture of a Fibrous Composite," Proc. R. Soc. London A, Vol. 319, pp. 95-116.
- Mah, T. et al, 1987, "Recent Developments in Fiber-Reinforced High Temperature Ceramic Composites," Am. Ceram. Soc. Bull., Vol. 66, No. 2, pp. 304-308.
- Mar, J.W., and Lin, K.Y., 1977, "Fracture Mechanics Correlation for Tensile Failure of Filamentary Composites with Holes," J. Aircraft, Vol. 14, pp. 703-704.
- Marshall, D.B., Cox, B.N., and Evans, A.G., 1985, "The Mechanics of Matrix Cracking in Brittle-Matrix Fiber Composites," Acta Metall., Vol. 33, pp. 2013-2121.
- Nahas, M.N., 1986, "Survey of Failure and Post-Failure Theories of Laminated Fiber-Reinforced Composites," J. Composites Technol. and Res., Vol. 8, No. 4, pp. 138-153.
- Outwater, J.O., and Murphy, M.C., 1969, Proceedings of the 24th SPI/RP Conference, Society of Plastics Industry, New York.
- Phillips, D.C., 1983, Fabrication of Composites, North-Holland, Amsterdam, p. 373.
- Poe, C.C., Jr., and Sova, J.A., 1980, "Fracture Toughness of Boron Aluminum Laminates with Various Proportions of 0° and +45° Plies," NASA TP-1707.
- Tsai, S.W., and Wu, E.M., 1971, "A General Theory of Strength for Anisotropic Materials," J. Comp. Materials, Vol. 5, pp. 58-80.
- Waddoups, M.E., Eisenmann, J.R., and Kaminski, B.E., 1971, "Macroscopic Fracture Mechanics of Advanced Composite Materials," J. Comp. Materials, Vol. 5, pp. 446-454.
- Wetherhold, R.C., and Pipes, R.B., 1984, "Statistics of Fracture of Composite Materials under Multiaxial Loading," Materials Science and Engineering, Vol. 68, pp. 113-118.
- Whitney, J.M., and Nuismer, R.J., 1974, "Stress Fracture Criteria for Laminated Composites Containing Stress Concentrations," J. Comp. Materials, Vol. 8, pp. 253-265.
- Wu, E.E., 1974, "Phenomenological Anisotropic Failure Criterion," Composite Materials, Broutman, L.J. and Krock, R.H., Eds., Vol. 2, Academic Press, New York, pp. 353-431.

NONDESTRUCTIVE EVALUATION

SESSION OVERVIEW

Alex Vary
Structural Integrity Branch
Lewis Research Center

The usual emphasis in nondestructive evaluation (NDE) is on detection and characterization of a variety of discrete, hidden flaws that can impair structural integrity and reduce life (i.e., cracks in metals, delaminations in composites, inclusions in ceramics, etc.). In failure prevention schemes, the specification of flaw criticality and the prediction of safe life depend on the assumption of a realistic set of extrinsic properties. Fracture analysis models presuppose flaw development in materials with known moduli, ultimate strengths, fracture toughness, and fatigue and creep properties.

Emerging NDE techniques may be used to verify the mechanical properties mentioned above and to assess their degradation in service. Ultimately, these techniques may be adapted for application to a variety of materials and actual structural parts and help circumvent sole reliance on handbook or representative values based on previous screening or sampling tests. A holistic approach to reliability assurance would combine the nondestructive characterization of flaws with the characterization of the material environments in which the flaws reside (Ruud and Green, 1983; Buck and Wolf, 1981; Vary 1984). This approach would engender more realistic assessments of structural integrity and service degradation by providing a better information base for fracture analysis and life prediction. Development and adaptation of the types of techniques discussed are needed to assure structural reliability and safe service life of components made of advanced materials in systems that demand efficient performance under extreme operating conditions.

The need for nondestructive materials characterization is indicated where local properties are critical or where the presence, identity, and distribution of potentially critical flaws can only be assessed statistically. In the latter case, flaws can be so microscopic, numerous, and dispersed that it is impractical to resolve them individually. Large populations of nonresolvable flaws may interact with each other (e.g., surface with volume flaws) or with morphological anomalies. These interactions would be manifested as degraded bulk properties (e.g., deficiencies in strength, and toughness). While a structure may be free of discrete critical flaws, it may still be susceptible to failure because of inadequate or degraded intrinsic mechanical properties. This can arise from faulty material processing and/or aggressive service environments. For these reasons it is important to have nondestructive methods for quantitatively characterizing mechanical properties.

Ultimately, mechanical properties are controlled by composition, microstructure, and morphology. These factors also influence various NDE probe media

(ultrasonic waves, electric currents, magnetic fields, x rays). Modulations of probe media by materials give quantitative measurements that correlate to differing degrees with strength, hardness, toughness, and other properties (see examples in the following table, which is based on Vary and Klima, 1986).

The approach at Lewis Research Center is to develop what we term "analytical NDE" for characterizing materials factors that govern mechanical properties. Analytical NDE refers to an emerging body of technology dedicated to assessing flaw, damage, and degradation states in structural materials (Vary, 1987). This requires advances in signal transmission, acquisition, and analysis. Although analytical NDE is currently in its infancy, it is being employed in materials research. At Lewis the emphasis is on the use of analytical ultrasonic NDE for advanced materials such as metal and ceramic matrix composites, particulate- and whisker-toughened ceramics, and carbon-carbon composites. The objective is to generate know-how for use in flaw detection; in integrity, degradation, and damage assessment; and in fracture analysis on structures and components.

REFERENCES

- Buck, O., and Wolf, S.M., 1981, Nondestructive Evaluation - Microstructural Characterization and Reliability Strategies, The Metallurgical Society of America, Warrendale, Pennsylvania.
- Ruud, C.O., and Green, R.E., Jr., 1983, Nondestructive Methods for Materials Property Determination, Plenum Press, New York, New York.
- Vary, A., 1984, "Ultrasonic Nondestructive Evaluation, Microstructure, and Mechanical Property Interrelations," NASA TM-86876.
- Vary, A., 1987, Material Analysis by Ultrasonics - Metals, Ceramics, Composites, Noyes Data Corporation, Park Ridge, New Jersey.
- Vary, A., and Klima, S.J., 1986, "Nondestructive Techniques for Characterizing Mechanical Properties of Structural Materials - An Overview," NASA TM-87203.

Quantitative nondestructive evaluation techniques for indirect characterization of material strength

Principal techniques	Operational techniques	Directly measured quantities	Indirectly measured quantities
Dynamic excitation	Sonic vibration, eddy sonic	Natural frequencies, forced frequencies	Dynamic moduli, elastic constants, density, composite morphology, bond strength
	Forced flexure, torsion	Amplitude, energy dissipation	Damping capacity, density, texture, hardness, alloying effects, cold work
Ultrasonic, acoustic	Continuous wave, transmission, resonance	Phase/group velocities, dispersion, damping, resonance frequencies	Elastic constants, moduli, anelasticity, microstructure, grain/phase morphology, residual stress state/distribution
	Broadband pulse-echo, spectrum analysis	Rayleigh/phase/diffuse scatter, attenuation coefficients	Hardness, tensile/shear/yield strengths, fracture toughness, microstructure, texture, grain/phase size/morphology
	Mechanical scan imaging	Signal intensity, diffraction effects	Macro- and microstructural variations/anomalies, bond/weld integrity/strength
	Acoustic microscopy	Spatial frequency image, interference fringes	Elastic/anelastic microstructural variations, grain texture, porosity, stress
	Acoustic emission	Emission rate, amplitude distribution, spectrum	In situ metallurgical transformation, creep, fatigue damage, microcracking
Electromagnetic	Eddy current	Electrical conductivity, magnetic permeability	Polycrystalline grain/domain anisotropies, alloy composition, hardness, porosity
	Magnetic field	Coersive force, flux leakage/signature	Ferroalloying content/distribution, age/case hardening, stress fields
Penetrating and particle radiation	X, gamma, neutron radiography and radiation gauging	Absorption and scatter radiation/attenuation, backscatter	Macro- and microstructural variations/anomalies, density, porosity, grain texture, chemistry, moisture ingress, corrosive/chemical attack
	X-ray diffraction	Scatter goniometry	Residual stress state, lattice spacing
	Mössbauer method	Gamma-Doppler velocity	Subsurface gradients, corrosion products
	Positron annihilation	Annihilation event count	Fatigue microcracking, plastic deformation, grain-boundary voids, strain hardening
	Exoelectron emission	Emission current, photo-emission image	Fatigue damage, plastic strain/deformation
Photooptical	Neutron activation	Gamma spectrum analysis	Alloy/chemical content, impurities
	Induced strain laser holography	Interference fringe spatial frequency	Stress/strain condition, deformation, macro- and microstructural anomalies

ANALYTICAL NONDESTRUCTIVE EVALUATION (A-NDE)

- **ANALYTICAL NDE REFERS TO AN EMERGING BODY OF TECHNOLOGY DEDICATED TO ASSESSING FLAW, DAMAGE, AND DEGRADATION STATES IN STRUCTURAL MATERIALS**
- **THIS REQUIRES ADVANCEMENTS IN SIGNAL TRANSMISSION, ACQUISITION, AND ANALYSIS FOR NONDESTRUCTIVE INTERROGATION AND INTERPRETATION**
- **ANALYTICAL NDE IS BEING USED IN ADVANCED MATERIALS RESEARCH (WITH MAJOR EFFORTS IN ULTRASONIC AND RADIOGRAPHIC NDE)**
- **THE OBJECTIVE IS TO GENERATE NDE KNOW HOW FOR USE IN FLAW DETECTION, INTEGRITY, DEGRADATION, AND DAMAGE ASSESSMENT, AND FRACTURE ANALYSIS**

CD-88-32706

BENEFITS OF ANALYTICAL ULTRASONIC NDE

- **IMPROVED BASES FOR ASSESSMENT OF FLAW CRITICALITY, FRACTURE ANALYSIS, AND MECHANICAL MODELING**
- **ABILITY TO DEAL MORE EFFECTIVELY WITH ADVANCED MATERIALS SUCH AS METAL AND CERAMIC MATRIX COMPOSITES, TOUGHENED CERAMICS, AND CARBON-CARBON COMPOSITES**
- **ABILITY TO VERIFY AND CERTIFY MATERIAL QUALITY AND KEY MATERIAL PROPERTIES**

CD-88-32707

NONDESTRUCTIVE EVALUATION BY ACOUSTO-ULTRASONICS

Harold E. Kautz
Structural Integrity Branch
NASA Lewis Research Center

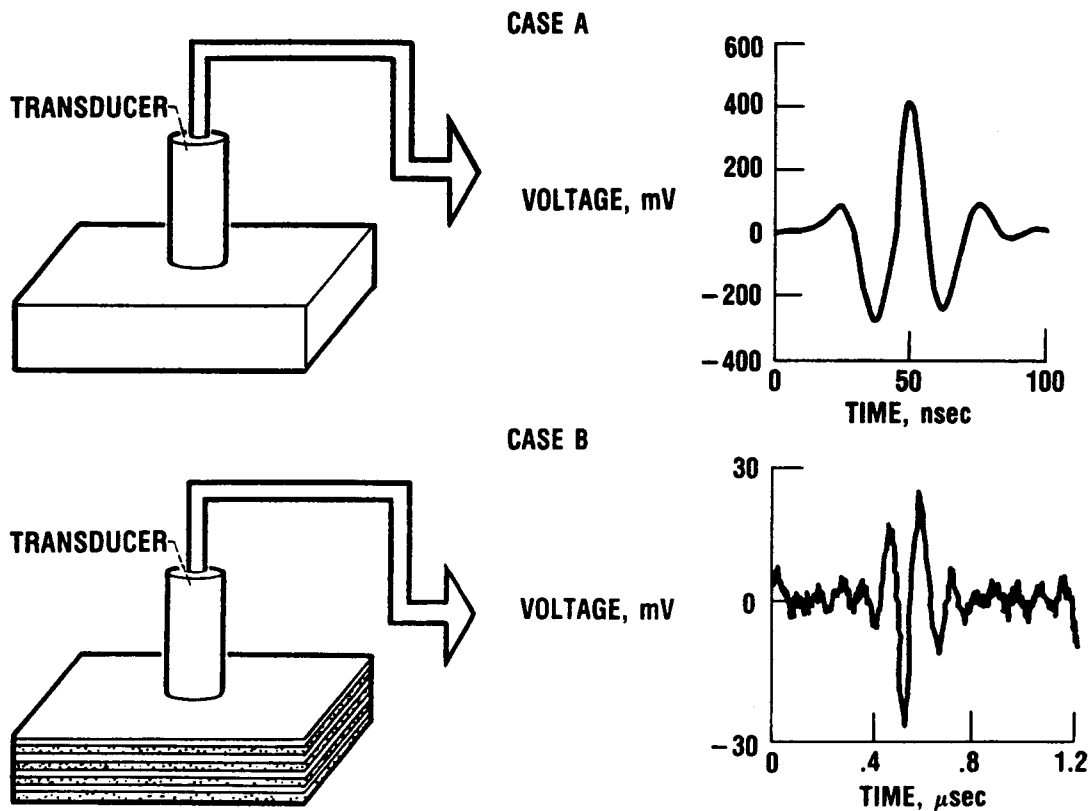
ABSTRACT

Acousto-ultrasonics is an ultrasonic technique that was originally devised to cope with the particular problems associated with nondestructive evaluation (NDE) of fiber/polymer composite structures. The fiber/polymer composites are more attenuating to ultrasound than any other material presently of interest. This limits the applicability of high-frequency ultrasonics. A common use of ultrasound is the imaging of flaws internal to a structure by scattering from the interface with the flaw. However, structural features of composites can scatter ultrasound internally, thus obscuring such flaws.

A somewhat unique need relative to composites is to be able to nondestructively measure the strength of laminar boundaries in order to assess the integrity of a structure. Acousto-ultrasonics has exhibited the ability to use the internal scattering to provide information for determining the strength of laminar boundaries. Analysis of acousto-ultrasonic signals by the wave ray paths that compose it leads to waveform partitioning that enhances the sensitivity to mechanical strength parameters.

PROBLEM: ULTRASONIC CHARACTERIZATION OF COMPOSITES

It is difficult to analyze ultrasonic signals recovered from composites by conventional methods. This is demonstrated below for "pulse-echo" ultrasonics (Hull et al., 1985). Case A shows an echo recovered from a metal specimen as used for precise velocity and attenuation determination. Case B is an echo from a laminated composite where considerable internal scattering has introduced ambiguity into the signal. These "noisy" signals can be difficult to interpret, necessitating a different approach. An approach referred to as acousto-ultrasonics is described next.



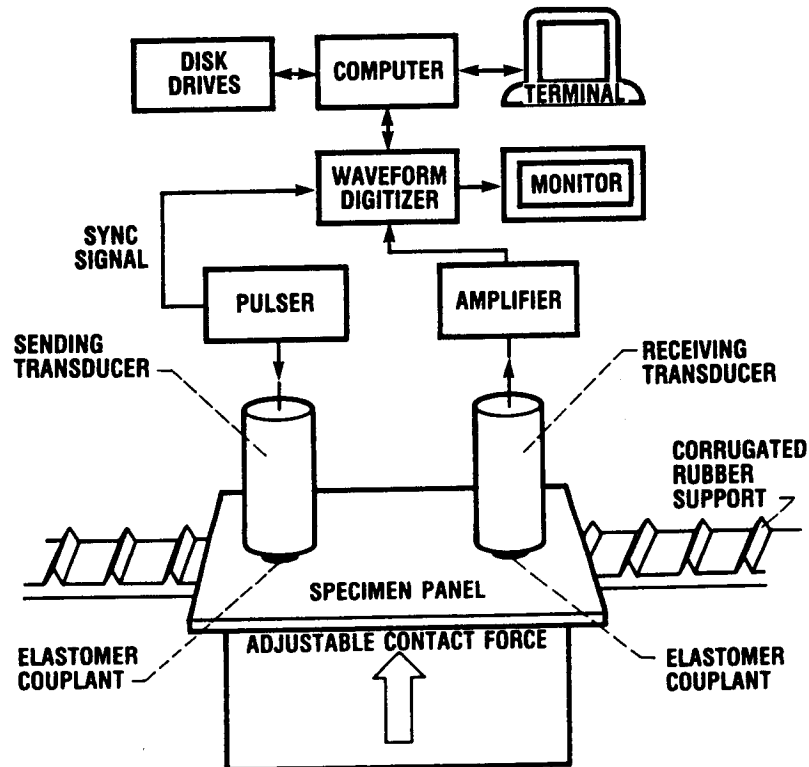
CD-88-32283

THE ACOUSTO-ULTRASONIC TECHNIQUE

Acousto-ultrasonics (A-U) employs two transducers:

- (1) A sender injects ultrasonic energy into the specimen.
- (2) A receiver detects the energy after interacting with the specimen.

Rather than avoiding the multiple reflections in a composite, A-U uses them to sense mechanical strength. A-U imitates the stress waves of acoustic emission with ultrasonics in place of mechanical stress. This is totally nondestructive (Vary and Bowles, 1979; Vary, 1979, 1982, 1987).



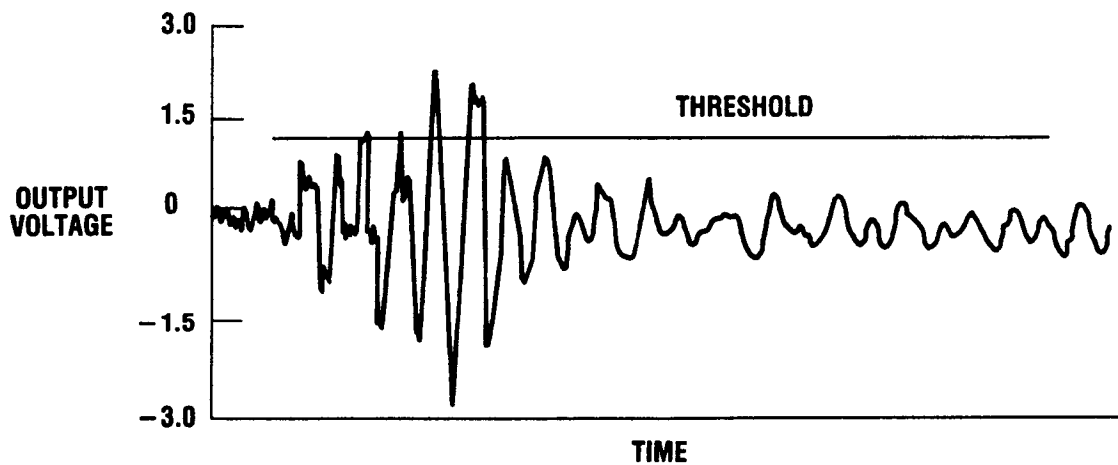
CD-88-32284

THE STRESS WAVE FACTOR

Acousto-ultrasonic signal strength is calculated as the stress wave factor (SWF). Two common measures of SWF are energy and ringdown count. Energy is measured by

$$SWF = \int_{t_1}^{t_2} V^2 dt$$

where V is receiver output voltage. Ringdown count measured by the number of voltage peaks above threshold is illustrated below.

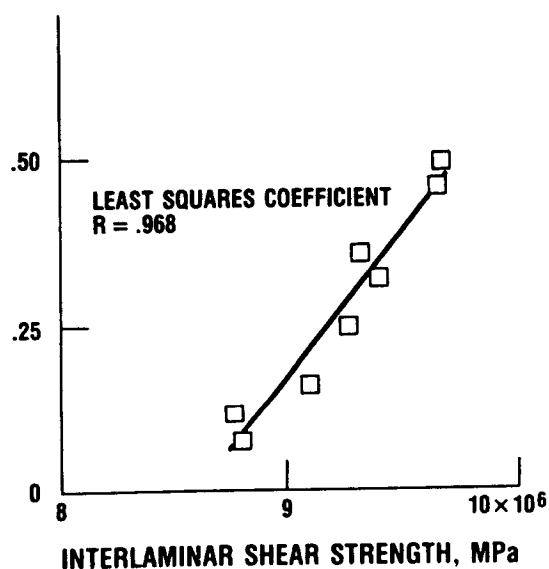
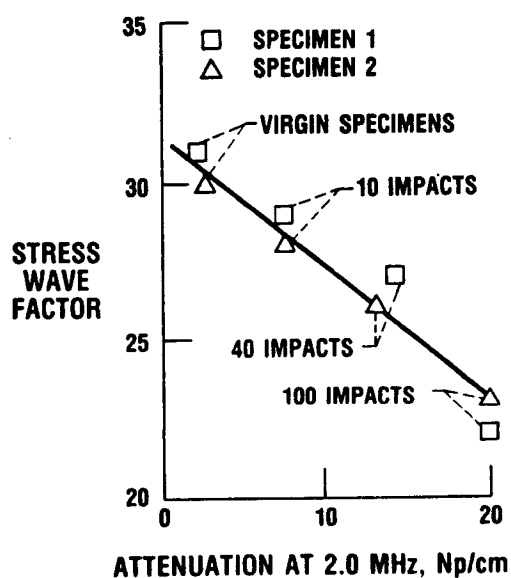


CD-88-32285

EARLY RESULTS WITH THE STRESS WAVE FACTOR AND GRAPHITE/POLYMER COMPOSITES

Acousto-ultrasonic and ultrasonic attenuation measurements were made on graphite fiber/polymer matrix panels at various stages of impact damage. The SWF and ultrasonic attenuation were calculated for each stage and compared with the number of impacts (Williams and Lampert, 1980), as shown in the figure on the left side.

Acousto-ultrasonic measurements were made on bend specimens prior to destructive testing. The SWF was compared to the interlaminar shear strength (ISS) as calculated from the bend test results (Kautz, 1986). These are shown in the figure on the right side.

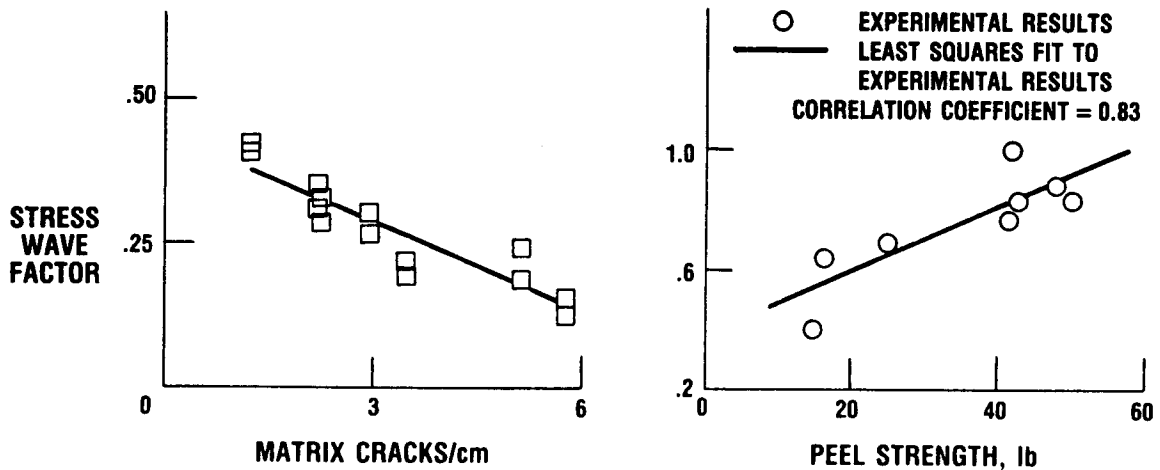


CD 88 32286

MORE RECENT RESULTS WITH SWF

Graphite fiber/polymer matrix specimens were put under tensile stress to produce a range of matrix crack densities through the central lamina. The SWF was measured after each tensile experiment and was compared with the crack density (Hemann et al., 1987), as shown in the figure on the left.

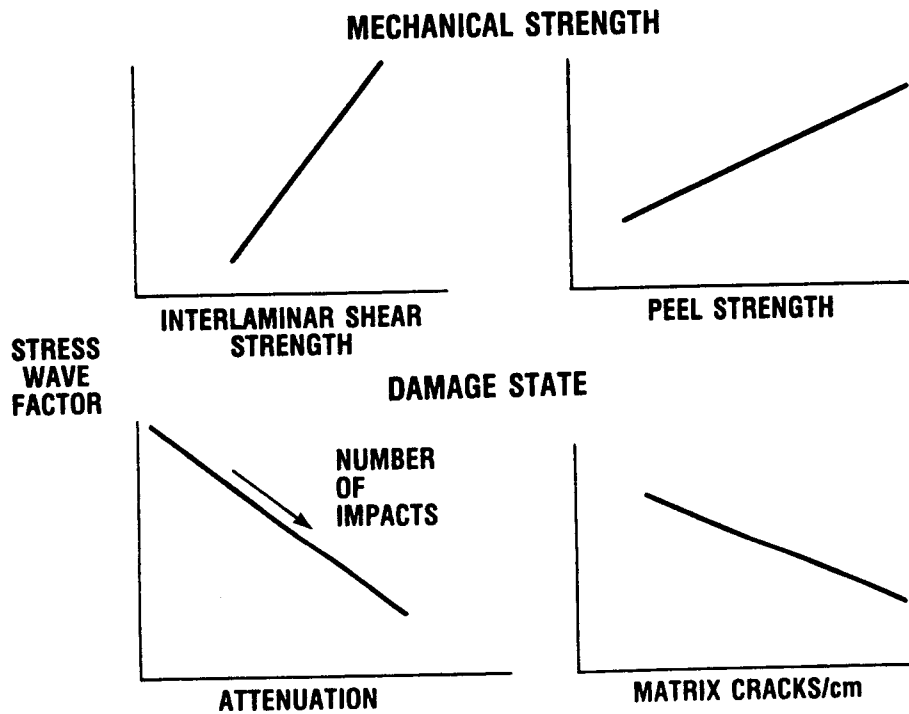
Acousto-ultrasonic measurements were done on specimens with vulcanized steel-rubber bonds. The SWF was compared with the strength coefficient from subsequent peel tests (Reis and Kautz, 1986), as shown in the figure on the right.



CO BB 32287

GENERAL CONCLUSIONS FOR SWF

When SWF was compared to a bond strength, such as interlaminar shear or against peel, the SWF was found to increase with the strength. When SWF was compared to a damage state, such as number of impacts or matrix cracks per centimeter, the SWF was found to decrease with increasing damage. In all these cases the SWF was larger for specimens with greater mechanical strength.

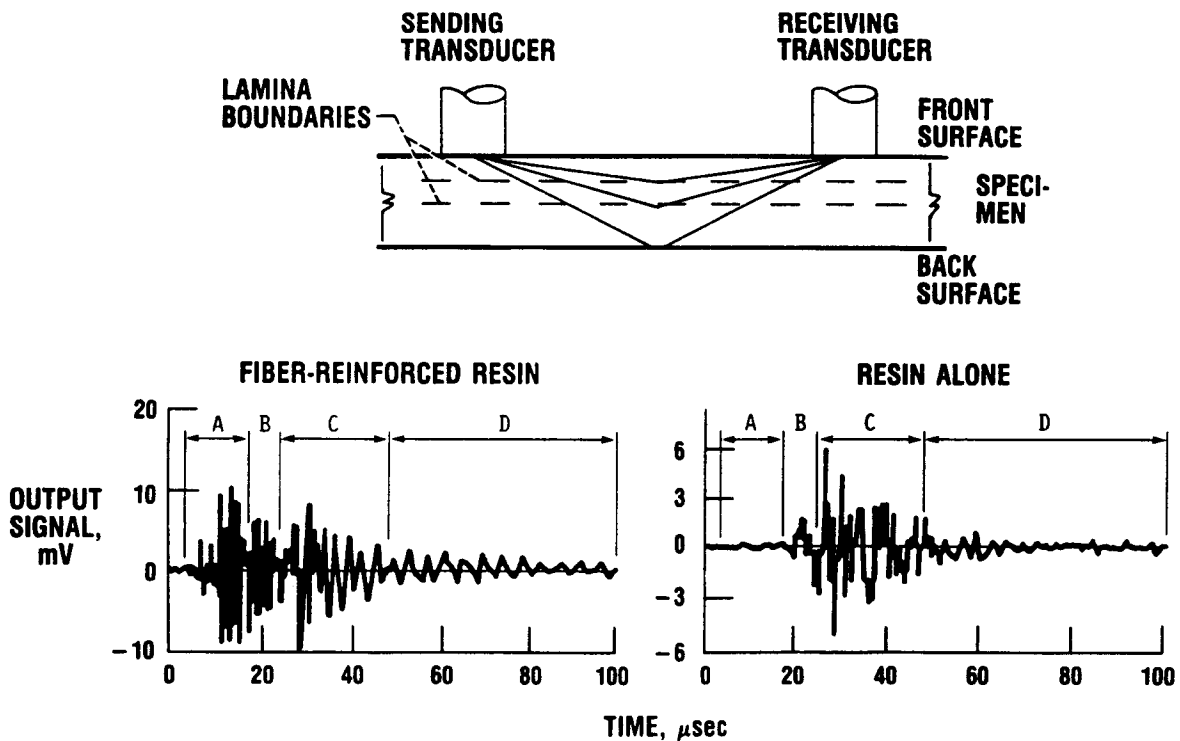


CD-88-32288

ANALYSIS OF PROPAGATION PATHS

The acousto-ultrasonic signal that arrives at the receiving transducer is the superposition of pulses that have traveled different paths and arrive there over a range of time (Kautz, 1986). This is illustrated below.

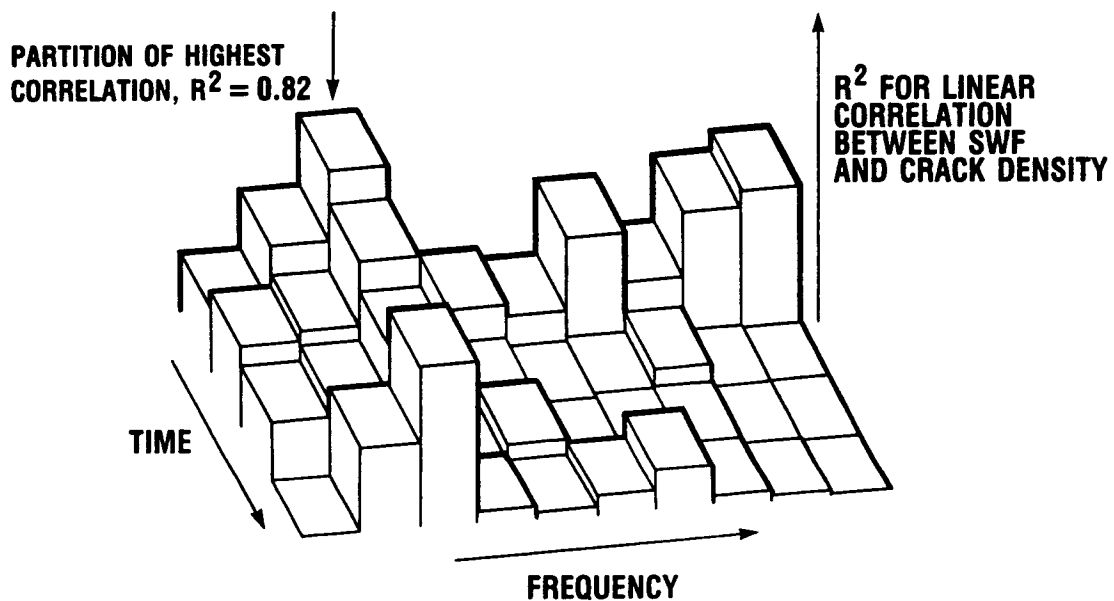
Signal propagation paths can be traced experimentally by comparing a fiber-reinforced resin specimen with a resin alone specimen (Kautz, 1987). Parts A of the time records shown below reveal a strong fiber path signal in the composite but nothing in the resin alone specimen. Parts B still show a strong fiber path signal. But in this time region the resin alone shows that signals are just beginning to arrive at the receiver. Parts C are dominated by resin path signal arrivals. Parts D are still dominated by resin path signal components. However, we see that they are enhanced in the composite by the presence of the fibers.



CD-88-32289

ACOUSTO-ULTRASONIC WAVEFORM PARTITIONING

Propagation path analysis can be used to enhance the sensitivity of SWF to mechanical properties. This is done by calculating SWF for partitions of the acousto-ultrasonic signal (Kautz, 1986). Correlation coefficients are shown for a 10×4 matrix of partition SWF values versus crack density for graphite/polymer specimens. The partitions that extend the highest are portions of the time-frequency field of the acousto-ultrasonic signal that are most sensitive to the crack density.



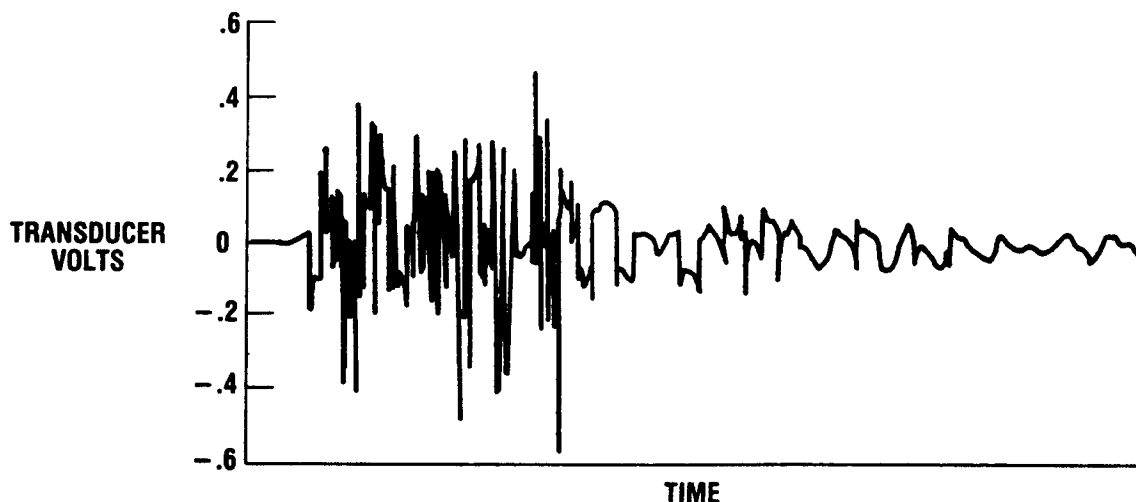
CD-88-32290

LASER ACOUSTO-ULTRASONICS

Laser in and laser out acousto-ultrasonics will improve reproducibility by eliminating piezoelectric transducer coupling. Input and output position will be more precisely defined while at the same time permitting better automation for scanning large panels or other hardware.

Shown below is a laser acousto-ultrasonic signal induced in a fiber/polymer composite as detected with a piezoelectric transducer. The laser-induced signal exhibits similar fiber-matrix distribution of ray paths to the one obtained with a transducer-induced signal.

The laser pulse used to produce this signal was 4 nsec in duration. The pulse should have a frequency spectrum envelope that is about 250 MHz. However the frequency spectrum of the induced ultrasonic signal is typical of that produced by a 1-MHz or a 2.25-MHz broadband transducer. This makes it quite appropriate for acousto-ultrasonics.



CD-88-32291

FURTHER APPLICATION OF ACOUSTO-ULTRASONICS

Acousto-ultrasonics has shown itself to be sensitive to the strength of structures at boundaries between both similar and dissimilar materials. For this reason it is actively being explored as a means of assessing the fiber-to-matrix bonding in ceramic composites. Similar studies are being conducted to compare SWF to strength parameters in metal matrix composites as well.

In order to understand and interpret acousto-ultrasonics in ceramic matrix and metal matrix composites it is necessary to identify the propagation paths that constitute the signals that are observed.

REFERENCES

- Hemann, J.H., Bowles, K.J., Kautz, H.E., and Cavano, P., 1987, "Transply Crack Density Detection by Acousto-Ultrasonics," Conference on Acousto-Ultrasonics: Theory and Application, cosponsored by NASA and ASNT, NASA TM-100224.
- Hull, D.R., Kautz, H.E., and Vary, A., 1985, "Measurement of Ultrasonic Velocity Using Phase-Slope and Cross-Correlation Methods," Materials Evaluation, Vol. 43, No. 11, pp 1455-1460.
- Kautz, H.E., 1986, "Acousto-Ultrasonic Verification of the Strength of Filament Wound Composite Material," Pressure Vessel Conference of ASME, NASA TM-88827.
- Kautz, H.E., 1987, "Ray Propagation Path Analysis of Acousto-Ultrasonic Signals in Composites," Conference on Acousto-Ultrasonics: Theory and Application, cosponsored by NASA and ASNT, NASA TM-100148.
- Reis, L.M., and Kautz, H.E., 1986, "Nondestructive Evaluation of Adhesive Bond Strength Using the Stress Wave Factor Technique," Journal of Acoustic Emission, Vol. 5, pp. 144-147.
- Vary, A., 1979, "A Review of Issues and Strategies in Nondestructive Evaluation of Fiber Reinforced Structural Composites," New Horizons - Materials and Processes for the Eighties, National SAMPE Technical Conference Series, Vol. 11, SAMPE, pp. 166-177.
- Vary, A., 1982, "Acousto-Ultrasonic Characterization of Fiber Reinforced Composites," Materials Evaluation, Vol. 40, pp. 650-654, 662.
- Vary, A., 1987, "The Acousto-Ultrasonic Approach," Conference on Acousto-Ultrasonics: Theory and Application, cosponsored by NASA and ASNT.
- Vary, A., and Bowles, K.J., 1979, "An Ultrasonic-Acoustic Technique for Non-destructive Evaluation of Fiber Composite Quality," Polymer Engineering and Science, Vol. 19, pp. 373-376.
- Williams, J.H., Jr., and Lampert, N.R., 1980, "Ultrasonic Evaluation of Impact-Damaged Graphite Fiber Composites," Materials Evaluation, Vol. 38, pp. 68-72.

CHARACTERIZATION OF SINTERED SiC BY USING NDE

George Y. Baaklini
Structural Integrity Branch
NASA Lewis Research Center

ABSTRACT

Capabilities of projection microfocus x-radiography and of ultrasonic velocity and attenuation for characterizing silicon carbide specimens were assessed. Silicon carbide batches covered a range of densities and different microstructural characteristics. Room-temperature, four-point flexural strength tests were conducted. Fractography was used to identify types, sizes, and locations of fracture origins. Fracture toughness values were calculated from fracture strength and flaw characterization data. Detection capabilities of radiography for fracture-causing flaws were evaluated. Applicability of ultrasonics for verifying material strength and toughness was examined. Radiography proved useful in detecting high-density inclusions and isolated voids, but failed in detecting surface and subsurface agglomerates and large grains as fracture origins. Ultrasonic velocity dependency on density was evident. Attenuation dependency on density and mean pore size was clearly demonstrated. Understanding attenuation as a function of toughness was limited by shortcomings in K_{IC} determination.

PRECEDING PAGE BLANK NOT FILMED

SPECIMEN SINTERING AND HOT ISOSTATIC PRESSING CONDITIONS

Twenty-five modulus of rupture (MOR) bars were prepared from -100-mesh α -SiC powder containing boron and carbonaceous resin binders. Compaction of the green specimens included dry pressing the powder by using a double-action, tungsten-lined die, vacuum sealing the green bars in thin-wall latex tubing, and cold isopressing the bars at 420 MPa. These bars represent five different batches which were sintered or sintered and hot isostatically pressed (HP) in order to tailor their density and microstructure. All bars were machined, the four long edges beveled, and further polished to a 0.07- μ m rms surface finish. Nominal test bar dimensions were 2.72 by 5.58 by 31.71 mm.

Batch number	Sintering			Hot isostatic pressing			Density, g/cm ³ , ±0.01 g/cm ³
	Temperature, °C	Time, hr	Argon pressure, MPa	Temperature, °C	Time, hr	Argon pressure, MPa	
1	2200	0.5	0.1	----	---	---	3.12
2HP	2200	1.5	↓	2100	0.5	138	3.14
4	2300	1.0	↓	----	---	---	3.05
4HP	2300	1.0	↓	2150	1.0	138	3.10
5HP	2100	.75	↓	2100	1.0	138	2.92

CD-88-32633

MICROSTRUCTURAL CHARACTERIZATION

Mean pore size, shape, and orientation were determined from photomicrographs of polished representative samples from each batch by applying two-dimensional Fourier transform theory (Generazio, 1986). Mean grain size was determined from photomicrographs of polished and etched representative samples of each batch by using an interactive image analysis system where grain boundaries could be traced at a digitizer tablet.

Batch number	Density, g/cm ³	Mean grain size, ^a μm			Mean pore size, ^{a,b} μm			Grain shape
		Circle ^c	Ellipse ^d		Circle ^e	Ellipse ^{a,f}		
		Diameter	Major	Minor	Diameter	Major	Minor	
1	3.12	5.76	7.94	4.56	1.60	1.61	1.59	Equiaxed and elongated
2HP	3.14	6.75	9.61	5.15	1.63	1.75	1.50	Equiaxed and elongated
4	3.05	11.56	19.39	7.73	3.82	4.00	3.64	Elongated
4HP	3.10	11.18	18.08	7.82	3.44	3.60	3.27	Elongated
5HP	2.92	3.36	4.40	2.78	2.29	2.38	2.19	Equiaxed

^a±0.2 μm.

^bNo preferred orientation.

^cAssuming all grains are equiaxed.

^dAssuming all grains are elongated.

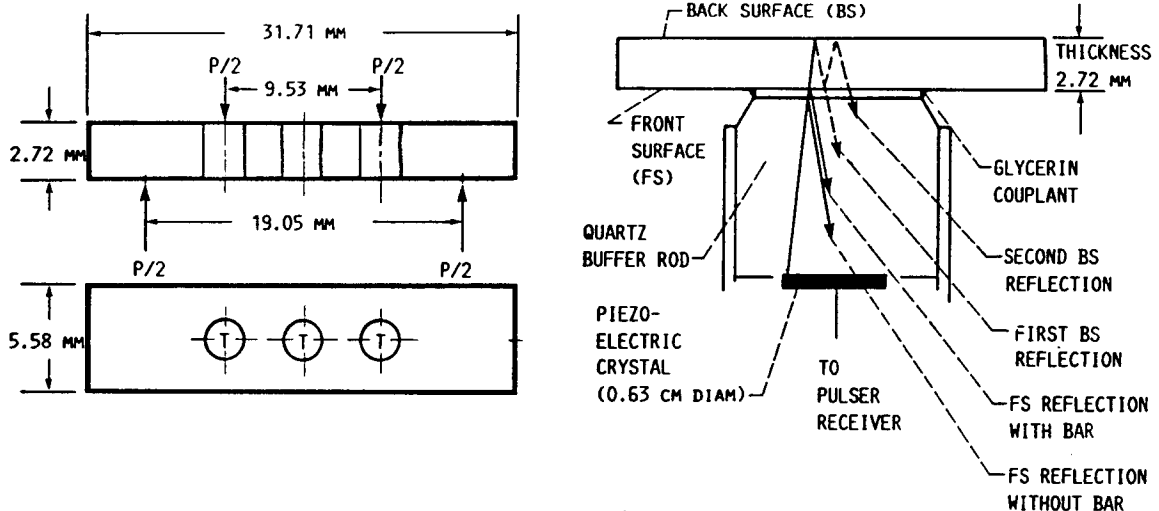
^eCalculated average from f.

^fReal measurements off the mean shape.

CD-88-32734

PULSE-ECHO ULTRASONICS OF MOR BARS

Velocity and attenuation measurements were determined for all samples through the thickness at three different locations in the highest stressed area of the test specimen. The pulse-echo technique, with a 100-MHz broadband longitudinal-wave transducer, was used to measure the cross correlation velocity (Hull et al., 1985) and the attenuation coefficient from the first and second back surface reflections. The front surface reflections obtained with and without the bar in place were used to calculate the reflection coefficient of the buffer rod-couplant-sample interface. This frequency-dependent reflection coefficient was incorporated for precision attenuation measurements (Generazio, 1985).

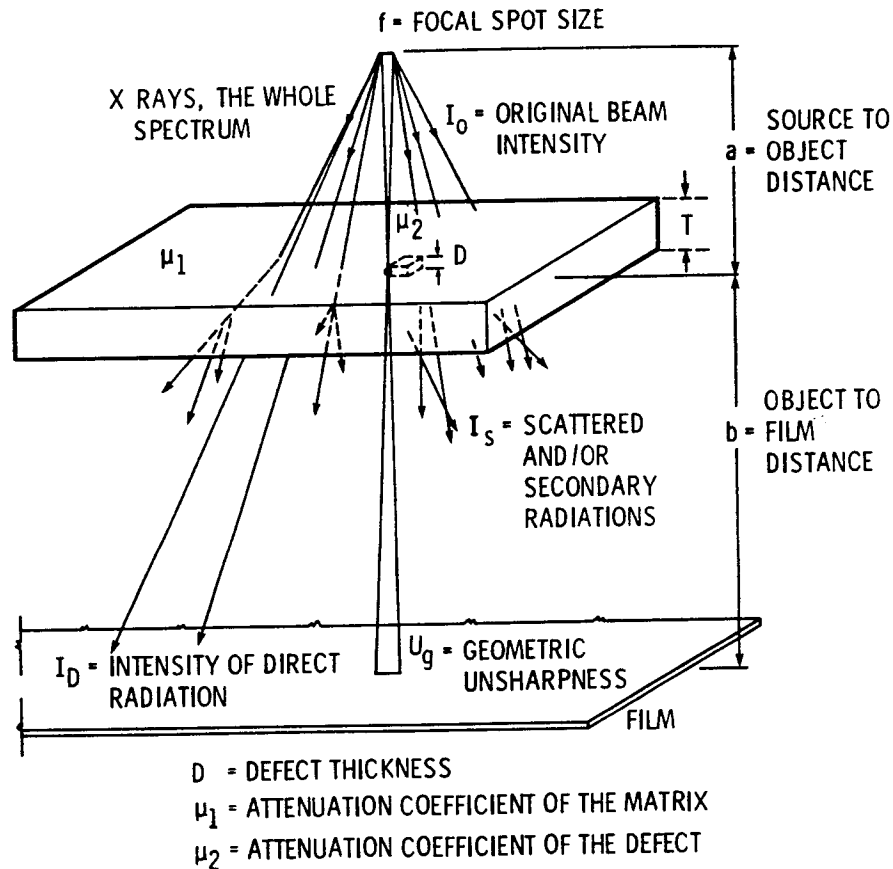


LOCATION OF TRANSDUCER FOR ULTRASONIC MEASUREMENTS IS DENOTED BY T, AND P IS APPLIED LOAD

CD-88-32735

RADIOGRAPHIC EVALUATION

All specimens were film radiographed in order to detect potential fracture-causing flaws. The microfocus system used was operated in the projection mode (x5 magnification) and in the 30 to 60 kV range with a beam current range of 0.25 to 0.32 mA. The system had a molybdenum anode and a 10- μm focal spot. All radiographs were manually developed, and were examined with the aid of a x7 optical measuring magnifier under variable-intensity backlighting (1000 to 9000 lm/m^2) in subdued room lighting. Test bars were radiographed in two modes, the (W,L) mode, where x rays were transmitted through the thickness, and the (T,L) mode, where x rays were transmitted through the width. When combined, they form a three-dimensional radiographic location of flaws.



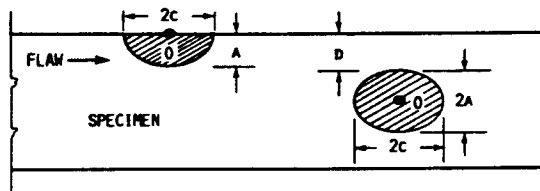
CD-88-32736

ASSESSMENT OF FRACTURE ORIGINS

Out of 25 specimens tested, 17 fracture origins were identifiable. The type, shape, size, and location of fracture origins are tabulated below. The 17 fracture origins identified were 5 bulk voids, 2 surface voids, 1 iron-rich inclusion, 1 large grain, 3 bulk agglomerates, and 5 surface agglomerates.

Batch number	Specimen number	Type	Shape	D, ^a μm	A ^a or 2A, μm	2C, ^a μm
1	3	Unidentified	-----	---	---	---
	5	Agglomerate	Circular	6	45	45
	8	Void	Irregular	14	69	69
	12	Agglomerate	Elliptical	60	40	70
	13	Void	Elliptical	40	80	104
2HP	2	Void	Semi-elliptical	0	19	67
	5	Agglomerate	Elliptical	12	65	127
	8	Void	Elliptical	120	58	92
	11	Unidentified	-----	---	---	---
	23	Agglomerate	Semi-elliptical	0	46	92
4	4	Void	Elliptical	50	69	127
	14	Void	Semi-elliptical	0	58	117
	15	Unidentified	-----	---	---	---
	16	Unidentified	-----	---	---	---
	18	Large Grain	Trapezoidal	7	34	58
4HP	1	Unidentified	-----	---	---	---
	5	Unidentified	-----	---	---	---
	8	Fe inclusion	Irregular	50	140	140
	9	Unidentified	-----	---	---	---
	24	Unidentified	-----	---	---	---
5HP	35	Agglomerate	Semi-elliptical	0	50	150
	36	Agglomerate	Irregular	0	35	55
	37	Agglomerate	Semicircular	0	30	200
	46	Void	Elliptical	120	100	120
	59	Agglomerate	Circular	0	60	60

^aSee sketch below.



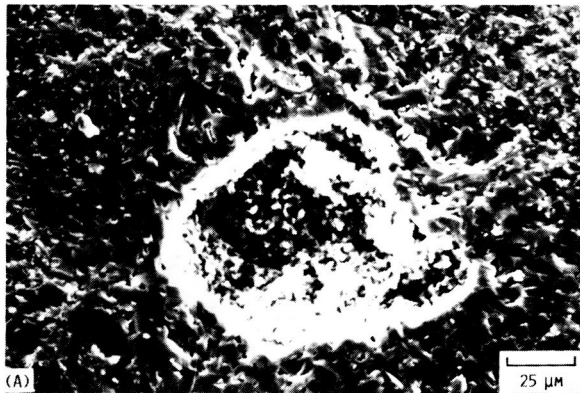
CD-88-32737

ORIGINAL PAGE IS
OF POOR QUALITY

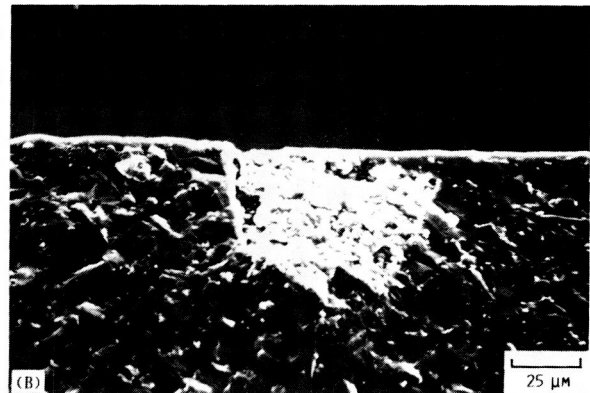
FRACTOGRAPHY

Shown below are scanning electron micrographs typical of fracture origins in sintered SiC MOR bars:

BULK VOID

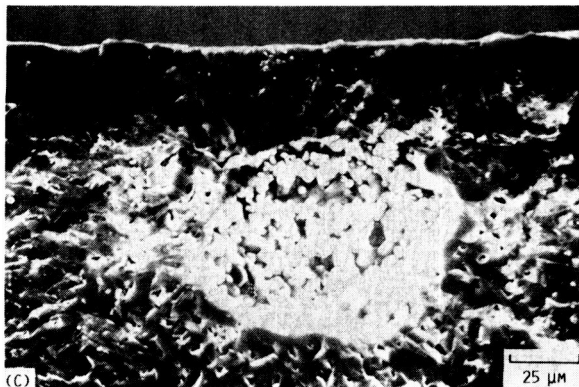


SURFACE AGGLOMERATE

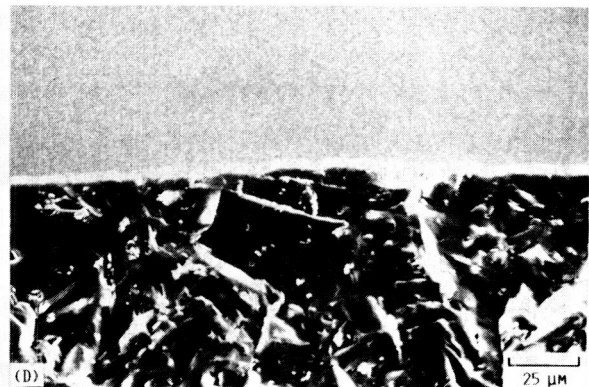


CD-88-32738

BULK VOID (AGGLOMERATE-LIKE)



LARGE GRAIN



CD-88-32739

RADIOGRAPHIC DETECTION OF FRACTURE ORIGINS

Seven out of seventeen identified fracture origins were radiographically detected. All five bulk voids, one out of two surface voids, and the iron-rich inclusion, were detected. All surface and subsurface agglomerates and the large grain were missed. In general, the flaw size as it appeared on the radiograph was less than or equal to its real size as determined optically.

Batch number	Specimen number	Type ^a	Optical flaw dimensions, μm		Sensitivity, ^b percent		Flaw detected		Radiographic flaw dimensions, μm	
			XT	XW	T	W	T	W	XW, XL	XT, XL
1	3	U	---	---	---	---	---	---	-----	-----
	5	BA	45	45	1.6	0.8	No	No	-----	-----
	8	BV	69	69	2.5	1.2	Yes	Yes	43, 85	43, 85
	12	BA	40	70	1.4	1.3	No	No	-----	-----
	13	BV	80	104	2.9	1.9	Yes	No	43, 43	-----
2HP	2	SV	19	67	0.7	1.2	No	No	-----	-----
	5	BA	65	127	2.4	2.3	No	No	-----	-----
	8	BV	58	92	2.1	1.7	Yes	No	63, 43	-----
	11	U	---	---	---	---	---	---	-----	-----
	23	SA	46	92	1.7	1.6	No	No	-----	-----
4	4	BV	69	127	2.5	2.3	Yes	No	105, 105	-----
	14	SV	58	115	2.1	1.6	Yes	Yes	105, 42	42, 105
	15	U	---	---	---	---	---	---	-----	-----
	16	U	---	---	---	---	---	---	-----	-----
	18	LG	34	58	1.2	1.0	No	No	-----	-----
4HP	1	U	---	---	---	---	---	---	-----	-----
	5	U	---	---	---	---	---	---	-----	-----
	8	FeI	140	140	5.3	2.5	Yes	Yes	62, 62	62, 62
	9	U	---	140	---	---	---	---	-----	-----
	24	U	---	140	---	---	---	---	-----	-----
5HP	35	SA	50	150	1.8	2.7	No	No	-----	-----
	36	SA	35	55	1.3	1.0	No	No	-----	-----
	37	SA	130	200	4.8	3.6	No	No	-----	-----
	46	BV	100	120	3.8	2.2	Yes	Yes	106, 64	106, 64
	59	SA	60	60	2.2	1.1	No	No	-----	-----

^aU, unidentified; BA, bulk agglomerate; BV, bulk void; SA, surface agglomerate; SV, surface void; LG, large grain; FeI, iron inclusion.

^bSensitivity, 100(XT/T) or 100(XW/W).

[Specimen dimensions measured along thickness, T, width, W, and length, L.
Flaw dimensions XT, XW, and XL measured along T, W, and L, respectively.]

CD-88-32740

FLEXURAL STRENGTH AND FRACTURE TOUGHNESS RESULTS

Fracture toughness (K_{IC}) values were obtained from the relationship between fracture strength and flaw shape, size, and location based on the work by Brown and Srawley (1967), Evans and Tapin (1972), Bansal (1976), Bansal and Duckworth (1977), and Danforth and Richman (1983).

There is no reason to believe, on the basis of an f-test at the 95-percent confidence level (Natrella, 1963), that the five batches differ in strength variability. Further, there is only reason to believe that the mean strength for batch 1 exceeds that of batch 4HP; otherwise no differences in mean strengths of all other batches are noted. This is substantiated by a t-test at the 95-percent confidence level.

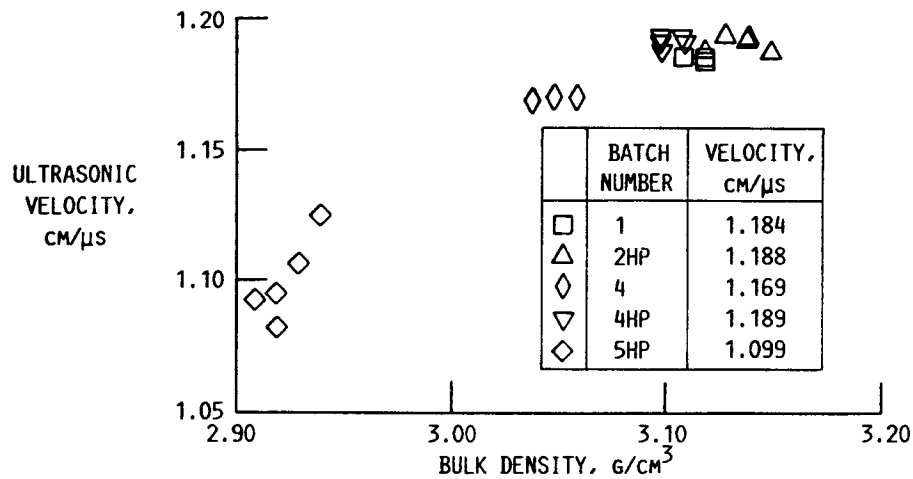
On the basis of an f- and t-test at the 95-percent confidence level, none of the four batches differed in toughness variability or in mean toughness.

Batch number	Specimen number	Fracture strength of tensile surface, σ_t , MPa	Fracture strength at origin, σ_f , MPa	$(\sigma_t)_{avg}$, standard deviation, MPa	Y/Z	Fracture toughness, K_{IC} , MN-m ^{-3/2}	$(K_{IC})_{avg}$, standard deviation, MN-m ^{-3/2}
1	3	356	---	338±48	---	---	3.26±0.26
	5	389	385		1.27	3.23	
	8	269	265		1.27	2.80	
	12	382	369		1.42	3.31	
	13	326	317		1.31	3.71	
2HP	2	319	319	319±52	1.60	2.23	2.88±0.65
	5	211	267		1.67	3.59	
	8	322	305		1.40	3.25	
	11	402	---		---	---	
	23	281	281		1.27	2.42	
4	4	265	256	315±40	1.44	3.06	3.22±0.39
	14	304	304		1.27	2.94	
	15	342	---		---	---	
	16	366	---		---	---	
	18	296	281		1.60	3.67	
4HP	1	251	---	273±51	---	---	-----
	5	334	---		---	---	
	8	209	201		---	---	
	9	306	---		---	---	
	24	271	---		---	---	
5HP	35	289	289	297±25	1.56	3.19	3.20±0.73
	36	324	324		1.25	2.40	
	37	288	288		1.25	4.10	
	46	319	298		1.26	3.75	
	59	264	264		1.26	2.57	

CD-88-32741

ULTRASONIC VELOCITY AND BULK DENSITY

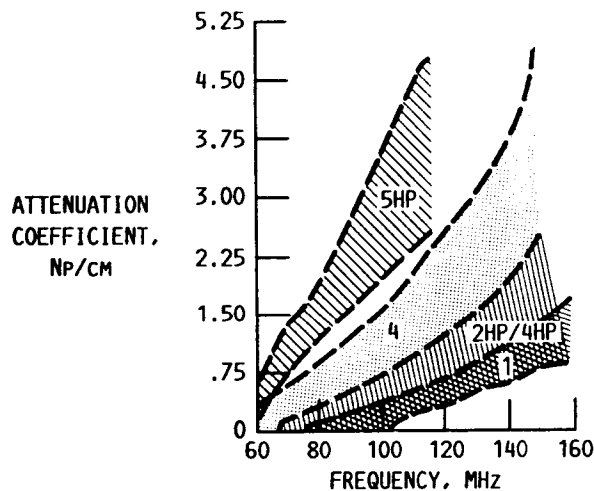
Average velocity based on three measurements at different locations in the MOR bar was plotted as a function of bulk density for all 25 bars. The data show that velocity is an increasing function of density. The average velocities are 1.184, 1.188, 1.169, 1.189 and 1.099 cm/ μ s for batches 1, 2HP, 4, 4HP, and 5HP, respectively. By comparing these results with corresponding average bulk densities, there is approximately a 1-percent change in velocity for a 1-percent change in density.



CD-88-32742

ULTRASONIC ATTENUATION, FLEXURAL STRENGTH, AND FRACTURE TOUGHNESS

Attenuation coefficient results are plotted as a function of frequency for all five batches. Plotted data are the measured attenuation at or very near the location where fracture took place. Dashed lines represent the upper and lower boundaries of the data of each batch of specimens. Attenuation coefficient in the frequency regime shown does differentiate substantially between batches on the basis of their density and microstructural characteristics. Attenuation dependency on density can be seen by comparing batch 4 and batch 4HP attenuation data, where a 1.6-percent difference in density (also a 1-percent difference in velocity) reflects a 56-percent difference in attenuation at a frequency of 100 MHz. Knowing a priori that attenuation is not due to grain boundary-scattering mechanism (Generazio, 1987), the attenuation data for batches 5HP, 4, and 1 therefore demonstrate the attenuation dependency on density and average pore size.



BATCH NUMBER	DENSITY, G/CM ³	MEAN PORE DIAMETER, μM	FLEXURAL STRENGTH, MPA	FRACTURE TOUGHNESS, MN · M ^{-3/2}
1	3.12	1.60	338±48	3.26±0.37
2HP	3.14	1.63	319±52	2.88±0.65
4	3.05	3.82	315±40	3.22±0.39
4HP	3.10	3.44	273±51	-----
5HP	2.92	2.38	297±25	3.20±0.73

CD-88-32743

CONCLUSIONS

1. Radiography proved useful in detecting high-density inclusions and isolated voids, but failed in detecting surface and subsurface agglomerates and large grains as fracture origins.
2. Ultrasonic dependency on velocity was evident.
3. Attenuation dependency on density and mean pore size was clearly demonstrated.
4. Understanding attenuation as a function of toughness was limited, first, by the fact that one dominant flaw can mask the effect of bulk porosity and microstructure on strength and toughness and, second, by shortcomings in K_{IC} determination.

REFERENCES

- Bansal, G.K., 1976, "Effect of Flaw Shape on Strength of Ceramics," J. Am. Ceram. Soc., 59 [1-2] 87-88.
- Bansal, G.K., and Duckworth, W.H., 1977, "Fracture Stress as Related to Flaw and Fracture Mirror Sizes," J. Am. Ceram. Soc., 60 [7-8] 304-310.
- Brown, W.F., Jr., and Srawley, J.E., 1967, Plane Strain Crack Toughness Testing of High Strength Metallic Materials. ASTM-STP-410, ASTM, Philadelphia, PA, pp. 1-15.
- Danforth, S.C., and Richman, M.H., 1983, "Strength and Fracture Toughness of Reaction-Bonded Si_3N_4 ," Am. Ceram. Soc. Bull., 62 [4] 501-505.
- Evans, A.G., and Tapin, G., 1972, "Effects of Microstructure on the Stress to Propagate Inherent Flaws," Proc. Br. Ceram. Soc., No. 20, 275-297.
- Generazio, E.R., 1985, "The Role of the Reflection Coefficient in Precision Measurement of Ultrasonic Attenuation," Mater. Eval., 43 [8] 995-1004.
- Generazio, E.R., 1986, "Determination of Grain Size Distribution Function Using Two-Dimensional Fourier Transforms of Tone Pulse Encoded Images," NASA TM-88790.
- Generazio, E.R., Roth, D.J., and Baaklini, G.Y., 1987, "Imaging Subtle Microstructural Variations in Ceramics with Precision Ultrasonic Velocity and Attenuation Measurements," NASA TM-100129.
- Hull, D.R., Kautz, H.E., and Vary, A., 1985, "Measurement of Ultrasonic Velocity Using Phase-Slope and Cross-Correlation Methods," Mater. Eval., 43 [11] 1455-1460.
- Natrella, M.G., 1963, Experimental Statistics. NBS Handbook No. 91, National Bureau of Standards, Washington, D.C.

C-2

SYSTEMS FOR ULTRASONIC SCANNING, ANALYSIS, AND IMAGERY

David B. Stang*, Edward R. Generazio, and Steve Abet†
Structural Integrity Branch
NASA Lewis Research Center

ABSTRACT

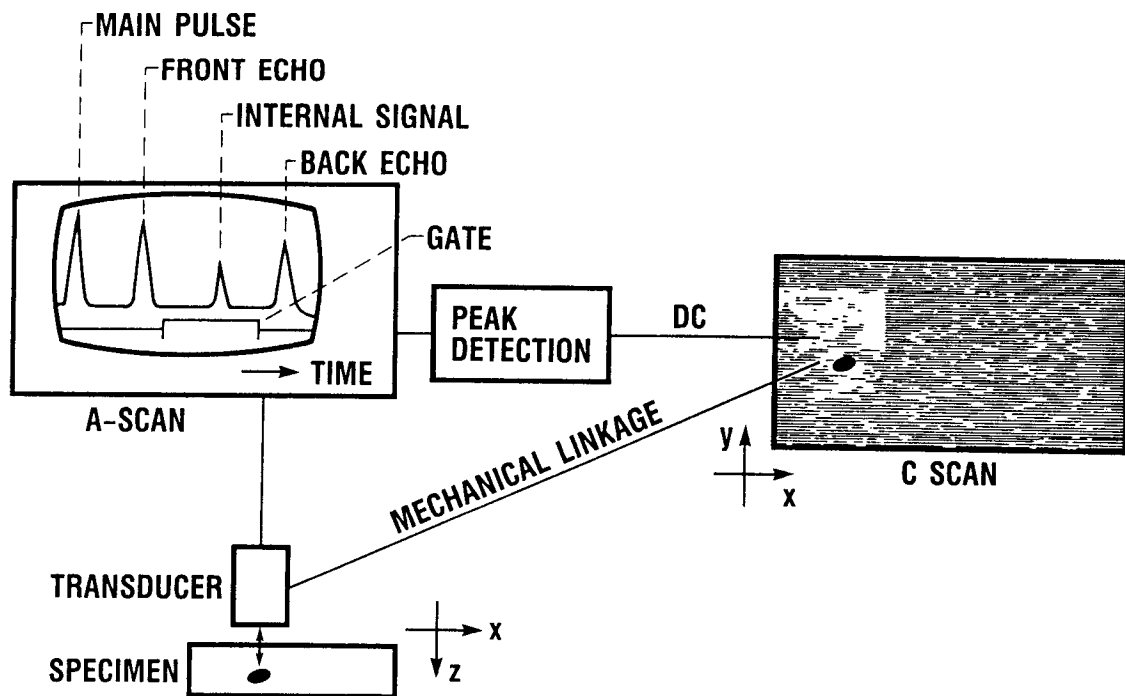
A variety of ultrasonic scanning and imagery techniques are used to investigate various aspects of materials and microstructures. Two ultrasonic scanning systems are in use by the Lewis Research Center's Structural Integrity Branch: an immersion scanner and a contact scanning system. The basic principles of scanning are reviewed, examples of images are presented, and structural features suggested by these images are discussed. Both of these systems are custom designed; their unique capabilities, advantages, and disadvantages are highlighted.

*Sverdrup Technology, Inc., Lewis Research Center Group. Work performed on-site at the Lewis Research Center under contract NAS3-2410S.

†Cleveland State University. Work funded under NASA Grant NCC3-24.

C-SCAN PRINCIPLES

In general, ultrasonic scans are based on the following procedures: A specimen with flat, parallel surfaces is immersed in water. A transducer is used to send a very short pulse which echoes off the front and back as well as flaws within the specimen. The transducer receives the echoes and they appear on an oscilloscope (A-scan trace) where echoes returning from points farther from the transducer are farther to the right on the time trace. Signals of interest are highlighted by an adjustable time gate, and the peak amplitude of the gated signal is converted to a dc signal. This signal is used to create an x-y image (C-scan), where traditionally the signal controls the intensity of an electrostatic pen moved as the scan progresses by a linkage attached to the transducer manipulator.

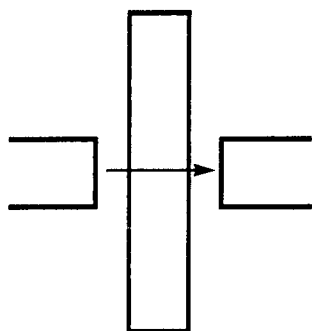


CD-88-31752

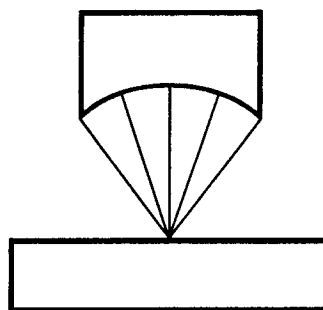
TYPES OF ULTRASONIC SCANS

In through-transmission scans, two transducers are used - a pulser and a receiver - and the signal transmitted through a relatively thin sample is examined in a plane parallel to the sample. In pulse-echo scans, the echoes are of interest and could be those from the specimen front or back surface or from inside. The transducer could be focused, where the sound waves converge to a point. In contact scans, a thin layer of oil or glycerin is used as couplant between the transducer and the sample in place of water.

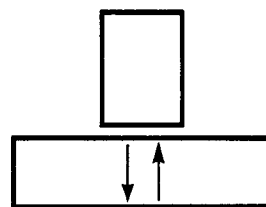
**IMMERSION
THROUGH TRANSMISSION**



**IMMERSION
PULSE-ECHO**



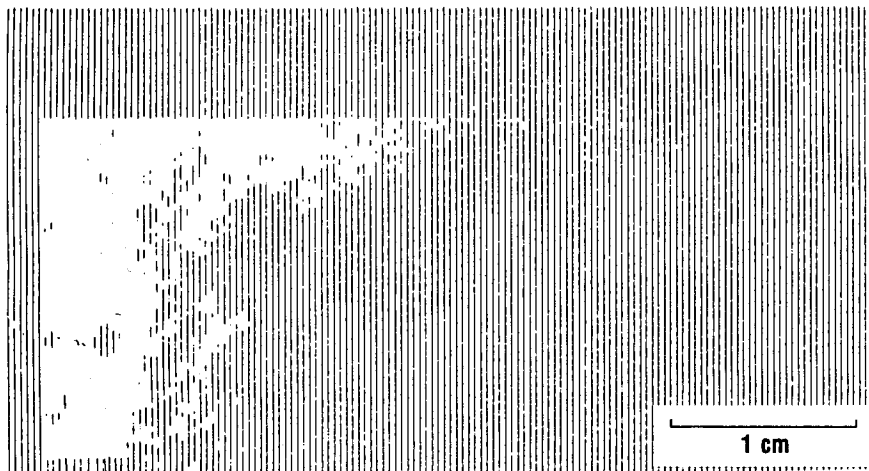
**CONTACT
PULSE-ECHO**



CD-88-31753

THROUGH-TRANSMISSION C-SCAN OF COMPOSITE PANEL

Displayed here is a conventional through-transmission C-scan image of a carbon composite panel produced by the electrostatic pen method. Higher amplitude transmitted signals are indicated by dark traces. The lower amplitude areas suggest poor bonding, but good contrast and quantitative results are difficult with this method.

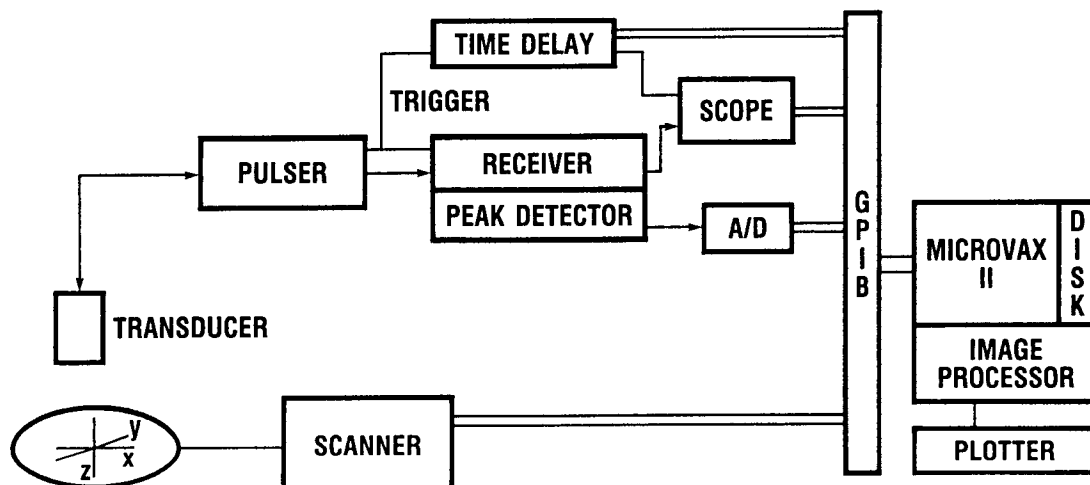


CD-88-31754

ORIGINAL PAGE IS
OF POOR QUALITY

MODIFIED IMMERSION ULTRASONIC SCANNING SYSTEM

An ultrasonic C-scan system was modified by omitting the use of the electrostatic pen plotter and sending the peak-detected dc signal to an analog-to-digital converter (A/D). This signal is sent to a MICROVAX II computer which controls the scan and acquires the digitized data through the IEEE-488 (general-purpose interface bus). A Grinnell image processor then displays a gray scale or color image of the scan.

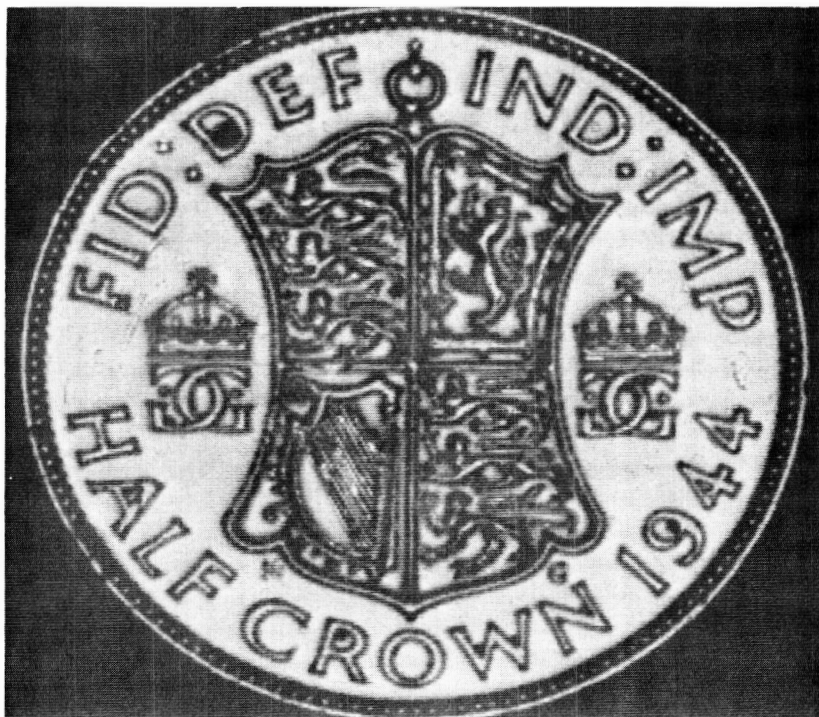


CD-88-31755

DIGITAL SURFACE SCAN IMAGE

This is an image obtained from a scan using a 75-MHz transducer focused at the surface. The scanner resolution is 96 μm (the limit of this system is 24 μm), and such an image can be zoomed to virtually any size. Note that not only are the coin's stamped features vividly brought out, but also small flaws such as nicks are imaged.

DIRECT SURFACE REFLECTION USING FOCUSED TRANSDUCER



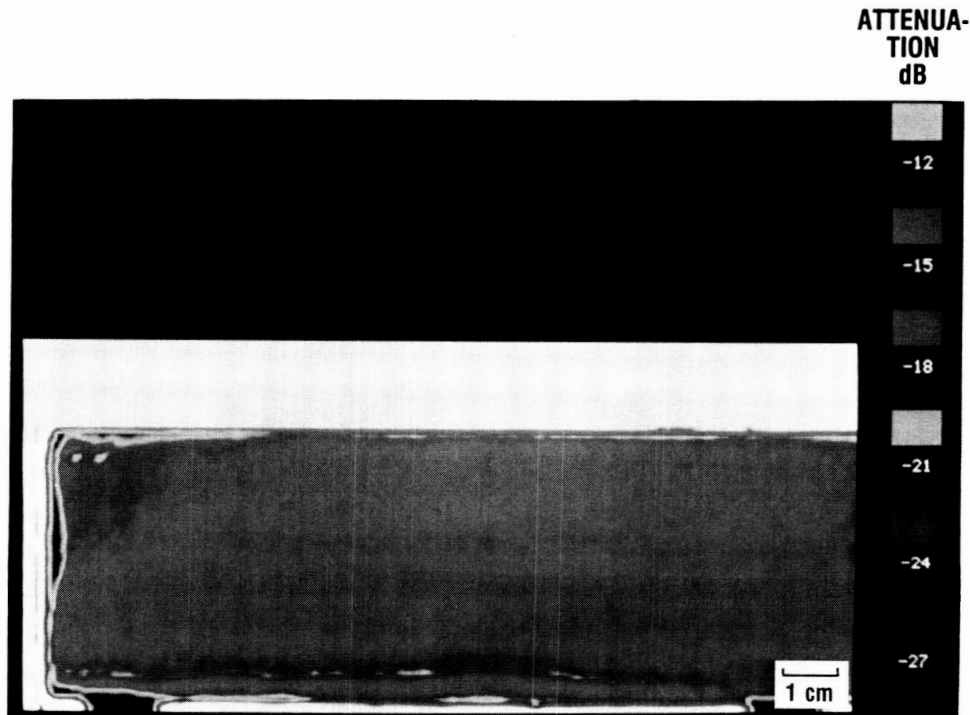
CD-88-31756

ORIGINAL PAGE IS
OF POOR QUALITY

DIGITAL THROUGH-TRANSMISSION IMAGE OF METAL MATRIX PANEL

Shown here is a through-transmission image of an iron-aluminum matrix, silicon carbide reinforced panel, produced using the modified C-scan system and 20-MHz transducers. The color scale indicates decibels of attenuation compared with a signal traveling through water unobstructed. This method of scanning creates a more quantitative and better contrasting result. The difference in attenuation can indicate the quality of bonding between matrix and reinforcement since a poor bond would cause ultrasonic energy to reflect rather than transmit through.

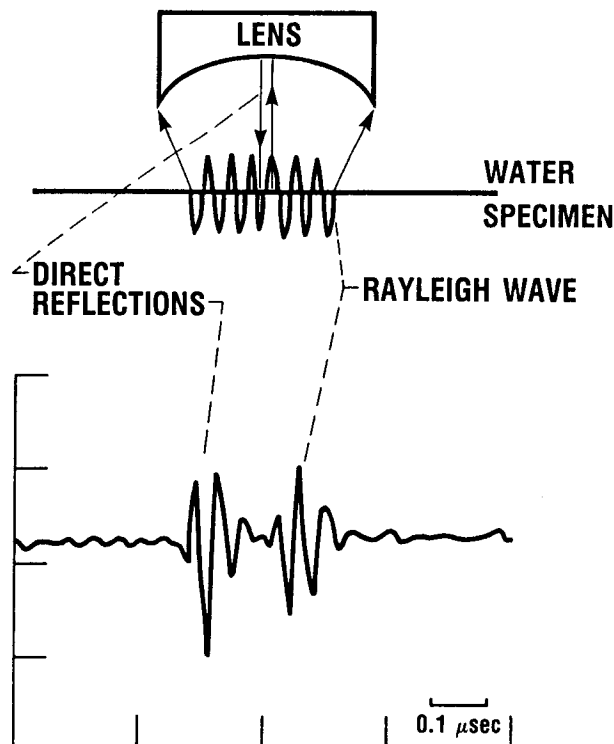
ORIGINAL PAGE IS
OF POOR QUALITY



CD-88-31757

RAYLEIGH WAVE SIGNAL

Another type of ultrasonic scan involves the recording of the surface (Rayleigh) wave signal by moving a focused transducer closer to the surface than the focal length. A wave traveling from the outer portions of the lens at some critical angle relative to the specimen surface will produce a surface wave in the sample and return again to the transducer lens. This signal appears slightly later than the main surface echo and can thus be recognized and gated (Gilmore et al., 1986; and Quate, 1980).



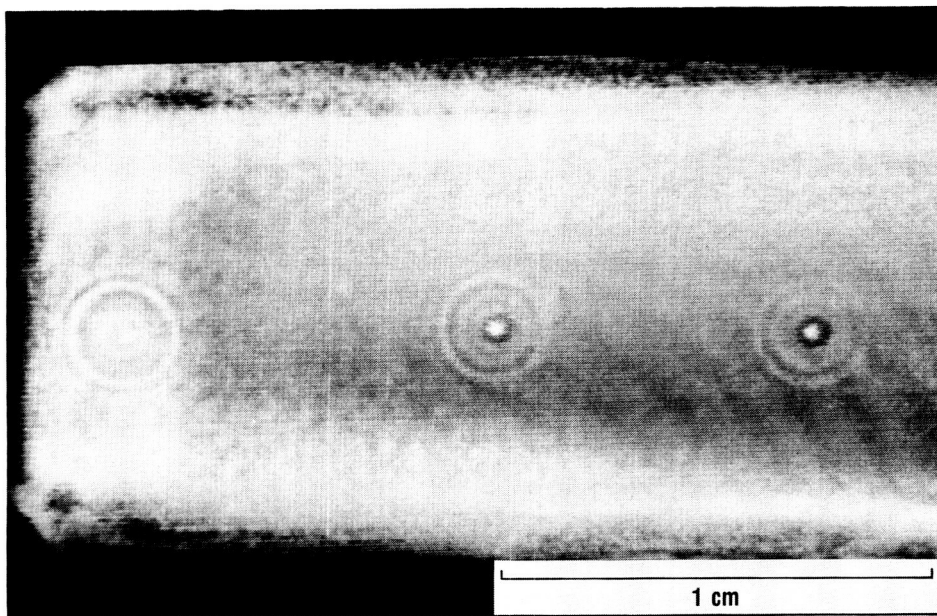
CD-88-31758

RAYLEIGH WAVE SCAN IMAGE

Images produced from the acquisition of the Rayleigh wave peak indicate features on the specimen surface as well as those near the surface (within a wavelength). Shown here is a scan using a 50-MHz transducer of a silicon carbide bar with seeded subsurface 50- μm voids. Such features cause disturbances in the Rayleigh signal, producing diffraction-like ring patterns.

ORIGINAL PAGE IS
OF POOR QUALITY

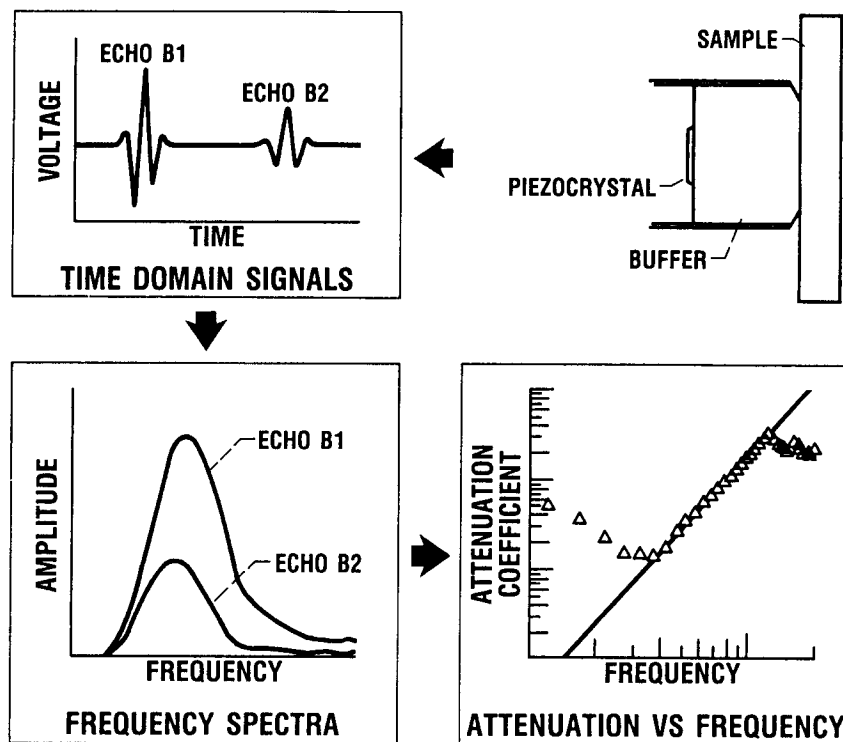
BAR WITH SEEDED VOIDS



CD-88-31759

CONTACT SCANNING AND ANALYTICAL ULTRASONICS

Analytical ultrasonics refers to any method where waveforms (as opposed to simply a peak) are processed to reveal how microstructure alters the wave. Here, two successive back wall echoes are processed to find attenuation versus frequency. Sound velocity can also be calculated by finding the travel time between pulses. These methods generally are used for finding bulk characteristics rather than individual defects (Vary, 1986).

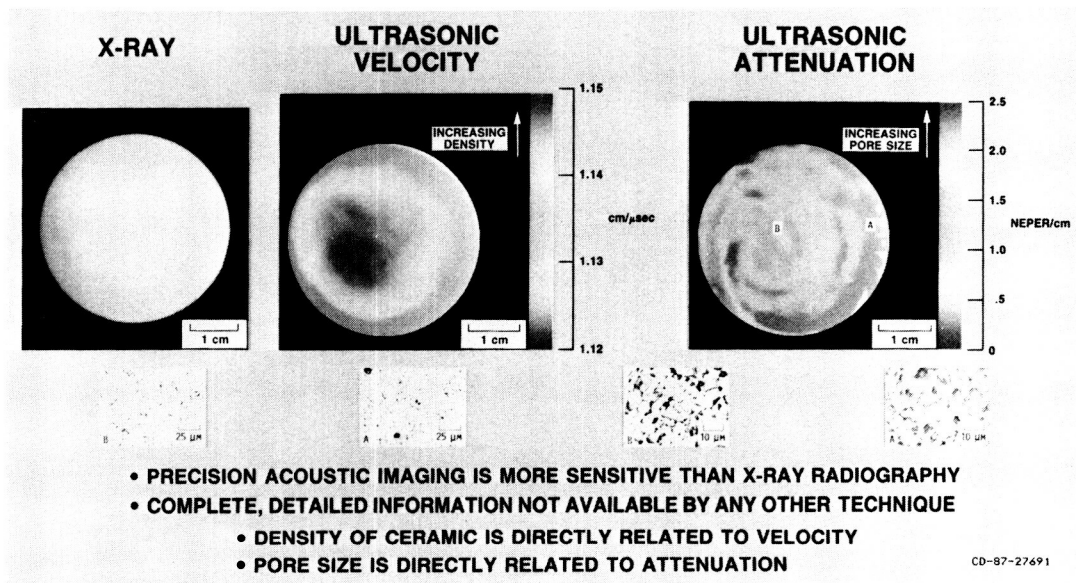


CD-88-31760

IMAGING SUBTLE FEATURES WITH ANALYTICAL ULTRASONICS

Shown here are contact scans of a monolithic silicon carbide disk. Variations in the sound velocity indicate differences in density over the area of the disk that x rays cannot image as well. In addition, differences in pore size are indicated by variations in ultrasonic attenuation (Generazio et al., 1988).

ORIGINAL PAGE IS
OF POOR QUALITY

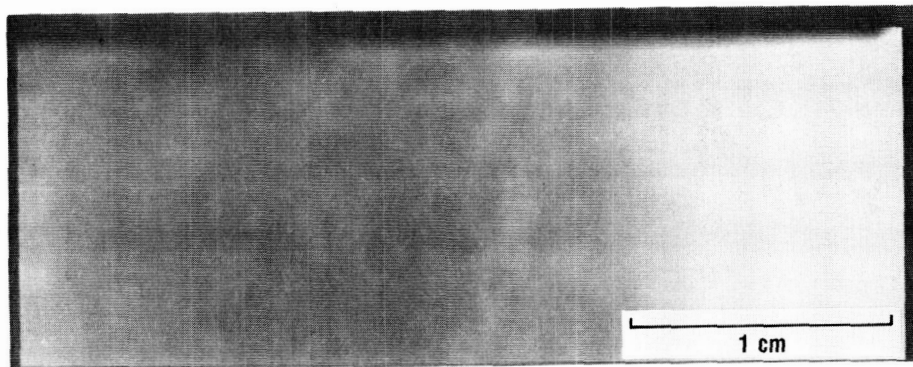


CD-88-33560

ULTRASONIC VELOCITY OF ALUMINA SAMPLE

This is an x-y image representing the velocity of sound through the bulk of an alumina specimen. The scan resolution is 0.5 mm; the sound velocity ranges from 0.984 (light areas) to 0.994 cm/ μ sec (dark areas). The regions of lower velocity are believed to be slightly more porous.

ORIGINAL PAGE IS
OF POOR QUALITY



CD-88-31761

REFERENCES

- Generazio, E.R., Roth, D.J., and Baaklini, G.Y., 1988, "Imaging Subtle Microstructural Variations in Ceramics With Precision Ultrasonic Velocity and Attenuation Measurements," NASA TM-100129.
- Gilmore, R.S., Tam, K.C., Young, J.D., and Howard, D.R, 1986, "Acoustic Microscopy From 10 to 100 MHz for Industrial Applications," Royal Society Transcripts, A320, pp. 215-235.
- Quate, C.F., 1980, "Microwaves, Acoustics, and Scanning Microscopy," Scanned Image Microscopy, Academic Press, pp. 23-55.
- Vary, A., 1986, "Concepts for Interrelating Ultrasonic Attenuation, Microstructure, and Fracture Toughness in Polycrystalline Solids," NASA TM-87339.

**FLAW CHARACTERIZATION IN STRUCTURAL CERAMICS USING SCANNING
LASER ACOUSTIC MICROSCOPY**

Don J. Roth
Structural Integrity Branch
NASA Lewis Research Center

ABSTRACT

The ability of scanning laser acoustic microscopy (SLAM) to characterize artificially seeded voids in sintered silicon nitride structural ceramic specimens was investigated. The voids ranged from 20 to 430 μm in diameter and were embedded up to 2 mm beneath the surface of the specimens. Probability of detection was determined as a function of void depth and size. Trigonometric relationships and Airy's diffraction theory were used to obtain predictions of void depth and size from acoustic diffraction patterns produced by the voids. Agreement was observed between actual and predicted void depths. However, predicted void diameters were generally much greater than actual diameters. Precise diameter predictions are difficult to obtain because of measurement uncertainty and the limitations of the 100-MHz SLAM applied to typical ceramic specimens.

PRECEDING PAGE BLANK NOT FILMED

OVERVIEW

FLAW CHARACTERIZATION IN STRUCTURAL CERAMICS USING SCANNING LASER ACOUSTIC MICROSCOPY

**OBJECTIVE: DETERMINE ABILITY OF SLAM TO CHARACTERIZE (SIZE, DEPTH)
INTERNAL FLAWS IN CERAMIC SPECIMENS**

**EXPERIMENTAL APPROACH: SINTERED SILICON NITRIDE SPECIMENS WITH
ARTIFICIALLY SEEDED INTERNAL VOIDS**

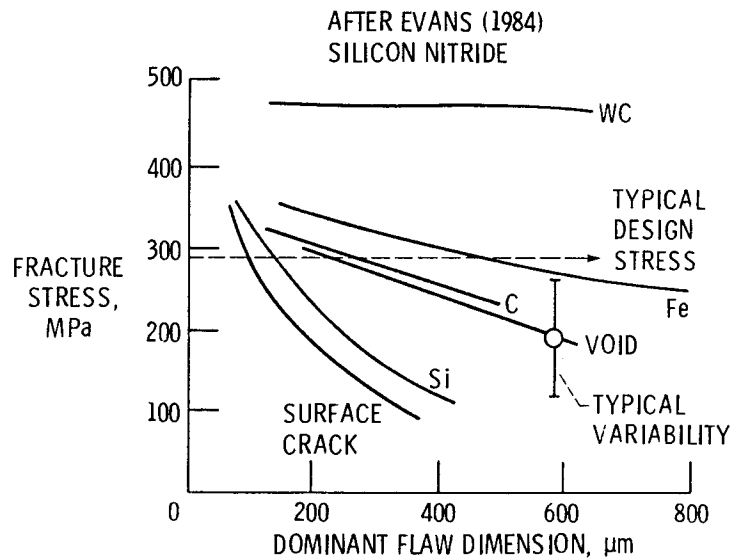
RESULTS AND CONCLUSION:

- (1) LARGE MEASUREMENT UNCERTAINTY DUE TO
EXPERIMENTAL CONFIGURATION**
- (2) UNCERTAINTY SEVERELY AFFECTED VOID SIZE
PREDICTIONS WHICH DEVIATED MORE THAN 100%
FROM ACTUAL SIZES**
- (3) REASONABLE AGREEMENT BETWEEN PREDICTED
AND ACTUAL VOID DEPTHS**

CD-88-32537

FRACTURE STRENGTH VERSUS FLAW TYPE AND SIZE

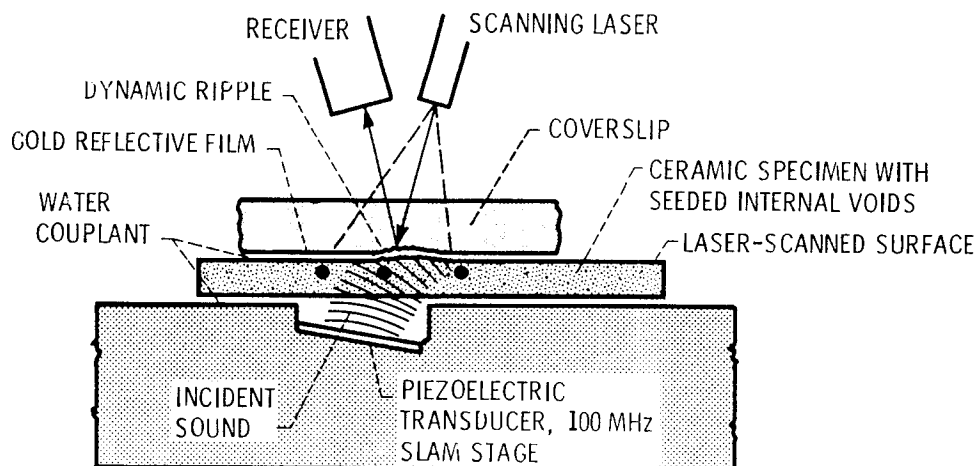
Experiment Rationale: Relationships between fracture strengths and flaw types, sizes, shapes, and locations are being actively investigated to promote understanding of structural ceramic mechanical behavior. Therefore, it is essential to develop accurate flaw characterization techniques for use on as-fabricated specimens.



CD-88-32538

SCANNING LASER ACOUSTIC MICROSCOPY (SLAM)

The experimental setup for scanning laser acoustic microscopy of ceramic specimens is shown below.

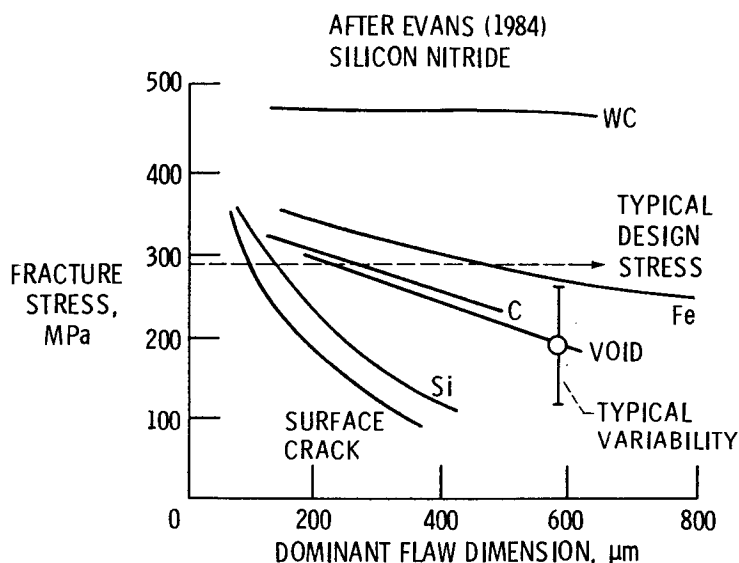


CD-88-32539

POSTER PRESENTATION

PURPOSE OF STUDY

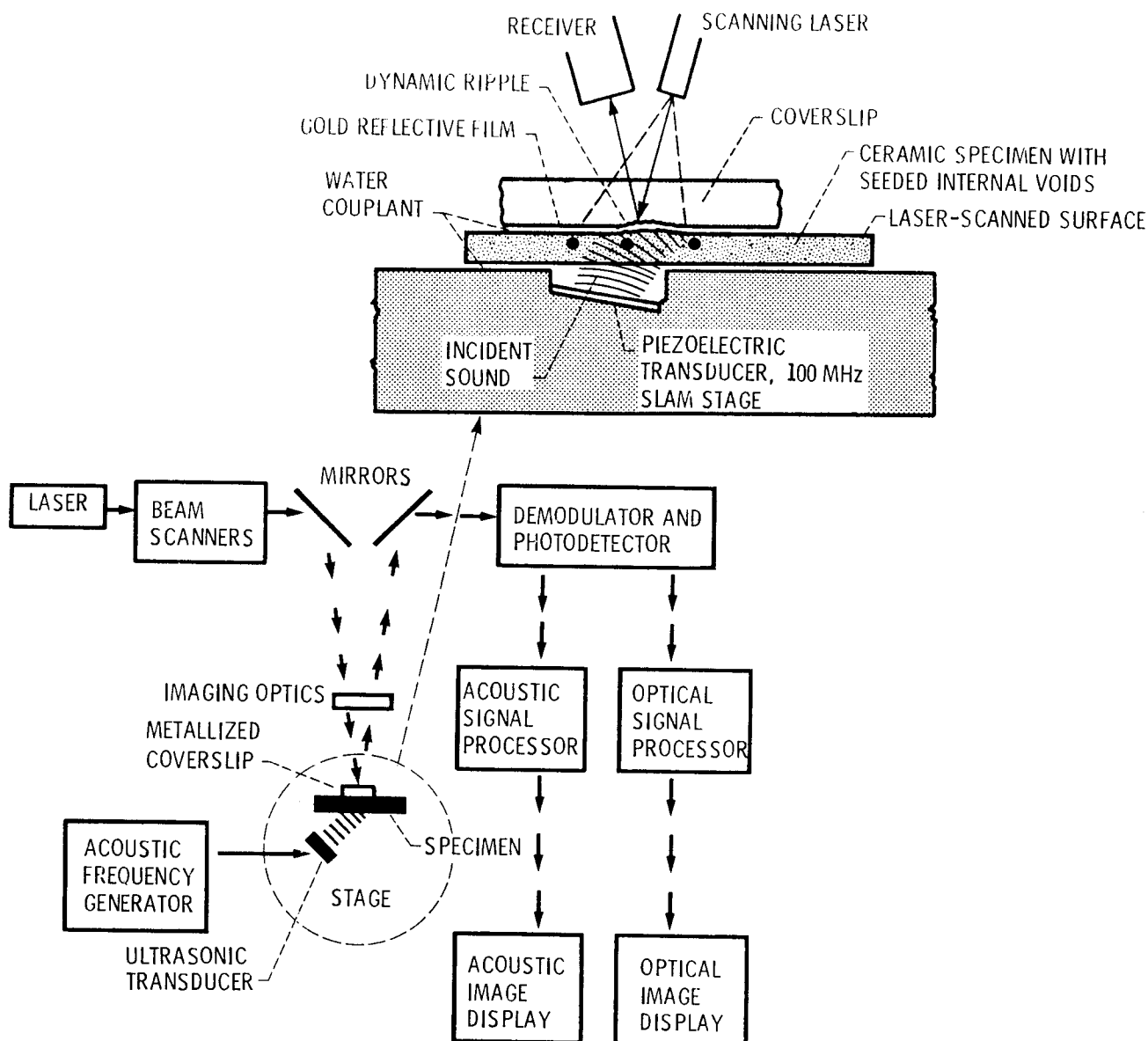
Structural ceramics exhibit wide variability in strength and low fracture toughness because of their brittle nature (Lenoe, 1983; Shannon, 1981; and Salem, 1985). Generally, failure is attributed to discrete flaws such as microcracks, voids, impurities, and oversized grains (Evans, 1984; Heitman, 1983; and Sanders, 1986). The relationships between fracture strengths and flaw types, sizes, shapes, and locations are being actively investigated for structural ceramics as indicated in the figure. Therefore, the ability to accurately characterize existing flaws in these materials by nondestructive evaluation (NDE) techniques has become extremely important.



CD-88-32538

SCANNING LASER ACOUSTIC MICROSCOPY (SLAM)

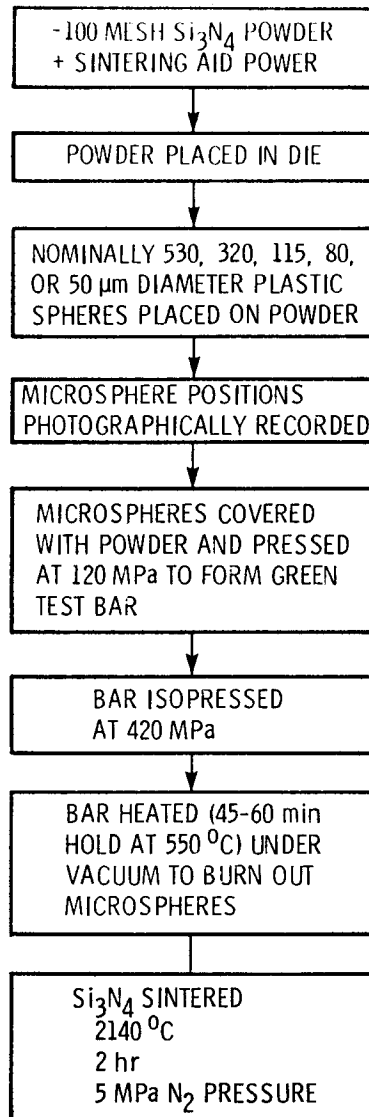
The following is a brief description of the principles of operation of SLAM. Continuous 100-MHz ultrasonic waves traveling through a specimen produce micro-distortions on the specimen surface farthest from the transducer. The distortion pattern is determined by the microstructural, bulk, and surface features of the material. A laser beam constantly raster scans a small area of the specimen. The laser beam, angularly modulated by the distortion pattern, is reflected to a photodetector and converted to an electronic signal. In this manner, an "acoustic" image of the specimen, including surface and internal flaws such as voids, inclusions, and cracks, is obtained and displayed on a video monitor in real time at approximately 100x (Roth, 1986a and b; Roth 1987; and Generazio, 1986).



CD-88-32540

SPECIMEN PREPARATION

Sintered Si_3N_4 specimens containing seeded internal voids were fabricated by using the processing steps shown in the figure and described in detail by Baaklini (1986). Briefly, plastic microspheres of various sizes were embedded in green specimens and later burned out to create voids within sintered specimens.

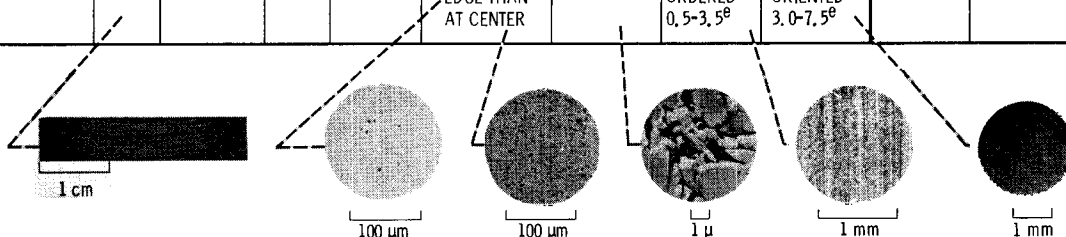


CHARACTERIZATION OF SPECIMENS

The seven sintered silicon nitride specimens were microstructurally characterized as shown in the table. The 12 internal voids seeded in the specimens ranged from 20 to 430 μm in diameter and from 0 to 2 mm in depth (Roth, 1987).

CHARACTERIZATION OF SPECIMENS

TEST BAR MATERIAL	NUMBER OF TEST BARS USED	LENGTH X WIDTH, (mm)	THICKNESS, (mm)	DENSITY		POROSITY DISTRIBUTION	AVERAGE GRAIN SIZE, (μm)	PEAK-TO-VALLEY ROUGHNESS, (μm), OF -		SEEDED INTERNAL VOIDS ^g		
				(g/cc)	% THEORETICAL			GROUND SURFACE	AS-FIRED SURFACE	TOTAL NUMBER	DIAMETER, (μm)	DEPTH BELOW SPECIMEN SURFACE (mm)
SINTERED Si_3N_4 (SSN)	7	30x6	2-4	3.230	~100	LESS AT EDGE THAN AT CENTER	0.5-1.5 ^c	RELATIVELY ORDERED 0.5-3.5 ^d	RANDOMLY ORIENTED 3.0-7.5 ^e	12	20-430	0-2



^aOPTICAL PHOTOGRAPH (GROUND SURFACE SHOWN).

^bOPTICAL MICROGRAPH OF METALLOGRAPHICALLY POLISHED SECTION (BLACK SPOTS INDICATE POROSITY).

^cAVERAGE GRAIN SIZES OBTAINED USING THE HEYN INTERCEPT (MEAN FREE PATH) METHOD GIVEN IN ASTM E112-81.

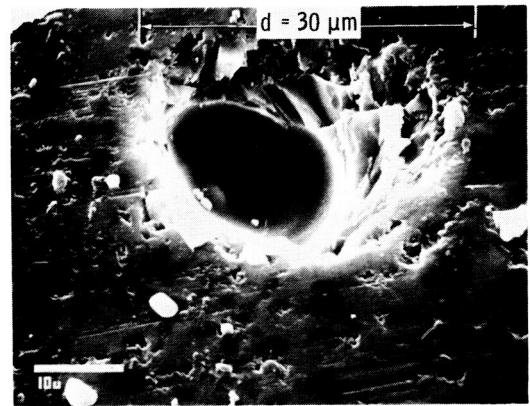
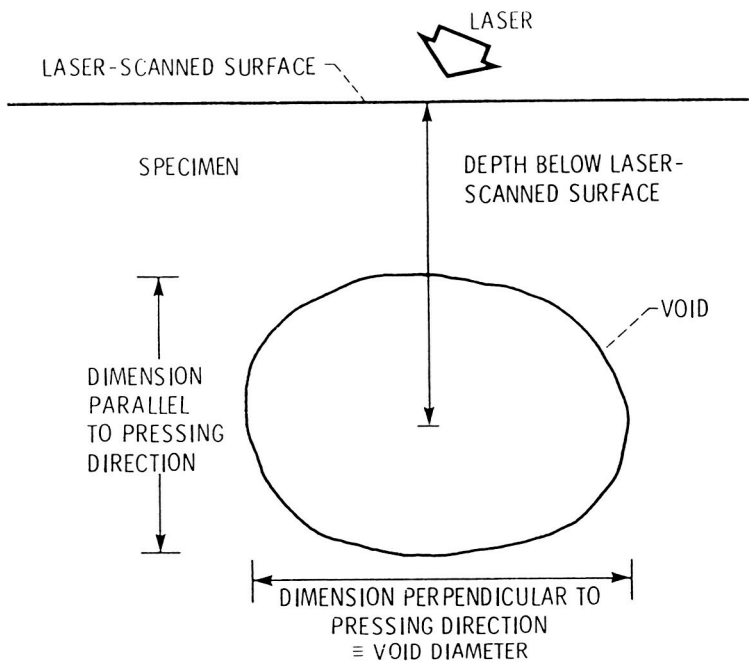
^dTRANSMISSION ELECTRON MICROGRAPH OF REPLICA OF METALLOGRAPHICALLY POLISHED AND ETCHED SECTION

^eSURFACE PROFILE (USING A 12.5 μm DIAMETER DIAMOND STYLUS) (PERPENDICULAR TO GRINDING MARKS FOR SPECIMEN WITH GROUND SURFACE).

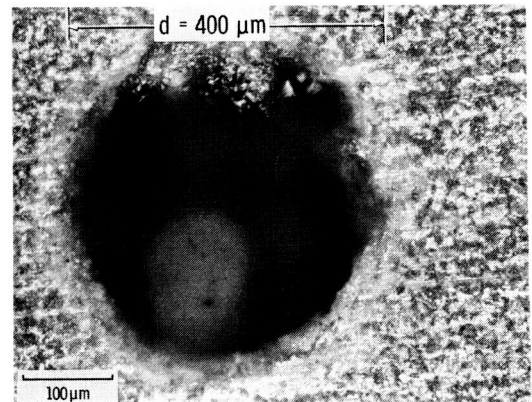
^fOPTICAL MICROGRAPH.

^gCHARACTERIZED AFTER SINTERING SPECIMEN AND EXPOSING VOIDS TO SURFACE.

The seeded internal voids were exposed to the surface by grinding. At this point, the void dimensions were measured optically, and the void depths at the various SLAM inspections were determined (Roth, 1987).



SEM MICROGRAPH (SILICON NITRIDE)

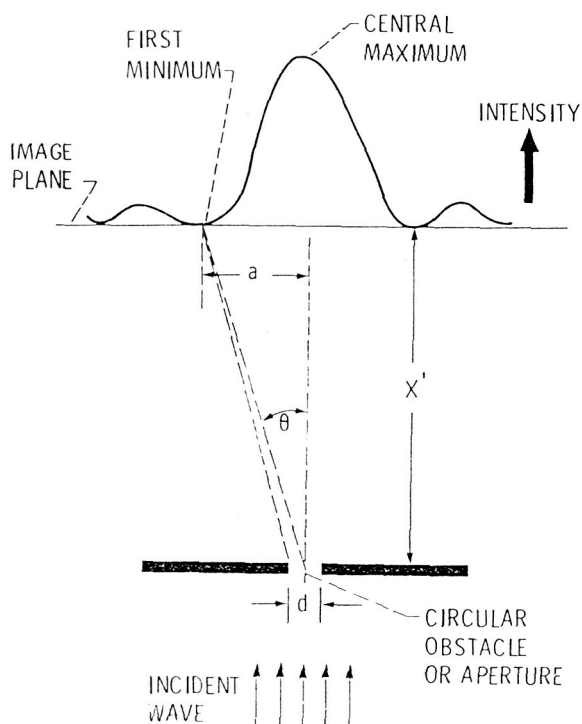


OPTICAL MICROGRAPH (SILICON NITRIDE)

CD-88-32543

ACOUSTIC IMAGE OF INTERNAL VOID

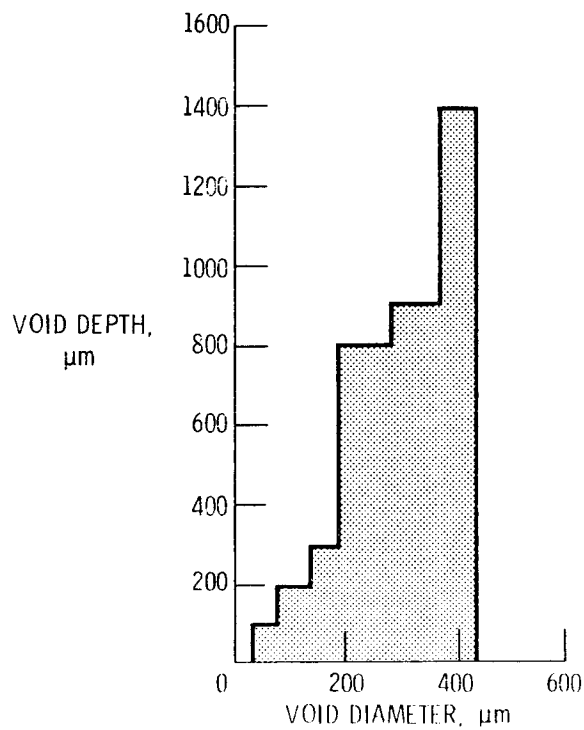
The acoustic image of an internal flaw often consists of a diffraction pattern rather than a facsimile image of the flaw. In this case, it is especially difficult to characterize the flaw. However, techniques have been investigated from which it is theoretically possible to predict flaw shape, size, and depth by using acoustic diffraction patterns (Generazio, 1986; Roth, 1986b and 1987). Measurements obtained from the acoustic images were used to obtain predictions of void diameter and depth (Roth, 1987).



CD-68-32544

PROBABILITY OF DETECTION OF INTERNAL VOIDS

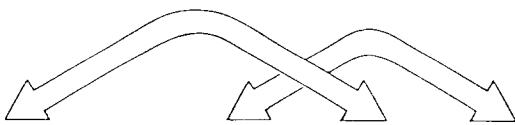
Probability-of-detection data for the seeded internal voids as a function of void diameter and void depth is shown (Roth, 1986b). The range of depths and diameters for which 90 percent or higher probability of detection (at a 95 percent confidence level) was achieved is indicated by the outlined region for sintered silicon nitride specimens (Roth, 1986).



CD 84 32545

PREDICTED VOID DEPTHS AND DIAMETERS USING SLAM

Predictions of depth and diameter were determined for 4 voids at 23 depths. The 23 predicted void depths deviated less than 70 percent from actual depths and 17 were within 20 percent of actual depths. Predicted void diameters deviated more than 100 percent from actual values in all cases but one (Roth, 1987). Examples are shown in the table.

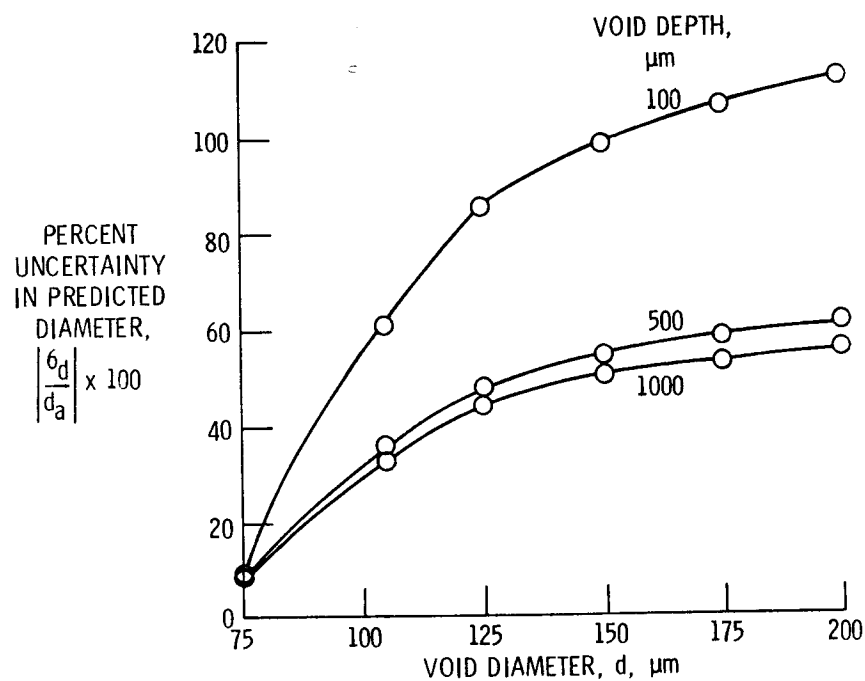


ACTUAL VOID DIAMETER, μm	AT	ACTUAL VOID DEPTH, μm	PREDICTED DIAMETER, μm	PREDICTED DEPTH, μm
403	AT	1897	1113	1917
252	AT	568	790	616
139	AT	197	571	153
30	AT	79	135	54

CD-88-32546

MEASUREMENT UNCERTAINTY

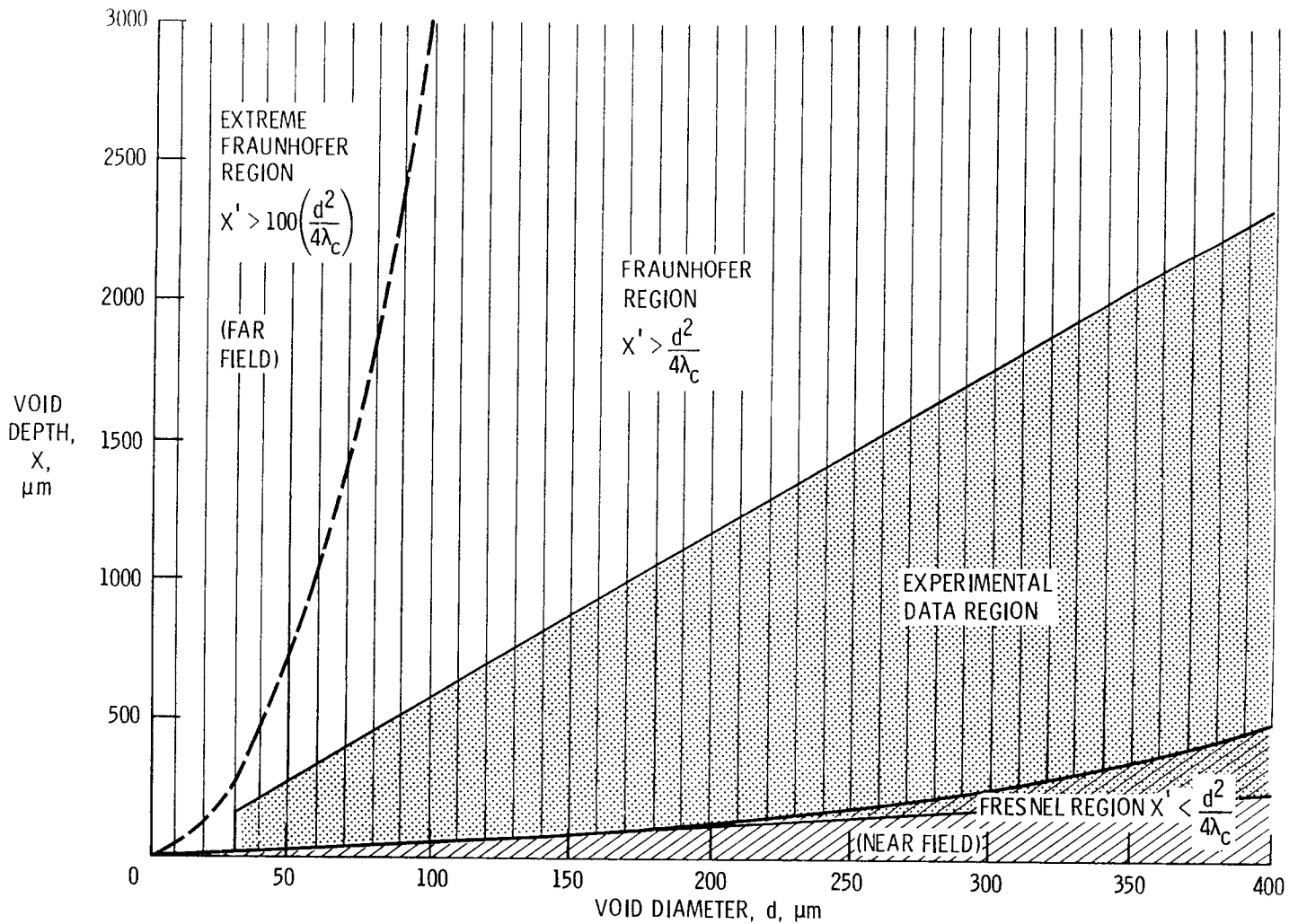
Measurements obtained from the acoustic images were used to obtain predictions of void diameter and depth. Precise measurements were not possible. Void diameter predictions were more severely affected by the measurement uncertainty than were void depth predictions. Measurement uncertainty was expected to increase with increasing void diameter and decreasing void depth (Roth, 1987).



CD-88-32547

VALIDITY OF RELATION USED TO PREDICT VOID DIAMETER

The range of void depths and diameters that produced discernible diffraction patterns is shown in the figure below in the area labeled "experimental data region." It is expected that for voids of these diameters and depths, the relation used to predict void diameter is of questionable validity. The relation is most valid for void depths and diameters in the "extreme Fraunhofer region" (far field). Extreme Fraunhofer conditions are difficult to approach with the 100-MHz SLAM configuration applied to typical ceramic specimens (Roth, 1987).



CD-88-32548

CONCLUSION

Probability of detection was determined for seeded internal voids in sintered silicon nitride specimens as a function of void size and depth. The acoustic images produced by the voids were used to obtain predictions of void size and depth.

The measurements taken from the acoustic images of the internal voids had large uncertainty associated with them (Roth, 1987). The measurement uncertainty severely affected the prediction of void diameter. Additionally, the relation used to predict void diameter may be of questionable validity for the conditions of this experiment. As a result, predicted void diameters were generally much larger than actual void diameters (Roth, 1987). The measurement uncertainty affected the prediction of void depth less severely. Hence, reasonable agreement was observed between predicted and actual void depths (Roth, 1987).

REFERENCES

- Baaklini, G.Y. and Roth, D.J., 1986, "Probability of Detection of Internal Voids in Structural Ceramics Using Microfocus Radiography," Journal of Materials Research, Vol. 1, No. 3, pp. 456-467. Also NASA TM-87164.
- Evans, A.G., 1984, "Aspects of the Reliability of Ceramics," Defect Properties and Processing of High-Technology Nonmetallic Materials, Ed. by J.H. Crawford, Jr., Y Chen, and W.A. Sibley, North Holland, New York, pp. 63-80.
- Generazio, E.R. and Roth, D.J., 1986, "Quantitative Flaw Characterization with Scanning Laser Acoustic Microscopy," Materials Evaluation, Vol. 44, No. 7, pp. 863-870.
- Heitman, P.W. and Khandelwal, P.K., 1983, "Development and Characterization of Ceramic Turbine Components," Ceramics for High-Performance Applications III: Reliability, Ed. by E.M. Lenoe, R.N. Katz, and J.J. Burke, Plenum Press, New York, pp. 645-664.
- Lenoe, E.M., 1983, "Recent Accomplishments and Research Needs in Structural Ceramics," Ceramics for High-Performance Applications III: Reliability. Ed. by E.M. Lenoe, R.N. Katz, and J.J. Burke, Plenum Press, New York, pp. 3-18.
- Roth, D.J. and Baaklini, G.Y., 1986b, "Reliability of Scanning Laser Acoustic Microscopy for Detecting Internal Voids in Structural Ceramics," Advanced Ceramic Materials, Vol. 1, No. 3, pp. 252-258. Also NASA TM-87222.
- Roth, D.J.; Klima, S.J.; Kiser, J.D.; and Baaklini, G.Y., 1986a, "Reliability of Void Detection in Structural Ceramics by Use of Scanning Laser Acoustic Microscopy," Material Evaluation, Vol. 44, No. 6, pp. 762-769.
- Roth, D.J.; Generazio, E.R.; and Baaklini, G.Y., 1987, "Quantitative Void Characterization in Structural Ceramics by use of Scanning Laser Acoustic Microscopy," Materials Evaluation, Vol. 45, No. 83, pp. 958-966.
- Salem, J.A. and Shannon, J.L., Jr., 1985, "Fracture Toughness of Si_3N_4 Measured with Short Bar Chevron-Notched Specimens," NASA TM-87153.
- Sanders, W.A and Baaklini, G.Y., 1986, "Correlation of Processing and Sintering Variables with the Strength and Radiography of Silicon Nitride," NASA TM-87251.
- Shannon, J.L., Jr.; Bubsev, R.T.; Muntz, D.; and Pierce, W.S., 1981, "Fracture Toughness of Brittle Materials Determined with Chevron Notch Specimens." Advances in Ceramic Research (Fracture '81), Ed. by D. Francois, Pergamon, New York, pp. 1127-1144.

NONDESTRUCTIVE EVALUATION OF SINTERED CERAMICS

George Y. Baaklini, Stanley J. Klima,
and William A. Sanders*
Structural Integrity Branch
NASA Lewis Research Center

ABSTRACT

Radiography and several acoustic and thermoacoustic microscopy techniques are investigated for application to structural ceramics for advanced heat engines. A comparison is made of the results obtained from the use of scanning acoustic microscopy (SAM), scanning laser acoustic microscopy (SLAM), and thermoacoustic microscopy (TAM). These techniques are evaluated on research samples of green and sintered monolithic silicon nitrides and silicon carbides in the form of modulus-of-rupture (MOR) bars containing deliberately introduced flaws. Strengths and limitations of the techniques are described, with the emphasis being on statistics of detectability of flaws that constitute potential fracture origins. Further, it is shown that radiographic evaluation and guidance helped develop uniform high-density Si_3N_4 MOR bars with improved four-point flexural strength (875, 544, and 462 MPa at room temperature, 1200 °C, and 1370 °C, respectively) and reduced scatter in bend strength.

*Materials Division.

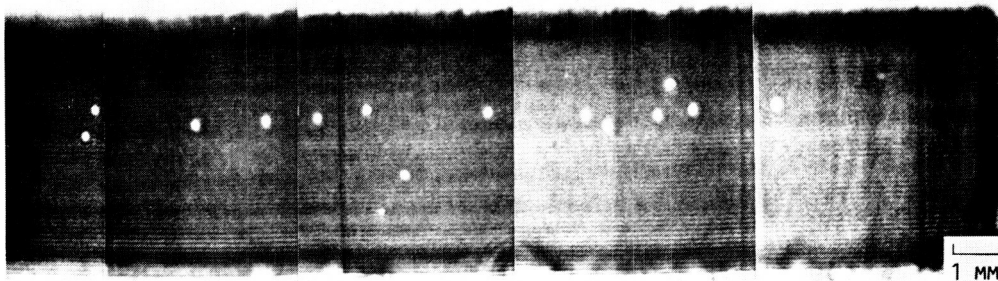
OVERVIEW

ORIGINAL PAGE IS
OF POOR QUALITY

ACOUSTIC MICROSCOPY

SAM uses a single transducer to generate and receive ultrasonic energy (Nikoonahad, 1984). Good resolution and sensitivity are achieved by focusing moderately high-frequency ultrasonic energy (30 to 100 MHz) on a small spot, raster-scanning the lens with respect to the sample, and then time-gate sampling the reflected ultrasonic pulse amplitude. Any features that produce an acoustic impedance mismatch within the sample, or that produce a change in acoustic impedance at the specimen surface, can cause detectable variations in the digitized and stored spatial map of reflected signal amplitude. Images of microflaws are generally sharp. Depth location of flaws is easy to determine. Access is needed to only one side of the test sample. Further, SAM can be adapted to handle curved surfaces. Detection and resolution of microflaws are affected by (1) surface roughness (2) ultrasound depth of penetration, and (3) the aperture size of the lens. SAM images are not generally displayed in real time because computer time is needed to process the entire block of data used to produce the image.

SAM IMAGE OF VOIDS IN A SILICON NITRIDE MOR BAR



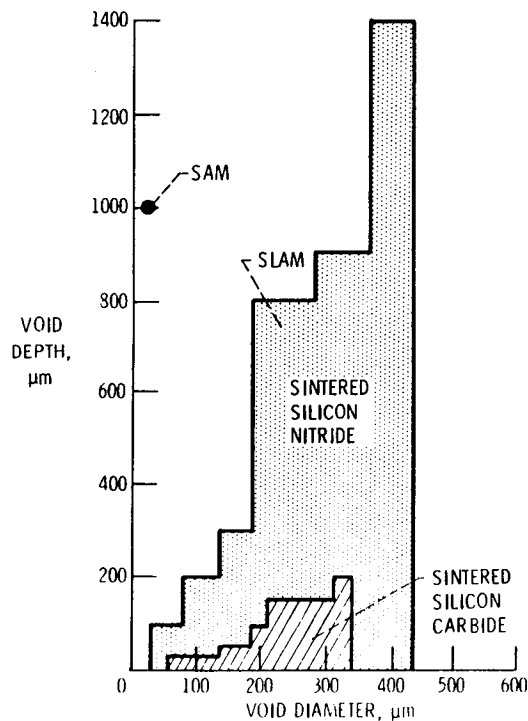
- SEEDED VOIDS (WHITE SPOTS) 20 μm DIAMETER, 1 mm DEEP
- DIAMOND GROUND SURFACE, 2 μm FINISH
- ULTRASONIC REFLECTION MODE
- 50 MHz TRANSDUCER, SPHERICALLY FOCUSED

CD-88-32329

DETECTION OF VOIDS WITH ACOUSTIC MICROSCOPY

Scanning laser acoustic microscopy (SLAM) uses 100 MHz ultrasonic waves that are transmitted through the specimen and are modulated by material surface and internal characteristics. The relative intensity and phase of the waves are detected by a laser beam that is raster-scanned over an area approximately 2 mm^2 . Features such as cracks, voids, density variations, etc. are displayed in real time on a video monitor at $\times 100$. SLAM images are affected by the surface roughness of the test object. Unlike SAM, SLAM has a limited capability for handling complex shaped objects, and also requires access to opposite sides of the sample. The plot below summarizes SLAM probability of detection (POD) data obtained for internal voids in specimens with diamond-ground surfaces (Roth and Baaklini, 1986). The boundaries of the bar graphs indicate the minimum void sizes and maximum depths (from the laser-scanned surface) at which the 0.90/0.95 POD/confidence level was achieved. Also shown is a single data point representing preliminary results obtained with the SAM technique. All of the 38 voids (nominal diameter $20 \text{ }\mu\text{m}$) were detected 1 mm below the surface of silicon nitride samples, yielding a POD better than 0.90/0.95 (Klima et al., 1986).

90% PROBABILITY OF DETECTION AT 95% CONFIDENCE LIMIT

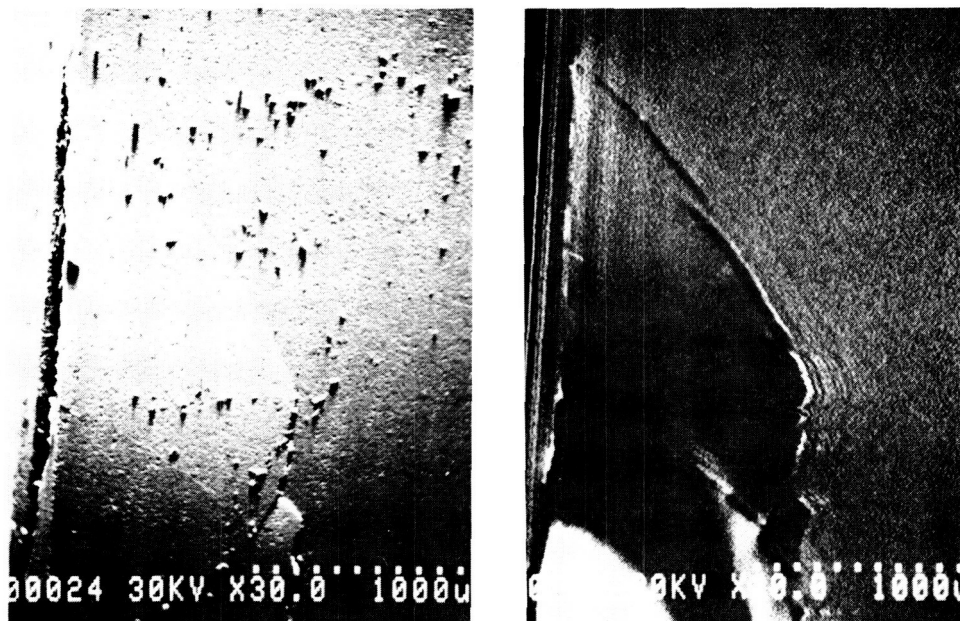


CD-88-32330

POSTER PRESENTATION

THERMOACOUSTIC MICROSCOPY

Thermoacoustic microscopy (TAM) measures relative differences in surface and near-surface thermal properties of the material being evaluated (Rosencwaig, 1980). The absorption of intensity-modulated electromagnetic radiation (usually a laser or an electron beam), focused at any point on the sample, gives rise to localized cyclic heating and cooling that, in turn, generates elastic waves at the modulation frequency. The amplitude and phase of these waves can be measured either at another location on the specimen surface by a piezoelectric crystal in contact with the specimen, or in the surrounding gas medium by a non-contacting method using a sensitive microphone. A sensitive, high-resolution image representing varying thermal characteristics of the sample can be generated point-by-point using this technique. Its applicability to engine parts can be limited by vacuum requirements, coating requirements, and shape complexity. By utilizing the electron beam method, TAM proved to be useful for detecting tight surface cracks and pits on research samples, as shown below (Klima et al., 1986).



CD-88-32331

DETECTABILITY OF FRACTURE-CAUSING TYPE OF FLAWS VIA RADIOGRAPHY AND ACOUSTIC MICROSCOPY

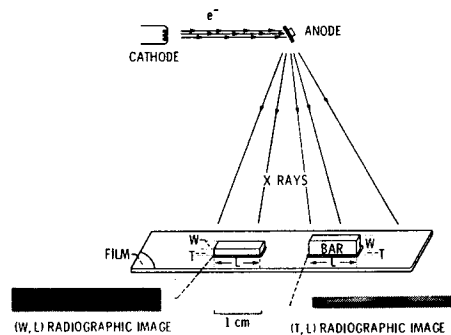
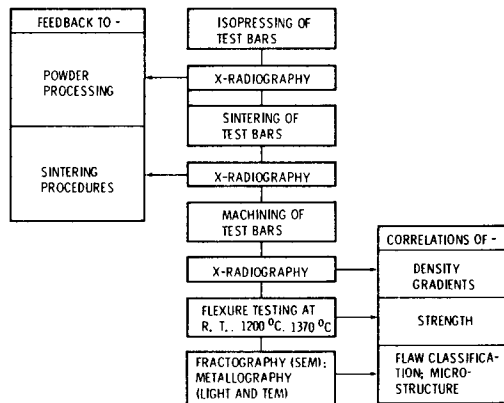
A comparison is made between acoustic and radiographic techniques for detecting fracture-causing defects such as voids, cracks, and inclusions. In general, acoustic microscopy is not applicable to green ceramics because either (1) the sample is damaged by the presence of a liquid-coupling medium or (2) the surface of the sample is damaged by the intensity of the laser or electron beam energy sources. However, acoustic microscopy can be successfully used to characterize small areas of sintered ceramic parts. Radiographic techniques are suitable for characterizing both green and sintered ceramics.

TECHNIQUE	DEFECT TYPE	RESOLUTION	LIMITATIONS	COMPONENT APPLICABILITY
SLAM	CRACKS	UNDEFINED	SURFACE ROUGHNESS, MATERIAL DEPENDENT, NEAR SURFACE	THIN SECTION, SIMPLE SHAPES
	VOIDS	25 μ m		
	INCLUSIONS	25 μ m		
SAM	CRACKS	UNDEFINED	SURFACE ROUGHNESS	SMALL AREAS
	VOIDS	20 μ m		
	INCLUSIONS	20 μ m		
TAM (LASER)	VOIDS	25 μ m	SURFACE CHEMISTRY, ABSORPTIVITY, NEAR SURFACE	SMALL AREAS
	INCLUSIONS	25 μ m		
TAM (ELECTRON BEAM)	CRACKS	1 μ m WIDE	SURFACE ROUGHNESS, REQUIRES VACUUM, REQUIRES COATING, NEAR SURFACE	SIMPLE SHAPES, SMALL AREAS
	VOIDS	10 μ m		
	INCLUSIONS	10 μ m		
MICROFOCUS X RAY	CRACKS	ORIENTATION DEPENDENT	SMALL ABSORPTIVITY DIFFERENCES	FILM-UNIFORM THICKNESSES REAL TIME-COMPLEX GEOMETRIES, REDUCED SENSITIVITY
	VOIDS	1-2%		
	INCLUSIONS	.5%		
	GRADIENTS	2%		
CT X RAY	CRACKS	ORIENTATION DEPENDENT	SLOW	COMPLEX GEOMETRIES
	VOIDS	< < 1%		
	INCLUSIONS	< < .5%		
	GRADIENTS	< < 2%		

CD-88-32332

RADIOGRAPHIC EVALUATION OF NASA 6Y Si₃N₄

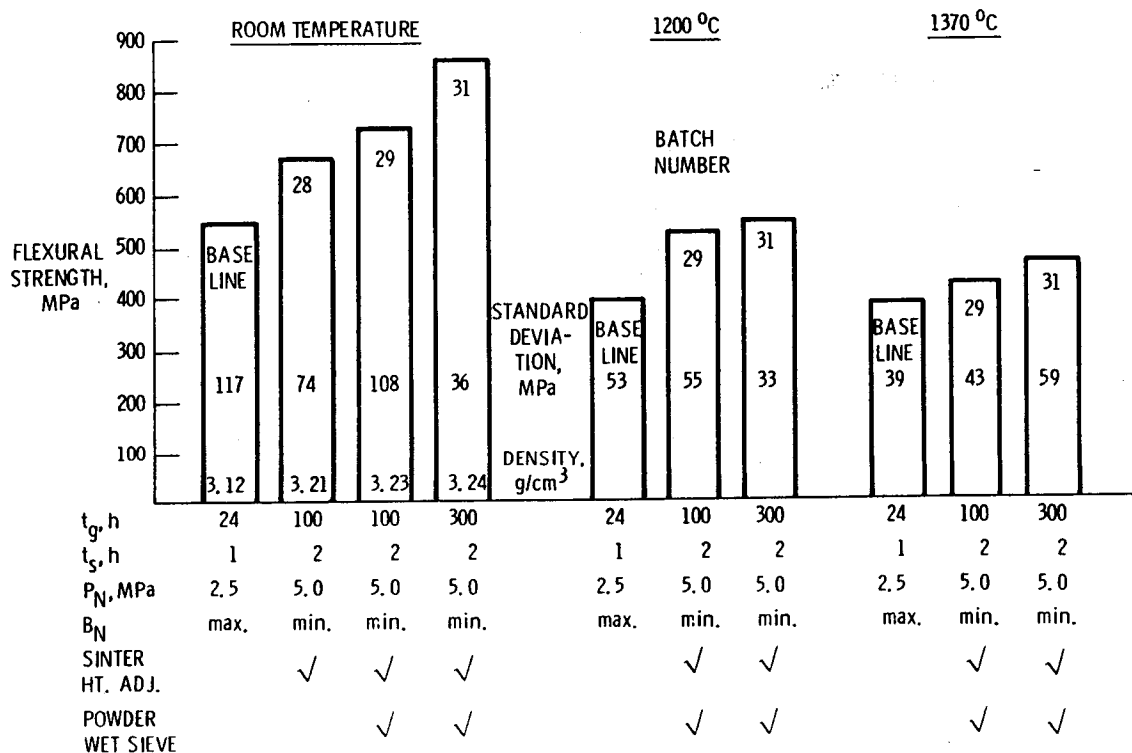
In mechanical properties of Si₃N₄, scatter is generally attributed to defects and inhomogeneities occurring during powder processing and/or during fabrication of parts (Bowen, 1980, and Evans, 1982). Based on preliminary x-radiographic characterization work on Si₃N₄ by Klima (1986), a program was undertaken to systematically investigate density-gradient, flexural-strength relationships as affected by sintering and powder-processing variables for sintered Si₃N₄. All batches were radiographically evaluated at all stages of fabrication. Test bars were radiographed in the (W,L) and (T,L) modes where x rays are transmitted through the thickness and the width of the bar, respectively.



CD-88-32333

COMBINED EFFECT OF MODIFIED PROCESSING/SINTERING PROCEDURES ON THE FLEXURAL STRENGTH OF NASA 6Y Si₃N₄

The sintering variables were (1) temperature (2) nitrogen pressure (P_N) (3) time (t_s) (4) spacer contact area (BN), and (5) furnace position. The powder-processing variables were (1) grinding time t_g and (2) inclusion or exclusion of powder wet-sieving procedures. The cumulative positive effects of all the variables on flexural strength are shown below. (For more information, see Sanders and Baaklini (1988).) In processing from batch to batch (baseline to 28 to 29 to 31), the room-temperature strength continually increased, with an overall improvement of 56 percent, and more than a threefold reduction in the standard deviation. The summary of individual parameter effects on room-temperature strength is shown in the table below. Strength improved 28 and 21 percent for 1200 and 1370 °C, respectively. All successive improvements in the mechanical properties were guided by x-radiographic characterization.



CD-88-32335

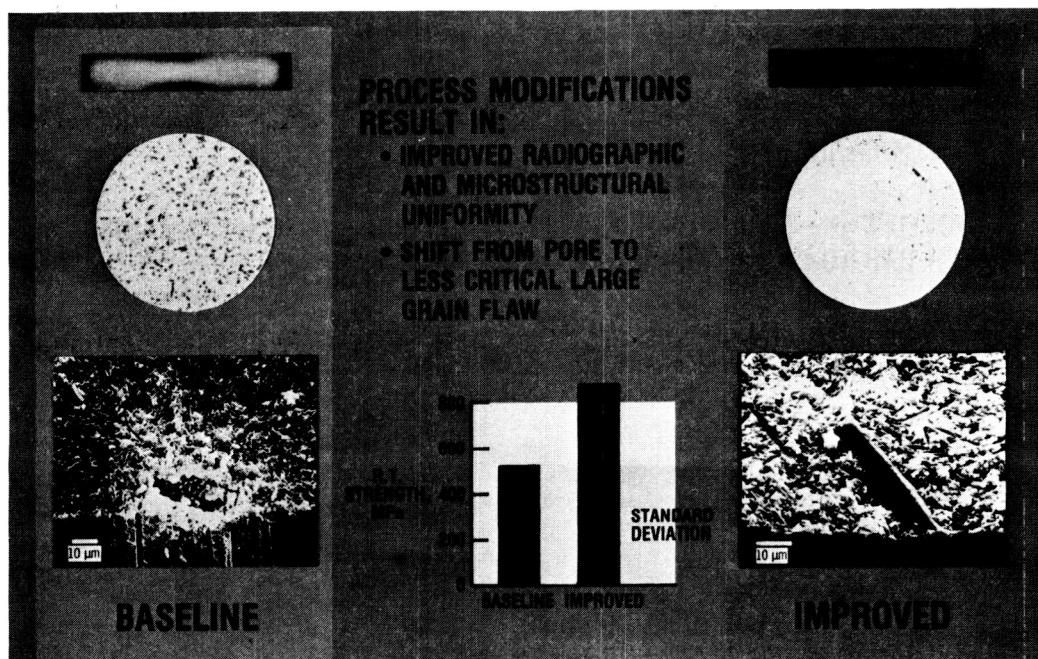
INDIVIDUAL PARAMETER EFFECTS ON ROOM-TEMPERATURE STRENGTH

VARIABLE	LEVELS	ROOM-TEMPERATURE STRENGTH CHANGES, MPa	CONCLUSIONS
BN SPACER CONTACT	MAX → MIN	+197, +157	EXTREMELY HELPFUL
SINTERING TIME	1 → 1.25 HR 1 → 1.5 HR 1 → 2 HR	+129 +87 +145	} VERY HELPFUL
SINTERING TEMPERATURE	2050 → 2140 °C	-117	
SIEVING	NO → YES	+60	
GRINDING TIME	24 → 100 HR 24 → 300 HR 100 → 300 HR	-61, -13 +41, +54 +102, +67, +62, +125	} VERY HELPFUL
SINTERING HEIGHT	LOW → HIGH	+24	
NITROGEN PRESSURE	2.5 → 3.5 MPa 3.5 → 5.0 MPa 2.5 → 5.0 MPa	-205 +45, +29, +24 -181	
			} INCONCLUSIVE

CD- 88-32334

NASA 6Y SINTERED SILICON NITRIDE IMPROVED BY RADIOGRAPHICALLY-GUIDED PROCESSING CHANGES

The successful use of conventional x-radiography in guiding the fabrication process resulted in denser and more uniform Si_3N_4 over the baseline materials. Previously dominant failure-causing voids were replaced by large grains, which are less detrimental to strength properties. The improved structure can be attributed to (1) increased powder fineness that improves sinterability and uniformity (2) powder wet sieving that results in reduction of agglomerates and certain impurity particles (3) minimizing BN spacer contact that results in more uniform densification as a consequence of more uniform heating (4) an increase in sintering time from 1 to 2 hr, thus improving density and uniformity, and (5) raising sinter cup height to reduce the top bar to bottom bar temperature gradient.



CD-88-32336

SUMMARY

- **ACOUSTIC MICROSCOPY CAN BE USED TO CHARACTERIZE SMALL AREAS OF SINTERED CERAMIC PARTS, BUT IT IS NOT APPLICABLE TO GREEN PARTS**
- **RADIOGRAPHY IS SUITABLE FOR CHARACTERIZING BOTH GREEN AND SINTERED CERAMIC PARTS**
- **RADIOGRAPHY IS VERY BENEFICIAL IN GUIDING POWDER PROCESSING AND SINTERING PARAMETER CHANGES FOR IMPROVED Si_3N_4**
 - IMPROVED Si_3N_4 EXHIBITED HIGHER DENSITY, LOWER DENSITY GRADIENT, AND BETTER BAR-TO-BAR UNIFORMITY**
 - IMPROVED Si_3N_4 POSSESSES LESS SCATTER IN BEND STRENGTH, IMPROVED STRENGTH, AND LESS CRITICAL DOMINANT FLAW**

CD-88-32337

REFERENCES

- Bowen, H.K., 1980, "Basic Research Needs on High Temperature Ceramics for Energy Applications," Mater. Sci. Eng., Vol. 44, pp. 1-56.
- Evans, A.G., 1982, "Consideration of Inhomogeneity Effects in Sintering," J. Am. Ceram. Soc., Vol. 65, No. 10, pp. 497-501.
- Klima, S.J., 1986, "NDE of Advanced Ceramics," Mater. Eval., Vol. 44, No. 5, pp. 571-576.
- Klima, S.J., Baaklini, G.Y., and Abel, P.B., 1986, "Nondestructive Evaluation of Structural Ceramics," NASA TM-88978, presented at the 24th Automotive Technology Development Contractors' Coordination Meeting, Dearborn, MI, Oct. 27-30.
- Nikoonahad, M., 1984, "Reflection Acoustic Microscopy for Industrial NDE," in Research Techniques in Nondestructive Testing, R.S. Sharpe (ed.), Academic Press, London, Vol. 7, pp. 217-257.
- Rosencwaig, A., 1980, Photoacoustics and Photoacoustic Spectroscopy, John Wiley and Sons, New York.
- Roth, D.J., and Baaklini, G.Y., 1986, "Reliability of Scanning Laser Acoustic Microscopy for Detecting Internal Voids in Structural Ceramics," Adv. Ceram. Mater., Vol. 1, No. 3, pp. 252-258.
- Sanders, W.A., and Baaklini, G.Y., 1988, "Correlation of Processing and Sintering Variables with the Strength and Radiography of Silicon Nitride," Adv. Ceram. Mater., Vol. 3, No. 1, pp. 88-94.

FRACTURE MECHANICS

SESSION OVERVIEW

John L. Shannon, Jr.
Fatigue and Fracture Branch
NASA Lewis Research Center

INTRODUCTION

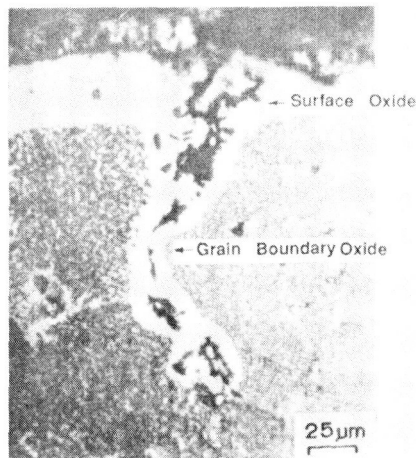
The topical areas of fatigue crack initiation, crack growth, and fracture are treated in Sessions 2 and 8 of this Symposium. Not all aspects of these complicated subjects have been studied. Therefore, past and current results are presented with the admission that much has yet to be learned.

PRECEDING PAGE BLANK NOT FILMED

GRAIN BOUNDARY OXIDATION AND LOW CYCLE FATIGUE AT ELEVATED TEMPERATURES

Fatigue life consists of crack initiation and subsequent propagation. Accurate life prediction requires a methodology for quantifying these two fatigue processes.

The two predominant high-temperature low cycle fatigue (LCF) damage mechanisms are creep and oxidation. The question that arises is - Which mechanism dominates at the temperature of concern? Understanding grain boundary oxidation kinetics, morphologies, and statistical distributions, plus factors which influence them for a range of practical structural alloys, is an important part of the work described in this Session by Liu and Oshida of Syracuse University. The principal product of their work is a method for extrapolating laboratory oxidation data to the prediction of life of engineering structures.

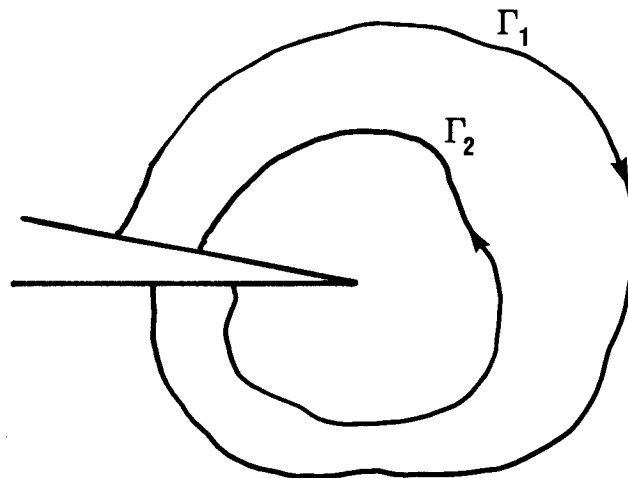


CD-88-33278

ORIGINAL PAGE IS
OF POOR QUALITY

ELASTOPLASTIC CRACK PROPAGATION AT ELEVATED TEMPERATURES

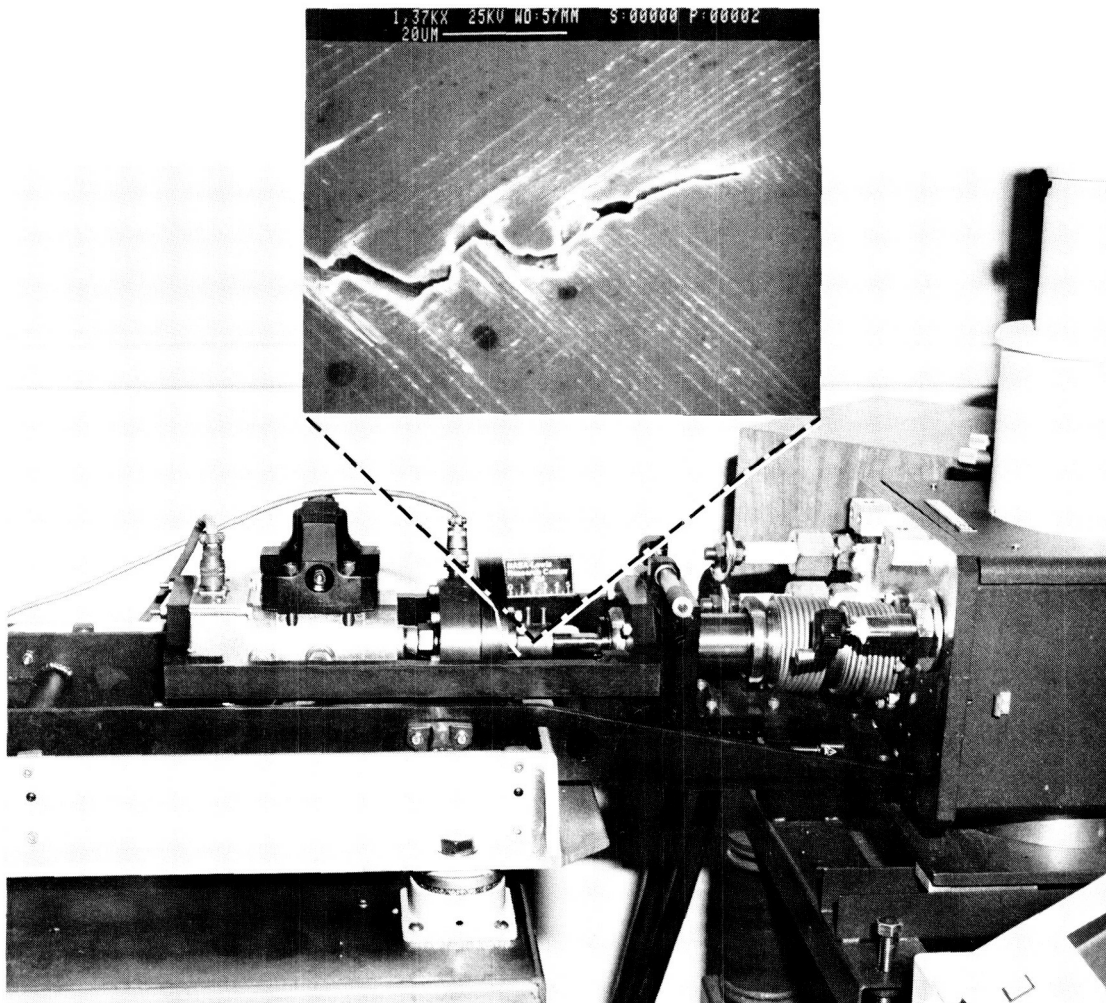
The work reported in this segment has the objective of developing methods for characterizing and predicting crack growth at elevated temperatures considering nonlinear material behavior (both time-dependent and time-independent), thermal gradients, and thermomechanical cycling. This work is being done at General Electric, Aircraft Engine Group, Evendale, Ohio, with the specific purpose of predicting crack growth rates and critical crack sizes in the hot section environment of turbine engines, relating the processes that control crack growth in the immediate vicinity of the crack tip to parameters that can be calculated from remote quantities such as forces, stresses, or displacements. The approach is to survey and compare, in comprehensible terms, the many current path-independent integrals; to computer test at least five of these using a common, simple problem; to validate them by laboratory experiment using extensive crack displacement measurements, first on an analog material at moderate temperatures (not exceeding 500 °F) and then a nickel-base alloy at temperatures approaching 2000 °F.; and finally to use the developed methodology to predict life of model structures in a laboratory situation where crack propagation within temperature gradients, with or without thermomechanical cycling and creep, is the operative life consuming process.



CD-88-33279

INSITU FATIGUE LOADING STAGE INSIDE A SCANNING ELECTRON MICROSCOPE

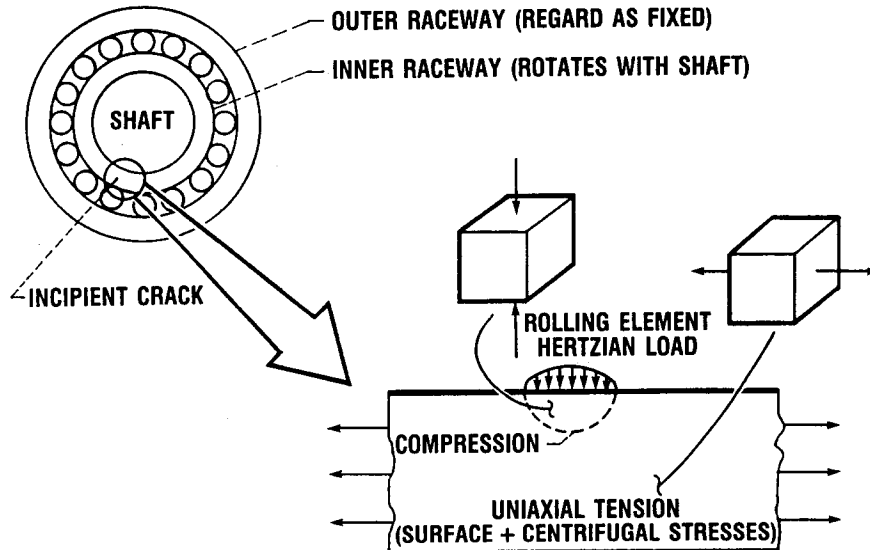
This work, which is being done by Telesman and Kantzos of Lewis and Brewer of the Army Propulsion Directorate (located at Lewis), recognizes the difficulty of explaining and predicting fatigue life without fully understanding the early stages of fatigue, which accounts for the greater part of total fatigue life. Telesman et al. describe a unique facility for observing in real time and at high magnification and resolution the damage mechanisms associated with fatigue crack initiation and propagation. The facility consists of a fatigue loading stage contained within a scanning electron microscope and operates at both ambient and elevated temperatures. Fatigue damage mechanisms are observed and coupled with quantitative data, such as crack tip strain field, to produce an improved understanding of fatigue behavior and life prediction methodology for engineering structures.



CD-88-33280

MIXED-MODE FRACTURE MECHANICS

Fatigue crack initiation and propagation under mixtures of loading modes I and II are operative in aircraft engine bearings. Current aircraft engines operate at load levels beneath concern. Tomorrow's aircraft engines, on the other hand, are intended to operate at load levels where catastrophic failure is a possibility. Experimental and analytical approaches to this potential problem are described by Buzzard and Ghosn of Lewis.

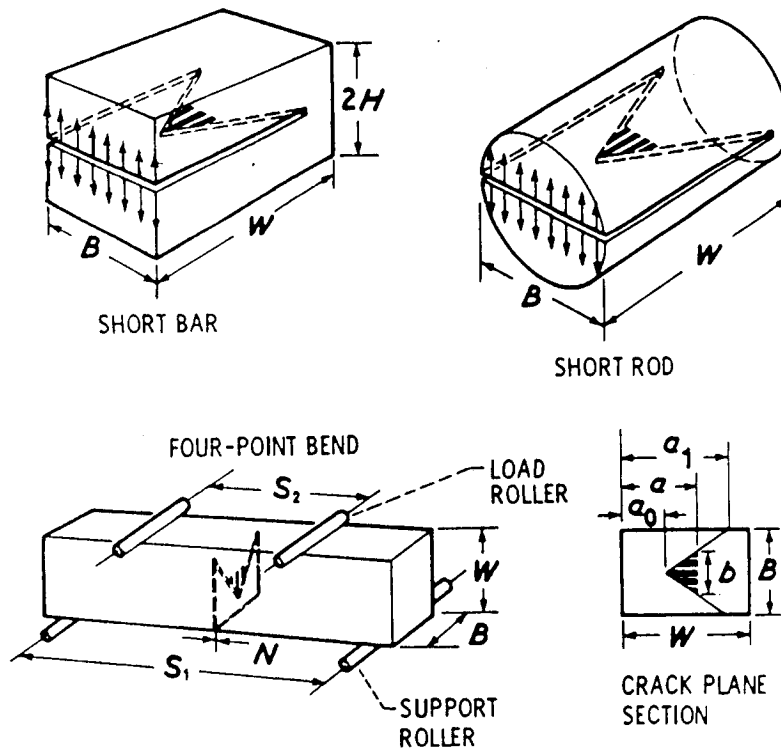


- ROLLING ELEMENT LOAD IS ADDED TO UNIAXIAL LOAD
- SUBSURFACE VOID FORMS
- CRACK AT SURFACE-SURFACE SPALLS
- CRACK GROWS DOWNWARD-RACE FAILS

CD-88-33281

FRACTURE TECHNOLOGY FOR BRITTLE MATERIALS

Research began at Lewis in 1977 on the challenge of measuring the fracture resistance of brittle nonmetallic materials in terms that can be used directly in design. The accomplishments toward standardizing a test method for measuring the plane strain fracture toughness of ceramics, coupled with observations of variable crack resistance behavior, are presented. Future directions are outlined.



CD-88-33282

FRACTURE TECHNOLOGY FOR BRITTLE MATERIALS

Jonathan A. Salem
Fatigue and Fracture Branch
NASA Lewis Research Center

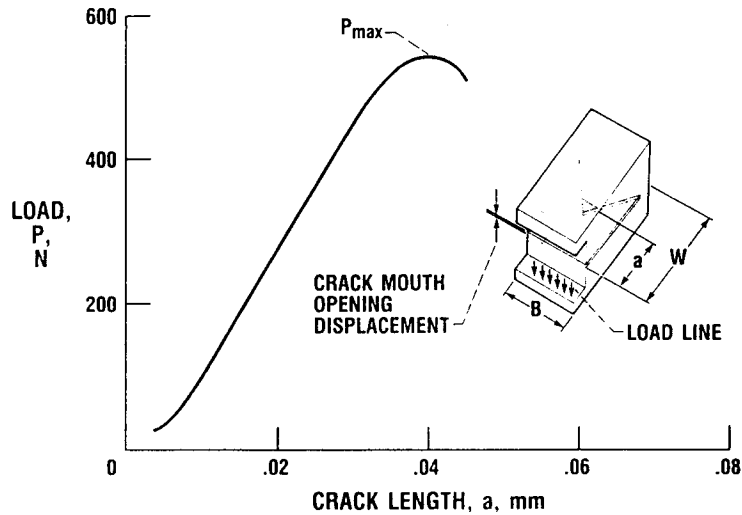
ABSTRACT

Ceramics materials have the potential for use in high-temperature, fuel-efficient engines. However, because these materials are brittle, their fracture characteristics must be well documented prior to their application. Thus Lewis is working to understand the fracture and strength properties of brittle ceramic and ceramic matrix materials. An understanding of fracture properties aids both designers who are attempting to design high-temperature structures and materials scientists who seek to design more temperature-resistant materials. Both analytical and experimental approaches to fracture analysis are being taken (Bubsey et al., 1983). Methods for testing fracture toughness, crack growth resistance, and strength are being developed (Salem and Shannon, 1987; Salem et al., 1988). The failure mechanisms at both room and elevated temperatures are also being investigated (Jenkins et al., 1988). Such investigations aid materials scientists in developing better high-temperature materials. Of concern is the anisotropy of ceramic materials and the experimental verification of ceramic design codes that will allow brittle material behavior to be accurately predicted at high temperature.

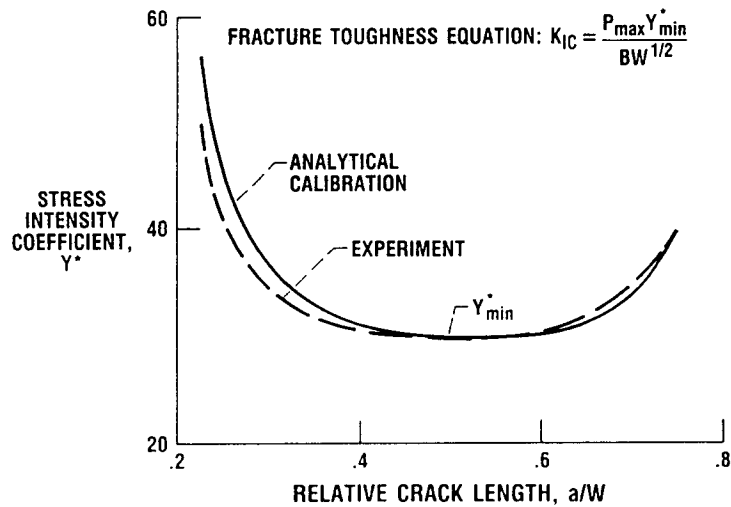
OVERVIEW

FRACTURE TOUGHNESS TEST METHOD FOR CERAMICS

Ceramic materials have potential applications in high-temperature, fuel-efficient engines, but these materials are brittle. Thus Lewis has developed a fracture testing methodology for brittle materials (Bubsey et al., 1983). The procedure accurately measures the fracture toughness of brittle, flat, crack-growth-resistant materials (Salem and Shannon, 1987).



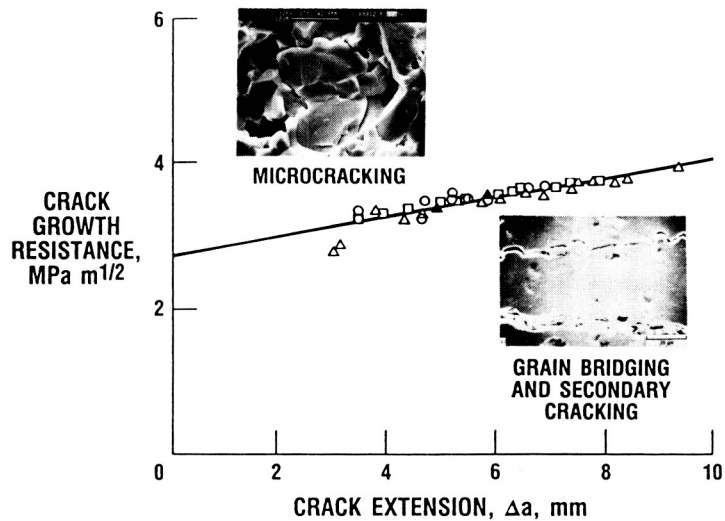
CD 88-31869



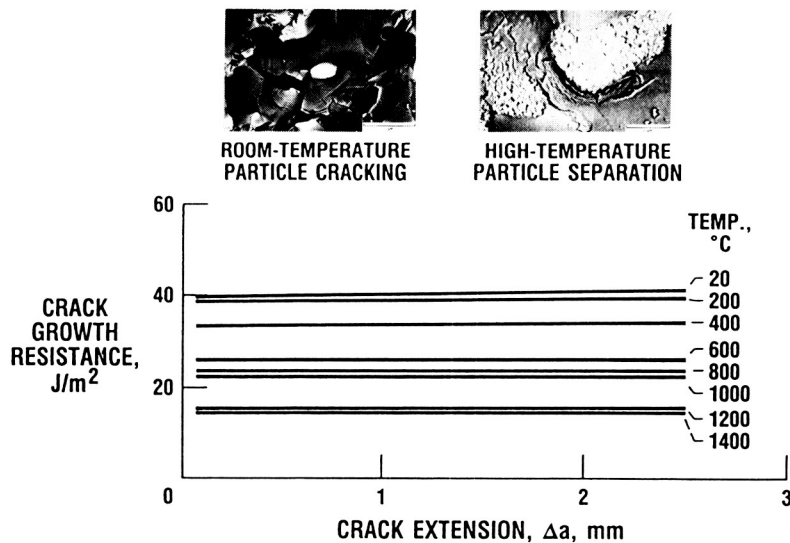
CD 88-32466

TOUGHENING MECHANISMS IN CERAMICS

The development of more crack-growth-resistant ceramic materials for use in high-temperature structures requires an understanding of energy-dissipative failure mechanisms. If these mechanisms are understood and related to the material's properties, better materials can be manufactured. In contrast to metals, where the energy-dissipative process that produces toughness is deformation accompanied by cracking, ceramics adsorb energy by plastic microcracking, crack surface friction, or both (Jenkins et al., 1988; Salem et al., 1988).



CD-88-31870

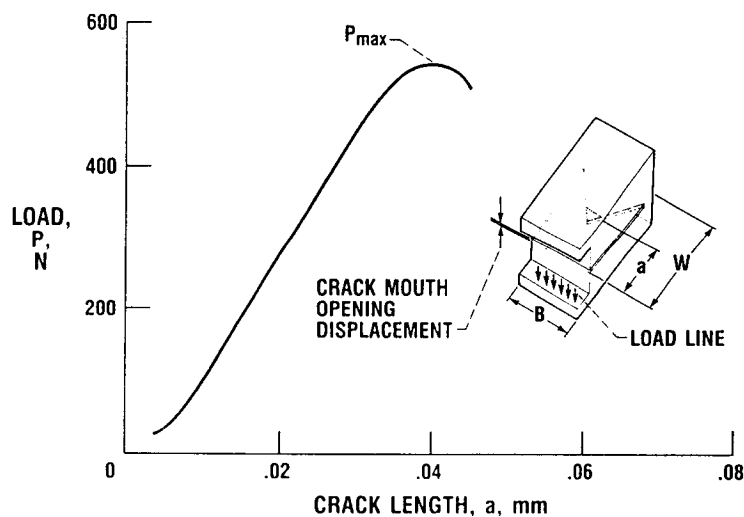


CD-88-32467

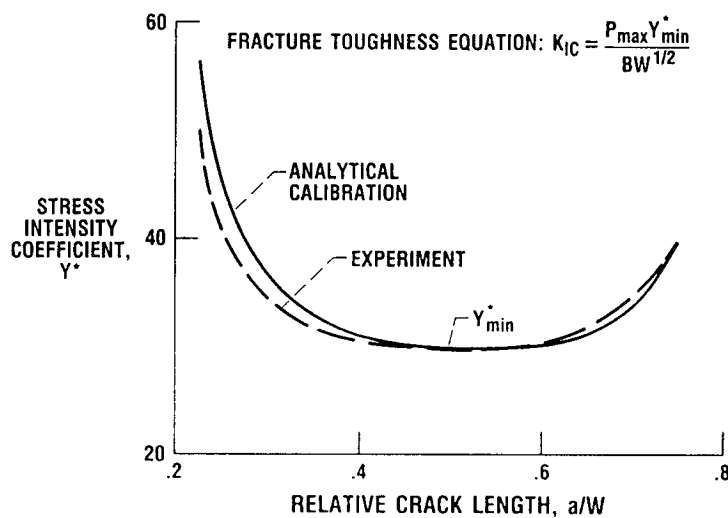
POSTER PRESENTATION

FRACTURE TOUGHNESS TEST METHOD FOR CERAMICS

Ceramic materials have potential applications in high-temperature, fuel-efficient engines, but these materials are brittle. Thus Lewis has developed a fracture testing methodology for such brittle materials (Bubsey et al., 1983; Salem and Shannon, 1987). The test specimen and the experimental load displacement record used to calculate the material's fracture toughness K_{IC} are shown below. The calculation defined in the lower graph involves the use of an experimental or analytical calibration known as a stress intensity coefficient Y^* (Munz et al., 1980). The coefficients are dependent on the specimen geometry and the loading configuration. The unique aspect of this method is that it does not require measurement of the crack length, as most test methods do.



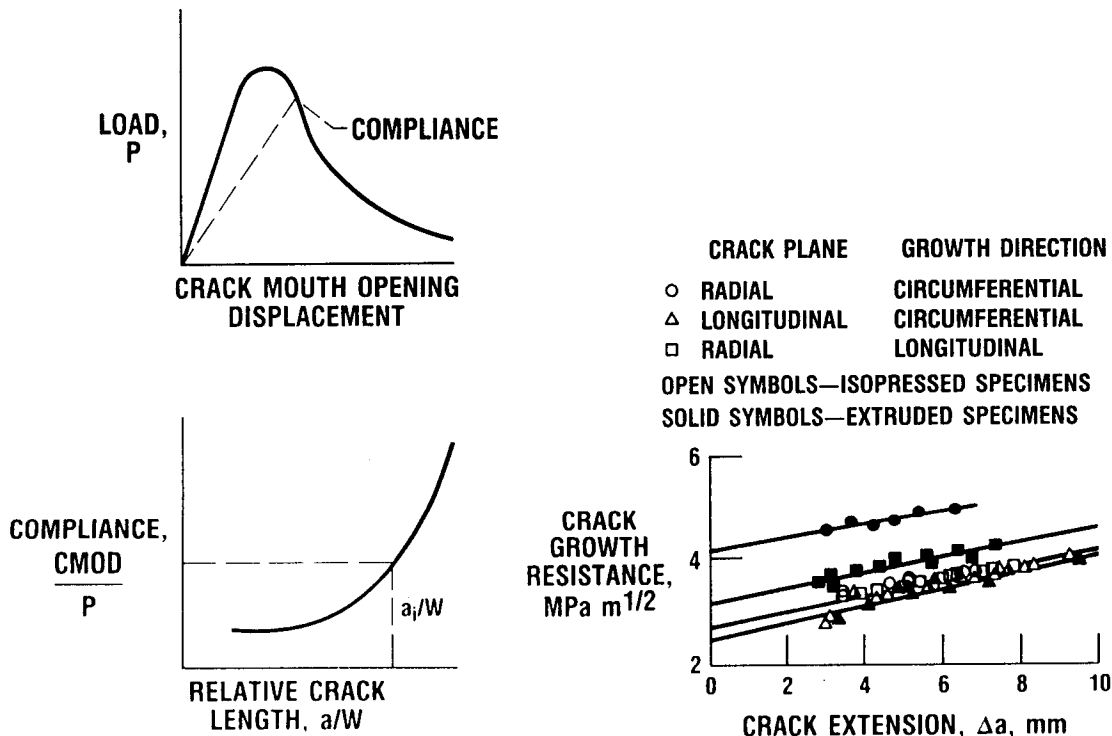
CD 88 31869



CD 88 32466

CRACK GROWTH RESISTANCE OF CERAMICS

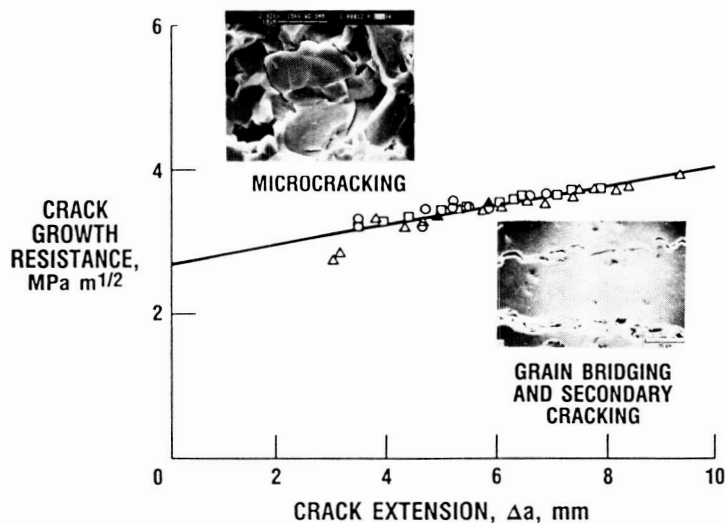
Brittle ceramic materials must be able to withstand crack-like damage. This ability is often referred to as "crack growth resistance." To determine the level of crack growth resistance in ceramics, Lewis has applied fracture mechanics measurement techniques to ceramics (Salem et al., 1988). The crack mouth opening displacement behavior of a specimen under load, or its compliance, is measured as shown below. The compliance is used with compliance - crack length relations to determine the crack length as shown in the lower left-hand graph. The crack growth resistance of the material can be calculated from the crack length and stress intensity coefficients (previous page). Results for various orientations of an extruded Al_2O_3 ceramic are also illustrated here.



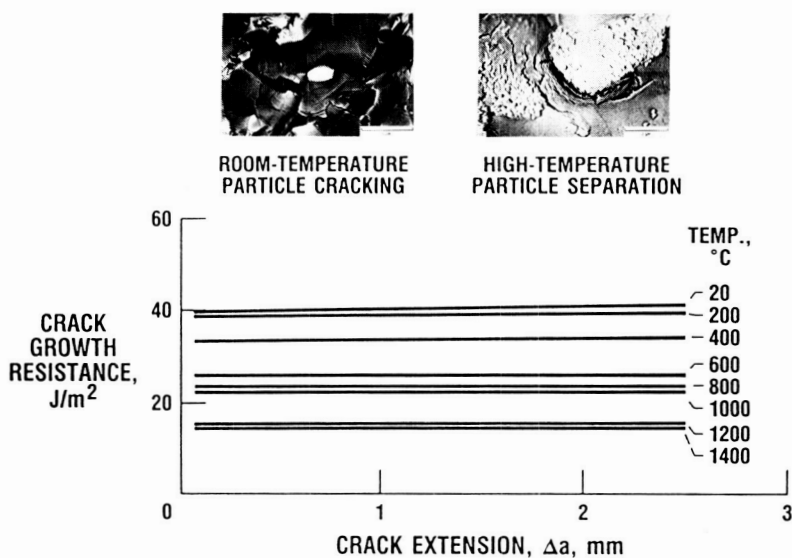
CD 88-31871

CRACK-GROWTH-RESISTANCE MECHANISMS IN CERAMICS

The development of more crack-growth-resistant ceramic materials for use in high-temperature structures requires an understanding of energy-dissipative failure mechanisms. If these mechanisms are understood and related to the material's properties, better materials can be manufactured. In contrast to metals, where the energy-dissipative process that produces toughness is plastic deformation accompanied by cracking, ceramics adsorb energy by microcracking, crack surface friction, or both. The upper graph shows microcracking, bridging, and secondary cracking in an alumina ceramic that exhibits rising crack growth resistance (Salem et al., 1988). Although cracking often imparts improved properties, in some cases it does not, as for the SiC/TiB₂ composite shown in the lower graph (Jenkins et al., 1988).



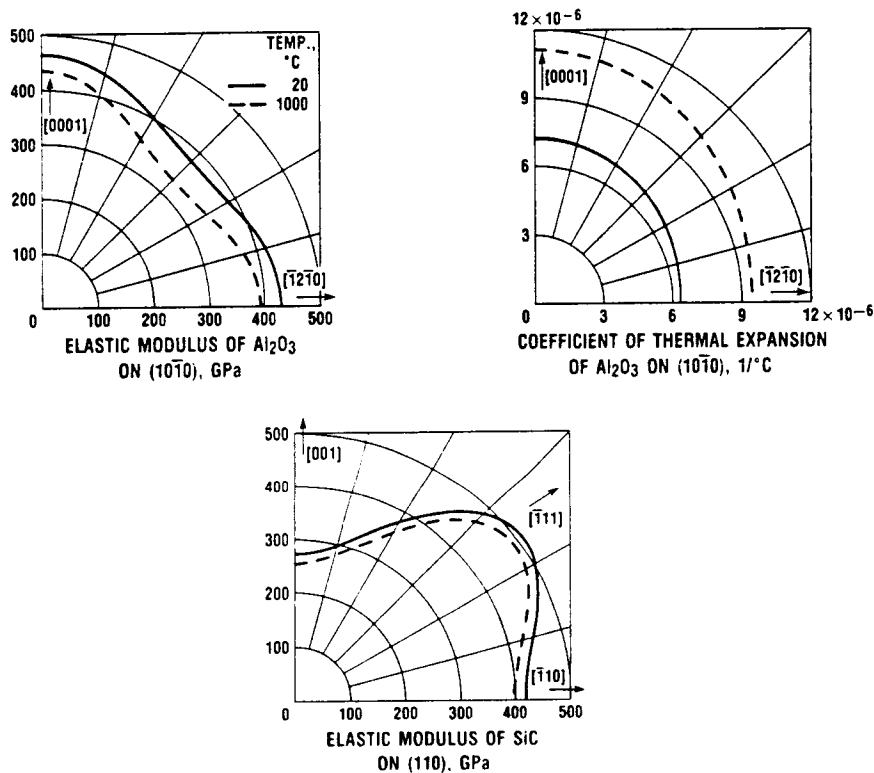
CD-88-31870



CD-88-32467

ANISOTROPY OF Al_2O_3 AND SiC WHISKERS FOR COMPOSITES

The introduction of ceramic whiskers into ceramic and metallic materials results in composite materials with unique properties. Single-crystal whiskers exhibit thermal and elastic anisotropy that can be used to tailor composite properties to the needs of designers. Thus an understanding of thermal and elastic properties of whiskers as a function of orientation is necessary in the design of ceramic- and metal-matrix composites. The property variations depend on the crystallographic structure of the material. Whiskers of Al_2O_3 have a hexagonal crystal structure, and both the elastic modulus and the coefficient of thermal expansion vary with crystal orientation, as shown in the upper two plots. SiC is a cubic crystal structure and therefore does not exhibit variation in the coefficient of thermal expansion but does exhibit a large variation in elastic modulus, as shown in the bottom figure (Salem et al., 1986).



CD-88-31872

REFERENCES

- Bubsey, R.T., Shannon, J.L., Jr., and Munz, D., 1983, "Development of Plane Strain Fracture Toughness Test for Ceramics Using Chevron Notched Specimens," in Ceramics for High Performance Applications, III: Reliability, E. Lenoe et al., eds., Plenum Publishing Corporation, pp. 753-771.
- Jenkins, M.G., Salem, J.A., and Seshadri, S.G., 1988, "Fracture Resistance of a TiB_2 Particle/ SiC Matrix Composite at Elevated Temperature," accepted by Journal of Composite Materials.
- Munz, D., Bubsey, R.T., and Srawley, J.E., 1980, "Compliance and Stress Intensity Coefficients of Short Bar Specimens With Chevron Notches," International Journal of Fracture, Vol. 16, No. 4, pp. 359-374.
- Salem, J.A. and Shannon, J.L., Jr., 1987, "Fracture Toughness of Si_3N_4 Measured With Short Bar Chevron-Notched Specimens," Journal of Materials Science, Vol. 22, pp. 321-324.
- Salem, J.A., Shannon, J.L., Jr., and Bradt, R.C., 1988, "Effects of Texture on the Crack Growth Resistance of Alumina," accepted by Journal of the American Ceramic Society.
- Salem, J.A., Li, Z., and Bradt, R.C., 1986, "Thermal Expansion and Elastic Anisotropy in Single Crystal Al_2O_3 and SiC Whiskers," Proceedings of ASME Symposium on Advances in Composite Materials and Structures, Vol. 82, S.S. Wang and Y. Rajapakse, ed.

MODE II FRACTURE MECHANICS

Robert J. Buzzard and Louis Ghosn*
Fatigue and Fracture Branch
NASA Lewis Research Center

ABSTRACT

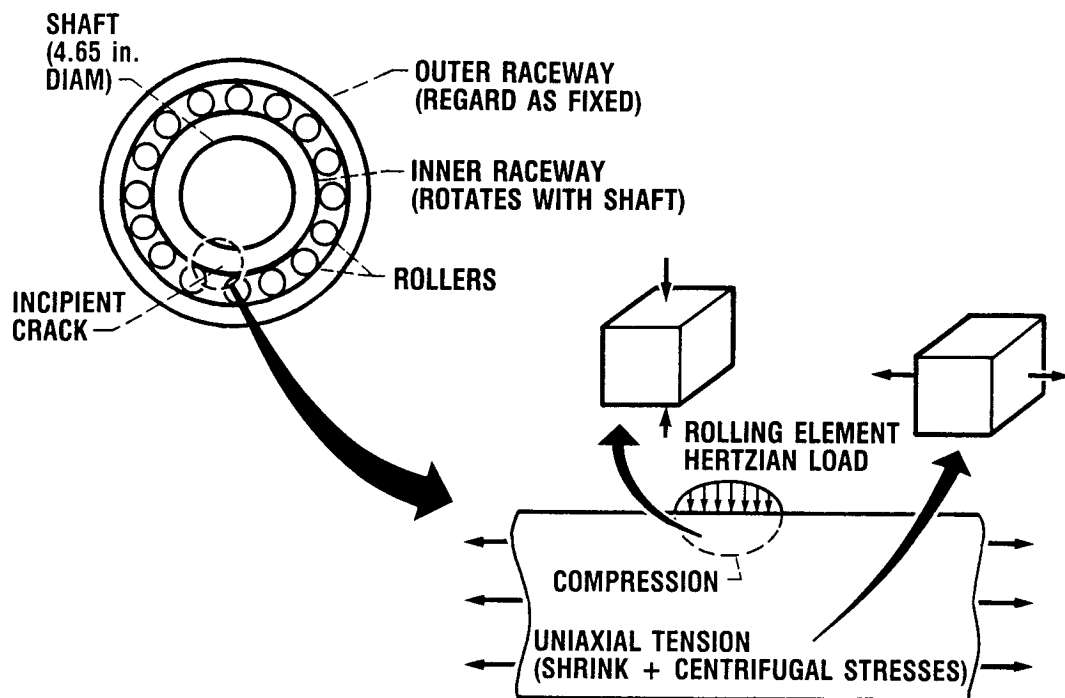
Current development of high-performance rolling element bearings for aircraft engines (up to 3 million DN, where DN is the product of shaft diameter in millimeters and speed in revolutions per minute) has aroused concern about fatigue crack growth in the inner bearing race that leads to catastrophic failure of the bearing and the engine. A failure sequence was postulated by Srawley (Buzzard et al., 1986), and an analytical program was undertaken (Ghosn, 1988) to simulate fatigue crack propagation in the inner raceway of such a bearing. A fatigue specimen has been developed at NASA (Buzzard et al., 1986) by which fatigue data may be obtained relative to the cracking problems. The specimen may be used to obtain either mode II data alone or a combination of mixed-mode (I and II) data as well and has been calibrated in this regard (Buzzard and Gross, 1988). Mixed-mode fracture data for M-50 bearing steel are presented herein, and a method for performing reversed-loading tests is described (Buzzard, 1988).

*Cleveland State University, Cleveland, Ohio 44115 (work funded under NCC3-46; monitor: John L. Shannon, Jr.) and NASA Resident Research Associate.

OVERVIEW

MODE II MECHANISM AND MODEL

High-performance rolling element aircraft engine bearings may become vulnerable to catastrophic fatigue failure as future requirements push them to ever higher operational limits. A postulated mechanism is described (Buzzard, et al., 1986) and an analytical model developed (Ghosn, 1988).



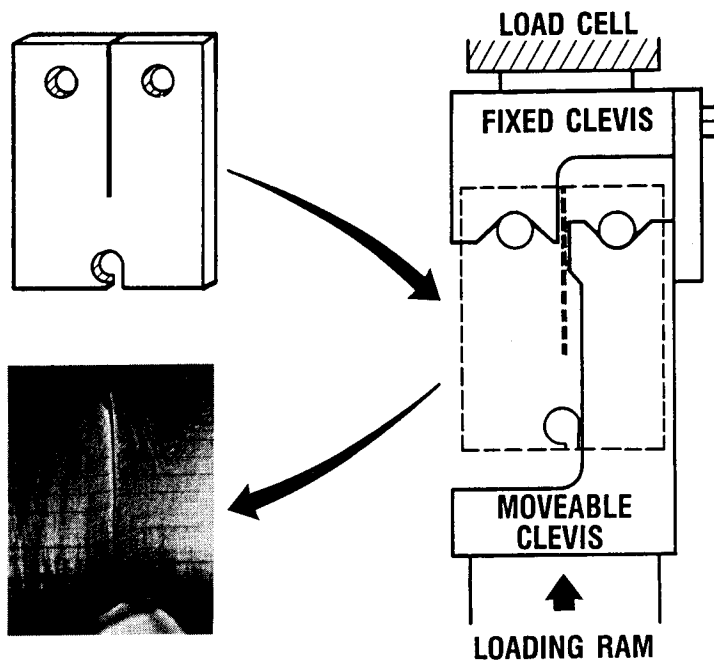
- ROLLING ELEMENT LOAD IS ADDED TO UNIAXIAL LOAD.
- SUBSURFACE VOID FORMS.
- CRACK REACHES SURFACE; SURFACE SPALLS.
- CRACK GROWS DOWNWARD; RACE FAILS.

CD-88-31739

MODE II TEST METHOD

A mode II fatigue and fracture specimen and test method have been developed at NASA for use in addressing the potential bearing failure problem (Buzzard et al., 1986). Use of the method has been extended to include mixed-mode testing (Buzzard and Gross, 1988) and reversed load testing (Buzzard, 1988).

ORIGINAL PAGE IS
OF POOR QUALITY



CD-88-31740

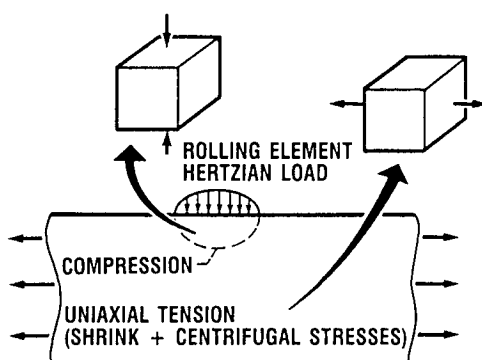
POSTER PRESENTATION

BEARING RACE FAILURE SEQUENCE

High-performance rolling element aircraft engine bearings are being developed for operation at very high rotational speeds (i.e., high DN values). This gives rise to concern regarding possible fatigue cracking of the inner bearing race and subsequent catastrophic failure of the bearing and the engine.

The following basic model was suggested by Srawley (Buzzard et al., 1986). Consider a section of a bearing race in which a location just below the surface is vulnerable to void initiation and growth resulting from the intense shear associated with the passage of individual rolling elements during engine operation. At DN values of about 1.7 million (the present commercial limit) this repetitive loading, in addition to constant hoop stress resulting from centrifugal force and the shrink fit of the race over the shaft, can cause crack growth from the void location to the surface, resulting in a spall. This situation can be monitored by various means and the bearing eventually retired. Under these loading conditions the critical crack size for continued growth is larger than the thickness of the race and therefore further crack growth would not be catastrophic. However, at DN values near 3 million (expected in the near future) the critical crack size is only about 1/5 of the thickness of the race. A small crack may be driven toward this size by alternating mode II stresses as the rolling elements pass by, followed by catastrophic mode I failure when the crack reaches its critical size.

It was primarily to address this problem in the laboratory that a specimen and a loading method were developed at Lewis. The specimen must contain a single notch to simplify data analysis and the monitoring of fatigue crack propagation, and the initial mode I stresses must be insignificant in comparison with the mode II stresses. Self-similar crack growth under mode II loading is desired but is obtainable only for structural materials that are less brittle than hardened bearing steel. Fatigue data for materials that do not exhibit self-similar crack extension must be analyzed in mixed-mode terms.

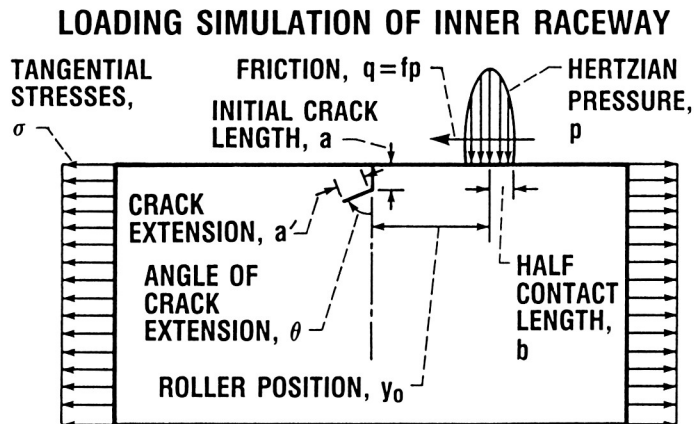


- ROLLING ELEMENT LOAD IS ADDED TO UNIAXIAL LOAD.
- SUBSURFACE VOID FORMS.
- CRACK REACHES SURFACE; SURFACE SPALLS.
- CRACK GROWS DOWNWARD; RACE FAILS.

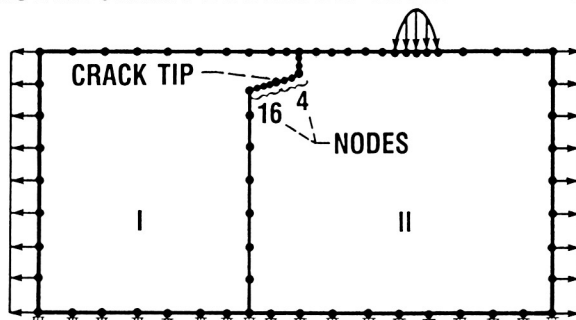
CD-88-31741

NUMERICAL SIMULATION

An analytical program was undertaken to simulate fatigue crack propagation in the inner raceway of high-speed bearings (Ghosn, 1988). The analysis makes use of the boundary integral method with a multidomain formulation. The multidomain formulation allows the two faces of the crack to be modeled in two different subregions, making it possible to analyze crack closure when the roller is positioned on or close to the crack tip. The stress intensity factors K_I and K_{II} along any direction are computed. These calculations permit determination of the crack growth direction along which the crack driving force is maximum. For brittle materials the fatigue crack driving force is the alternating K_I , but since the mean stress intensity is not constant during the loading cycle, the alternating K_I is an insufficient parameter. The mean stress effect is corrected for by assuming the crack driving force to be the product of the mean times the alternating K_I .



MULTIDOMAIN BOUNDARY INTEGRAL MESH



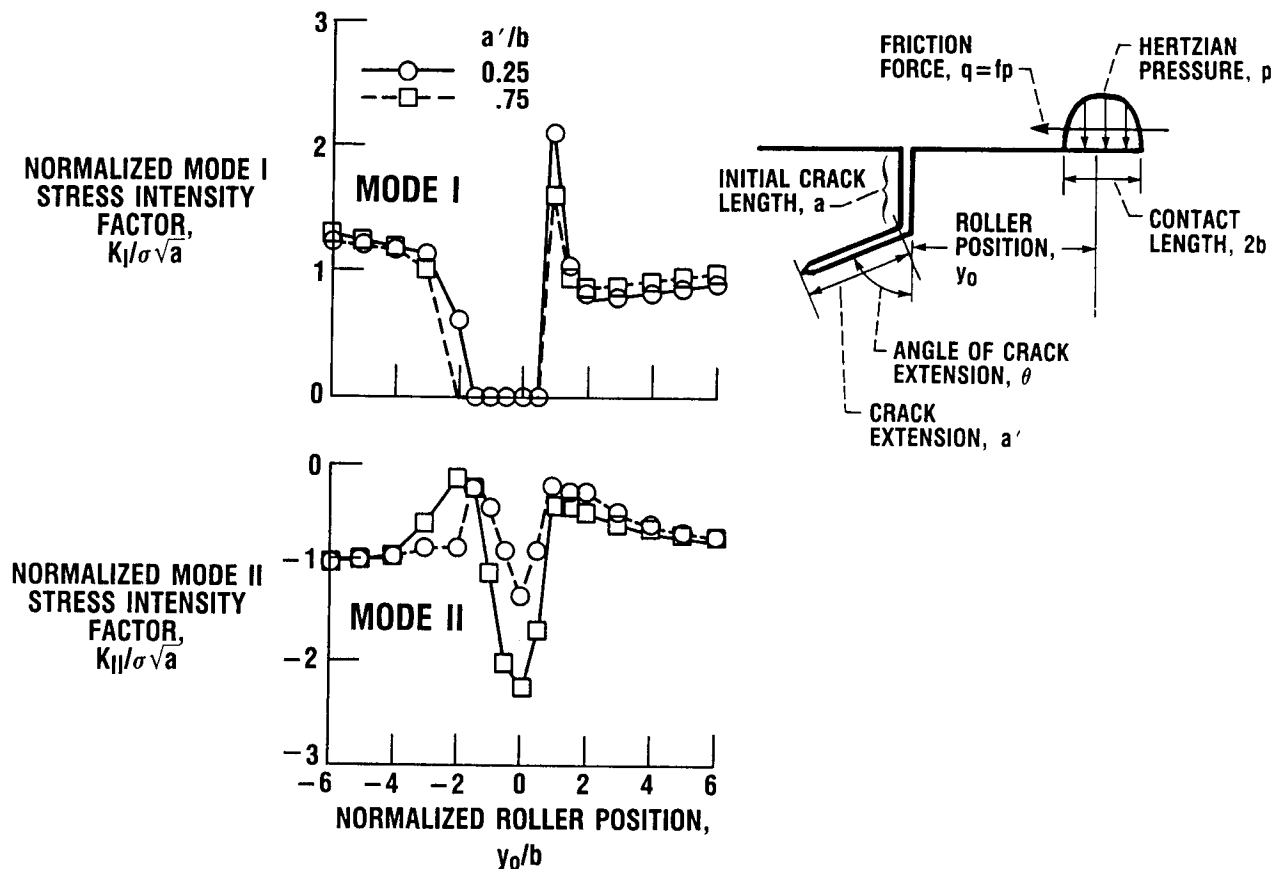
ACTUAL CRACK PROFILE
IN INNER RACEWAY OF
HIGH-SPEED BEARINGS

CD-88-31742

STRESS INTENSITY FACTOR VARIATIONS

The crack extension in a high-speed bearing was simulated numerically by using the multidomain boundary integral equation method (Ghosn, 1988). The graphs show typical variations of the normalized mode I and mode II stress intensity factors ($K_I/\sigma \sqrt{a}$ and $K_{II}/\sigma \sqrt{a}$, respectively). An original straight crack, $a/b = 1.0$, was extended in the direction of the maximum crack driving force. For $a/b = 1.0$, the maximum crack driving force was along an angle θ equal to 71° . As the Hertzian load passed over the crack, the stress intensity factors, K_I and K_{II} , decreased and then increased. These variations in K_I and K_{II} can result in a fast-growing crack in the inner raceway that can cause the complete failure of the bearing.

TYPICAL VARIATION OF STRESS INTENSITY FACTORS WITH ROLLER POSITION FOR KINKED CRACK ($a/b = 1.0$, $\theta = 71^\circ$, $f = 0.2$)



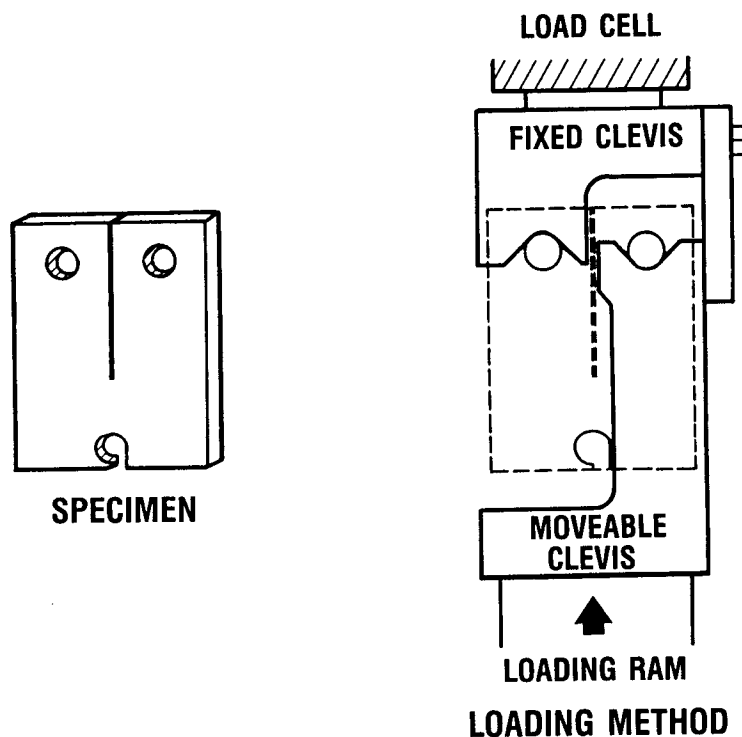
CD-88-31743

MODE II TEST METHOD

A novel mode II test specimen and testing fixture have been developed at Lewis that may aid in understanding phenomena associated with mixed-mode fatigue failures in high-performance aircraft engine bearing races (Buzzard et al., 1986 and 1987). The specimen contains one single-ended notch, which simplifies data gathering and reduction; the fatigue crack grows in-line with the direction of load application in many engineering materials; a single-axis test machine is sufficient to perform testing; and the mode I component can be practically eliminated if so desired.

The figure shows the shape of the specimen and the testing fixture/loading method. As a compressive load is applied, relative movement of the clevises causes a shearing force to be applied to the specimen along the loading axis. Rotation of the specimen is prevented by the lower loading pin.

The specimen has been calibrated (Buzzard and Gross, 1988) and analyzed by photoelastic and finite element methods (Gross et al., 1986).



CD-88-31744

MODE II FRACTURE PATH

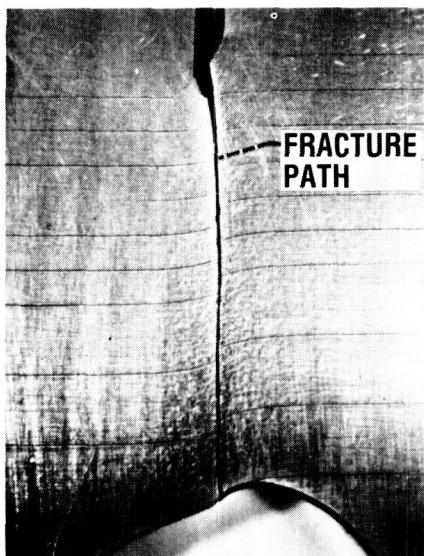
Mode II fracture and fatigue tests have been performed for hardened M-50 bearing steel and for less brittle engineering materials (steels and aluminum alloys). Under identical loading conditions the fatigue and fracture paths for the two classes of materials are quite different, as shown below for the test zone of a specimen of each class.

The fracture and high-load fatigue crack path for an aluminum engineering alloy is shown (in the photograph on the left) to extend in-line with the axis of major load application. It is reasoned that relative displacement of the two specimen halves along the loading line, promoted by plasticity and possible void growth at the crack tip, contribute to this observed behavior. At low fatigue loads, however, the crack proceeds in a direction of about 70° toward the tensile-loaded leg of the specimen (crack not shown). This direction is predicted by the maximum tangential stress and minimum strain energy criteria. The "threshold" load responsible for the difference in behavior has yet to be investigated more thoroughly (Buzzard et al., 1986).

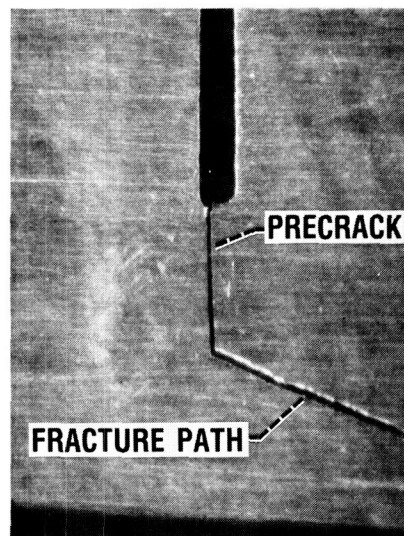
The fracture and fatigue path at both high and low loads for the brittle bearing steel (shown in the photograph on the right) extends only in the direction of about 70° from the tip of the precrack toward the tensile-loaded leg of the specimen, as predicted by theory.

This "dual" behavior suggests that the type of material, the loading restraints affecting structural mobility, and the magnitude of the load, in addition to the possibility of plasticity or void growth at the crack tip, must be given consideration when analyzing the direction of mode II crack progression.

ALUMINUM ALLOY



BEARING STEEL



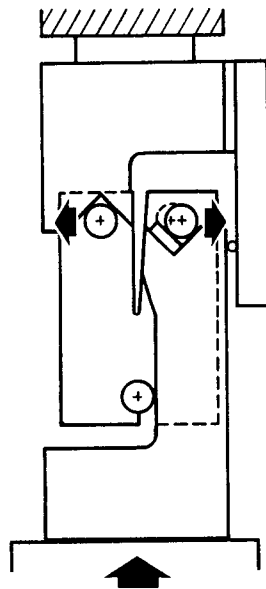
MIXED-MODE AND REVERSED-LOAD TEST METHODS

Mixed-mode (I and II) testing, wherein the mode I component is fixed and the mode II component is variable, may be accomplished with the NASA mode II test system (Buzzard and Gross, 1988). Spacers are placed beneath one of the loading pins as shown on the left. Application of a compressive load causes this loading pin to move outward (or inward, if desired) by a fixed distance determined by the thickness of the spacers. This distance is monitored by a standard ASTM clip gage, which spans the specimen along the loading pins' horizontal centerline. As the moving pin becomes seated in the vee-notch, lateral movement ceases and further load application results in loading in the shear direction only.

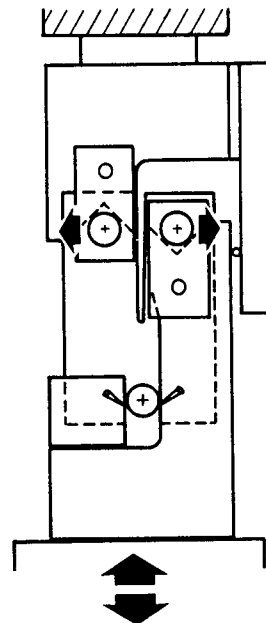
Reversed loading, or loading the specimen through zero load, may also be accomplished by modifying the testing fixture as shown on the right (Buzzard, 1988). Adding the loading pin retainer straps allows a tensile load as well as a compressive load to be applied. Rotation of the specimen when under reversed loading is prevented by adding a block at the lower loading pin.

Both of these modifications may be incorporated simultaneously if so desired.

MODES I AND II MIXED



MODE II REVERSED



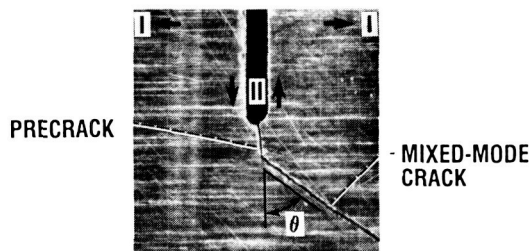
CD-88-31746

MIXED-MODE TESTING

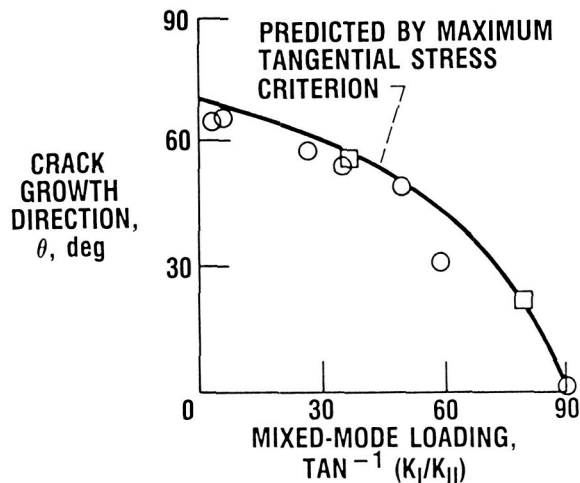
A knowledge of the mode I and mode II fracture characteristics of a material is essential to understanding failure initiation in a structure made of that material and subject to mode I and mode II loading. However, failures in a structure rarely progress by either of these two modes alone, but rather by a combination of modes. It therefore becomes necessary to obtain data that describe the mixed-mode fracture properties of structural materials. Such data have been recently obtained by Buzzard for hardened M-50 bearing steel and are presented below.

The plot at the left shows the path taken by a crack under various combinations of mode I and mode II loading to failure. Experimentally obtained data agree well with values predicted by the maximum tangential stress theory. Under mixed-mode loading the fracture path ranges from 0° to about 70° from the tip of the precrack toward the tensile-loaded leg of the specimen. The photograph shows a typical cracked M-50 steel specimen that fractured at an angle of about 65° under mixed-mode loading.

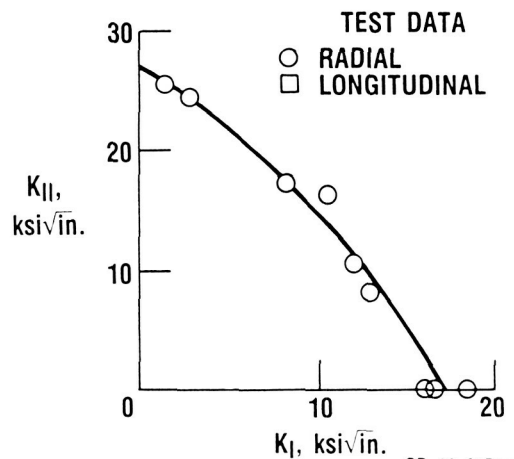
The plot at the right shows the relative amounts of K_I and K_{II} at fracture for this series of tests.



CRACK PROPAGATION DIRECTION AS
FUNCTION OF K_I/K_{II} RATIO FOR
M-50 BEARING STEEL



STRESS INTENSITY AT FRACTURE FOR
MIXED MODES I AND II IN
M-50 BEARING STEEL



CD-88-31747

REFERENCES

- Buzzard, R.J., Gross, B., and Srawley, J.E., 1986, "Mode II Fatigue Crack Growth Specimen Development." ASTM STP 905.
- Buzzard, R.J., Succop, G., and Gross, B., 1987, "Mode II Test Specimen and Method." NASA Tech Brief No. LEW-14281. NASA Tech Briefs, Vol. 11, No. 3, pp. 55-56.
- Buzzard, R.J., and Gross, B., 1988, "Calibration of a Mode II Test Specimen." ASTM STP 945, March 30, pp. 1083-1088.
- Buzzard, R.J., 1988, "Mode II Fatigue Testing Apparatus." NASA Patent Application LEW 14124-1.
- Ghosn, L., 1988, "Crack Propagation in Roller Bearings Using the Boundary Integral Equation Method - A Mixed-Mode Loading Problem." ASME Journal of Tribology, vol. 110, July 1988.
- Gross, B., Buzzard, R.J., and Brown, W.F., Jr., 1986, "Elastic Analysis of a Mode II Fatigue Crack Test Specimen." International Journal of Fracture, pp. 151-157.

IN SITU FATIGUE LOADING STAGE INSIDE SCANNING

ELECTRON MICROSCOPE

Jack Telesman,* Peter Kantzos,† and David Brewer‡
Fatigue and Fracture Branch
NASA Lewis Research Center

ABSTRACT

A fatigue loading stage inside a scanning electron microscope (SEM) has been developed at the NASA Lewis Research Center. The stage allows dynamic and static high-magnification and high-resolution viewing of the fatigue crack initiation and crack propagation processes. The loading stage is controlled by a closed-loop servohydraulic system. Maximum load is 1000 lb (4450 N) with test frequencies ranging up to 30 Hz. The stage accommodates specimens up to 2 in. (50 mm) in length and tolerates substantial specimen translation to view the propagating crack. At room temperature, acceptable working resolution is obtainable for magnifications ranging up to 10 000X. The system is equipped with a high-temperature setup designed for temperatures up to 2000 °F (1100 °C). The signal can be videotaped for further analysis of the pertinent fatigue damage mechanisms.

The design allows for quick and easy interchange and conversion of the SEM from a loading stage configuration to its normal operational configuration and vice versa. Tests are performed entirely in the in situ mode. In contrast to other designs, the NASA design has greatly extended the life of the loading stage by not exposing the bellows to cyclic loading.

The loading stage has been used to investigate the fatigue crack growth mechanisms in the (100)-oriented PWA 1480 single-crystal, nickel-based superalloy. The high-magnification observations revealed the details of the crack growth processes.

PRECEDING PAGE BLANK NOT FILMED

*NASA Lewis Research Center.

†Co-op Student with Case Western Reserve University.

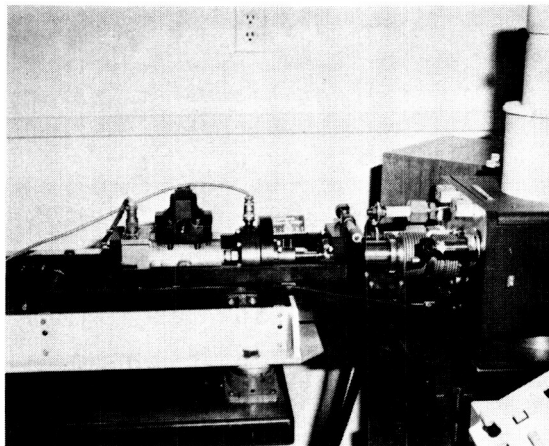
‡Army Propulsion Directorate.

OVERVIEW

MAIN FEATURES OF LOADING STAGE

Some of the main features of an in situ loading stage system developed at NASA Lewis are highlighted below. A photograph of the loading frame and some of the major system components are shown.

- o Dynamic observations of fatigue up to 10 000X
- o Loads up to 1000 lb; frequency up to 30 Hz
- o High-temperature capability
- o Interchangeable with normal SEM configuration



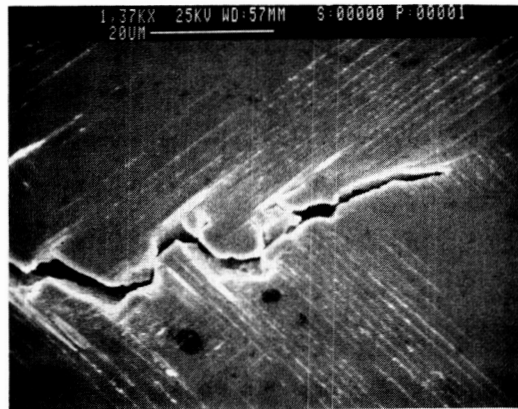
- DYNAMIC OBSERVATIONS OF FATIGUE UP TO 10 000X
- LOADS UP TO 1000 lb; FREQUENCY UP TO 30 Hz
- HIGH-TEMPERATURE CAPABILITY
- INTERCHANGEABLE WITH NORMAL SEM CONFIGURATION

CD-88-32381

ORIGINAL PAGE IS
OF POOR QUALITY

SAMPLE FRACTOGRAPH OF SINGLE CRYSTAL

The fatigue processes in a PWA 1480 single-crystal, nickel-base superalloy were examined by using the loading stage system. Some of the major observations are described in this paper. The poster session includes a videotape presentation of the observed fatigue damage mechanisms. A sample fractograph is included below.



- FATIGUE PROCESSES IN PWA 1480 SINGLE-CRYSTAL, NICKEL-BASE SUPERALLOY
- FATIGUE CRACK GROWTH BY PLANAR SLIP
- CRACK CLOSURE AND SECONDARY CRACK BRANCHING
- VIDEOTAPE PRESENTATION OF FATIGUE IN A SINGLE CRYSTAL

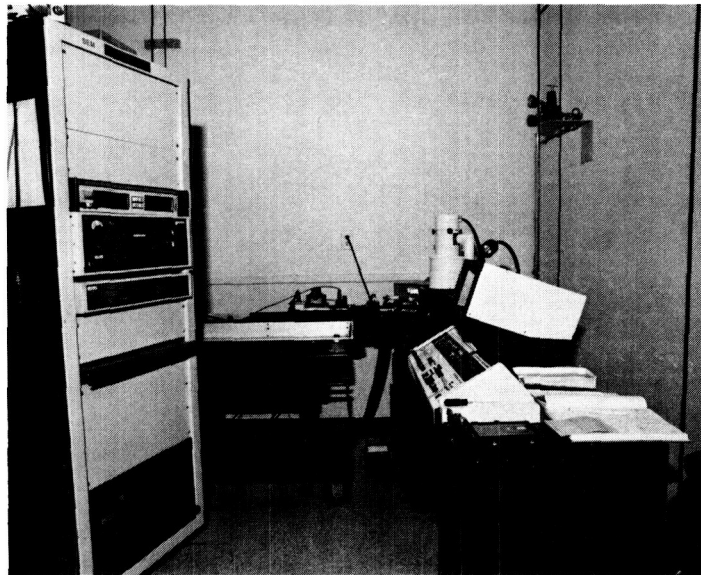
CD-88-32382

POSTER PRESENTATION

LOADING STAGE

An overall view of the loading stage, the scanning electron microscope, and accessories is shown below. On the right is the SEM, in the center is the loading frame mounted on a four-wheel adjustable height cart, and to the left is the console housing the controls for the servohydraulic system and the high-temperature equipment. Not shown in the figure are the color monitor and the video tape recorder, which are also part of the system.

During the operation of the in-house designed loading stage, the regular SEM chamber door and the attached specimen stage are swung out of the way. If the loading stage is no longer needed, the entire assembly is rolled away on the service cart and the regular specimen stage is swung back into its normal operating position. This interchange is quick and easy, typically being performed in only 2 to 3 minutes.

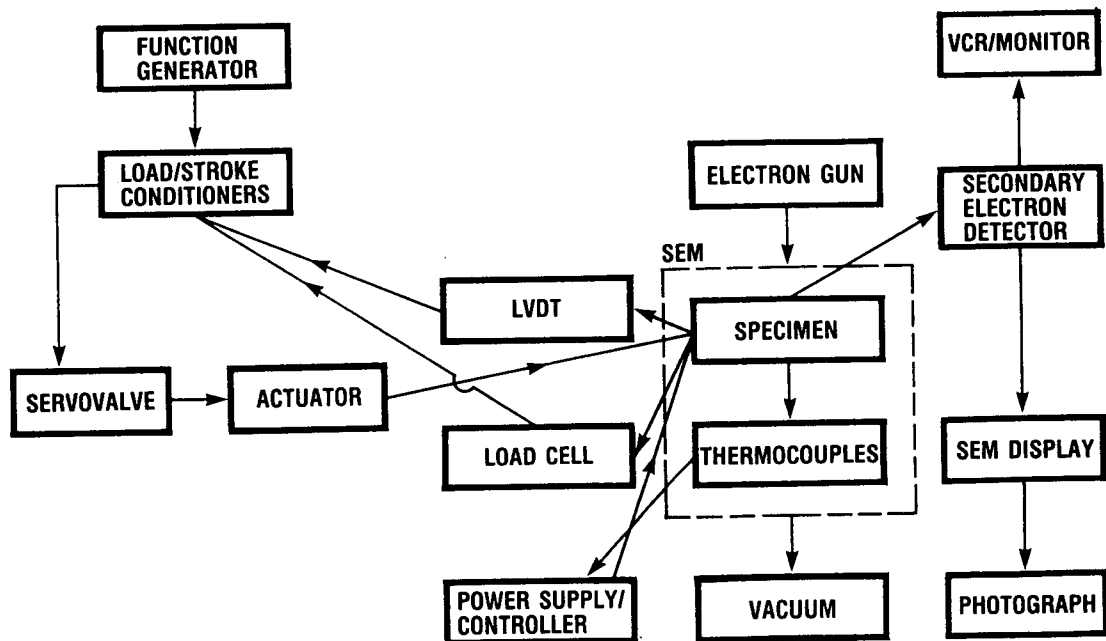


CD-88-32383

ORIGINAL PAGE IS
OF POOR QUALITY

SCHEMATIC OF LOADING STAGE

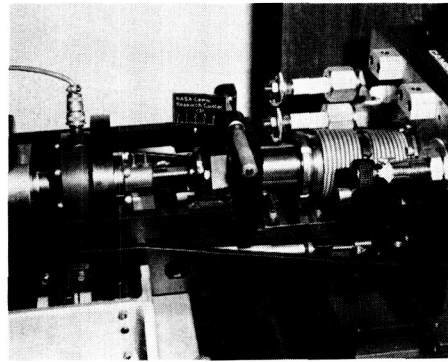
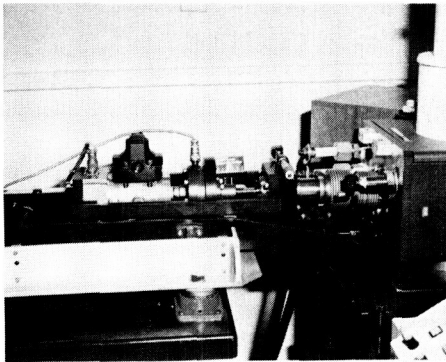
The entire loading stage system is shown here in schematic form. The system can be operated either in load or stroke control. The closed-loop servohydraulic portion of the system consists of a function generator, load and stroke conditioners and transducers, and a servovalve mounted to an actuator. The high temperature is achieved by passing a high current directly through a heating element surrounding the specimen. The current is applied from a dc power supply and controlled through standard means. The signal emanating from the specimen in the SEM can be sent to either a Polaroid camera or a video cassette recorder.



CD-88-32384

LOADING FRAME AND COMPONENTS

Detailed views of the loading stage are shown below. A 1-in. (25-mm) full-stroke axial actuator is attached to the loading frame. The actuator is driven by a 1-gal/min (4-liter/min) servovalve. Other components such as the load cell and the linear variable-differential transformer (LVDT) are attached to either the actuator or the loading rod. The entire assembly is connected to a support frame by two precision x-y translation stages and is also connected by a flexible bellows to a specially machined SEM door. The specimen is translated in the x and y directions by turning the micrometers mounted to the two translation stages.



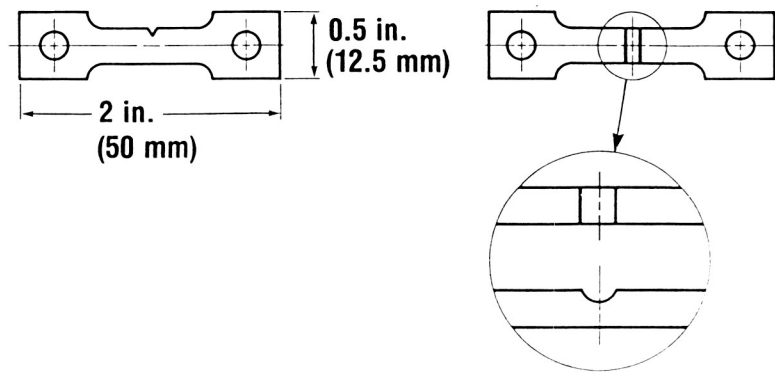
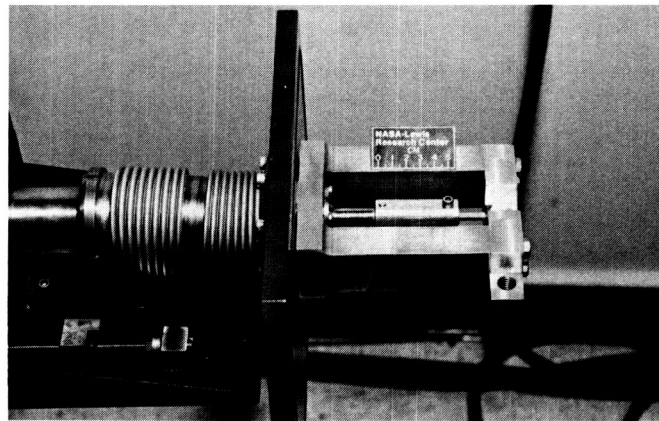
ORIGINAL PAGE IS
OF POOR QUALITY

CD-88-32385

GRIP FIXTURES AND SPECIMEN

The specimen is mounted in the grip fixture as shown in the photograph. The setup illustrated below is for room-temperature testing only. The simplicity of the room-temperature setup allows for a reduction in the working distance to 0.8 in. (20 mm) and this significantly increases the maximum useful resolution of the image.

Two examples of the type of specimen geometries used to date are shown below. Other configurations are possible because the allowable specimen viewing area is 0.7 by 0.7 in. (18 by 18 mm).



CD-88-32386

PERFORMANCE CHARACTERISTICS AND SPECIFICATIONS

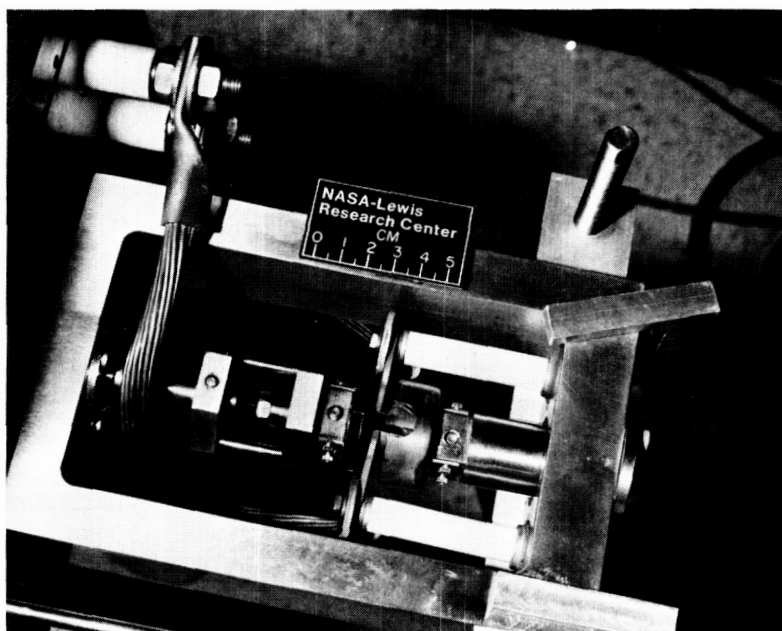
The design of the NASA Lewis in situ loading stage offers a number of important advantages. Because the bellows are not exposed to fatigue loading, long-duration tests can be performed in the in situ mode. Testing can be performed over a wide range of frequencies and temperatures. The system is also easily interchangeable with a normal SEM configuration. No other existing design has all of these advantages.

MAXIMUM CYCLIC LOAD, lb (N)	1000 (4450)
MAXIMUM CYCLIC RATE, Hz	30
MAXIMUM TEMPERATURE (DESIGNED), °F (°C)	2000 (1100)
USEFUL MAXIMUM MAGNIFICATION	
ROOM-TEMPERATURE STAGE	10 000X
HIGH-TEMPERATURE STAGE	3000X
WORKING DISTANCE, mm	
ROOM-TEMPERATURE STAGE	20
HIGH-TEMPERATURE STAGE	55
VIEWING AREA, in. (mm)	0.7 BY 0.7 (18 BY 18)

CD-88-32387

HIGH-TEMPERATURE SETUP

High-temperature operation is achieved by resistance heating of a cylindrical tantalum element surrounding the specimen. The power is supplied by a 625-A-maximum-current controlled dc power supply. The specimen is heated by radiation from the heating element. The cylindrical heating element is designed with a slit that enables the electron beam to impinge on the specimen and permits the escape of secondary electrons to the SEM collector. The heat is removed from the system through a water-cooled loading rod, and the SEM components are protected from overheating by three tantalum shields. Six thermocouples monitor the temperature of the specimen as well as the temperature of the critical SEM components.



CD-88-32388

PLANAR SLIP IN PWA 1480 SINGLE CRYSTALS

The fatigue loading stage has been used to investigate fatigue crack propagation mechanisms in (100)-oriented PWA 1480 single-crystal, nickel-based super-alloy specimens. The fractographs reveal that the mechanism by which the crack propagated consisted of planar slip on two different slip planes. The slip planes were identified later to be $(1\bar{1}1)$ and $(\bar{1}11)$. The fractographs also make it possible to measure crack tip opening displacements and the extent of damage occurring ahead of the crack tip.



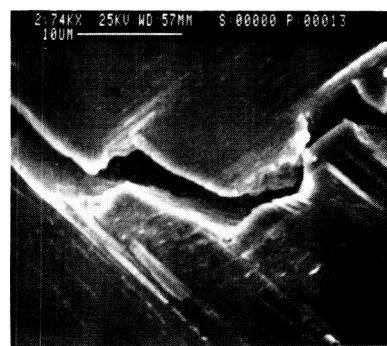
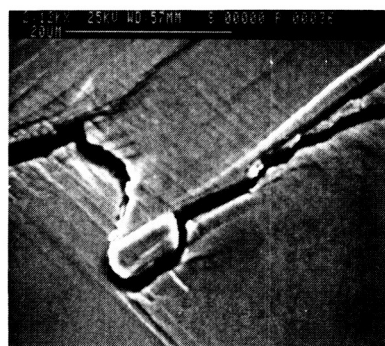
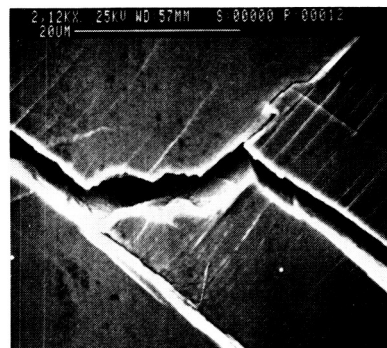
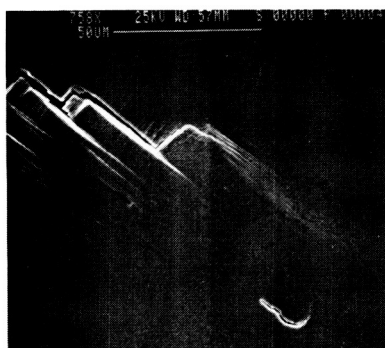
CD-88-32389

ORIGINAL PAGE IS
OF POOR QUALITY

DAMAGE AHEAD OF CRACK TIP AND CRACK CLOSURE

ORIGINAL PAGE IS
OF POOR QUALITY

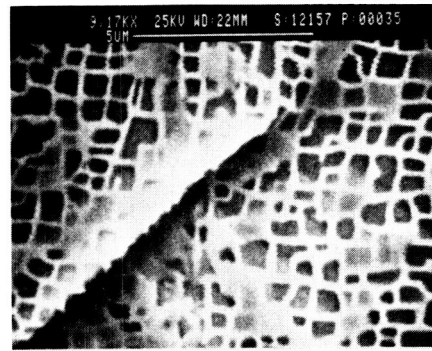
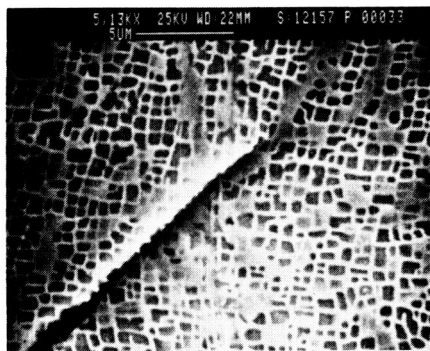
Observation of the fatigue damage processes in PWA 1480 single crystals reveals cracking ahead of the crack tip and the extent of the damage zone. The upper fractographs reveal the details of the damage occurring from planar slip as well as secondary branch cracking taking place between slip bands. The two bottom fractographs reveal regions of crack closure behind the crack tip even though the pictures were taken with the specimen under a relatively high axial tensile load.



CD-88-32390

INTERACTION OF CRACK WITH STRENGTHENING PRECIPITATES

High-magnification micrographs reveal the interaction of a crack in a PWA 1480 single crystal with the gamma prime strengthening precipitates. Instances of small-scale vibrations are noticeable at these high magnifications.



CD-88-32391

ORIGINAL PAGE IS
OF POOR QUALITY

GRAIN BOUNDARY OXIDATION AND LOW-CYCLE FATIGUE
AT ELEVATED TEMPERATURES*

H.W. Liu and Y. Oshida
Syracuse University
Syracuse, NY

ABSTRACT

Fatigue life consists of fatigue crack nucleation and propagation periods. In order to predict fatigue life accurately, a methodology for the quantitative assessment of these two fatigue damage processes had to be devised.

Grain boundary oxidation penetrates faster than does oxidation within a grain. This faster oxidation penetration causes intergranular fatigue failures at elevated temperatures. Grain boundary oxidation accelerates both crack nucleation and propagation.

Grain boundary oxidation kinetics and the statistical distribution of grain boundary oxide penetration depth were measured. Quantitative applications of the grain boundary oxidation kinetics to fatigue crack nucleation and propagation were analyzed. A method, based on the Weibull distribution, of extrapolating the laboratory oxidation data measured with small samples to large engineering structures is presented.

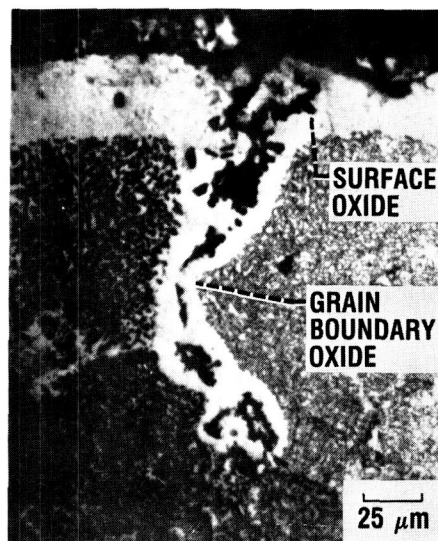
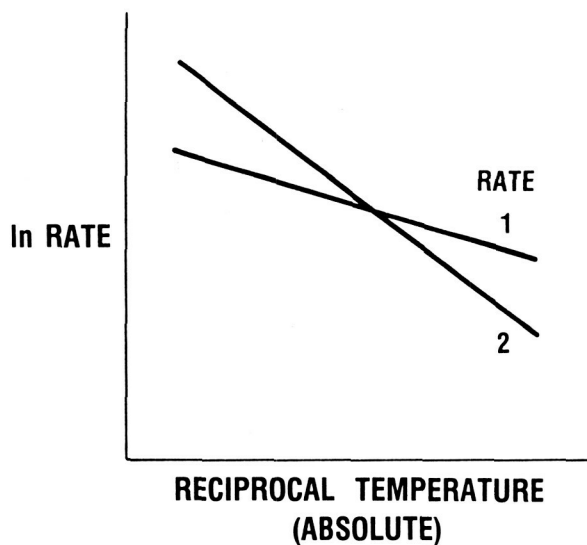
* Work performed for Fatigue and Fracture Branch and funded under NASA Grant NAG3-348 (monitor: Jack Telesman).

ORIGINAL PAGE IS
OF POOR QUALITY

OVERVIEW

DAMAGE MECHANISMS OF HIGH-TEMPERATURE, LOW-CYCLE FATIGUE

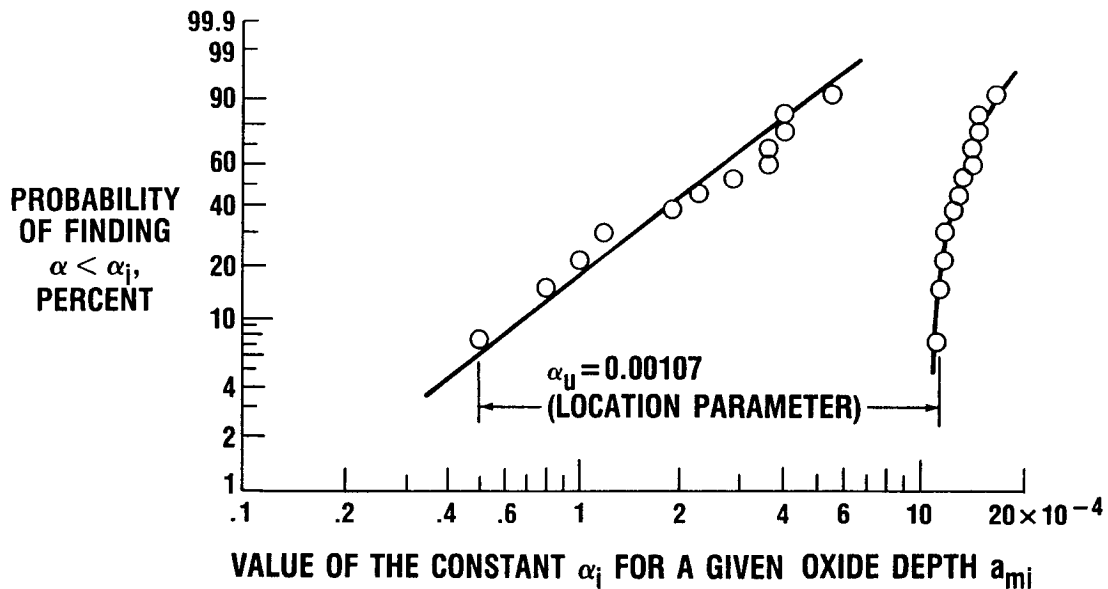
At high temperature both creep and oxidation are distinctive LCF damage mechanisms. Need exists to identify the regions at which each mechanism is dominant. A quantitative study of grain boundary oxidation and its effects on fatigue life was conducted.



CD-88-31859

STATISTICAL DISTRIBUTION OF GRAIN BOUNDARY OXIDE PENETRATION

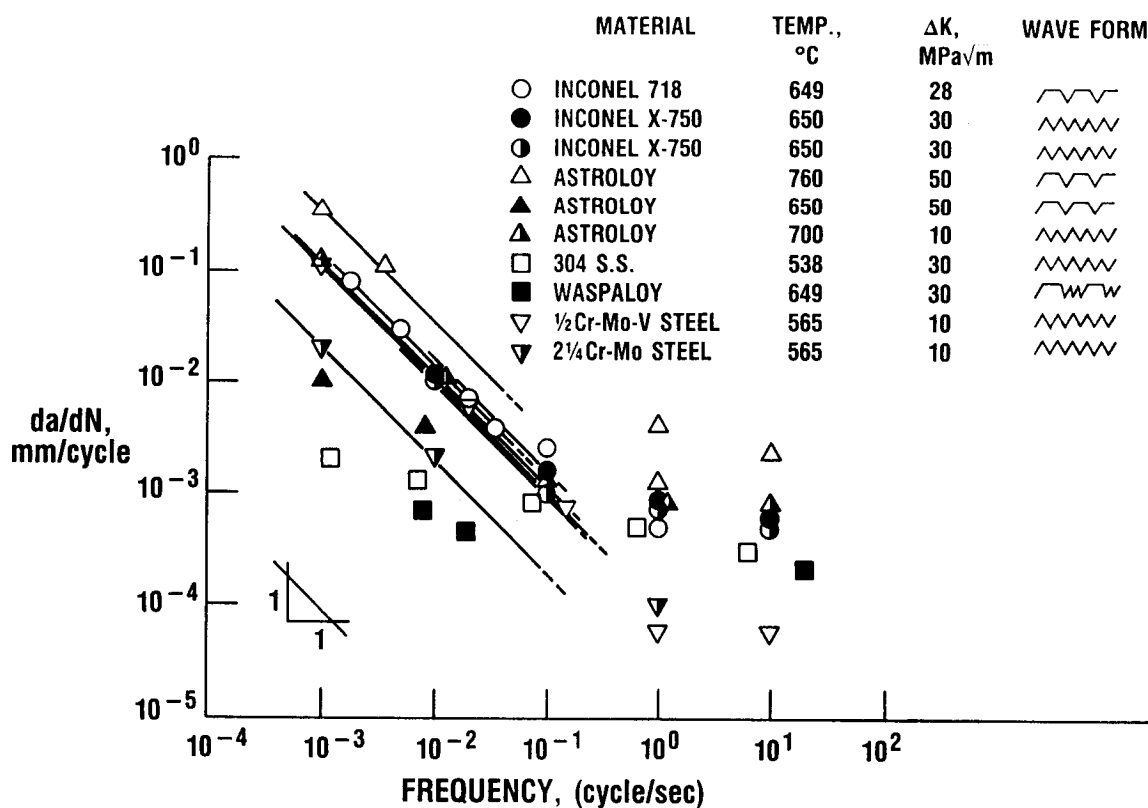
Grain boundary oxide penetration depth was measured as a function of oxidation temperature T and exposure time t . The penetration depth exhibited a wide statistical scatter which followed the Weibull distribution function as shown below. The distribution function allowed the extrapolation of the small laboratory samples to the large engineering components in service.



CD-88-31865

FREQUENCY EFFECTS ON FATIGUE CRACK GROWTH AT HIGH TEMPERATURE

A model is proposed that predicts fatigue crack propagation behavior of high temperatures. The model is based on an intermittent microrupture of oxide particles which is controlled by grain boundary oxidation kinetics. The model predicts an inverse relationship between da/dN and cyclic frequency. This relationship agrees with observed behavior of a number of materials.



CD-88-31866

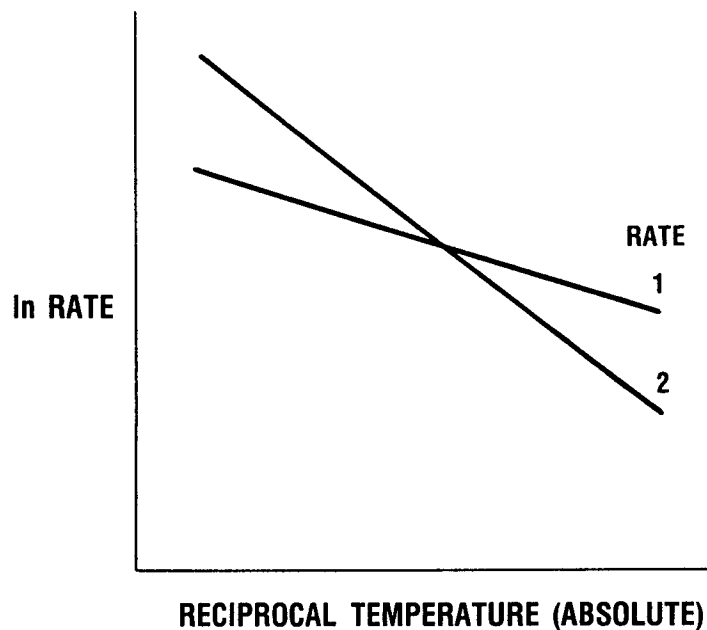
POSTER PRESENTATION

DAMAGE MECHANISMS OF HIGH-TEMPERATURE, LOW-CYCLE FATIGUE

Two primary damage mechanisms of high-temperature, low-cycle fatigue are creep and oxidation. Both mechanisms are thermally activated as illustrated schematically below.

The question is not which of these two mechanisms is dominant. The pertinent question is rather which one is dominant in the high-temperature region and which in the low-temperature region. Quantitative studies on creep and oxidation damage mechanisms are necessary in order to answer this question.

A quantitative study on grain boundary oxidation and its effects on fatigue life was conducted.



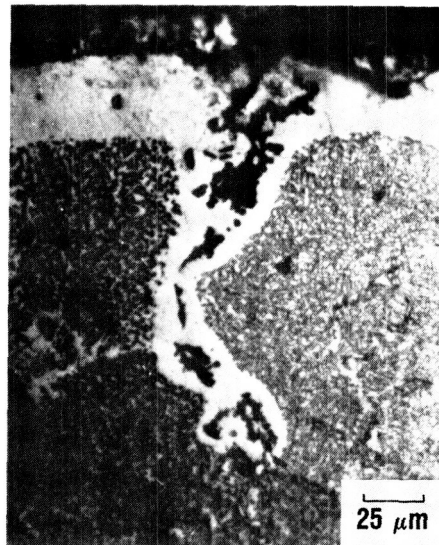
CD-88-31860

ORIGINAL PAGE IS
OF POOR QUALITY

OXIDATION AT GRAIN BOUNDARIES

A grain boundary is a path for rapid diffusion. Grain boundary oxidation is controlled by the diffusion of oxygen along the boundary. The rapid oxygen diffusion causes a deep grain boundary oxidation penetration, and the fast oxidation penetration causes the accelerated intergranular fatigue fractures at high temperatures.

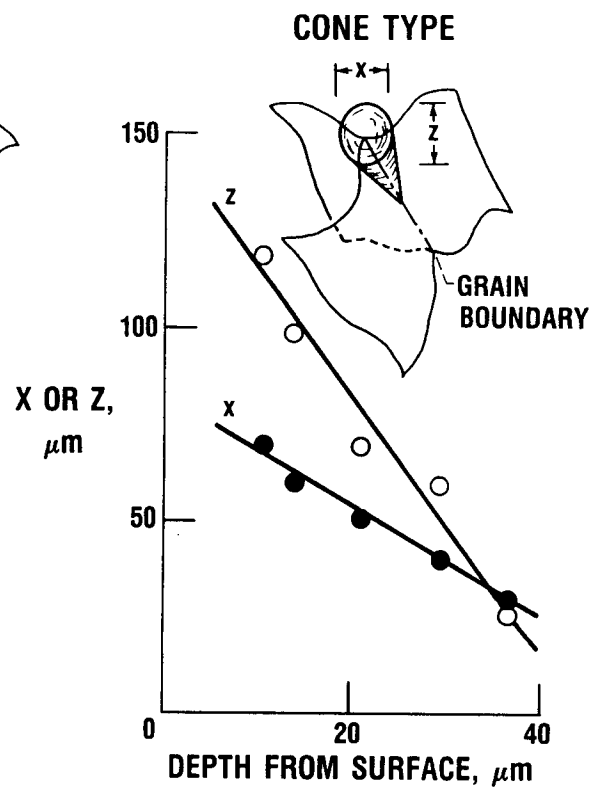
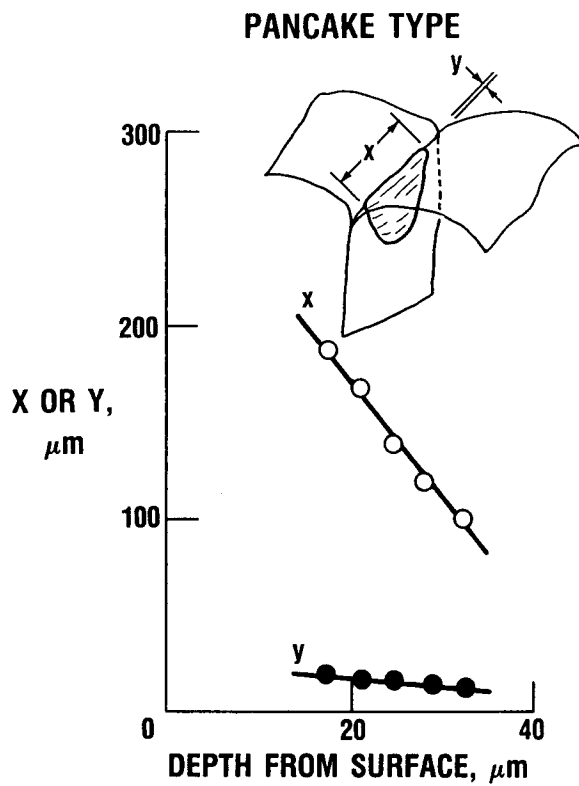
TAZ-8A AT 1000 °C FOR 500 HOURS



CD-88-31861

GRAIN BOUNDARY OXIDE MORPHOLOGIES

Two different grain boundary oxide morphologies were found: the pancake type and the cone type. The larger and deeper pancake type is more damaging.



CD-88-31862

RELATIONSHIPS MEASURING OXIDE PENETRATION OF GRAIN BOUNDARY

Grain boundary oxide penetration a_m in the cobalt-base superalloy, TAZ-8A, was measured by Liu and Oshida (1984 and 1985) and Oshida and Liu (1985 and 1988) as a function of oxidation temperature T and exposure time t .

The coefficient of correlation is 0.96 for 144 data points. This quantitative relation was used to study the accelerated fatigue crack nucleation and fatigue crack growth rate at elevated temperatures.

$$\begin{aligned} A_m &= \alpha t^n \exp\left(\frac{-Q}{RT}\right) \\ &= 1.34 t^{0.25} \exp\left(\frac{-4.25}{RT}\right) \end{aligned}$$

WHERE

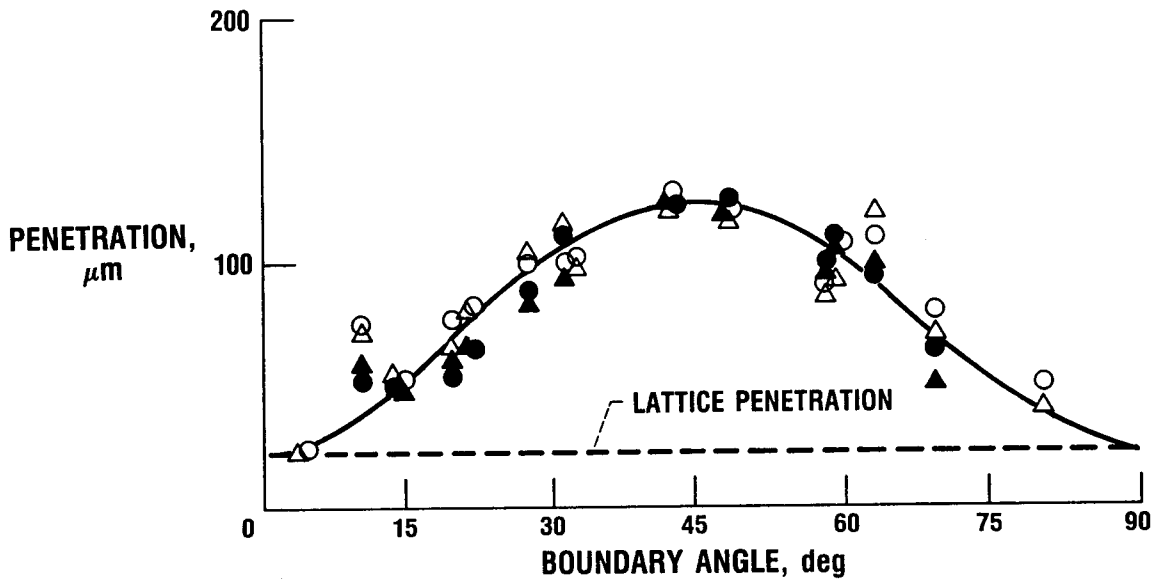
Q = APPARENT ACTIVATION ENERGY

R = GAS CONSTANT

CD-88-31863

RADIOACTIVE NICKEL PENETRATION AT GRAIN BOUNDARY

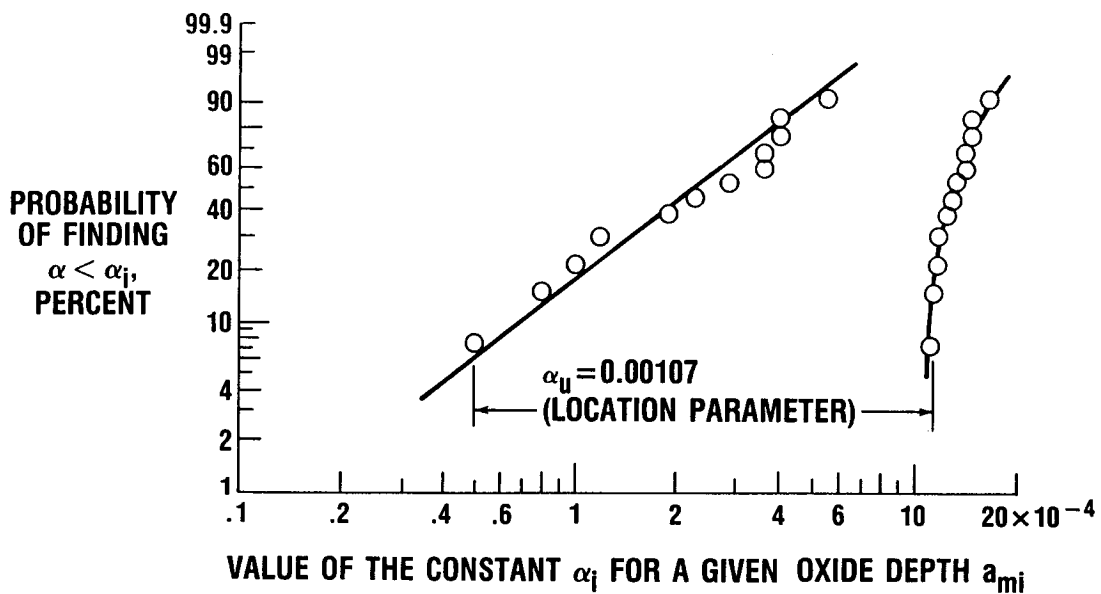
Grain boundary morphology and the chemical elements in a grain boundary may also cause the wide variation in the grain boundary oxide penetration. This wide variation may cause wide variations in the rates of crack nucleation and growth and fatigue life. Grain boundary penetration by impurities (radioactive nickel) is a function of the orientations of neighboring grains as shown below.



CD-88-31864

STATISTICAL DISTRIBUTION OF GRAIN BOUNDARY OXIDE PENETRATION

The statistical scatter of the grain boundary oxide penetration depth follows Weibull's distribution law as shown below. The variation of the calculated values reflects the statistical scatter of the measured oxide values. The empirical distribution law can be used to extrapolate the data obtained in a laboratory by using small samples to a much larger structural component in service.



CD-88-31865

EFFECT OF PRECRACK ON LOW-CYCLE FATIGUE

When an oxide reaches a critical size under given loading conditions, it will fracture. A grain boundary oxide crack becomes a fatigue crack nucleus, or a precrack. The precrack will shorten the crack nucleation period and the total fatigue life. This reduction in nucleation life will be significant if the cyclic frequency is very low, the temperature is very high, and the oxidation exposure time is very long.

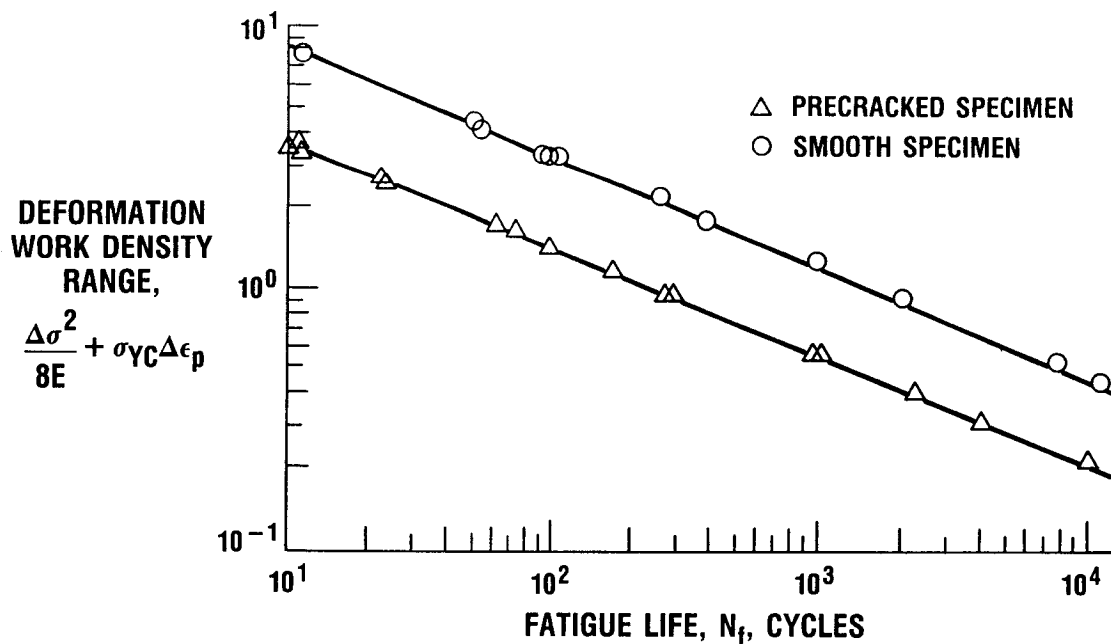
The ratio between the fatigue life of a precracked specimen and the fatigue life of a smooth specimen is a function of the precrack size:

$$N_{fi}/N_{fo} = f(\text{precrack size})$$

where N_{fi} is the fatigue life of a precracked specimen and N_{fo} is the fatigue life of a smooth specimen. The functional relationship between the ratio and the precrack size can be found empirically.

The wide variations in oxidation penetration and oxide crack size may cause a wide variation in N_{fi} and the total fatigue life. A large structural component has a high probability of having a large oxide crack and a short fatigue life. The empirical relation of the equation, together with the grain boundary oxide penetration kinetics and the Weibull distribution, would be able to predict the effect of the oxide crack on the nucleation life of a structural component.

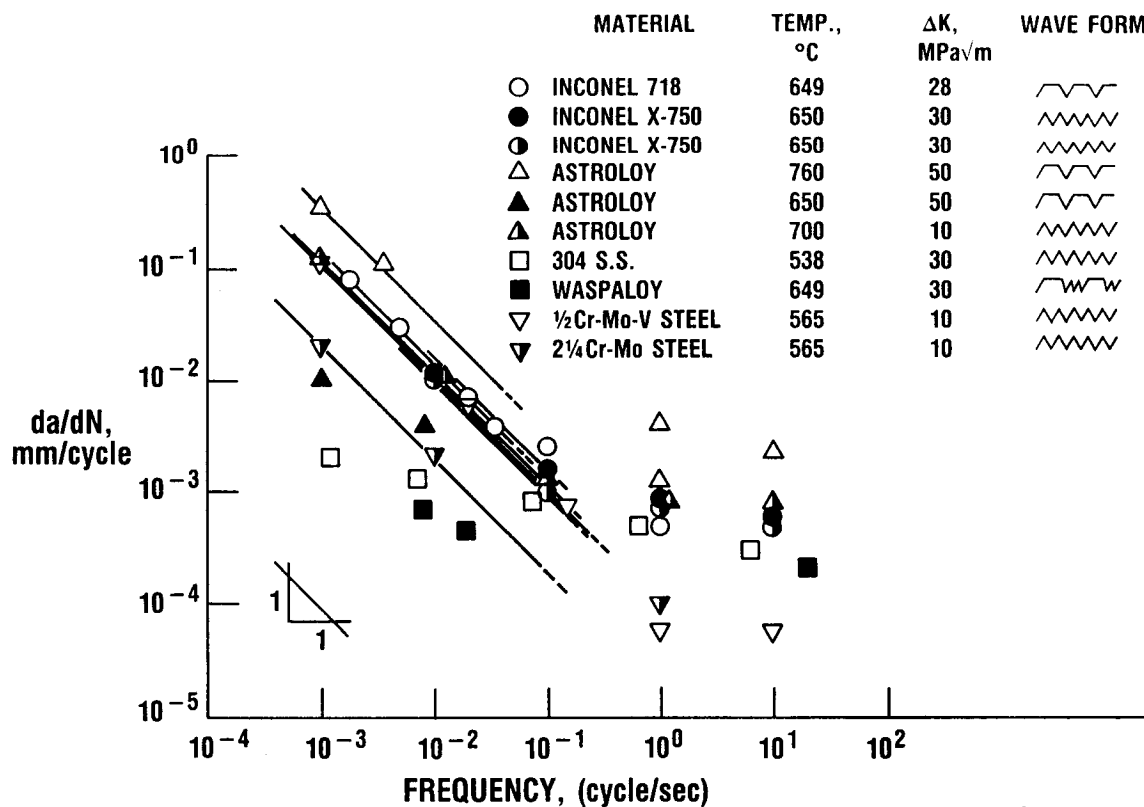
In conclusion, quantitative studies based on the physical damage mechanisms will lead to an improved life-prediction methodology.



CD-88-31867

FREQUENCY EFFECTS ON FATIGUE CRACK GROWTH RATE AT HIGH TEMPERATURE

The basic concept of grain boundary oxidation kinetics was used to analyze fatigue crack growth rate at the elevated temperatures. A high-temperature fatigue crack growth model based on intermittent microruptures of grain boundary oxides was proposed. The model is consistent with the observed intergranular fracture and the observed inverse relationship between crack growth rate and the cyclic frequency in the low-frequency region as shown in the figure (Oshida and Liu, 1984 and 1985), Liu and Oshida (1985 and 1986). In the high-frequency region fatigue failure could be mixed intergranular and transgranular or transgranular entirely.



REFERENCES

- Liu, H.W., and Oshida, Y., 1984, "Literature Survey on Oxidation and Fatigue Lives at Elevated Temperatures," NASA CR-174639.
- Liu, H.W., and Oshida, Y., 1985, "Grain Boundary Oxidation and Oxidation Accelerated Fatigue Crack Nucleation and Propagation," Proceedings of the Minnowbrook Conference on Life Prediction for High Temperature Gas Turbine Materials, Blue Mountain Lake, NY.
- Liu, H.W., and Oshida, Y., 1986, "Grain Boundary Oxidation and Fatigue Crack Growth at Elevated Temperatures," Theoretical and Applied Fracture Mechanics, vol. 6, no. 2, pp. 85-94.
- Oshida, Y., and Liu, H.W., 1984, "Oxidation and Low Cycle Fatigue Life Prediction," Turbine Engine Hot Section Technology - 1984, NASA CP-2339, pp. 321-329.
- Oshida, Y., and Liu, H.W., 1985, "Grain Boundary Oxide Crack, Oxidation Accelerated Fatigue Crack Growth and Fatigue Life," Proceedings of the 40th Meeting of the Mechanical Failures Prevention Group, Symposium on the Use of New Technology to Improve Mechanical Readiness, Reliability and Maintainability, National Bureau of Standards, Gaithersburg, MD, Cambridge University Press, pp. 287-295.
- Oshida, Y. and Liu, H.W., 1988, "Grain Boundary Oxidation and an Analysis of the Effects of Pre-oxidation on Subsequent Fatigue Life," ASTM Symposium on Low Cycle Fatigue - Direction for the Future, ASTM STP 942, pp. 1199-1217.

ELEVATED TEMPERATURE CRACK GROWTH

KS Kim, RH Van Stone, SN Malik, & JH Laflen

GE-AE, Evendale, Ohio 45215

ABSTRACT

The problem of crack growth in hot path components such as combustor liners is complicated by several practical and theoretical considerations. The loading environment of such components involves high temperature levels and gradients that lead to considerations such as thermal stresses, crack closure, hold time, inelastic strains - both time dependent and independent, and Thermal Mechanical Fatigue (TMF). In general, a good understanding of the influence of these factors on crack growth has not been obtained. At the same time, several nonlinear fracture mechanics parameters have been suggested for such applications; however, most of the proposed methods have not been tested for broad applications such as required for hot section components. It was the purpose of this program to evaluate proposed nonlinear methods by performing a thorough experimental and analytical study. The results illustrated that much progress has been made in developing nonlinear methods. This work was performed on contract NAS3-23940 with the NASA-Lewis Research Center.

EXECUTIVE OVERVIEW OF: ELEVATED TEMPERATURE CRACK GROWTH

The development of suitable predictive methods for high temperature inelastic crack growth involved several technology considerations. The important factors were an outgrowth of the hot path problems, but there were several factors that called for technology assessments and development. These latter factors included selection of a lower temperature alloy to simplify the experimental work; development of detailed, but proper, experimental methods; selection of appropriate parameters from a long list of nonlinear Path-Independent fracture mechanics integrals; and correlation of experimentally measured crack growth through detailed finite element simulations of the tests to calculate the nonlinear Path-Independent integrals.

- | | |
|---|--|
| <ul style="list-style-type: none">• Alloy selection• Experimental considerations<ul style="list-style-type: none">- Specimen development- Closure measurement- Temperature gradients and cycling• Nonlinear fracture mechanics<ul style="list-style-type: none">- Numerous path-independent integrals- Detailed review- FEM post-processor- Initial evaluation | <ul style="list-style-type: none">• Experimental simulations<ul style="list-style-type: none">- Crack release- Measured boundary conditions- PI integral correlation |
|---|--|

Figure 1. Technology Considerations

EXECUTIVE OVERVIEW OF: ELEVATED TEMPERATURE CRACK GROWTH

The results of the current program strongly suggest that significant progress has been made in the development of nonlinear fracture mechanics for application to problems of importance to hot section components of gas turbine engines. This conclusion is based on a thorough analytical and experimental evaluation of crack growth in the nonlinear regime. There, nevertheless, remain areas of developmental activities such as thermo mechanical fatigue, thermal gradients, and time dependence.

- Developed new specimen geometry
- Path-independent integrals are available for hot part applications
- Extensive data base collected
- Excellent isothermal data correlation obtained at 538C
- TMF data tended to agree with max stress isothermal data
- Additional work:
 - TMF, thermal gradient, and time dependence
 - Crack closure
 - Geometry verification
 - Numerical improvements

Figure 2. Program Results and Conclusions

SPECIMEN DESIGN AND MEASUREMENTS

The attached figure shows a schematic of the gage section of the buttonhead single edge notch specimen that was developed during this program. Shown in the figure are the locations of the three extensometers and the potential drop leads (for monitoring crack length). The control extensometer was used to simulate strain control, and its value was controlled to vary in a specified way throughout an experiment. The CMOD gage was used to measure the occurrence of crack opening and closure. The back surface extensometer was used with the control extensometer to help establish the boundary conditions in the FEM analyses. The specimen met often conflicting goals of the program, and proved to be easy to analyze via FEM by using the extensometer measurements for boundary conditions.

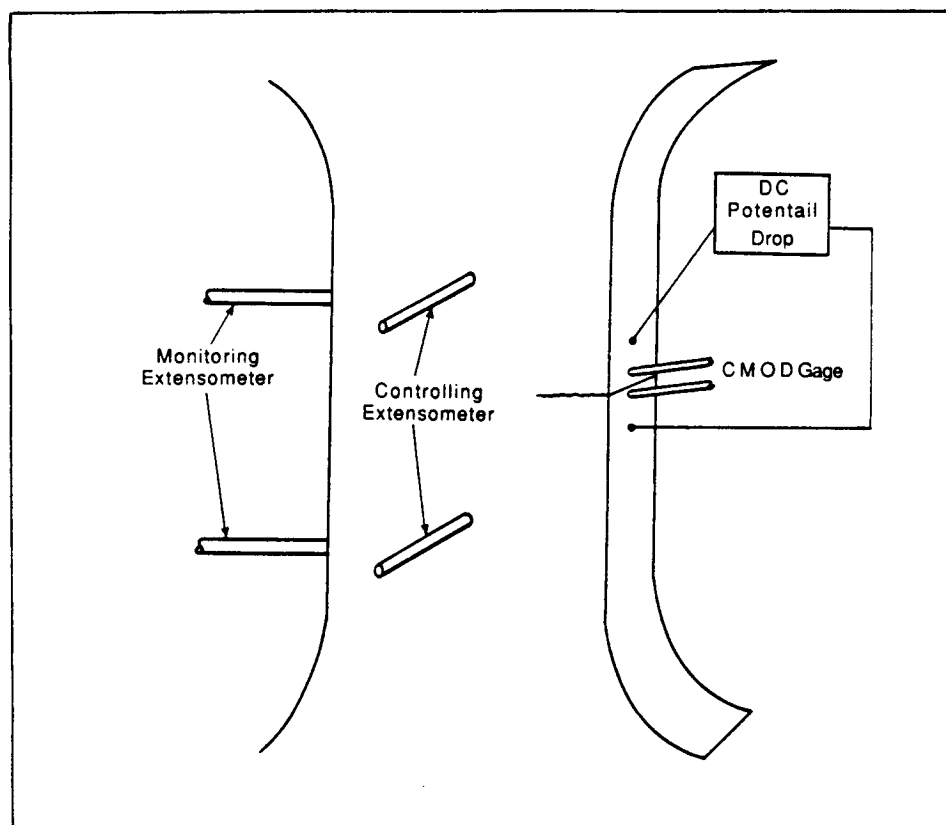


Figure 3. Schematic Drawing of SEN Test Method

LIMITATIONS OF LINEAR ELASTIC FRACTURE MECHANICS

Using the SEN specimen, crack growth properties were measured for a variety of conditions of interest to hot section components. One basic property is the effect of inelastic strain on crack growth rate. As shown in the figure, increasing strain range increases the measured crack growth rate, even though a linear elastic fracture mechanics parameter, the stress intensity factor, is used. This result shows that the effect of inelastic strains is to make predictions based on elastic fracture mechanics potentially nonconservative. It was for this reason that the various nonlinear PI integrals were developed, and it was a purpose of this contract to determine which approach would provide the best method for analyzing such conditions.

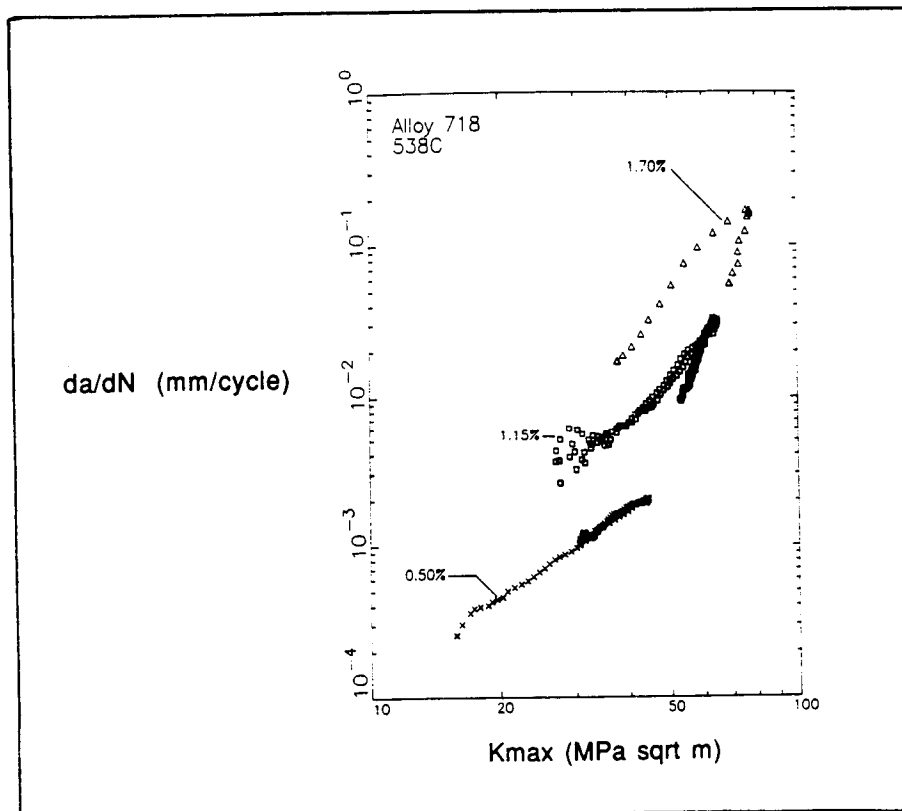


Figure 4. Limitation of Linear Elastic Fracture Mechanics

PROPOSED PATH INDEPENDENT INTEGRALS

A critical element in the program was to evaluate proposed nonlinear fracture mechanics parameters which are Path Independent integrals. The attached figure shows several proposed methods. For a given application the easiest way to calculate the value of the parameter is to perform a FEM analysis, and then use a post processor to evaluate the integral; this was the approach used in this program. A finite element post processor was written to calculate the PI integrals for conditions of interest to hot section components.

Rice's J-Integral

$$J = \int_{\Gamma} (n_1 W - t_i u_{i,1}) ds$$

$$\text{where } W = \int_0^{\epsilon_{ij}} \sigma_{ij} d\epsilon_{ij}$$

Wilson and Yu's Thermoelastic Integral

$$J_W = \int_{\Gamma} (n_1 W - t_i u_{i,1}) ds - \alpha(3\lambda + 2\mu) \int_A [\frac{1}{2}(\theta \epsilon_{ii}),_1 - \epsilon_{ii} \theta,_1] dA$$

Where

$$W = \frac{1}{2} \sigma_{ij} \epsilon_{ij}$$

Gurtin's Thermoelastic Integral

$$J_G = \int_{\Gamma} [n_1 W - t_k u_{k,1} - \frac{\alpha^2(3\lambda+2\mu)^2}{2(\lambda+\mu)} \theta^2 n_1 + \frac{\alpha\mu(3\lambda+2\mu)}{(\lambda+\mu)} (\theta \frac{\partial u_1}{\partial n} - u_1 \frac{\partial \theta}{\partial n})] ds$$

Where

$$\frac{\partial}{\partial n} = n_j \frac{\partial}{\partial x_j}$$

and

$$W = \mu \epsilon_{ij} + \frac{\lambda}{2} (\epsilon_{kk})^2$$

The J_{θ} -Integral by Ainsworth et al.

$$J_{\theta} = \int_{\Gamma} (n_1 W - t_i u_{i,1}) ds + \int_A \sigma_{ij} \epsilon'_{ij,1} dA$$

where

$$W(\epsilon'_{ij}) = \int_0^{\epsilon'_{ij}} \sigma_{ij} d\epsilon'_{ij}, \text{ and } \epsilon'_{ij} = \epsilon_{ij} - \epsilon_{ij}^{\theta}$$

Figure 5. Proposed Path Independent Integrals

FEM MESH AND BOUNDARY CONDITIONS

To do a FEM analysis, it is, of course, necessary to develop a mesh of the specimen that is being studied. The attached figure shows the mesh of the buttonhead SEN specimen that was used in the simulation of the experimental results. The plane stress model consisted of 421 nodes and 688 constant strain triangular shaped elements. There were also 33 gap elements located along the plane of symmetry where the crack was assumed to be propagating. The gap elements allowed the model to simulate the effect of crack opening and closure. Along the top half of the model the measured displacements were used as displacement boundary conditions, so that an exact geometric model of the specimen was not needed. A large effort including three dimensional analyses was made to verify that this analysis method was accurate.

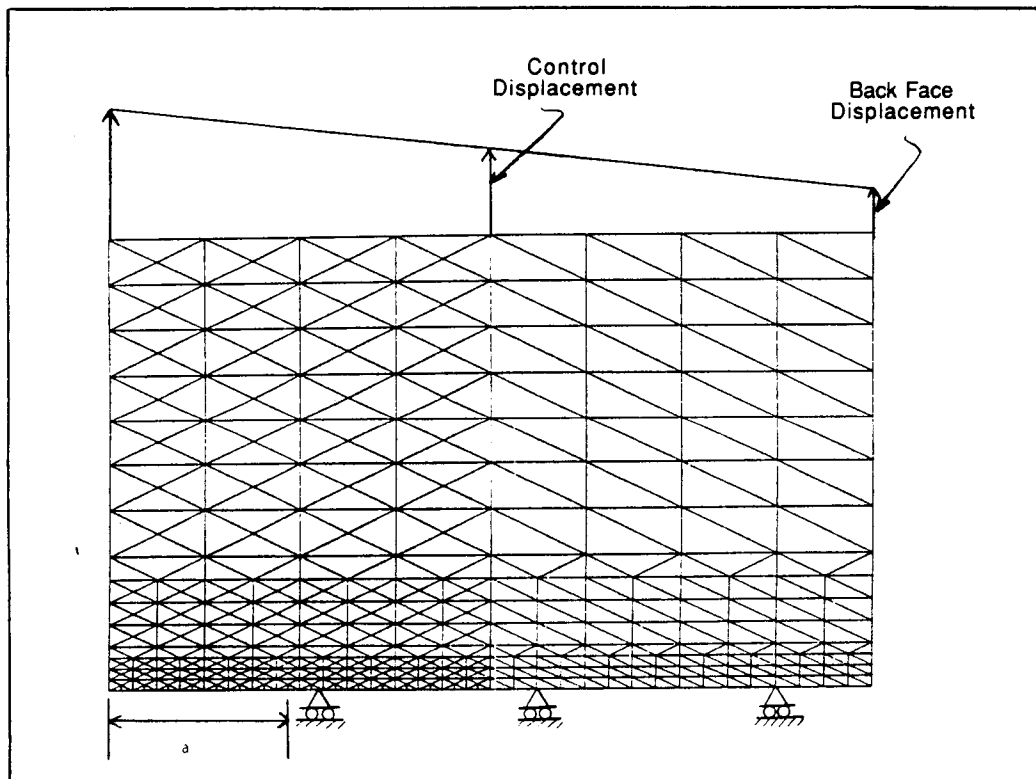


Figure 6. Finite Element Model of the Gage Section of Single Edge Notch Specimen

ANALYTICAL SIMULATION OF CRACK GROWTH

Besides understanding the boundary conditions, it is also necessary to simulate the influence of crack closure in the FEM analysis, to correctly calculate the value of the fracture mechanics parameters while the crack is open. To include the closure effect, it is necessary to simulate the plastic wake that is created by a growing crack. The attached figure schematically shows how the crack was incremented in the analyses. After a complete loading cycle, simulated by the control displacement going through a complete cycle, the crack is incremented over the length of a couple of element widths. Another cycle is then simulated before the crack is incremented again. In this manner, the whole history of the loading sequence can be simulated giving confidence in the resulting PI integrals. It should be noted that this process is inherently nonlinear; thus, the analysis has two nonlinear loops since the material is also nonlinear because of plastic strains.

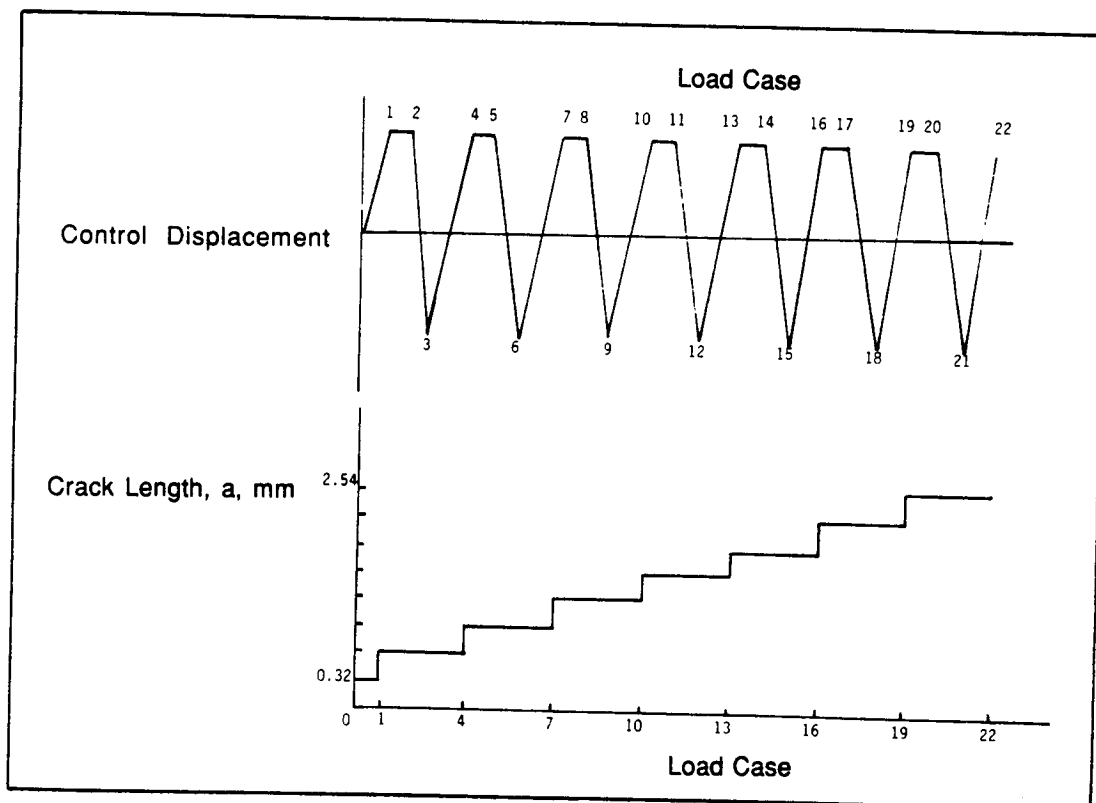


Figure 7. Schematic of Loading Steps in Crack
LeRC-LST '88 Growth Simulation

CORRELATION OF FEM AND EXPERIMENTAL RESULTS

After each finite element simulation, it is possible to compare the accuracy of the analysis with the experiment. This is accomplished by comparing two test measurements not used in generating the analysis: neither the applied load (or nominal stress) nor the measured crack mouth opening displacement, CMOD, are used in the analytical simulations. The attached figure shows two such comparisons from a single test with a strain range of 1.15% at two different crack lengths. As shown, the analytical procedure very accurately predicts the variation in nominal stress with CMOD for both short and long cracks.

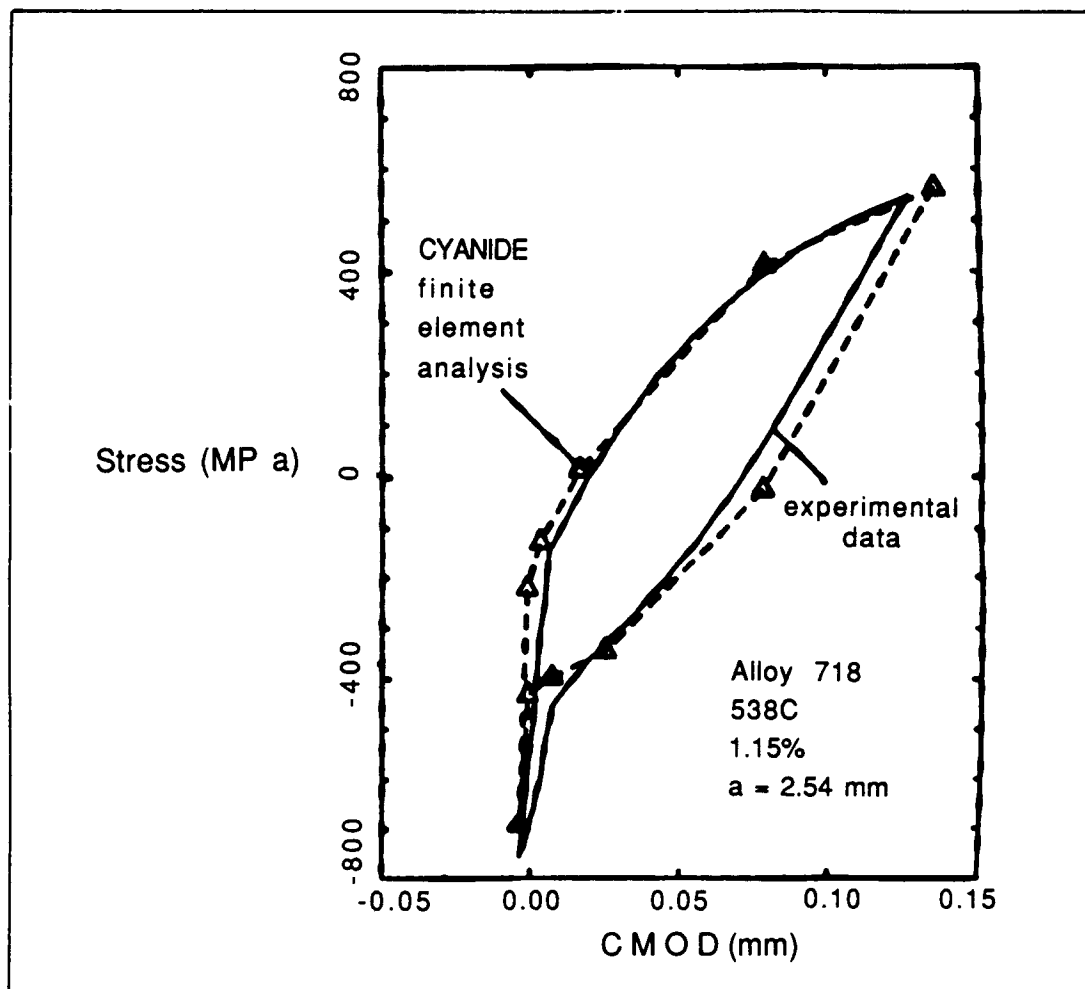


Figure 8. Average Cross Section Stress -CMOD Hysteresis Loop

PATH INDEPENDENCE

Once the analysis has been shown to correlate with the experimental measurements, the results can be used with confidence to calculate the PI integrals. A fundamental property of the nonlinear fracture mechanics integrals is path independence. The attached figure shows that this property was maintained in the current analyses for one of the integrals that was found to be capable of correlating inelastic strain crack growth.

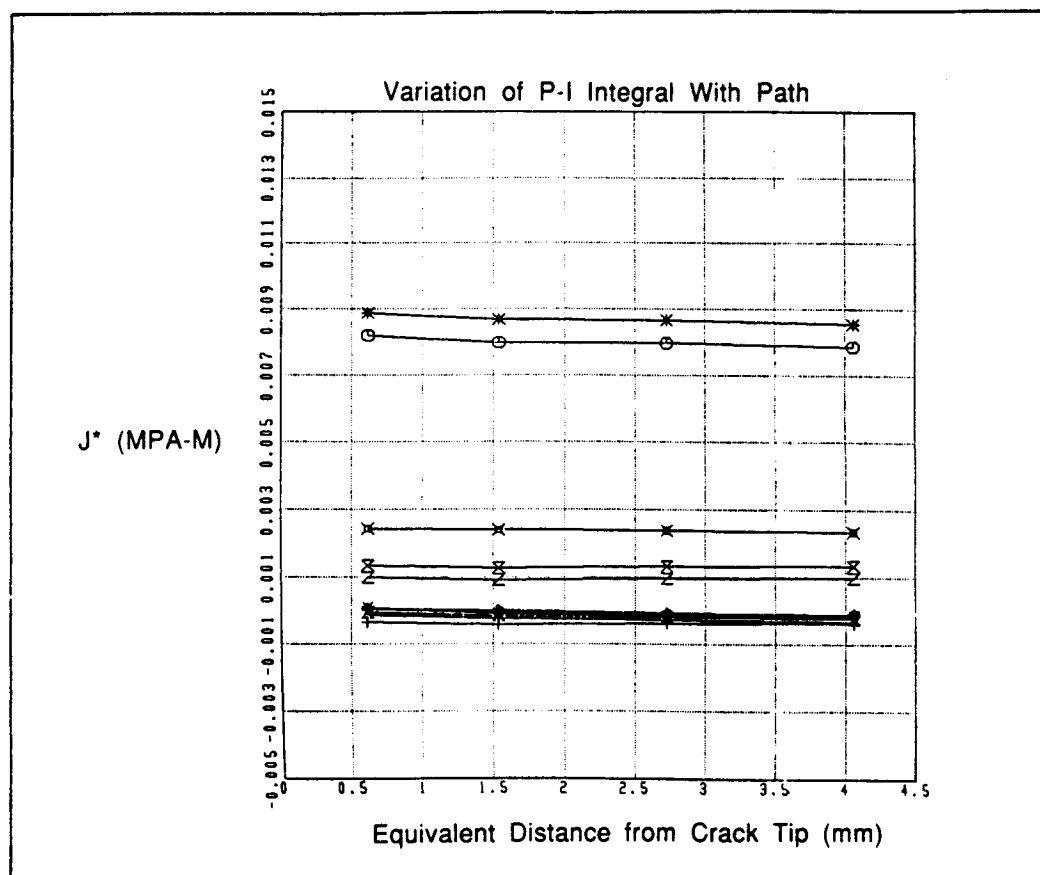


Figure 9. Path Independence

CORRELATION OF CRACK GROWTH DATA

Using the PI integrals and knowing the measured crack growth rates from a given test, it is possible to determine whether a parameter can correlate the measured crack growth rates from several different tests. The attached figure shows that one PI integral can correlate the crack growth rate results at one temperature with different strain ranges. The same test results were shown earlier in a plot which compared the data on the basis of the stress intensity factor. It was found that several nonlinear parameters were capable of correlating these data. With parameters such as these, better predictions of crack growth in hot path components will be possible.

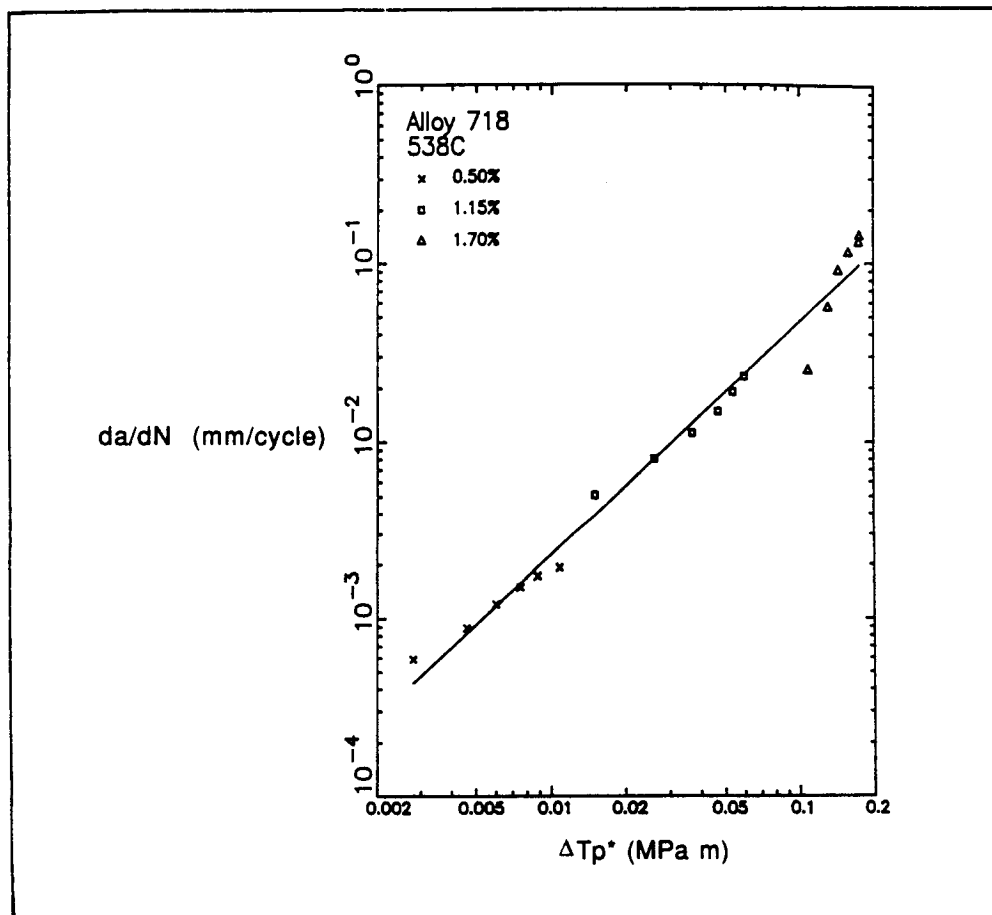


Figure 10. da/dN Versus ΔT_p^*

ANALYSIS OF TEMPERATURE GRADIENT EXPERIMENT

Another factor of importance to predicting crack growth in hot path components, is the influence of temperature gradients. The attached figure shows a comparison of predicted load with control displacement for a cracked SEN specimen which was tested with a temperature gradient of over 175C maintained over the gage section. As shown, the response is well predicted using nonlinear FEM analysis.

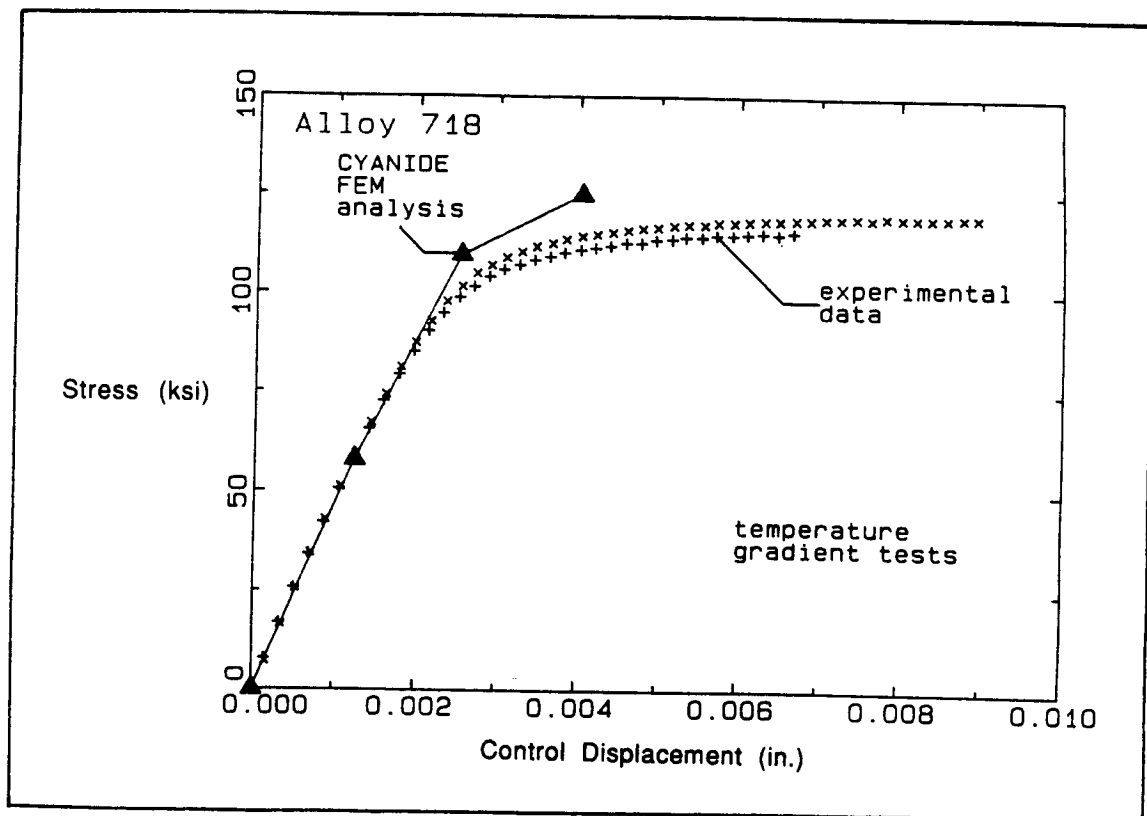


Figure 11. Analysis of Temperature Gradient Experiment

FATIGUE AND DAMAGE

SESSION OVERVIEW

Marvin H. Hirschberg
Structures Division
NASA Lewis Research Center

There are seven presentations scheduled for this session. Each presenter will give an executive overview of approximately 5 minutes followed by a question-and-answer period of another 5 minutes. All the presenters will also be making subsequent poster presentations where you will have an opportunity to discuss the work in much greater detail.

It should be noted that the fatigue and damage and life prediction papers being presented in this session are all focused on the most significant kinds of problems and environments associated with hot sections of propulsion systems. We find, from experience, that the hot section components are the most life-limiting parts of the systems and have a major impact on both cost and reliability of these systems. To develop the ability to understand and predict the structural life of such systems is very difficult and challenging but, as we will hear, substantial progress has and is being made.

The presentations for this session are as follows:

1. Cumulative Fatigue Damage Models. M.A. McGaw, NASA Lewis.
2. Fatigue Damage Mapping. D. Socie, University of Illinois.
3. Bithermal Fatigue: A Simplified Alternative to Thermomechanical Fatigue. M.J. Verrilli, NASA Lewis.
4. Life Prediction Modeling Based on Strainrange Partitioning. G.R. Halford, NASA Lewis.
5. Life Prediction Modeling Based on Cyclic Damage Accumulation. R.S. Nelson, Pratt & Whitney.
6. Fatigue Damage Modeling for Coated Single Crystal Superalloys. D.M. Nissley, Pratt & Whitney.
7. Life and Reliability of Rotating Disks. E.V. Zaretsky, NASA Lewis.

CUMULATIVE FATIGUE DAMAGE MODELS

Michael A. McGaw
Fatigue and Fracture Branch
NASA Lewis Research Center

ABSTRACT

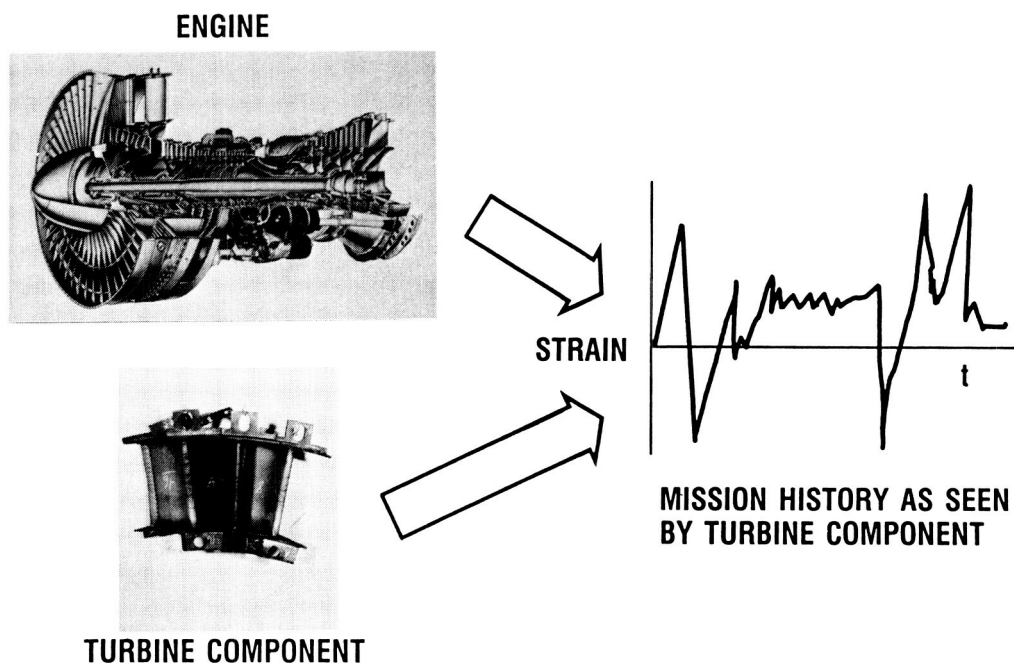
The problem of calculating expected component life under fatigue loading conditions is complicated by the fact that component loading histories contain, in many cases, cyclic loads of widely varying amplitudes. In such a case one requires a cumulative damage model, in addition to a fatigue damage criterion, or life relationship, in order to compute the expected fatigue life. The traditional cumulative damage model used in design is the linear damage rule. This model, while being simple to use, can yield grossly unconservative results under certain loading conditions. Research at the NASA Lewis Research Center has led to the development of a nonlinear cumulative damage model, named the double damage curve approach (DDCA), that has greatly improved predictive capability. This model, which considers the life (or loading) level dependence of damage evolution, has been applied successfully to two polycrystalline materials, 316 stainless steel and Haynes 188. The cumulative fatigue behavior of the PWA 1480 single-crystal material is currently being measured to determine the applicability of the DDCA for this material.

PRECEDING PAGE BLANK NOT FILMED

OVERVIEW

MISSION HISTORY PRODUCES COMPLEX COMPONENT LOADING HISTORIES

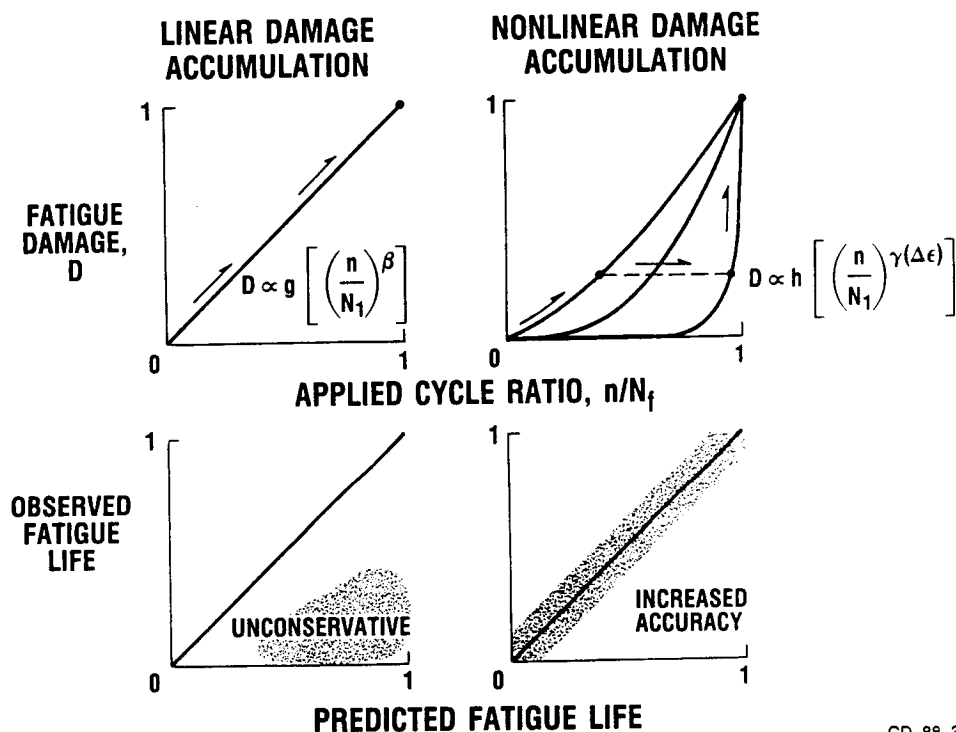
Mission profiles derived from aircraft gas turbine engine usage resolve into complex thermal and mechanical loading histories on many hot-section components. Components whose useful life is limited by such loadings experience creep and fatigue in varying and interacting degrees, both within a cycle and over the service life. A typical component is a hot-section turbine blade. The figure shows the strain history resulting from thermal and mechanical loading induced by the mission history. The strain history is that experienced at the life-limiting, or critical, location of the turbine blade.



CD-88-32318

A MORE ACCURATE CUMULATIVE FATIGUE DAMAGE RULE

When considering the life of components subjected to complex fatigue loading histories in the interest of predicting the useful component life as limited by fatigue, it is common practice to employ a fatigue crack initiation life relationship in conjunction with a cumulative damage model. Traditionally the cumulative damage model used is the linear damage rule. Although using this rule greatly simplifies life prediction calculations, it can lead to unconservative results under certain loading conditions. Research at NASA Lewis has led to the development of a nonlinear cumulative damage model that greatly increases the accuracy of such calculations. Named the double damage curve approach (DDCA), this new model considers the life (or loading) level dependence of fatigue damage evolution. In certain cases the predictions resulting from using the DDCA are nearly an order of magnitude more accurate than those made under the linear damage rule. Example applications are given below.



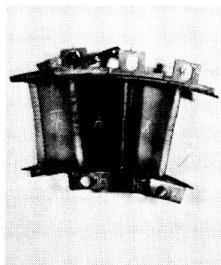
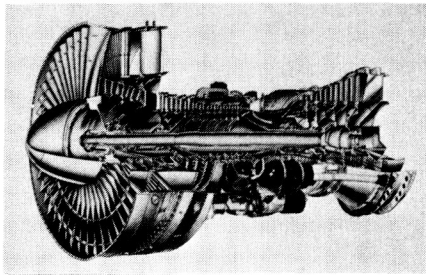
CD-88-32319

POSTER PRESENTATION

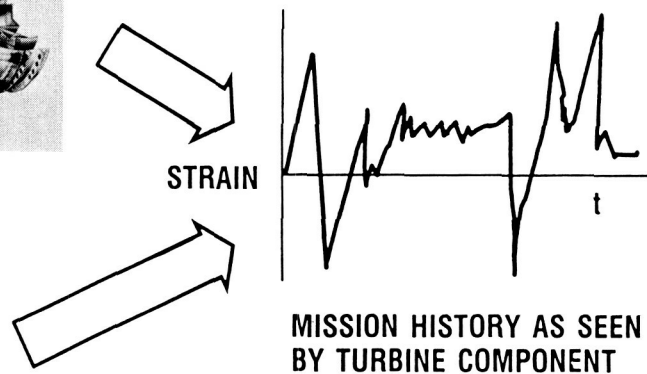
MISSION HISTORY PRODUCES COMPLEX COMPONENT LOADING HISTORIES

Mission profiles derived from aircraft gas turbine engine usage resolve into complex thermal and mechanical loading histories on many hot-section components. Components whose useful life is limited by such loadings experience creep and fatigue in varying and interacting degrees, both within a cycle and over the service life. A typical component is a hot-section turbine blade. The figure shows the strain history resulting from thermal and mechanical loading induced by the mission history. The strain history is that experienced at the life-limiting, or critical, location of the turbine blade.

ENGINE



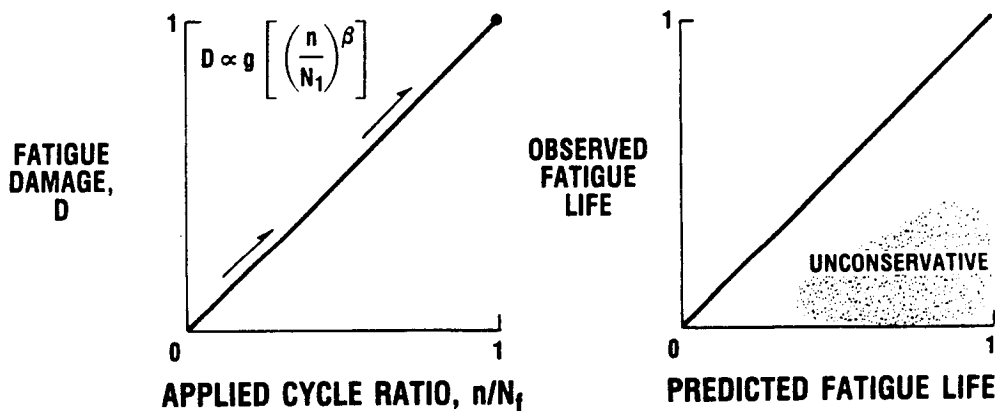
TURBINE COMPONENT



CD-88-32318

LINEAR DAMAGE RULE

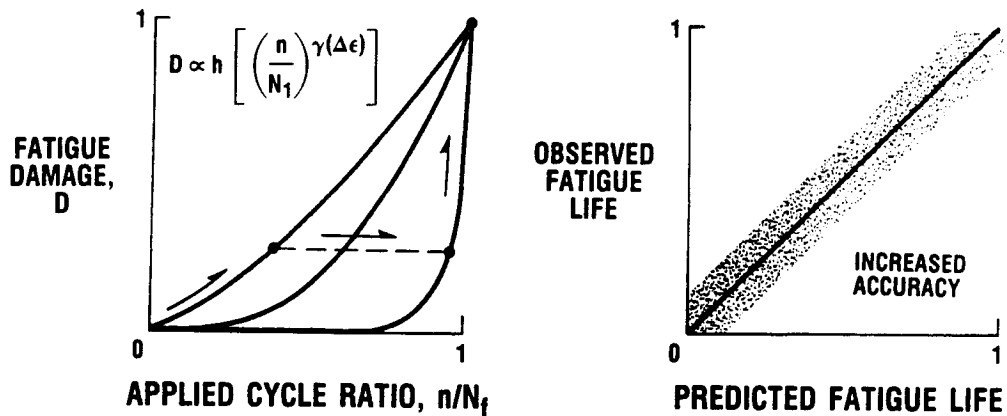
When considering the life of components subjected to complex fatigue loading histories in the interest of predicting the useful component life as limited by fatigue, it is common practice to employ a fatigue crack initiation life relationship in conjunction with a cumulative damage model. Traditionally the cumulative damage model used is the linear damage rule (Miner, 1945). This rule considers the evolution of fatigue damage to be independent of the life (or loading) level. This implies that all life levels share the same fatigue damage evolution curve, regardless of the shape of this curve. Although this assumption greatly simplifies life prediction calculations, in certain cases it can lead to unconservative results. An example of this is high-amplitude straining (low-cycle fatiguing) followed by low-amplitude straining (high-cycle fatiguing). The life predicted by the linear damage rule for this case can be in error from that observed in experiment by as much as nearly an order of magnitude, depending on the relative life levels involved (Manson and Halford, 1981).



CD-88-32320

A MORE ACCURATE CUMULATIVE FATIGUE DAMAGE RULE

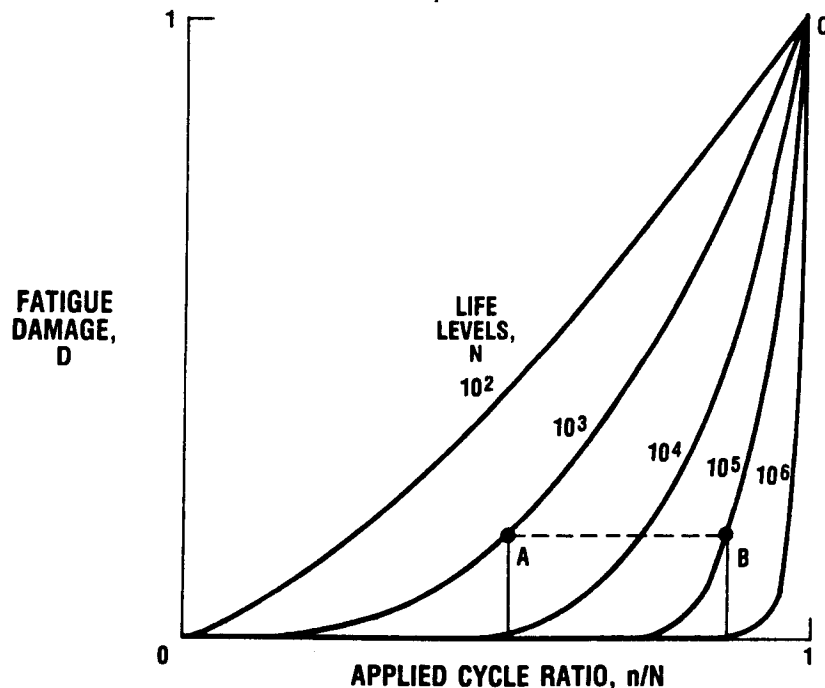
Research at NASA Lewis has led to the development of a nonlinear cumulative damage model that greatly increases the accuracy of cumulative fatigue life calculations. Named the double damage curve approach (DDCA), this new model considers the life (or loading) level dependence of fatigue damage evolution (Manson and Halford, 1986). In this way each life level possesses an individual damage evolution curve, the shape of which may vary to the extent that the relationship to the other life curves is maintained. In certain cases such as in the previous example, wherein a block of low-cycle fatigue is followed by high-cycle fatigue to failure, the predictions resulting from the use of the DDCA are nearly an order of magnitude more accurate than those made under the linear damage rule. These predictions thus more realistically model the fatigue damage interaction behavior of polycrystalline materials.



CD-88-32321

DEVELOPMENT OF DAMAGE CURVE APPROACH

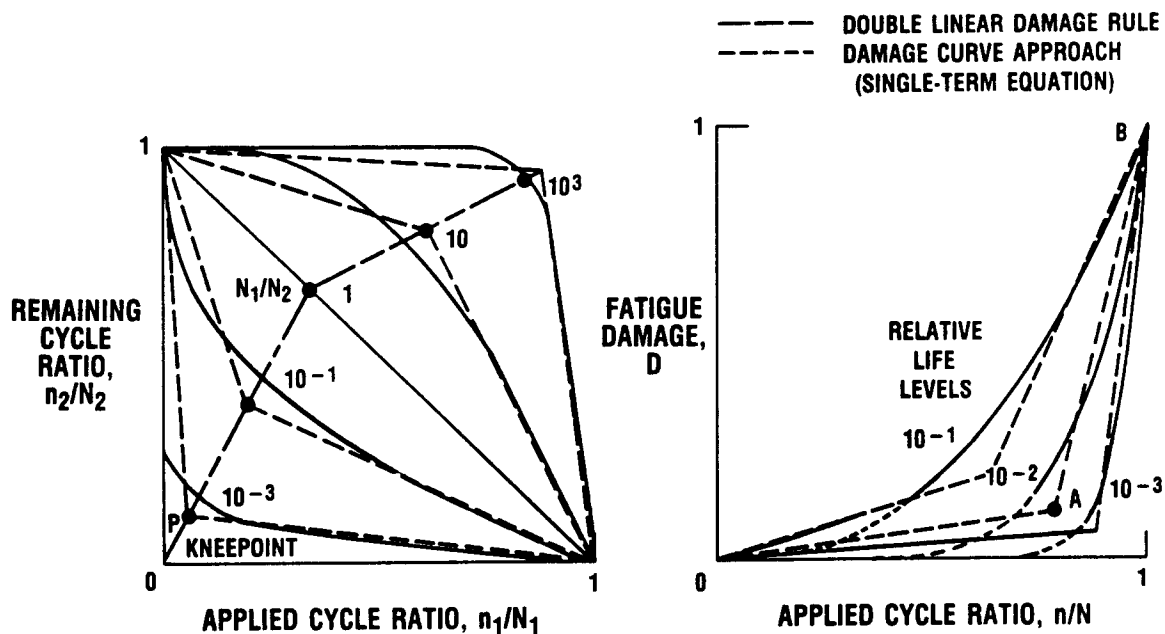
The approach taken at Lewis has been to phenomenologically model the damage accumulation process. It is generally recognized that the major manifestation of fatigue damage is the creation, nucleation, and growth of cracks. Although the usual approach is to treat a single, dominant crack, the early stages of development of such a crack are characterized by many complicated processes, including dislocation agglomeration, subcell formation, multiple microcrack formation, and the growth of these cracks to the point of linkup to form the dominant crack. Clearly the mechanisms by which fatigue damage occur are complex, and thus an empirical formulation of the "effective crack growth" equation was developed that accounts for the effects of these processes without specifically identifying them (Manson and Halford, 1981). Taking the effective crack growth as the measure of fatigue damage and applying it to the multiple loading level case resulted in the damage curve approach (DCA). A schematic representation of the damage evolution described by this approach is shown in the figure. Note that, in contrast to the linear damage rule, the dependence of damage evolution on life (or loading) level is accounted for in the damage curve approach.



CD-88-32322

DEFICIENCIES OF DCA AND DLDR

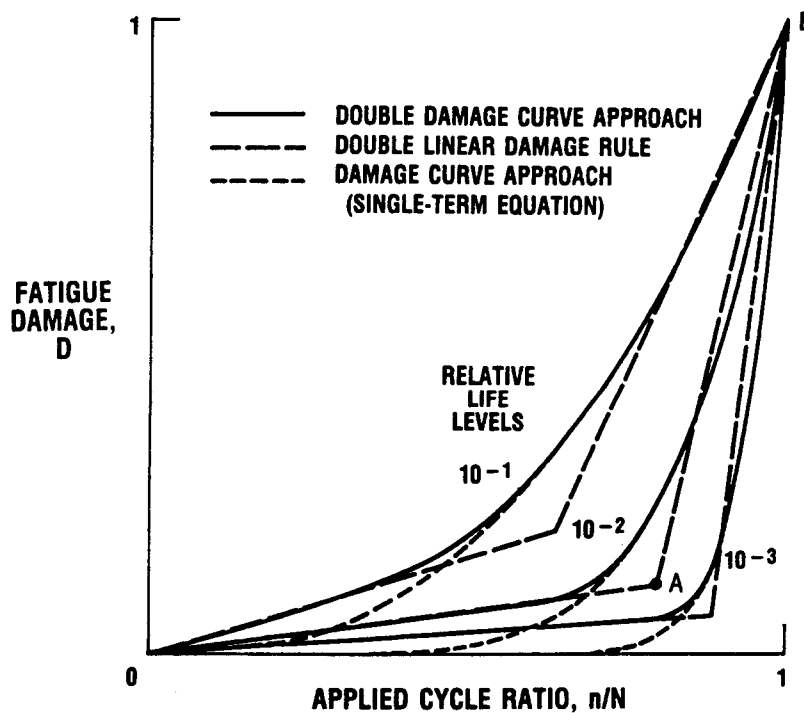
The damage curve approach provided a much more realistic picture of fatigue damage accumulation under variable amplitude loading. However, experience with the approach in conjunction with prior work on another cumulative damage method, the double linear damage rule (DLDR), suggested that the single-term DCA was perhaps overly conservative in certain cases (Manson and Halford, 1985). This was especially evident in the two-level loading case, wherein low-cycle fatiguing for a certain number of cycles is followed by high-cycle fatiguing to failure. In this case the DCA predicts a substantial reduction in remaining high-cycle-fatigue capability for small amounts of low-cycle fatigue. In contrast, the double linear damage rule, a method that models the accumulation of fatigue damage by considering the process as the sum of two linear damage accumulation regimes, predicts a more physically realistic behavior in this case. This leads to the consideration of a double-term damage curve equation that would accurately model damage accumulation behavior while retaining the attractive aspects of the DCA.



CD-88-32323

DEVELOPMENT OF DOUBLE DAMAGE CURVE APPROACH

To ameliorate this difficulty with the DCA, we developed another term, guided by the experience provided by the double linear damage rule (DLDR). The resulting expression was termed the double damage curve approach (DDCA) (Manson and Halford, 1985). As the figure shows, at low values of the cycle fraction, the DDCA followed closely the damage accumulation behavior predicted by the DLDR, but at mid to high values of the cycle fraction it followed the DCA. The resulting cumulative damage equation retains the attractive features of the DCA, viz, no specialized materials tests are required and the equation is cast in terms of the life level, so that any appropriate fatigue life expression may be used to relate the fatigue life to macroscopic variables such as strain or stress. Note that in the DDCA (and the DCA as well) the degree of damage interaction depends on the ratio of the life levels involved; the further apart the respective low- and high-cycle-fatigue life levels are, the more pronounced is the interaction.

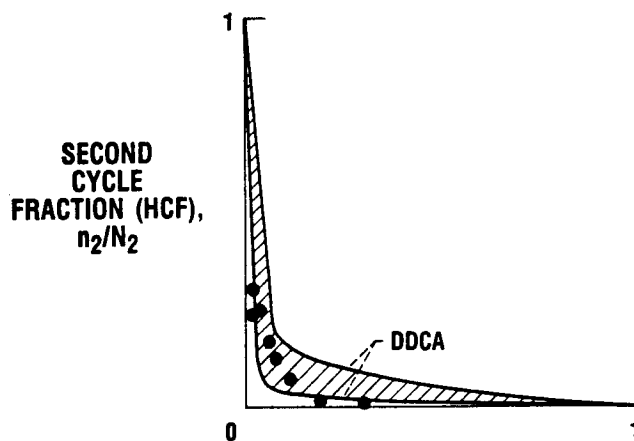


CD-88-32324

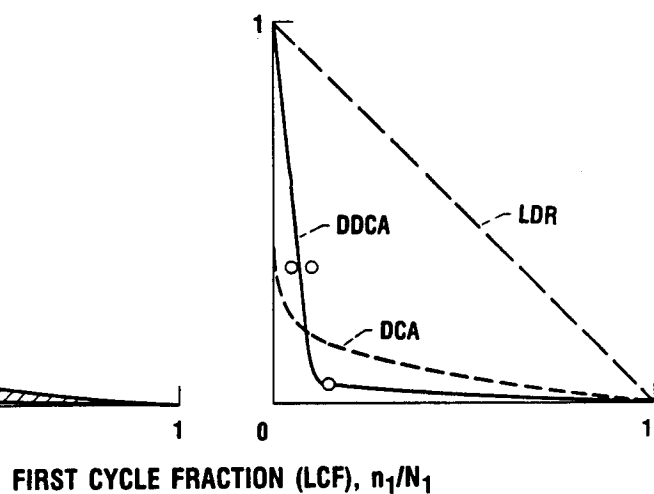
APPLICATION OF DDCA TO POLYCRYSTALLINE ALLOYS

The DDCA has been applied to two polycrystalline materials: 316 stainless steel and Haynes 188, as shown in the figures (Manson and Halford, 1985). For the 316 stainless steel the low-cycle-fatigue portion of the tests was conducted under thermomechanical conditions and the high-cycle-fatigue portion under isothermal conditions to loosely approximate the loading experienced by a component in a rocket engine undergoing initial firing and subsequent operation. The nature of the thermomechanical cycle used for the low-cycle fatigue was such that a negligibly small amount of creep was introduced, so that the failure mode was by transcrystalline cracking (fatigue failure). The cumulative damage analysis of these experiments could therefore be made only on considerations of fatigue damage. The tests conducted on the Haynes 188 material were performed under isothermal conditions, with the strain rates such that creep was precluded. In general, the predictive accuracy of the DDCA in these two cases was quite good and represented a substantial improvement over the linear damage rule.

HAYNES 188 AT 1400 °F (BIZON, ET AL.)



316 STAINLESS STEEL

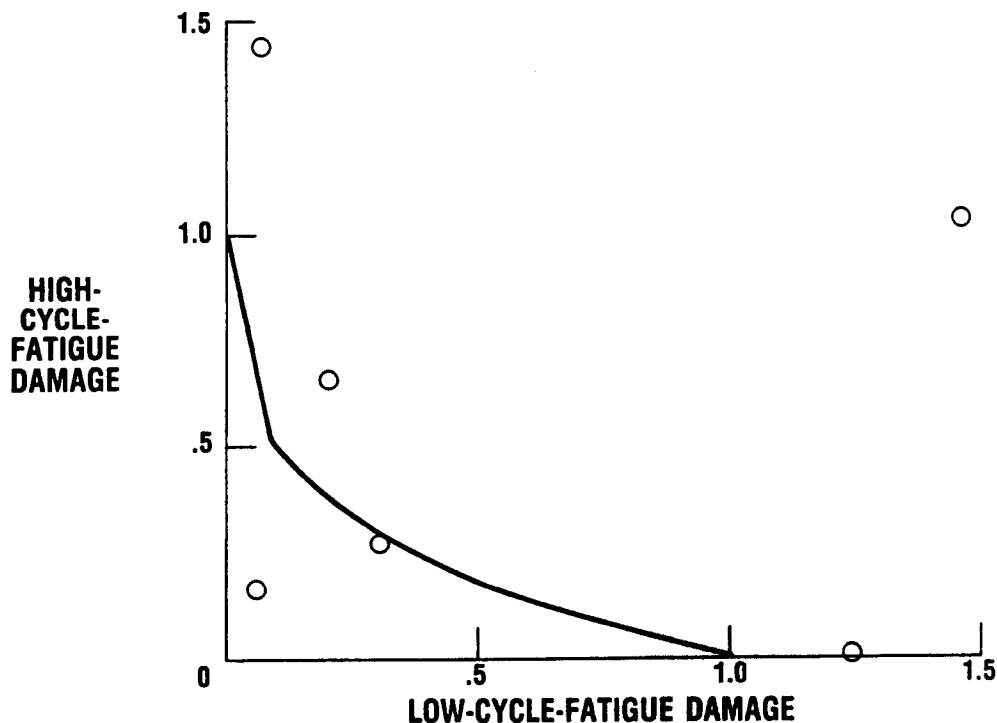


CD-88-32325

APPLICATION OF DDCA TO SINGLE-CRYSTAL ALLOY PWA 1480

Recent cumulative damage work being carried out at Lewis concerns the cumulative fatigue damage behavior of two materials of interest in space shuttle main engine (SSME) turbopump applications: MAR-M 246 + Hf, the current bill of materiel for SSME turbine blading, and a single-crystal superalloy, PWA 1480, a candidate replacement material for turbopump blading. The work will identify the cumulative damage behavior of these materials, so that the relative applicability of the polycrystalline-based DDCA may be determined. Experimental results to date have only been obtained for the single-crystal material, with limited cumulative fatigue data having been generated. This material contains significant levels of microporosity as a result of current processing techniques; microporosity is generally responsible for producing failure in fatigue. The effects of microporosity have been incorporated into the baseline fatigue life relationship for this material (McGaw, 1987), so that the reference life levels can be more accurately determined for the cumulative fatigue analysis. The microporosity-compensated interaction data generated to date are shown in the figure, with the DDCA prediction. Additional experiments are being conducted to more clearly determine the cumulative fatigue behavior of this material.

MICROPOROSITY COMPENSATED



CD-88-32326

REFERENCES

- Manson, S.S., and Halford, G.R., 1981, "Practical Implementation of the Double Linear Damage Rule and Damage Curve Approach for Treating Cumulative Fatigue Damage," Int. J. Fract., vol. 17, pp. 169-172.
- Manson, S.S., and Halford, G.R., 1985, "Re-examination of Cumulative Fatigue Damage Analysis - An Engineering Perspective," NASA TM-87325.
- McGaw, M.A., 1987, "The Fatigue Damage Behavior of a Single Crystal Superalloy," M.S. Thesis, Case Western Reserve University, Cleveland, Ohio.
- Miner, M.A., 1945, "Cumulative Damage in Fatigue," J. Appl. Mech., vol. 67, pp. A159-A164.

FATIGUE DAMAGE MAPPING

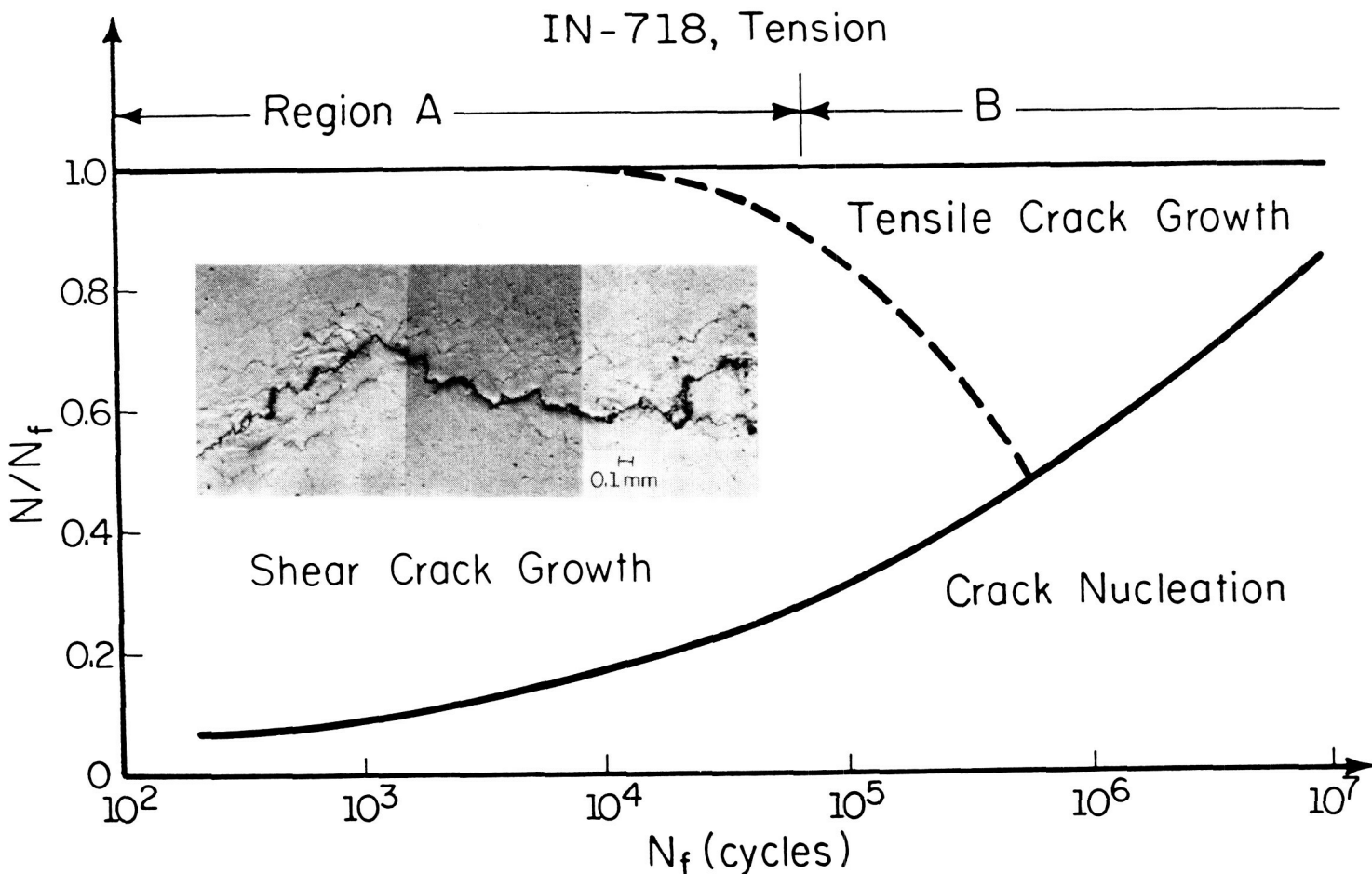
Darrell Socie

Department of Mechanical and Industrial Engineering
University of Illinois at Urbana-Champaign

Observations of fatigue crack nucleation and early growth are presented. The state of stress/strain has been shown to play a significant role in this process. Early growth occurs on planes experiencing the largest range of shear strain (Mode II) or normal strain (Mode I) depending on the stress state, strain amplitude, and microstructure. These observations have been summarized in a fatigue damage map for each material. These maps provide regions where one fatigue failure mode dominates the behavior. Each failure mechanism results in a different failure mode. Once the expected failure mode has been identified, bulk deformation models based on the cyclic stresses and strains can be used to obtain reliable estimates of fatigue lives for complex loading situations.

EXECUTIVE OVERVIEW OF FATIGUE DAMAGE MAPPING

A fatigue damage map for Inconel 718 loaded in cyclic tension is given below. The vertical scale is presented in terms of life fraction and the horizontal scale in terms of fatigue life. The solid line represents the first observation of a surface crack 100 μm long and serves as a demarcation between initiation and growth. The dashed line represents the demarcation between crack growth on planes of maximum shear strain amplitude and crack growth on planes of maximum principal strain amplitude. Region A is characterized by shear initiation followed by extensive shear crack growth with final failure occurring by a linking of shear cracks similar to the tearing of perforated paper. Region B is characterized by shear initiation followed by crack growth along the principal stress direction. A third region is often observed at long lives and small strains where there is no observable initiation or shear initiation resulting in nonpropagating cracks. A separate damage model is required for each region.

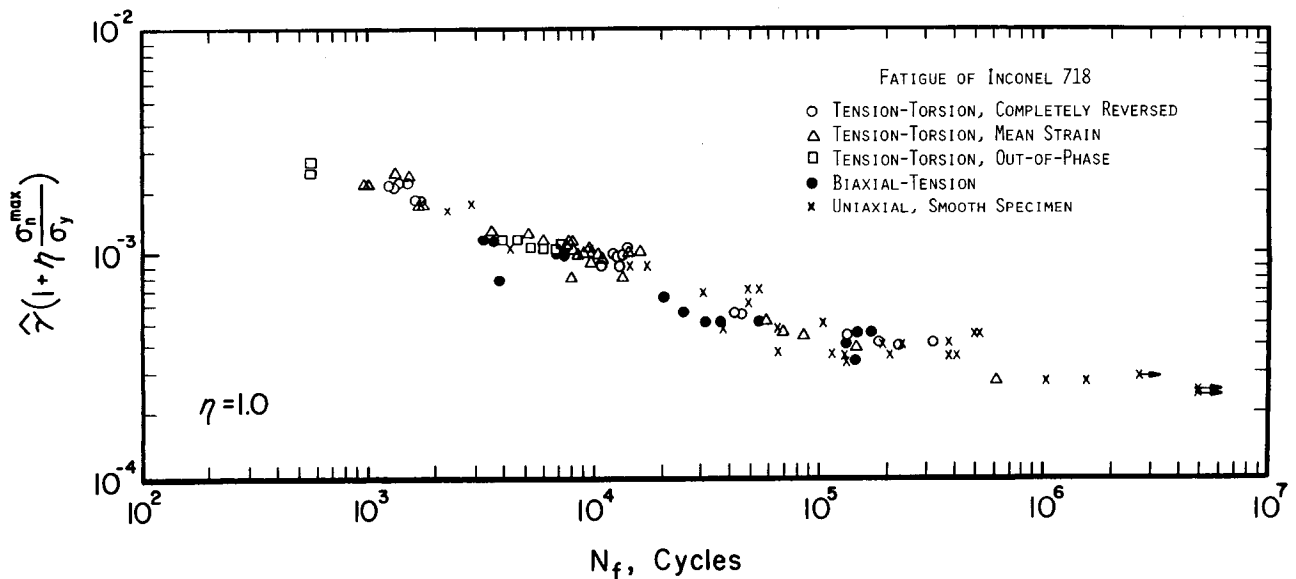


EXECUTIVE OVERVIEW OF FATIGUE DAMAGE MAPPING

The damage maps indicate that a shear strain based theory is most appropriate for this material for lives below about 10^5 cycles. One such damage parameter has been proposed by Fatemi and Socie (1985)

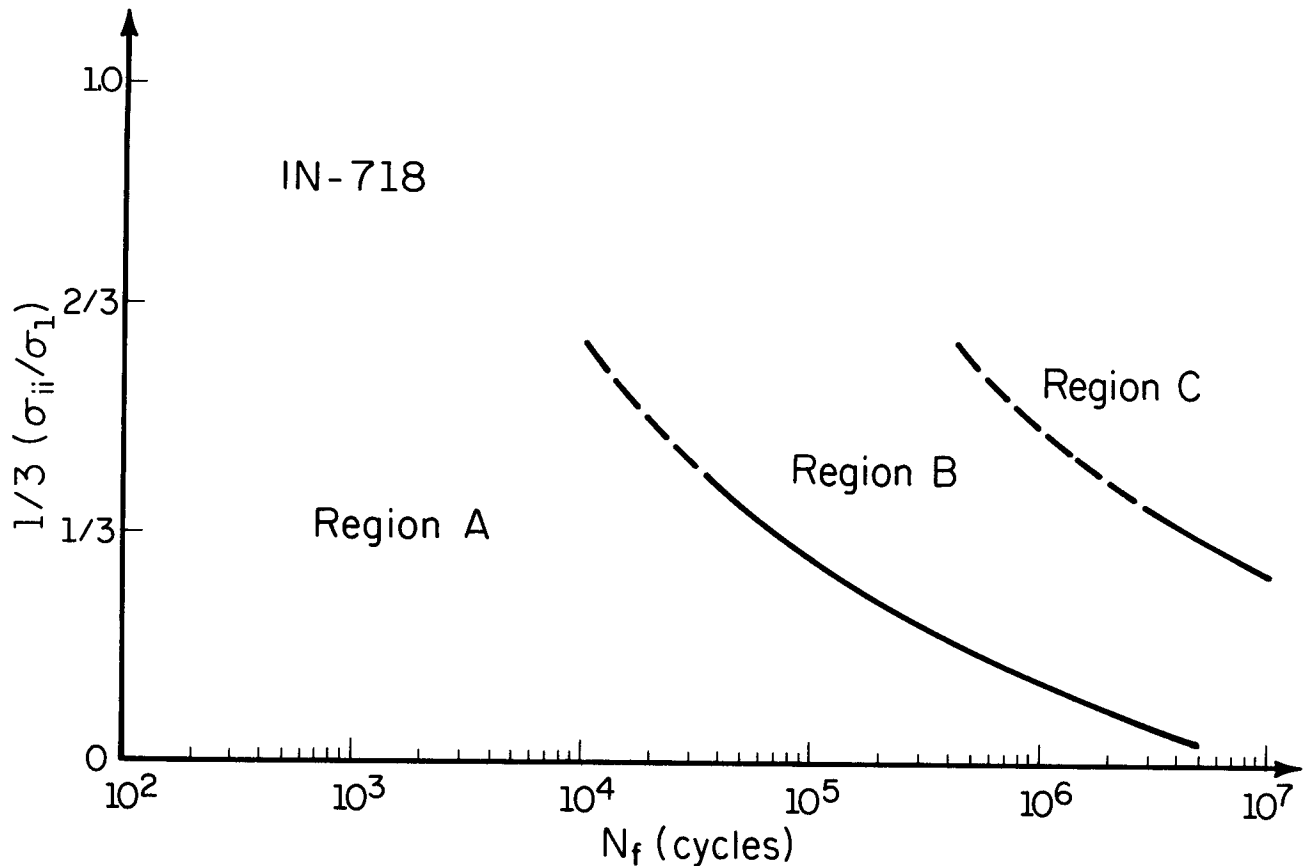
$$\gamma \left(1 + \frac{\sigma_n}{\sigma_y} \right)$$

Two parameters are considered to cause fatigue damage. The primary damage is caused by the cyclic shear strains (γ). Stresses normal to the cyclic shear strain tend to open any microcracks and enhance their growth. Hence the second term can be interpreted as including crack closure effects. The term also includes effects from any additional cyclic hardening that is often observed during nonproportional loading. The stress normal to the shear crack (σ_n) is normalized with the yield strength (σ_y) to retain the dimensionless features of strain. In this formulation no fatigue damage is computed for planes in the material that do not experience cyclic shear strain. Results are presented for a wide variety of loading histories including tension, torsion, biaxial tension, and tests with complex multiaxial mean stresses. Both proportional and nonproportional tests are included. This degree of correlation is only possible because the damage mechanism does not change for the variety of tests considered here.



FATIGUE DAMAGE MAP FOR INCONEL 718

Test data from individual stress states are summarized in the fatigue damage map for Inconel 718 given below. The vertical axis has now been plotted in terms of hydrostatic stress normalized by the maximum principal stress. Torsion, tension and biaxial tension have values of 0, 1/3, and 2/3, respectively. Regions of similar fatigue failure modes are given. Little data exists for the case of biaxial tension and these lines are shown as dashed. The map shows that over a wide range of stress states and strain amplitudes the primary failure mechanism is one of shear crack growth. The x symbols in the preceding figure that fall to the right of the central tendency of the test data represent large compressive mean stress tests. This type of behavior is expected since the fatigue damage map shows a transition from shear to tensile dominated behavior at longer lives. In this failure mode, compressive stresses would retard crack growth and prolong fatigue lives.

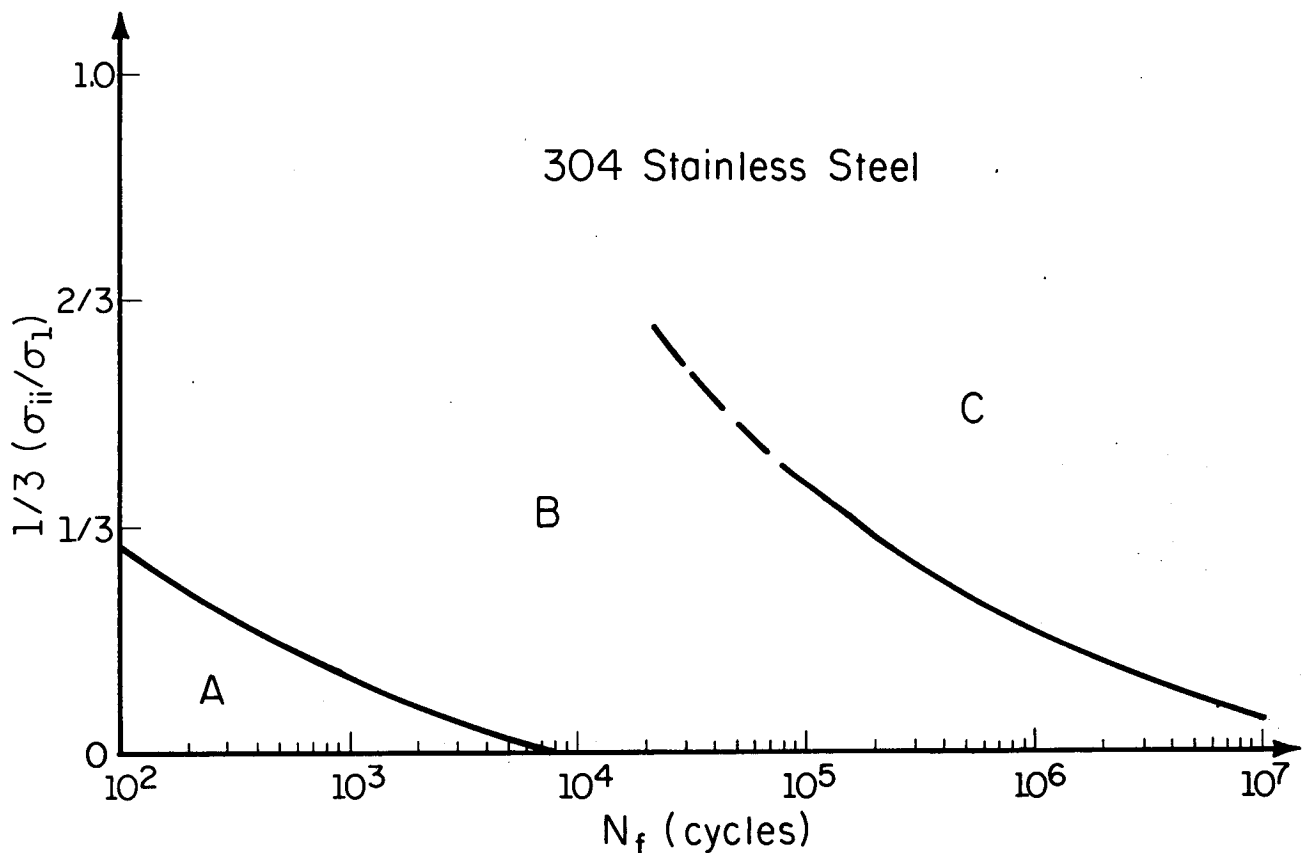


FATIGUE DAMAGE MAP FOR 304 STAINLESS STEEL

The fatigue damage map for 304 stainless steel is given below. Note that the region of shear behavior found in Inconel 718 is restricted to a narrow range in 304 stainless steel. There is a large region of tensile dominated behavior. It is suggested that a tensile strain based model is most appropriate here. One such model has been proposed by Smith, et al. (1970), and has found widespread use in uniaxial fatigue situations.

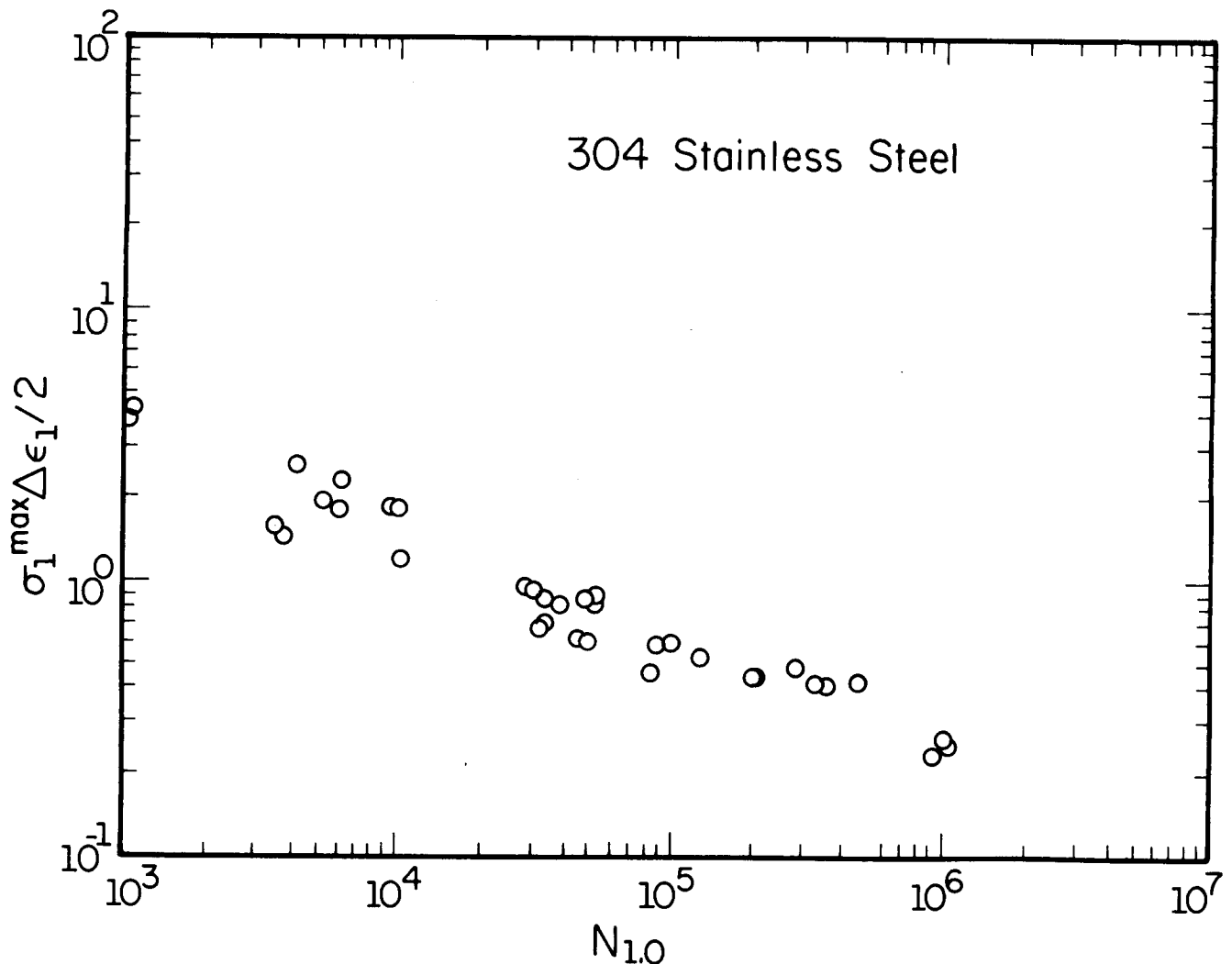
$$\sigma_{\max} \epsilon_a$$

Two parameters are considered to be the driving force for fatigue damage. The maximum principal strain amplitude, ϵ_a , and the tensile stress normal to that plane, σ_{\max} .



LIFE ESTIMATIONS FOR 304 STAINLESS STEEL

Test data for 304 stainless steel from Socie (1987) for both proportional and nonproportional tests are given below. This material cyclically hardens under nonproportional loading to a stable stress level that is nearly double that of a proportional test. The increase in cyclic stress is very damaging and must be accounted for in the model. For the same total strain range, uniaxial loading has the largest plastic strain range and longest life. Nonproportional loading tests have the smallest plastic strain range, largest stress range and shortest life.

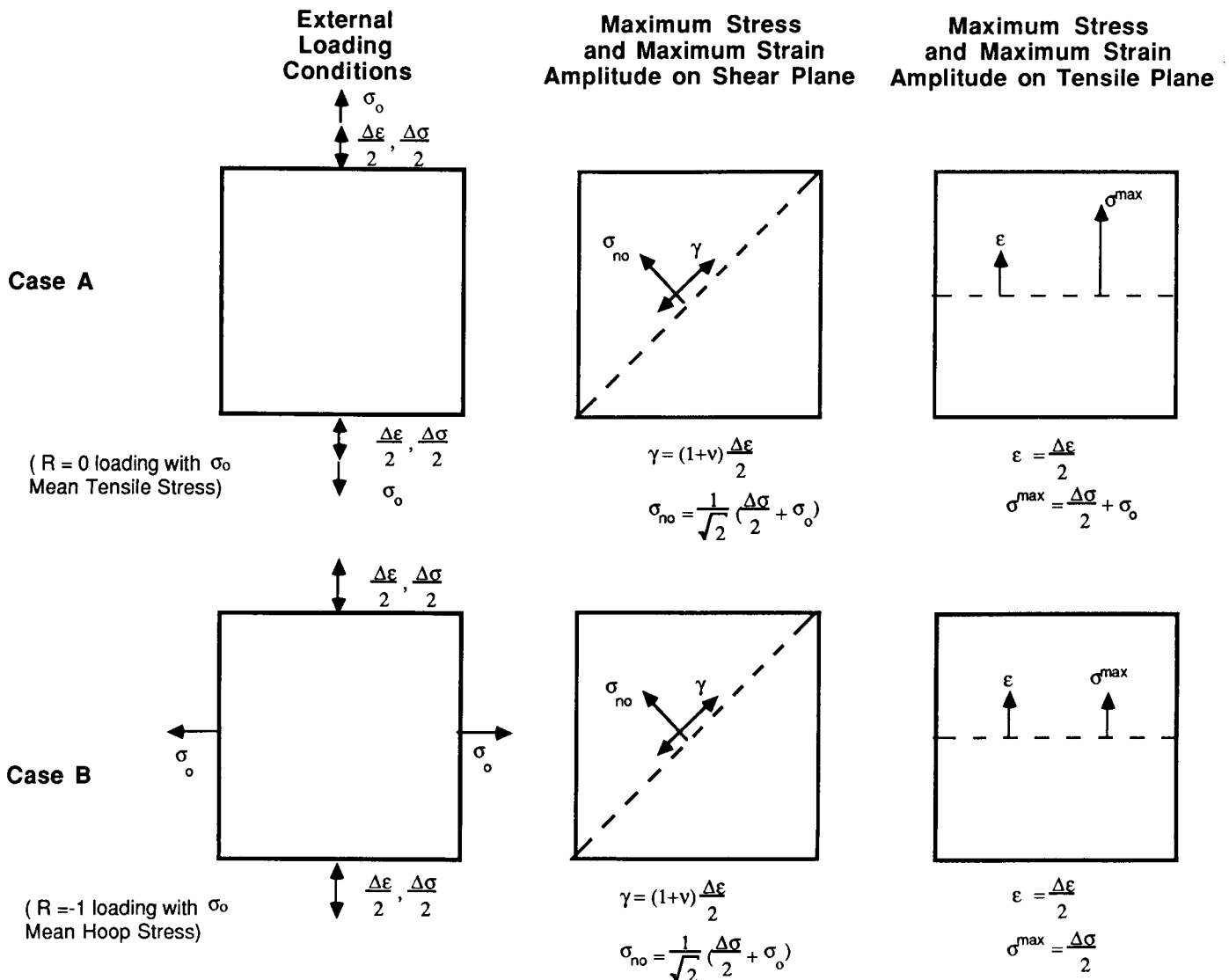


MULTIAXIAL MEAN STRESS EXAMPLE

Two loading cases that have the same shear damage parameter are given below. Consider a standard uniaxial test specimen, Case A, tested in zero to maximum strain cycling. A tensile mean stress σ_o will result. Now consider a second test, Case B, of a tubular specimen tested with the same axial strain range only in completely reversed loading. The magnitude of the mean stress in the first test is applied as a hoop stress in the second test. Since the shear damage parameter is the same for both tests the fatigue lives would be expected to be similar for a material that fails in a shear mode. Note that the tensile damage parameter for the second test is much lower since there is no mean stress in the plane experiencing the largest range of cyclic principal strain. Results for Inconel 718 are as follows:

$\Delta\epsilon/2$	σ_o	Case A	Case B
0.0005	270	4245	6735
		9768	7221

These tests confirm the selection of the damage parameter since the lives are the same for both tests. The tensile model predicts an increase in fatigue life for Case B that was not observed experimentally.



REFERENCES

Fatemi, A., and Socie, D. F. (1987), "A Critical Plane Approach to Multiaxial Fatigue Damage Including Out-of-Phase Loading," accepted for publication in Fatigue and Fracture Engineering Materials and Structures.

Smith, R. N., Watson, P., and topper, T. H. (1970), "A Stress-Strain Function for the Fatigue of Metals," Journal of Materials, JMLSA, Vol. 5, No. 4, pp. 767-778.

Socie, D. F. (1987), "Multiaxial Fatigue Damage Models," Journal of Engineering Materials and Technology, Vol. 109, No. 4, pp. 293-298.

**BITHERMAL FATIGUE: A SIMPLIFIED ALTERNATIVE
TO THERMOMECHANICAL FATIGUE**

Michael J. Verrilli
Fatigue and Fracture Branch
NASA Lewis Research Center

ABSTRACT

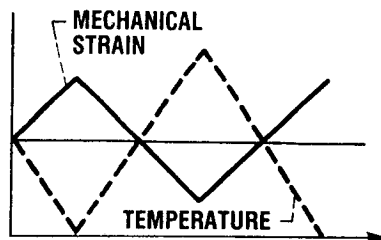
A bithermal fatigue test technique has been proposed as a simplified alternative to the thermomechanical fatigue test. Both the thermomechanical cycle and the bithermal technique can be used to study nonisothermal fatigue behavior. The difference between the two cycles is that in a conventional thermomechanical fatigue cycle the temperature is continuously varied concurrently with the applied mechanical strains, but in the bithermal fatigue cycle the specimen is held at zero load during the temperature excursions and all the loads are applied at the two extreme temperatures of the cycle. Experimentally, the bithermal fatigue test technique offers advantages such as ease in synchronizing the temperature and mechanical strain waveforms, in minimizing temperature gradients in the specimen gauge length, and in reducing and interpreting data. In addition, the bithermal cycle captures first-order effects of nonisothermal fatigue such as the influence of alternate high and low temperatures on the cyclic stress-strain response characteristics, the effects of thermal free-expansion mismatch straining between the oxide (or coating) and the substrate, and the possibility of introducing high- and low-temperature deformation mechanisms within the same cycle. The bithermal technique has been used to study nonisothermal fatigue behavior of alloys such as single-crystal PWA 1480 (Gayda et al., 1987), single-crystal René N4, cast B1900+Hf (Halford et al., 1988a), and wrought Haynes 188 (Halford et al., 1988b).

OVERVIEW

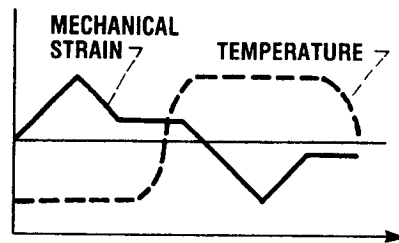
BITHERMAL VERSUS TMF

In studying TMF the bithermal cycle is a simplified alternative to the more conventional continuously varying temperature TMF cycle. Pictured below are an out-of-phase bithermal cycle and an out-of-phase TMF cycle. In an out-of-phase cycle the tensile mechanical strain is imposed at the low temperature. In the bithermal cycle the mechanical strain excursions and the temperature excursions are decoupled, whereas in the TMF cycle both temperature and mechanical strains are cycled simultaneously.

OUT-OF-PHASE TMF

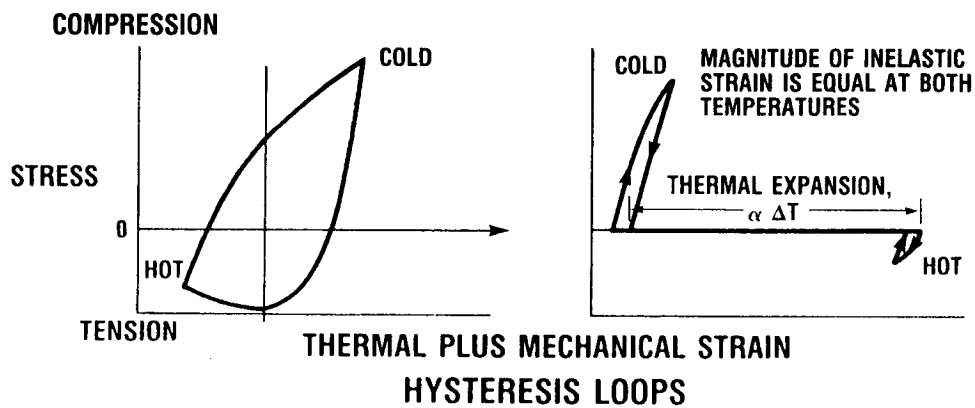


OUT-OF-PHASE BITHERMAL



TIME

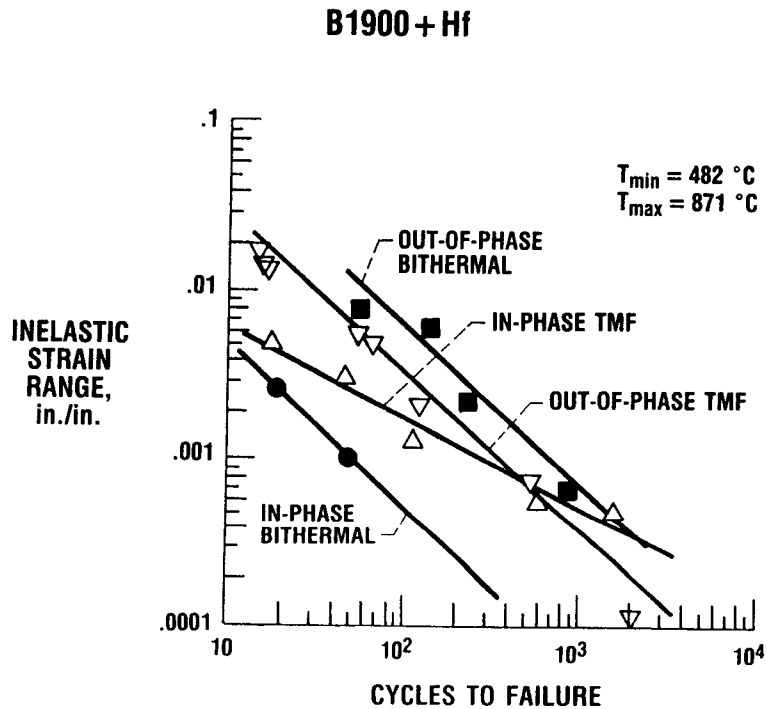
TEMPERATURE AND STRAIN WAVEFORMS



CD-88-31682

COMPARISON OF TMF AND BITHERMAL FATIGUE DATA

Does the bithermal technique really capture the important effects of a cycle that combines thermally and mechanically induced strains? For one material investigated, B1900+Hf, conventional TMF and bithermal results are similar. As the results show, the bithermal fatigue behavior bounds the TMF results (Halford et al., 1988b). One would expect that bithermal fatigue would result in slightly shorter lives than TMF. However, in this case the slightly longer life of the out-of-phase bithermal fatigue may be attributable to the longer TMF cycle time.

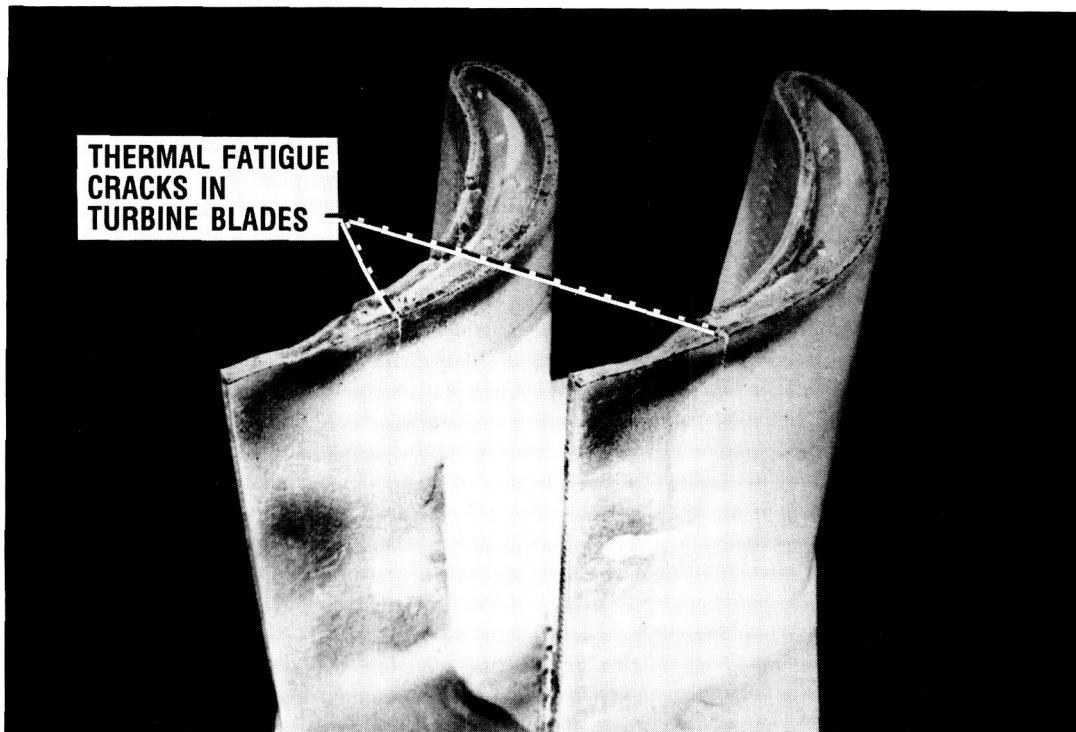


CD-88-31685

POSTER PRESENTATION

WHAT IS TMF?

Many high-temperature components, such as gas turbine blades, experience both temperatures and mechanical strains that vary with time. Thermal fatigue is the result of constrained thermal expansion in solids undergoing cyclic temperature gradients. Superimposed mechanical loadings may also be involved. The cracks in the pictured turbine blades are a result of thermal fatigue. Thermomechanical fatigue (TMF) is an experimental simplification of thermal fatigue. During TMF a material specimen is subjected to both temperatures and mechanical strains that vary cyclically.

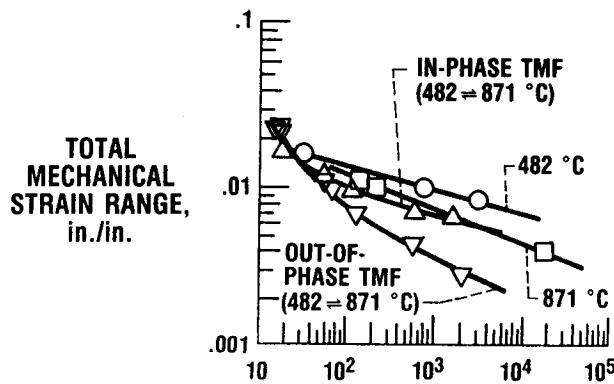


CD-88-31679

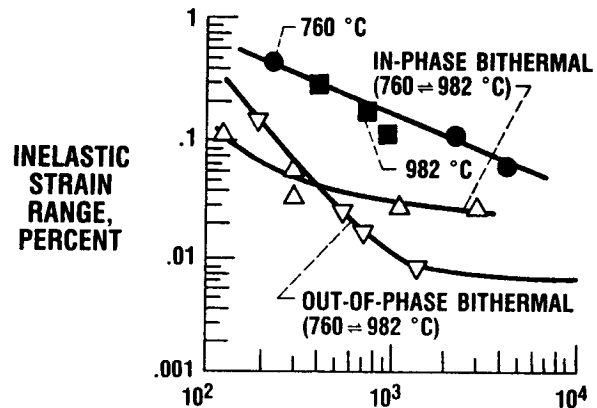
HOW DOES TMF COMPARE WITH ISOTHERMAL LCF?

For some alloys, such as the nickel-base superalloys single-crystal René N4 and polycrystalline B1900+Hf, thermomechanical fatigue has been found to yield significantly lower fatigue lives than does fatigue at either the minimum or maximum cycle temperatures. Major design codes have assumed fatigue at the maximum service temperature to be a conservative design parameter. Consequently most high-temperature, low-cycle fatigue data have been generated under isothermal conditions. This approach has been assumed to be conservative, but it is not.

B1900 + Hf



RENÉ N4 (SINGLE CRYSTAL)

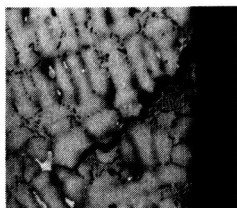


CD-88-31680

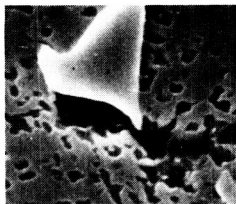
TEMPERATURE-STRAIN PHASING EFFECTS DURING TMF

Not only can thermomechanical fatigue life data vary significantly from isothermal data, but variation in the phasing of the temperature and mechanical strain can also drastically affect the crack initiation and growth mechanisms during TMF. Pictured below is the effect of temperature and mechanical strain phasing on crack initiation and crack growth in Mar-M 200 (Bill et al., 1984).

IN PHASE



CRACK TIP AND CRACK
SURFACE OXIDATION

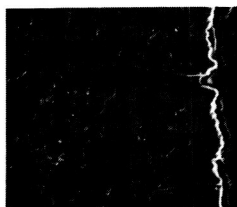


CARBIDE/MATRIX
PULL-AWAY



INTERGRANULAR
PROPAGATION

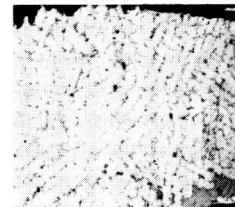
OUT OF PHASE



BLUNT CRACK TIP AND
LESS OXIDIZED
SURFACE



CRACKING WITHIN
CARBIDES



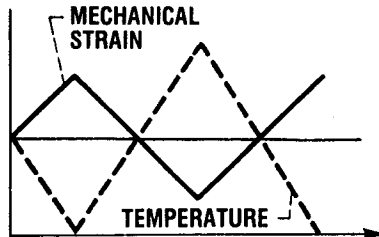
INTERGRANULAR AND
TRANSGRANULAR
PROPAGATION

CD-88-31681

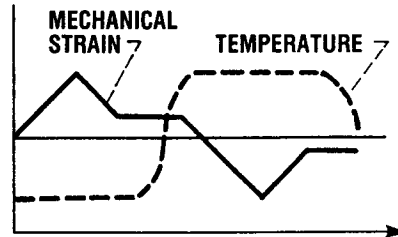
BITHERMAL VERSUS TMF

In studying TMF the bithermal cycle is a simplified alternative to the more conventional continuously varying temperature TMF cycle. Pictured below are an out-of-phase bithermal cycle and an out-of-phase TMF cycle. In an out-of-phase cycle the tensile mechanical strain is imposed at the low temperature. In the bithermal cycle the mechanical strain excursions and the temperature excursions are decoupled, whereas in the TMF cycle both temperature and mechanical strains are cycled simultaneously.

OUT-OF-PHASE TMF

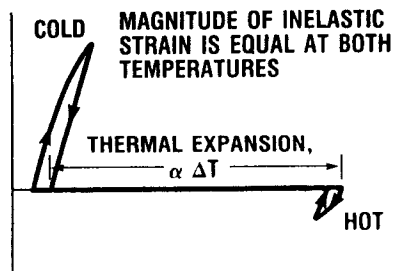
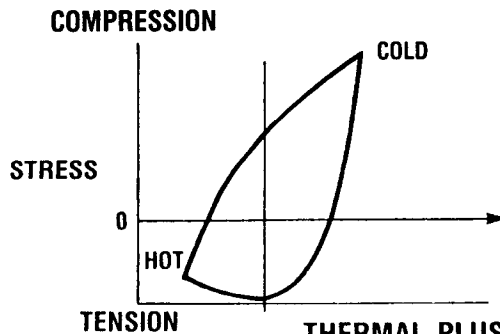


OUT-OF-PHASE BITHERMAL



TIME

TEMPERATURE AND STRAIN WAVEFORMS



HYSTERESIS LOOPS

CD-88 31682

PROS AND CONS OF BITHERMAL CYCLING

The bithermal cycling concept has advantages over TMF cycling that must be balanced against the disadvantages. Both the advantages and the disadvantages are listed below.

ADVANTAGES OF BITHERMAL CYCLING

- TEMPERATURE AND MECHANICAL STRAIN WAVEFORMS CAN BE EASILY SYNCHRONIZED.
- THERMAL-FREE EXPANSION STRAINS CAN BE EASILY SUBTRACTED FROM TOTAL (THERMAL PLUS MECHANICAL) STRAINS.
- NUMBER OF ACTIVE DEFORMATION MECHANISMS CAN BE LIMITED BY PROPER CHOICE OF TEMPERATURES.
- SAMPLES CAN DEFORM AT HIGH ENOUGH RATES TO PRECLUDE CREEP.
- TECHNIQUE CAPTURES EFFECT OF THERMAL-FREE EXPANSION MISMATCH STRAINING BETWEEN SUBSTRATE AND COATING OR OXIDE, OR BETWEEN MATRIX AND FIBERS IN A COMPOSITE.

CD-88-31683

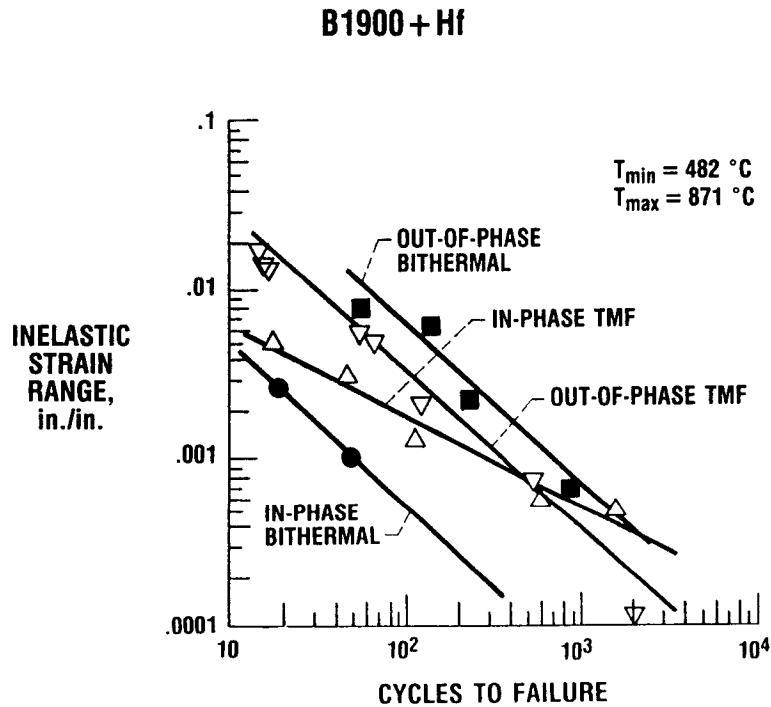
DISADVANTAGES OF BITHERMAL CYCLING

- HOLDING AT ZERO LOAD DURING TEMPERATURE EXCURSIONS CAN ALLOW UNDESIRABLE RECOVERY PROCESSES TO OCCUR.
- RESULTS CAN BE MISLEADING IF SIMULTANEOUSLY APPLIED MECHANICAL AND THERMAL STRAINS ARE IMPORTANT TO LIFE.
- THERMAL FREE-EXPANSION MISMATCH STRAINS ARE MORE SEVERE THAN THOSE OCCURRING DURING A TMF CYCLE.

CD-88-31684

COMPARISON OF TMF AND BITHERMAL FATIGUE DATA

Does the bithermal technique really capture the important effects of a cycle that combines thermally and mechanically induced strains? For one material investigated, B1900+Hf, conventional TMF and bithermal results are similar. As the results show, the bithermal fatigue behavior bounds the TMF results (Halford et al., 1988b). One would expect that bithermal fatigue would result in slightly shorter lives than TMF. However, in this case the slightly longer life of the out-of-phase bithermal fatigue may be attributable to the longer TMF cycle time.



CD-88-31685

REFERENCES

- Bill, R.C., Verrilli, M.J., McGaw, M.A., and Halford, G.R., 1984, "Preliminary Study of the Thermomechanical Fatigue of Polycrystalline Mar-M 200," NASA TP-2280.
- Gayda, J., Gabb, T.P., Miner, R.V., and Halford, G.R., 1987, "Bithermal Low-Cycle Fatigue Behavior of a NiCoCrAlY-Coated Single Crystal Superalloy," NASA TM-89831.
- Halford, G.R., McGaw, M.A., Bill, R.C., and Fanti, P.D., 1988a, "Bithermal Fatigue: A Link Between Isothermal and Thermomechanical Fatigue," ASTM STP 942, American Society for Testing and Materials, Philadelphia, pp. 625-637.
- Halford, G.R., Saltsman, J.F., Verrilli, M.J., Kalluri, S., Ritzert, F.J., and Duckert, R.E., 1988b, "A New Approach to Thermomechanical Fatigue Life Prediction Based on Bithermal Fatigue, Strainrange Partitioning and Unified Constitutive Models," to be presented at the Symposium on Constitutive Equations and Life Prediction Models for High Temperature Applications, Univ. of California, Berkley, CA, June 20-22, 1988.

LIFE PREDICTION MODELING BASED ON STRAINRANGE PARTITIONING

Gary R. Halford
Fatigue and Fracture Branch
NASA Lewis Research Center

ABSTRACT

Strainrange partitioning (SRP) is an integrated low-cycle-fatigue life prediction system. It was created by Manson et al. (1971) specifically for calculating cyclic crack initiation life under severe high-temperature fatigue conditions. The system has received exhaustive evaluation by Lewis personnel, contractors and grantees, and numerous independent industrial and research organizations around the world. Improvements and additions have been incorporated continuously, including some within the past year. The key feature of the SRP system is its recognition of the interacting mechanisms of cyclic inelastic deformation (i.e., strainrange) that govern cyclic life at high temperatures. Time-dependent, thermally activated deformation processes and time-independent dislocation glide, and their relative contributions (i.e., partitioning) within each strain cycle significantly affect fatigue crack initiation life. The SRP system is the engineering quantification, at the macroscopic level, of these microscopic influences on high-temperature fatigue life. For example, at the macroscopic engineering level, the micromechanisms of deformation are lumped into two major phenomenological categories, either creep (and attendant oxidation) or plasticity deformation.

The SRP system bridges the gap between the mechanistic level of understanding that breeds new and better materials and the phenomenological level wherein workable engineering life prediction methods are in great demand.

The system has recently been expanded to address engineering fatigue problems in the low-strain, long-life, nominally elastic regime. This breakthrough, along with other advances in material behavior and testing technology, has permitted the system to also encompass low-strain thermomechanical loading conditions. This is a critical durability problem area for a great number of engineering structural components subjected to high-temperature service.

Other important refinements of the originally proposed method include procedures for dealing with life-reducing effects of multiaxial loading, ratcheting, mean stresses, nonrepetitive (cumulative damage) loading, and environmental and long-time exposure. Procedures have also been developed for partitioning creep and plastic strains and for estimating strainrange-versus-life relations from tensile and creep-rupture properties.

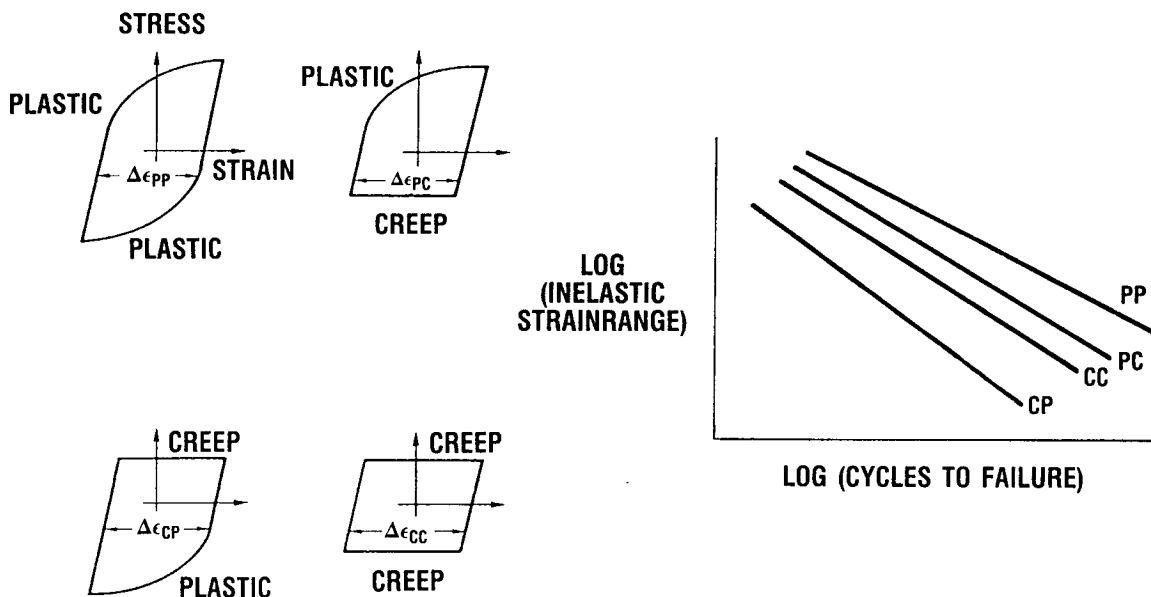
Each of the important engineering features of the SRP system are discussed and examples shown of how they help toward predicting high-temperature fatigue life under practical, although complex, loading conditions.

OVERVIEW

ORIGINAL BASIS OF SRP

Strainrange partitioning is an integrated system for calculating cyclic crack initiation life under severe high-temperature fatigue conditions. The key feature of the SRP system is its recognition of the interacting creep and plasticity mechanisms of cyclic inelastic deformation that govern cyclic life at high temperatures. Recent developments now permit the system to deal also with interactions due to effects of high-temperature oxidation. SRP has received extensive evaluation at Lewis, by contractors and grantees, and at numerous independent industrial and research organizations around the world. Improvements and additions are constantly being brought into the system.

The basics of SRP as it was first proposed several years ago are known to many and are illustrated below only for completeness. Since the introduction of SRP, it has been constantly improved upon in efforts to overcome recognized deficiencies. Despite its many improvements the basic concept remains valid and unchanged - the primary variable that governs low-cycle-fatigue life at high temperatures is the magnitude of the inelastic strainrange and the manner in which the time-dependent and time-independent inelastic deformations reverse themselves within a complete cycle. In the extreme there are only four different cycles that combine these two strain types in tension and compression loading. Each will potentially have its individual set of deformation mechanisms, and hence strainrange-versus-life relations, that are generalizations of the classical Manson-Coffin law of low-cycle fatigue.



CURRENT MODULES IN SRP SYSTEM

The numerous improvements to the SRP system are listed below and discussed in the text that follows. Each item is discussed from the standpoints of why the improvement was needed, how the improvement is implemented, the quantitative benefits of the improvement, and finally what remains to be done for further improvement.

The SRP system of life prediction has been created in a modular fashion, and a module is called upon only if the problem at hand warrants. In applying the system to the life prediction of a structural component, certain inputs are required from the structural analysis. These include the stress-strain-temperature-time history at the critical crack initiation location. Obviously the strainrange-versus-life relations for the material must also be known through measurement or estimation.

To date the SRP system has not been codified for computer application.

- BOUNDING LIFE AND TEMPERATURE INSENSITIVITY
- MULTIAXIAL EFFECTS
- MEAN STRESS EFFECTS
- CREEP AND PLASTIC RATCHETTING
- CUMULATIVE CREEP-FATIGUE DAMAGE
- DUCTILITY-NORMALIZED LIFE RELATIONS
- ENVIRONMENTAL AND LONG-TIME EXPOSURE EFFECTS
- TOTAL STRAINRANGE VERSION
- THERMOMECHANICAL FATIGUE

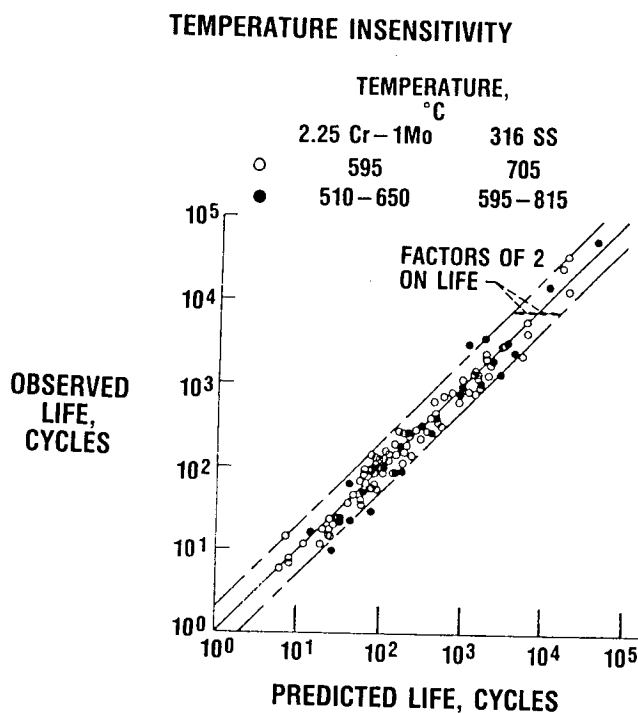
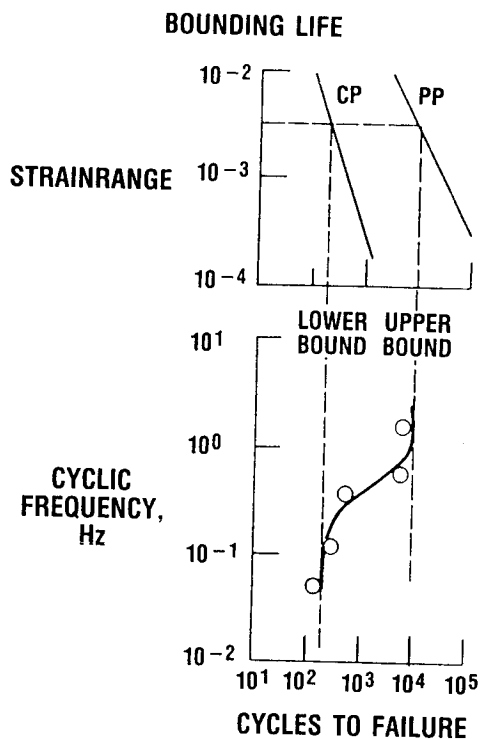
POSTER PRESENTATION

BOUNDING LIFE AND TEMPERATURE INSENSITIVITY

Two distinct features of the SRP system that offer significant advantages in performing engineering creep-fatigue life predictions are (1) the ability to provide upper and lower bounds on expected cyclic life with only limited analysis, and (2) the insensitivity to temperature of the life relations.

Upper and lower bounds on expected cyclic life for an imposed inelastic strain-range are given by the example figure on the left (Hirschberg and Halford, 1976). Typically the upper bound is given by the plastic-plastic (PP) life relation. The lower bound, although frequently being the creep-plastic (CP) life relation for materials that crack and fail intergranularly, could be the plastic-creep (PC) or creep-creep (CC) life relation, depending on which is the most damaging for the material in question.

Temperature insensitivity applies to materials whose creep-fatigue deformation mechanisms are not altered appreciably over a broad temperature range. This includes a large number of metallurgically stable engineering alloys whose creep and tensile ductilities remain reasonably constant over the temperature range of interest. The advantage to the analyst is in the reduced amount of temperature-dependent failure data that are needed to document the life equations. A secondary benefit is obtained from the reduced accuracy required in identifying the operating temperature. The graph on the right below illustrates the temperature insensitivity of strainrange-versus-life relations for two engineering alloys (Halford et al., 1973).

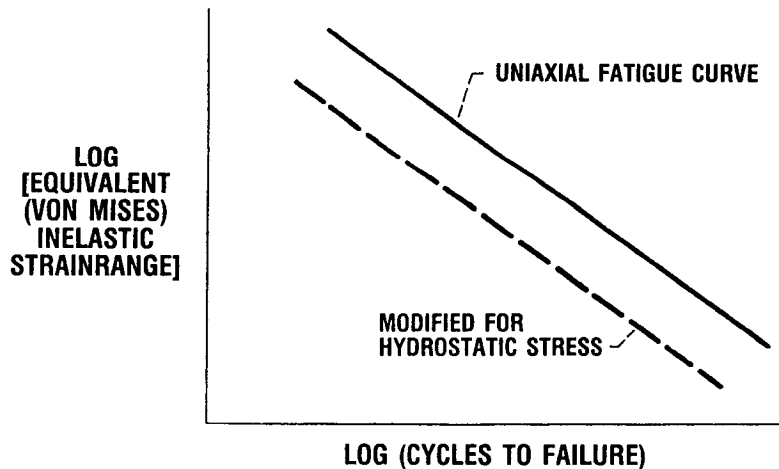


CD-88-32551

MULTIAXIAL EFFECTS

Multiaxial stress and strain states pose several special problems for creep-fatigue life prediction. Since most creep-fatigue results are generated for uniaxially loaded specimens, and quite rarely for multiaxial stress-strain states, the designer must rely on a multiaxial failure theory to relate complex states of loading to the simple uniaxial state. A relatively simple procedure for dealing with this problem was proposed by Manson and Halford (1977). The procedure involves using the von Mises theory for the distortional component of strain, and a multiaxiality factor for the hydrostatic component of stress. The greater the tensile hydrostatic state of stress, the lower the potential ductility, and hence the lower the strainrange-versus-life relations.

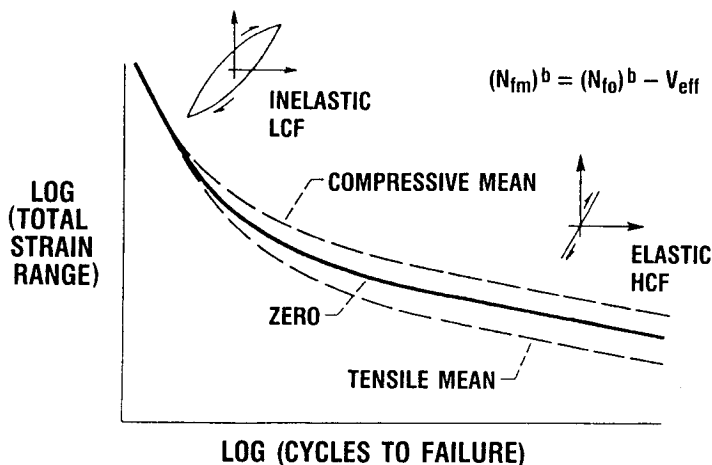
In addition, the concepts of "tension" and "compression" deformation for simple uniaxial loading must be generalized for multiaxial loadings in which both tensile and compressive stresses appear simultaneously but along different directions. Since the SRP system recognizes that the damaging nature of a cycle of inelastic strain at high temperatures depends strongly on whether the strains are tensile or compressive, the concept of tension and compression must be retained in any multiaxial creep-fatigue theory to be used by SRP. Procedures to establish dominant directions for classifying a stress-strain state as being predominantly tension or compression have been suggested by Manson and Halford (1976). The procedures apply to proportional multiaxial loading. Rules were not given for nonproportional loading because of the dearth of data to serve as a guideline. Limited experimental verification has been achieved to date for the multiaxial module in the SRP life prediction system.



CD-88-32552

MEAN STRESS EFFECTS

Although mean stress effects are usually associated with high-cycle fatigue, they are almost always present in high-temperature, low-cycle fatigue. In past years such mean stresses have been ignored. However, research at the Lewis Research Center has indicated that such stresses cannot always be ignored. Halford and Nachtigall (1980) developed a criterion for establishing the effectiveness of mean stresses under isothermal creep-fatigue conditions. The effectiveness criterion was used in conjunction with the Morrow equation (Morrow, 1968) for describing the Goodman diagram for mean σ_m and alternating σ_a stresses in fatigue. The equation has been recast in terms of the life N_{fm} with and N_{fo} without mean stress, the slope of the high-cycle-fatigue curve, and the mean stress ratio (V = mean/alternating). The principal feature of the criterion is that a transition period exists between high-cycle fatigue (nominally elastic stress-strain response), where the mean stress effect is 100 percent, and lower-cycle fatigue, where large inelastic strains nullify the mean stress effect. The isothermal mean stress equation is shown below. The constant, 70, was evaluated for the disk alloys, AF2-1DA and IN-100. Under thermal fatigue conditions, additional considerations must be examined since mean stresses can develop because of the temperature-dependent stress-strain characteristics of a material. Halford (1987) suggests a procedure for determining mean stress effectiveness under thermal cycling conditions. The terms are completely defined in the Halford (1987) paper.



ISOTHERMAL:

$$V_{eff} = V_{\sigma} \exp \left[-70 \left(\frac{\Delta \epsilon_{in}}{\Delta \epsilon_{el}} \right)^2 \right]$$

THERMOMECHANICAL:

$$V_{eff} = \frac{1 + \frac{R_{\sigma}}{R_y}}{1 - \frac{R_{\sigma}}{R_y}}$$

CD-88-32553

CREEP AND PLASTIC RATCHETTING

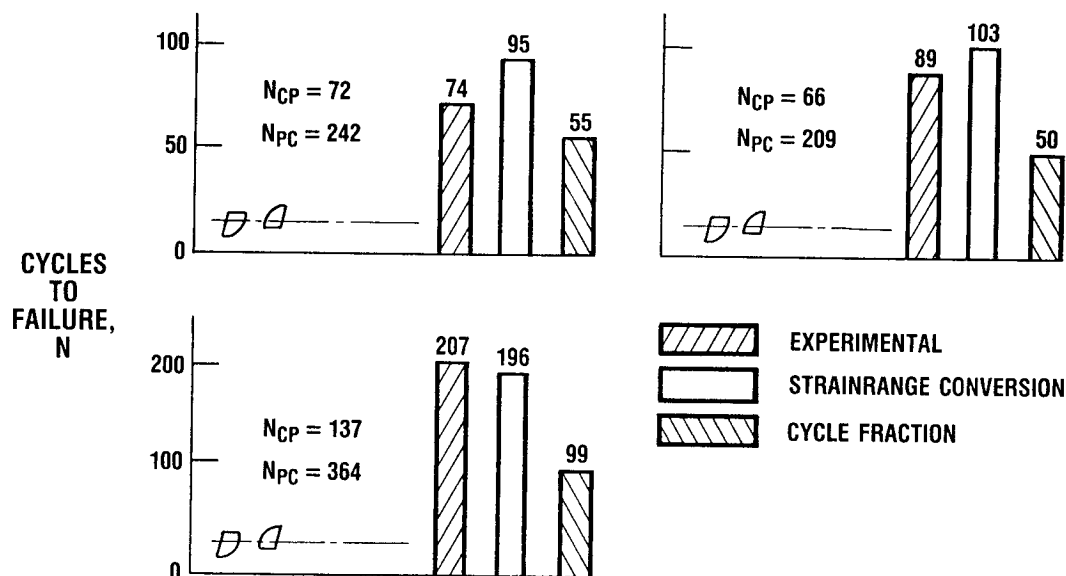
The damaging nature of creep or plastic ratchetting strains has received very little attention by researchers. Theoretical considerations have been nil, and few well-controlled experiments have been conducted. To provide a first-order approximation as to the damage imparted by ratchetting strains, an SRP system module has been adopted (Manson and Halford, 1976) that uses a simple linear exhaustion-of-ductility concept. Plastic ratchetting strain δ_p exhausts tensile ductility D_p ; creep ratchetting strain δ_c exhausts creep ductility D_c . The general inelastic strainrange SRP life equation for reversed strainrange damage and ratchetting strain damage is shown below. It is based on the interaction damage rule.

$$\text{DAMAGE CYCLE} = \underbrace{\frac{F_{PP}}{N_{PP}} + \frac{F_{CC}}{N_{CC}} + \frac{F_{CP}}{N_{CP}} + \frac{F_{PC}}{N_{PC}}}_{\text{CREEP-FATIGUE DAMAGE}} + \underbrace{\frac{\delta_p}{D_p} + \frac{\delta_c}{D_c}}_{\text{RATCHETTING DAMAGE}} = \frac{1}{N_F}$$

CD-88-32554

CUMULATIVE CREEP-FATIGUE DAMAGE

Cumulative creep-fatigue damage theories are in their infancy compared with lower temperature fatigue damage models. Creep-fatigue damage experimentation is also in its formative years. The SRP creep-fatigue life prediction system uses the recently proposed concept (Manson and Halford, 1983) called strain-range conversion. As a simple example to illustrate the concept, consider a repeating series of cycles in which each CP cycle is followed immediately by a PC cycle. Both strainranges are considered to be "unbalanced" since the tensile and compressive strains are different in each case. For alloys such as austenitic stainless steels, CP strainranges are more damaging, by about an order of magnitude, than PC strainranges. Thus from the CP strainrange alone one would expect (based on a simple cycle fraction approach) the block of CP + PC cycles to result in a block life that is always less than the number of cycles to failure. However, if this repeating series is shifted by one-half cycle of loading, it could be represented as a repeating series of CC-PP cycles. This sequence involves "balanced" cycles, which are generally less damaging than unbalanced ones. Since this sequence is actually the same as the first (with the exception of exactly one-half cycle), the experimental lives of the two will be the same. However, for the second sequence the "expected" number of blocks of loading (based on cycle fraction) should be greater than for the first sequence, since CC and PP strainrange damages are considerably more benign. The number of blocks should also be less than the number of CC cycles to failure, and more importantly, greater than the original number of CP cycles to failure. The principle of strainrange conversion (SRC) addresses the seeming contradiction in reasoning noted above and provides the rationale for synthesizing any series of SRP strain cycles.



DUCTILITY-NORMALIZED LIFE RELATIONS

The four SRP inelastic strainrange-versus-life relations may not be available for a particular material. Therefore a set of equations has been derived for estimating them from a knowledge only of a material's tensile plastic ductility D_p and creep ductility D_c . The equations are known as the ductility-normalized strainrange partitioning life relations (DN-SRP). The constants in these equations were determined empirically from a large number of data sets on a variety of alloy systems (Halford et al., 1977). Note that two equations exist for estimating the CP strainrange-versus-life relation. The first is for transcrystalline creep cracking alloys, and the second for intercrystalline creep cracking alloys.

The life relations estimated by the DN-SRP equations shown below are in agreement with measured life relations to within a factor of approximately 3 in cyclic life. The greater the ductility, the greater the resistance to failure by cyclic inelastic deformation. These equations also help to predict whether the strainrange-versus-life relations are sensitive to test temperature. If the ductility of an alloy does not change appreciably with temperature, the strainrange-versus-life relations will probably also be insensitive to test temperature.

$$\Delta\epsilon_{pp} = 0.50 D_p (N_{pp})^{-0.60}$$

$$\Delta\epsilon_{pc} = 0.25 D_p (N_{pc})^{-0.60}$$

$$\Delta\epsilon_{cc} = 0.25 (D_c)^{0.60} (N_{cc})^{-0.60}$$

$$\Delta\epsilon_{cp} = 0.20 (D_c)^{0.60} (N_{cp})^{-0.60} \text{ (TRANSCRYSTALLINE)}$$

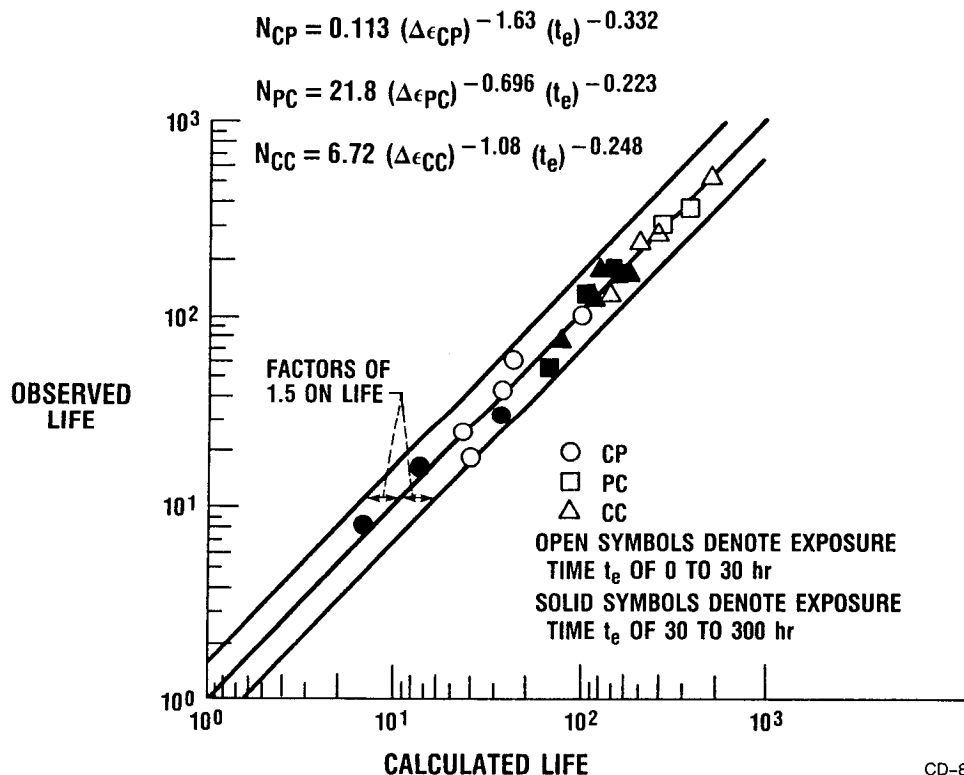
OR

$$\Delta\epsilon_{cp} = 0.10 (D_c)^{0.60} (N_{cp})^{-0.60} \text{ (INTERCRYSTALLINE)}$$

ENVIRONMENTAL AND LONG-TIME EXPOSURE EFFECTS

Procedures based on modification of the inelastic strainrange-versus-life relations have been proposed by Kalluri (1987) and Kalluri et al. (1987) to account for oxidation of alloys and other time-dependent degradation mechanisms. Excellent correlations of experimental results have been obtained with the modified life relations. Two forms of time-dependent strainrange-versus-life relations are available to choose from, depending on the information available to the user. One set is written in terms of the time of exposure, while the other is in terms of steady-state creep rates associated with the stresses encountered in a cycle. For brevity, only the exposure-time relations are shown here. An example set of equations for CP, PC, and CC inelastic strainranges are shown below for type 316 austenitic stainless steel evaluated at 816 °F. Exposure times are from a few minutes to about 300 hours. These equations have been highly effective in correlating time-dependent effects as indicated in the figure. Correlation of the experimental results to within a factor of only 1.5 in cyclic life is considered exceptionally good.

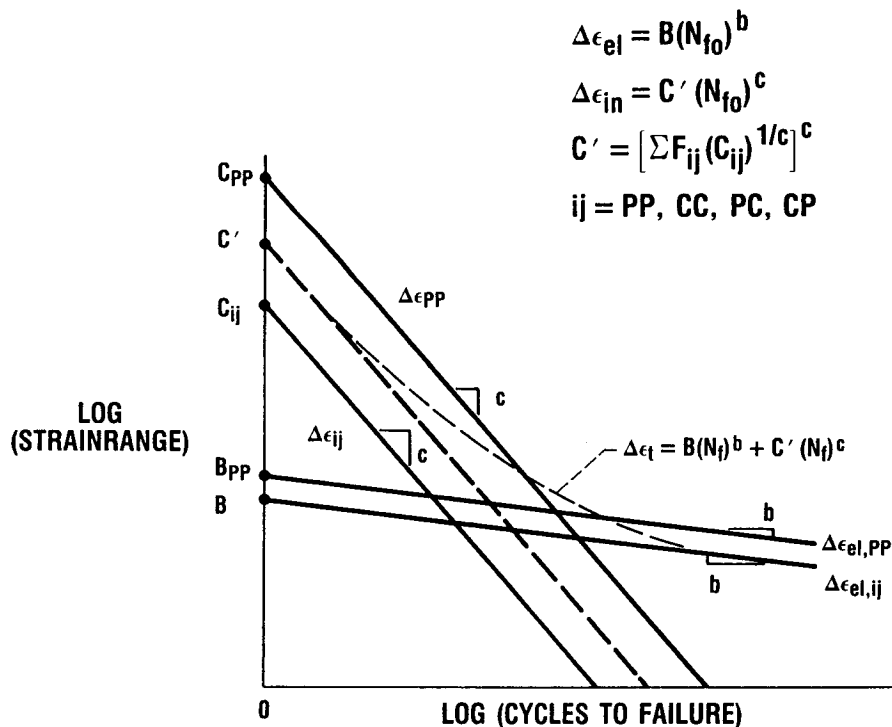
EXPOSURE-TIME-MODIFIED STRAINRANGE-VERSUS-LIFE RELATIONSHIPS



CD-88-32557

TOTAL STRAINRANGE VERSION

A workable total strainrange version of strainrange partitioning (TS-SRP) was first proposed by Halford and Saltsman (1983). Improvements have been made recently (Saltsman and Halford, 1988a). The TS-SRP module of the SRP life prediction system was designed to overcome the problems of applying SRP to the low-strain, long-life, nominally elastic regime of low-to-intermediate cycle fatigue. In that regime direct application of the classical inelastic strainrange-versus-cyclic-life relations of SRP is virtually impossible. The calculation accuracy would be totally unacceptable. In applying the TS-SRP version an alloy is characterized in much the same manner as for the original inelastic strainrange version. However, additional information concerning cyclic stress-strain characteristics is needed along with elastic strainrange-versus-cyclic-life data. Thus advantage is taken of recent advances made in the development of unified constitutive equations relating cyclic stresses, strains, temperature, and time. Using the TS-SRP module allows the life of a structural component to be calculated from the magnitude of the total strain response in the structure at the critical crack initiation location. The strain-time waveshape of the repetitive cycle is used in conjunction with a unified constitutive model to determine the partitioning of whatever inelastic strains may be present. The constitutive model along with pre-existing material property correlations can be used to identify the equation of the elastic strainrange-versus-cyclic-life relation that is to be added to the partitioned inelastic strainrange-versus-life relation to form the total strainrange-versus-life relation. It is this life relation that is entered by using the total strainrange determined for the critical location. Never once in the processes is it necessary to actually identify the magnitude of the inelastic strainrange. Example applications of TS-SRP to complex loadings of laboratory specimens has been provided by Moreno et al. (1985).



CD-88-32558

THERMOMECHANICAL FATIGUE

Thermomechanical fatigue problems pose special requirements for life prediction methods. Efforts to base thermomechanical fatigue life prediction methods on isothermal creep-fatigue behavior have not always met with success. The reason is that the thermal history of a thermal fatigue cycle can activate cyclic deformation and crack initiation mechanisms that simply are not present in isothermal strain cycles. To overcome this difficulty in a manageable manner, Saltsman and Halford (1988b) proposed that the life relations for the TS-SRP module be determined from tests involving two distinctly different isothermal temperatures -- one high and one low. This type of test has been termed the "bithermal fatigue test" and is reported upon in this conference by M.J. Verrilli. By using the bithermal test, it is possible to generate inelastic strainrange-versus-life relations for the unbalanced cycles of CP (in phase) and PC (out of phase). Almost all thermal and thermomechanical fatigue cycles are of the unbalanced type (i.e., the tensile and compressive paths of the cycle are not the same). It is also possible to perform bithermal PP tests by the proposed technique. Results of applying the TS-SRP module to thermomechanical fatigue for two engineering alloys, the cast nickel-base superalloy B1900 and the wrought cobalt-base alloy Haynes 188, are to be reported upon in June by Halford et al. (1988).

- BITHERMAL STRAINRANGE-VERSUS-LIFE RELATIONS
- UNIFIED CONSTITUTIVE MODELING
- TOTAL STRAINRANGE VERSION (TS-SRP)

REFERENCES

- Halford, G.R., Hirschberg, M.H., and Manson, S.S., 1973, "Temperature Effects on the Strainrange Partitioning Approach for Creep-Fatigue Analysis." Fatigue at Elevated Temperatures, ASTM STP 520, A.E. Carden, A.J. McEvily, and C.H. Wells, eds., American Society for Testing and Materials, Philadelphia, pp. 658-667.
- Halford, G.R., Saltsman, J.F., and Hirschberg, M.H., 1977, "Ductility-Normalized Strainrange Partitioning Life Relations for Creep-Fatigue Life Prediction." Proceedings of the Conf. on Environmental Degradation of Engineering Materials. Virginia Tech. Printing Dept., V.P.I. and State University, Blacksburg, VA, pp. 599-612.
- Halford, G.R., and Nachtigall, A.J., 1980, "The Strainrange Partitioning Behavior of an Advanced Gas Turbine Disk Alloy, AF2-1DA." J. Aircraft, Vol. 17, No. 8, pp. 598-604.
- Halford, G.R., and Saltsman, J.F., 1983, "Strainrange Partitioning - A Total Strainrange Version." Advances in Life Prediction Methods, ASME International Conference Proceedings, Albany, NY, pp. 17-26.
- Halford, G.R., 1987, "Low-Cycle Thermal Fatigue." Chapter 6, Thermal Stresses II, R.B. Hetnarski, ed., Elsevier Science Publishers B.V., Amsterdam, pp. 329-428.
- Halford, G.R., Saltsman, J.F., Verrilli, M.J., Kalluri, S., Ritzert, F.J., and Duckert, R.E., 1988, "A New Approach to Thermomechanical Fatigue Life Prediction Based on Bithermal Fatigue, Strainrange Partitioning, and Unified Constitutive Models." Accepted for presentation at the Symposium on Constitutive Equations and Life Prediction Models for High Temperature Applications, University of California, Berkeley, June 20-22.
- Hirschberg, M.H., and Halford, G.R., 1976, "Use of Strainrange Partitioning to Predict High-Temperature Low-Cycle Fatigue Life." NASA TN D-8072.
- Kalluri, S., 1987, "Generalization of the Strainrange Partitioning Method for Predicting High Temperature Low Cycle Fatigue Life at Different Exposure Times." Ph.D. Dissertation, Case Western Reserve University, Cleveland, OH.
- Kalluri, S., Manson, S.S., and Halford, G.R., 1987, "Environmental Degradation of 316 Stainless Steel in High Temperature Low Cycle Fatigue." Proceedings, Third International Conference Environmental Degradation of Engineering Materials, The Pennsylvania State University, pp. 503-519.
- Manson, S.S., Halford, G.R., and Hirschberg, M.H., 1971, "Creep-Fatigue Analysis by Strain-Range Partitioning." Symposium on Design for Elevated Temperature Environment, ASME, pp. 12-28.
- Manson, S.S., and Halford, G.R., 1976, "Treatment of Multiaxial Creep-Fatigue by Strainrange Partitioning." 1976 ASME-MPC Symposium on Creep-Fatigue Interaction, R.M. Curran, ed., MPC-3, pp. 299-322.

- Manson, S.S., and Halford, G.R., 1977, "Discussion to paper by J.J. Blass and S.Y. Zamrik, "Multiaxial Low-Cycle Fatigue of Type 304 Stainless Steel," 1976, ASME-MPC Symposium on Creep-Fatigue Interaction, ASME, 1976, pp. 129-159. J. Engineering Materials and Technology, Vol. 99, pp. 283-286.
- Manson, S.S., and Halford, G.R., 1983, "Complexities of High Temperature Metal Fatigue - Some Steps Toward Understanding." Israel J. Tech., Vol. 21, pp. 29-53.
- Moreno, V., Nissley, D.M., Halford, G.R., and Saltsman, J.F., 1985, "Application of Two Creep-Fatigue Life Prediction Models for the Prediction of Elevated Temperature Crack Initiation of a Nickel-Base Alloy." AIAA Preprint 85-1420.
- Morrow, J., 1968, "Fatigue Properties in Metals." Section 3.2, Fatigue Design Handbook, SAE Advances in Engineering, Vol. 4, J.A. Graham, ed., pp. 21-29.
- Saltsman, J.F., and Halford, G.R., 1988a, "An Update on the Total Strain Version of SRP." Low Cycle Fatigue, ASTM STP 942, H.D. Solomon, G.R. Halford, L.R. Kaisand, and B.N. Leis, eds., American Society for Testing and Materials, Philadelphia, pp. 329-341.
- Saltsman, J.F., and Halford, G.R., 1988b, "Life Prediction of Thermomechanical Fatigue Using Total Strain Version of Strainrange Partitioning (SRP) - A Proposal." NASA TP-2779.

LIFE PREDICTION MODELING BASED ON CYCLIC DAMAGE ACCUMULATION

Richard S. Nelson
United Technologies Corporation
Pratt & Whitney
East Hartford, Connecticut

A high temperature, low cycle fatigue life prediction method has been developed by Pratt & Whitney under the sponsorship of the Lewis Research Center's Gas Turbine Engine Hot Section Technology Program (HOST) (Moreno et al, 1984). This method, Cyclic Damage Accumulation, has been developed for use in predicting the crack initiation lifetime of gas turbine engine materials, where initiation has been defined as a 0.030 in. surface length crack. A principal engineering feature of the CDA method is the minimum data base required for implementation. Model constants can be evaluated through a few simple specimen tests such as monotonic loading and rapid cycle fatigue. The method has been expanded to account for the effects on creep-fatigue life of complex loadings such as thermomechanical fatigue, hold periods, waveshapes, mean stresses, multiaxiality, cumulative damage, coatings, and environmental attack (Nelson et al, 1986). A significant database has been generated on the behavior of the cast nickel-base superalloy B1900+Hf, including hundreds of specimen tests under such loading conditions. This information is being used to refine and extend the CDA life prediction model, which is now nearing completion. The model is also being verified using additional specimen tests on wrought INCO 718, and the final version of the model is expected to be adaptable to most any high-temperature alloy. The model is currently available in the form of equations and related constants. A proposed contract addition will make the model available in the near future in the form of a computer code to potential users.

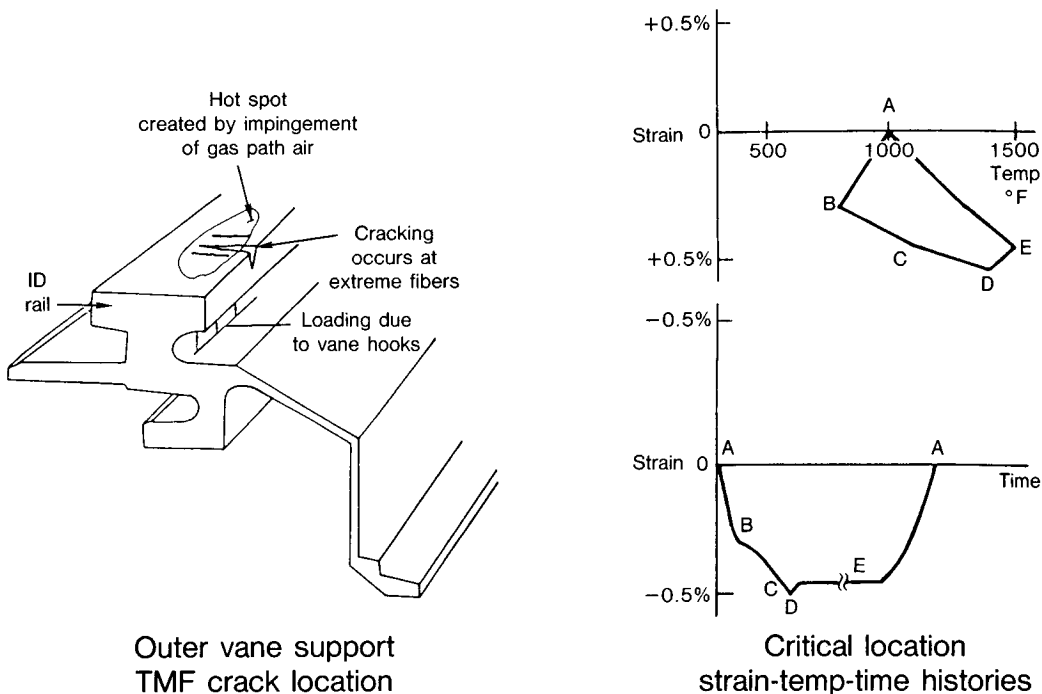
Work performed under NASA Contract NAS3-23288; Dr. Gary R. Halford, LeRC, serves as NASA Technical Monitor.

EXECUTIVE OVERVIEW OF:

LIFE PREDICTION MODELING BASED ON CYCLIC DAMAGE ACCUMULATION (CDA)

Modern applications of high strength materials often involve high homologous temperatures (greater than 0.5) combined with complex time-varying stresses and strains. The figure shown here depicts typical strain and temperature histories for such a location and shows the resulting damage to the structure after application of a sufficient number of these cycles. Clearly, this situation gives rise to many difficulties when life predictions are required for such service conditions, since several different damage mechanisms (such as creep, fatigue, and oxidation) may be activated simultaneously. Many researchers have devoted large portions of their careers to the solution of such problems and have developed several useful techniques for high temperature life prediction in the presence of creep-fatigue-environment interactions (Halford, 1986; Cailletaud et al, 1983). In order to build on their work and to enhance hot section durability, the current effort was sponsored by the Lewis Research Center's Gas Turbine Engine Hot Section Technology Program (HOST). The intent of this work has been to examine fundamental approaches to high temperature crack initiation life prediction, identify modeling strategies, and develop a practical model which can produce accurate life predictions for a wide range of component relevant conditions (Moreno et al, 1984). Though originally developed for aerospace use, the work is relevant to most high temperature applications of current and future isotropic alloys.

THE EFFECTS OF COMPLEX STRAIN AND TEMPERATURE HISTORIES MUST BE DETERMINED FOR ACCURATE LIFE PREDICTIONS

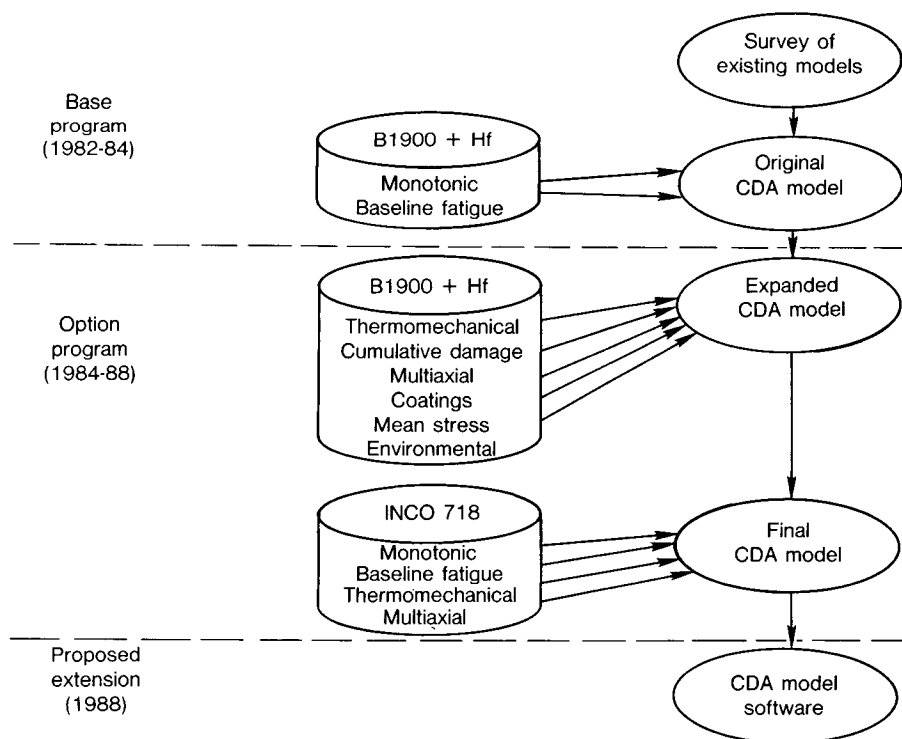


EXECUTIVE OVERVIEW OF:

LIFE PREDICTION MODELING BASED ON CYCLIC DAMAGE ACCUMULATION (CDA)

The work under the HOST contract began with a base program during which existing life prediction approaches were examined in detail. Monotonic tests and continuously cycled strain controlled isothermal fatigue tests of cast B1900+Hf specimens were performed to provide baseline data for comparison. Desirable features from several of these methods were identified, and the result was a new approach for life prediction called Cyclic Damage Accumulation (CDA). This is being expanded during the option portion of the program to account for the effects of thermomechanical fatigue, multiaxiality, cumulative damage, environment, coatings, and mean stresses (Nelson et al, 1986). The B1900+Hf specimen database has been greatly expanded during this work to provide clear data regarding material behavior under such complex conditions. Finally, the CDA model is being refined and modified to account for the behavior of other types of high temperature engineering alloys, wrought INCO 718 being used as the alternate model material for this work. It should be noted that these databases will, when completed, comprise the results of approximately 350 specimen tests of B1900+Hf and 110 specimen tests of INCO 718. By themselves, they are therefore of great interest to any researcher in the field of high temperature life prediction. A proposed extension to the contract would also provide software of immediate value to those desiring to perform high temperature life predictions using the CDA method.

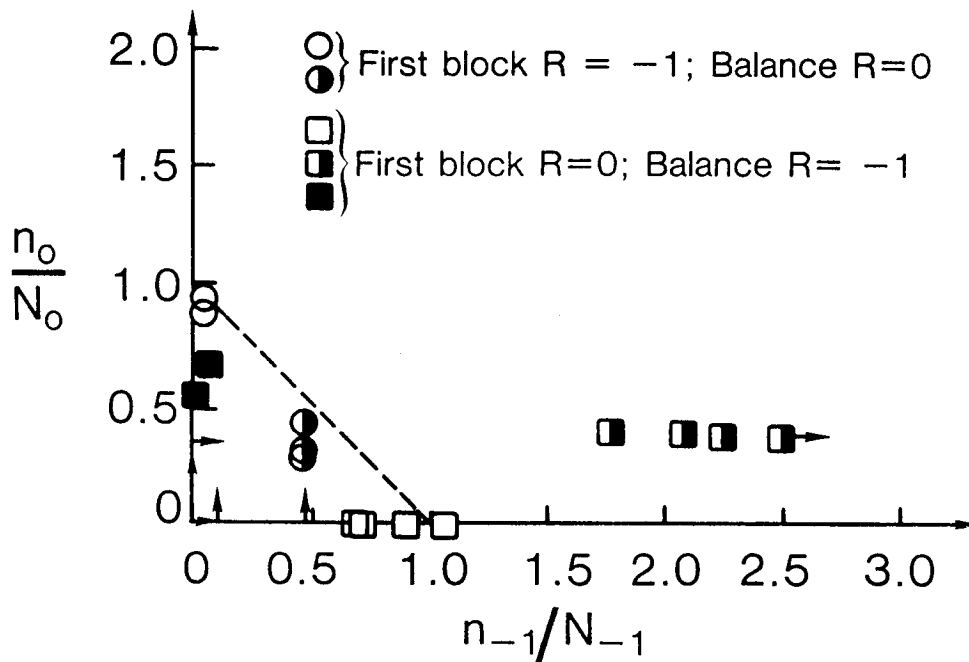
HOST ISOTROPIC CREEP-FATIGUE CONTRACT HAS PRODUCED EXTENSIVE DATABASES AND PRACTICAL LIFE MODEL



CUMULATIVE DAMAGE TESTS DEMONSTRATED THE USEFULNESS OF THE BASIC CDA APPROACH

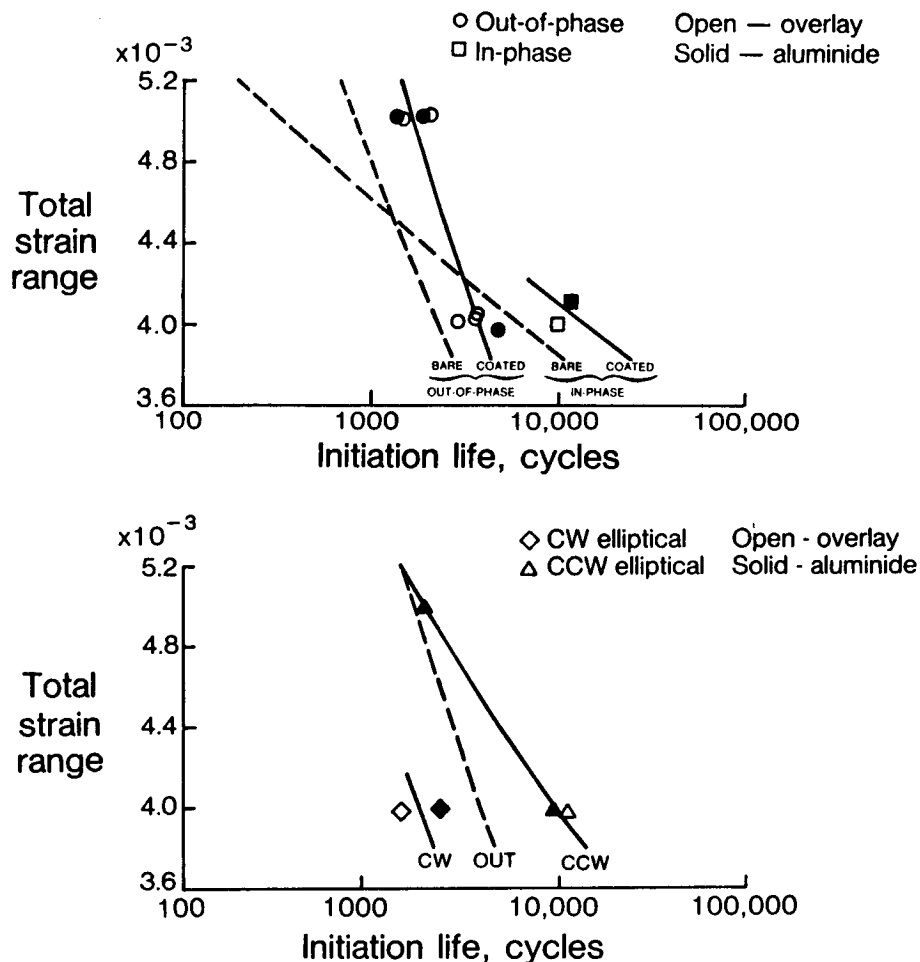
One of the important features of the Cyclic Damage Accumulation (CDA) life prediction model developed during the base portion of this contract is the use of a ductility variable which represents the fatigue capability of the material as a function of the loading history. It was observed that the dislocation structure produced during the primary phase of a creep test was very similar to that which developed during fatigue. The amount of total accumulated primary creep was found to be a function of both temperature and maximum applied stress. The CDA life prediction model therefore uses primary creep ductility as a measure of fatigue capability, and the damage accumulation rates for the various temperatures are calculated using this concept.

Cumulative damage tests were completed as part of the option program, including block tests (strain ratio, temperature, and hold time), sequenced tests (strain range and rate), and interrupted tests (prior creep and interspersed exposure time). The block strain ratio results are shown below, where the level of prior loading and its duration are seen to have pronounced effects on the life of subsequent block loading. This effect is easily captured using the CDA concept of primary creep ductility, since this variable will depend on the prior loading history. The cumulative damage tests also showed the need to incorporate a non-linear damage accumulation function to predict sequence effects correctly.



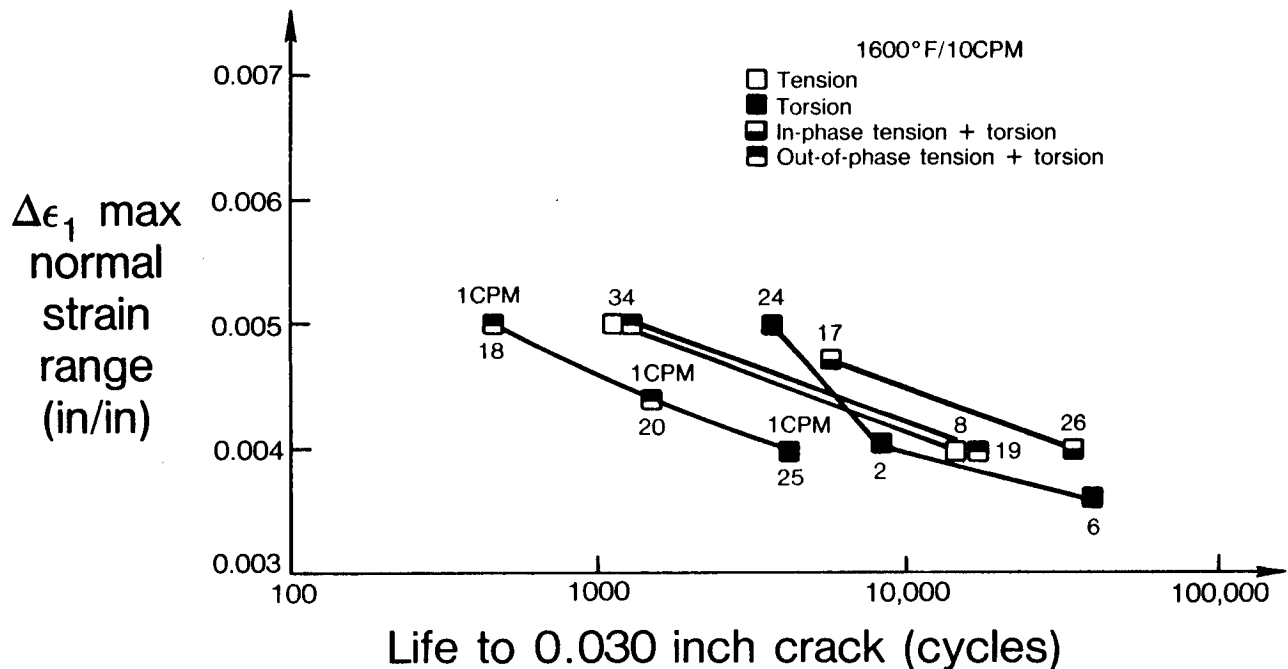
TMF LIFE PREDICTION MUST ACCOUNT FOR STRONG INFLUENCES SUCH AS COATINGS AND CYCLE PATH

Prediction of initiation life under conditions of thermomechanical fatigue is one of most important practical applications of any advanced creep-fatigue life model. Such conditions of simultaneously varying strain and temperature are typical of what is experienced by many components of modern turbomachinery and powerplants. To complicate matters further, the alloys used in such applications are often coated to prevent oxidation or other environmental attack. Such conditions were simulated during the option portion of this program using many types of strain-temperature cycle paths, including in-phase, out-of-phase, "dogleg" (non-isothermal holds), and elliptical cycles. The B1900+Hf specimens were run in one of three conditions: uncoated, overlay coated, or diffusion aluminide coated. The INCO 718 TMF specimens were run using similar strain-temperature cycles and were all uncoated. The results shown below are typical of the effects produced by such variables, indicating that successful life models must be able to account for these effects. The modifications to the CDA model currently in progress will enable it to accept completely arbitrary histories of stress-strain-temperature and thereby make accurate TMF life predictions. A constitutive and life model for coatings from a companion HOST contract will also be incorporated (Swanson et al, 1987).



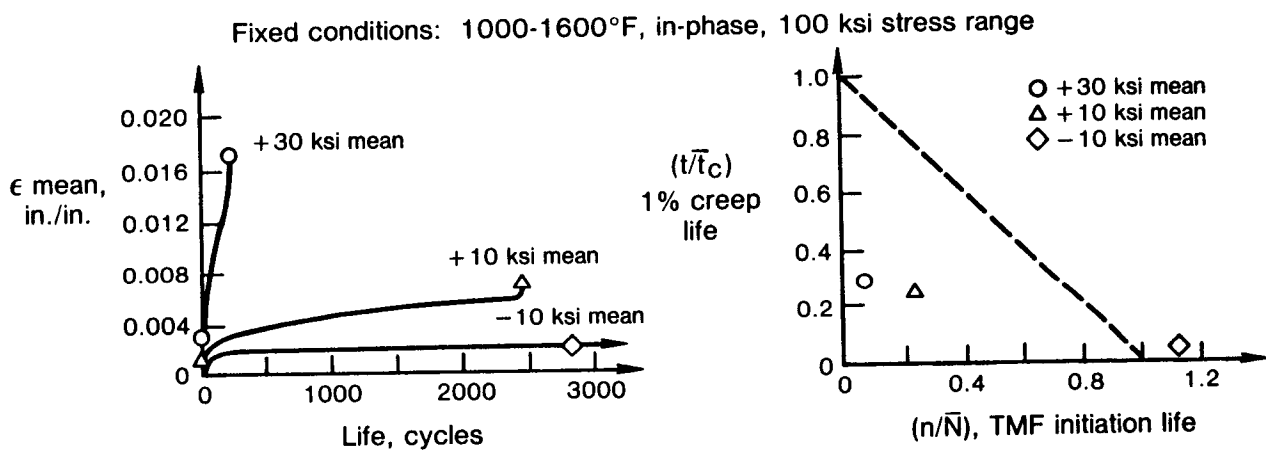
MULTIAXIAL EFFECTS HAVE BEEN INVESTIGATED
AND ARE BEING INCORPORATED INTO CDA MODEL

Certain areas of high temperature components, such as blade/platform intersections and disk webs, may be subject to loading conditions which have a high degree of multiaxiality. Also, three-dimensional analysis programs often express calculated stress and strain tensors in coordinate systems which are not aligned with the local component loads. In both of these cases, some method is needed to determine the invariant parameter(s) which best characterize the initiation life under such conditions. As part of the option program, both alloys were tested under strain controlled multiaxial conditions at elevated temperatures by Prof. Eric Jordan at the University of Connecticut. Part of the data generated for B1900+Hf are shown in the figure below, where it can be seen that maximum normal strain range does a reasonably good job of correlating the data at 871°C (1600°F). Preliminary indications are that a modified maximum shear strain range parameter will provide the best correlation for the INCO 718 multiaxial data. A preprocessor module currently being developed will allow the CDA model to incorporate the flexibility needed to adjust to such differences in modern engineering alloys.



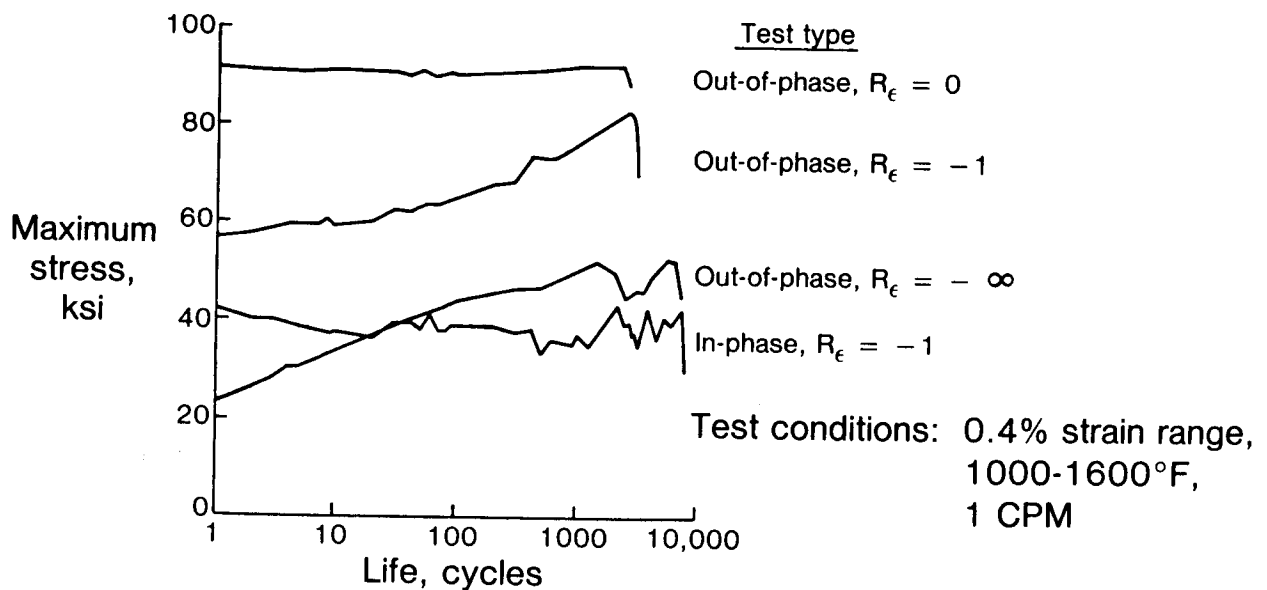
MEAN STRESS EFFECTS CAN BE NON-LINEAR FOR BOTH ISOTHERMAL AND TMF CONDITIONS

It has been known for many years that a superimposed mean stress can have pronounced effect on fatigue life. Such conditions occur in both high and moderate temperature applications and can have different effects, depending on what types of damage modes are active at the temperatures involved. Isothermal experiments during which both the strain range and the mean stress are independently controlled are underway at the University of Rhode Island under the direction of Prof. Hamouda Ghonem. The temperatures chosen for these tests will span a range of active damage mechanisms for both B1900+Hf and INCO 718. Thermomechanical load controlled experiments have been completed on both alloys at Pratt & Whitney, and the figures shown below present the results of three of these tests. Clearly, the influence of mean stress cannot be predicted using a linear damage interaction rule combined with lives predicted for pure creep or TMF under similar conditions. The CDA model is being refined to account for this type of effect as part of its basic formulation. The inherent capability of the primary creep ductility variable will provide the basis for this work.



ADVANCED VISCOPLASTIC CONSTITUTIVE MODELS ARE
AVAILABLE FROM A COMPANION HOST CONTRACT

Advanced life prediction models such as CDA rely heavily on accurate knowledge of the local stress-strain conditions at the point of interest. With specimen data, these variables can be measured and used for direct correlation of the life results. For example, the figure shown below shows the measured stress response of B1900+Hf to various TMF cycles. The obvious differences in maximum stress history will significantly affect the crack initiation life and therefore must be well known. However, for design and analysis of actual components, the stress-strain behavior will generally have to be predicted using some kind of analytical method. For the base alloy from this program, two advanced viscoplastic constitutive models have been produced by a companion HOST contract (Chan et al, 1986). The basic methods used for these models can be expanded to predict the behavior of most alloys for which CDA life model constants would be desired, thus providing the framework for a complete analysis system for high temperature life prediction.



CDA LIFE PREDICTION MODEL IS BASED ON INTEGRATION OF DAMAGE RATES FOR VARIOUS MODES

The fundamental equations of the CDA life prediction model are based on the integration of damage rates for various mechanisms for a particular material. For example, shown below are the two basic integrals which must be evaluated for the transgranular and intergranular damage modes for B1900+Hf. Note the incorporation of the primary creep ductility term and the non-linear damage accumulation function, both of which have been previously described. It is important also to note that, wherever possible, the actual calculations are based on ratios of current parameters relative to those from simple tests (the "reference" values shown in the equations with "R" subscripts). This enables the CDA life constants to be determined from low cost, simple tests rather than expensive, complex tests. Other damage modes (such as environmental) will be incorporated using the same methodology, including interaction with current modes through appropriate factors and equations. The final form of the CDA equations is still under development but will continue to include the same features. All modes for a given material will be evaluated simultaneously on a cycle-by-cycle basis using efficient adaptive techniques.

- Transgranular damage mode:

$$1 = \int_0^{N_i} \left(\frac{1}{\bar{\epsilon} p} \right) \left(\frac{1}{G_{NL}} \right) \left(\frac{dD}{dN} \right)_R \left[\left(\frac{\Delta\sigma}{\Delta\sigma_R} \right) \left(\frac{\sigma_T}{\sigma_{TR}} \right) + D_{TD} \left(\frac{fox}{fox_R} \right) \right] dN$$

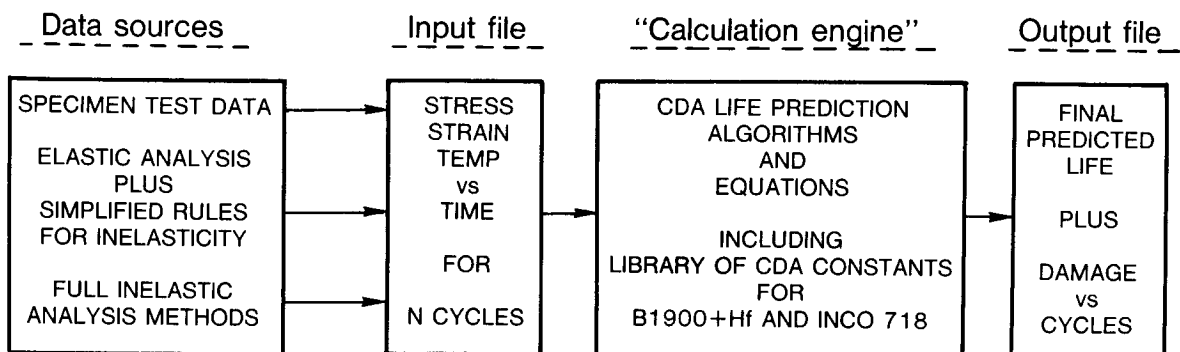
- Intergranular damage mode:

$$1 = \int_0^{N_i} \left(\oint_{\text{cycle } i} \frac{dt}{t_{cr}(\sigma, T)} \right) \left(\frac{fox}{fox_R} \right) dN$$

- Constants derived from simple tests

PROGRAM IS MODULAR TO PROVIDE MAXIMUM
EFFICIENCY AND FLEXIBILITY FOR EXPANSION

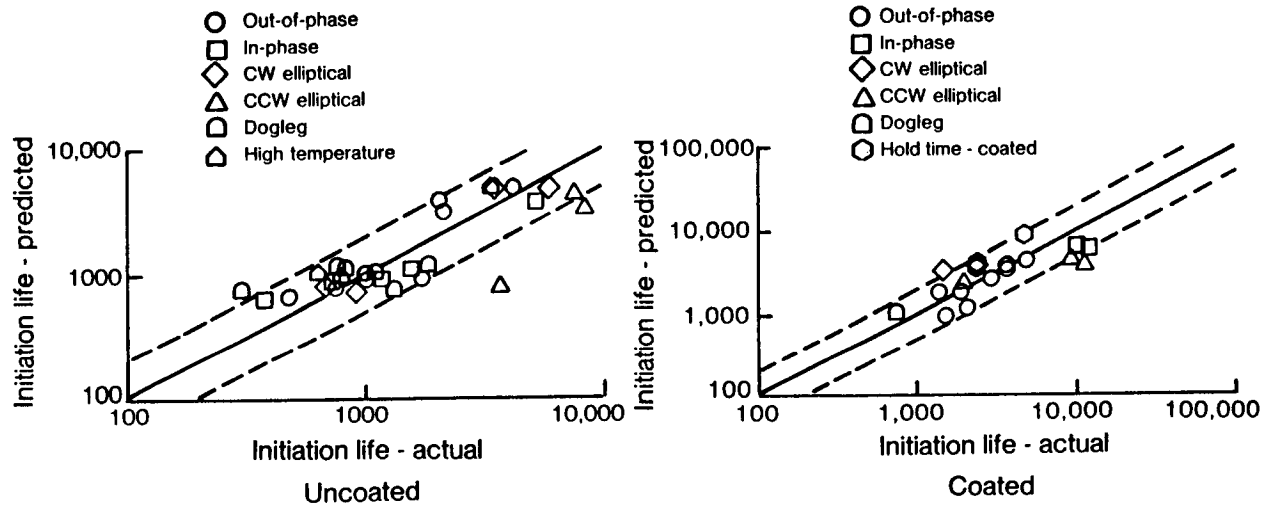
From the very beginning of this contract, it was decided that flexibility would be very important for high temperature life prediction. It was therefore decided to keep the method to be developed as modular as possible so that only those aspects which were relevant to the particular application at hand would need to be exercised. This also permits modification or upgrading of selected portions of the method as new techniques become available. The CDA life model software currently under development is designed to reflect this philosophy and therefore incorporates several features worthy of mention. As shown in the figure below, the input will be an ASCII file which can be created as required from whatever source of information is available. Similarly, the output will be an ASCII file containing the actual life prediction(s) plus (optionally) the evolution of damage variables versus cycles. This file input/output system will permit the use of any of the many available software packages for editing, plotting, and display of these results. The internal structure will make use of generic variables and arrays which can be defined as needed by the particular damage mode being evaluated. The whole code will be written in FORTRAN-77 for use on mainframes, minis, or micros, and will be heavily commented for ease of modification by end users.



PRELIMINARY TMF MODEL SHOWS GOOD CORRELATION AND POTENTIAL FOR PRACTICAL APPLICATION

A preliminary version of the CDA life prediction model was used to correlate the B1900+Hf TMF data for both coated and uncoated specimens. The figures below show that these predicted lives mostly fall within a factor of 2 relative to the actual life data. The model used for these correlations exercised only the basic transgranular damage mode, and work is still continuing to improve the correlation. Also, these figures indicate the potential of the method for improved design predictions after all damage modes are activated and integrated into the final system.

B1900+Hf TMF data



CYCLIC DAMAGE ACCUMULATION MODEL WILL PRODUCE
ACCURATE HIGH TEMPERATURE LIFE PREDICTIONS

In summary, it should be clear that this HOST contract has produced information which is valuable to any who wish to make life predictions for structures subjected to high temperature, complex loading conditions, especially those situations which can cause creep-fatigue-environment interactions. The large, self-consistent databases for both cast B1900+Hf and wrought INCO 718 are by themselves of great value to any who wish to understand the effects of thermomechanical fatigue, cumulative damage, multiaxiality, environment, coatings, and mean stresses. The test matrices have been designed to show how the multiple damage mechanisms which are characteristic of this regime can occur and interact in actual component-relevant conditions. The development of the Cyclic Damage Accumulation life prediction model is well along and will result in a practical, accurate life model with flexibility and efficiency for many types of engineering alloys. The method is also complemented by the development of advanced viscoplastic constitutive models for stress-strain predictions for the base alloy. Finally, the availability of the CDA model as a software package will facilitate its use and further enhancement by the engineering community.

- Broad spectrum of B1900 + Hf testing is nearly complete, providing consistent database for model development
- INCO 718 testing is underway to establish high temperature database for forged material
- Test results are showing how multiple damage modes occur and interact under complex loading conditions
- Model evaluation is being pursued for several types of loadings and will result in practical, accurate life prediction method

REFERENCES

Cailletaud, G., Nouailhas, D., Escaravage, C., Heliot, J., Kang, S., Grattier, J., Levailant, C., Mottot, M., Tortel, J., 1983, "A Review of Creep Fatigue Life Prediction Methods," ONERA TP 1983-122.

Chan, K. S., Lindholm, U. S., Bodner, S. R., Hill, J. T., Weber, R. M., and Meyer, T. G., 1986, "Constitutive Modeling for Isotropic Materials (HOST)," NASA CR-179522.

Halford, G. R., 1986, "Low-Cycle Thermal Fatigue," NASA TM 87225.

Moreno, V., Nissley, D. M., and Lin, L. S., 1984, "Creep Fatigue Life Prediction for Engine Hot Section Materials (Isotropic) Second Annual Report," NASA CR-174844.

Nelson, R. S., Schoendorf, J. F., and Lin, L. S., 1986, "Creep Fatigue Life Prediction for Engine Hot Section Materials (Isotropic) Interim Report," NASA CR-179550.

Swanson, G. A., Linask, I., Nissley, D. M., Norris, P. P., Meyer, T. G., and Walker, K. P., 1987, "Life Prediction and Constitutive Models for Engine Hot Section Anisotropic Materials Program," NASA CR-179594.

FATIGUE DAMAGE MODELING FOR COATED SINGLE CRYSTAL SUPERALLOYS*

David M. Nissley
United Technologies Corporation
Pratt & Whitney
East Hartford, Connecticut

A high temperature, low-cycle fatigue life prediction method for coated single crystal nickel-base superalloys is being developed under the sponsorship of the Lewis Research Center's Gas Turbine Engine Hot Section Technology Program (HOST) by the Pratt & Whitney Division of United Technologies. The method is being developed for use in predicting the crack initiation (.010" depth in single crystal) life of coated single crystal turbine airfoils. Although the models are being developed using coated single crystal PWA 1480, they should be readily adaptable to other coated nickel-base single crystal materials. The coatings chosen for this effort were of two generic types: 1) a low pressure plasma sprayed NiCoCrAlY overlay, designated PWA 286, and 2) an aluminide diffusion, designated PWA 273 (Swanson et al., 1987).

In order to predict the useful crack initiation life of airfoils, the constitutive and failure behavior of the coating/substrate combination must be taken into account. Coatings alter the airfoil surface microstructure and are a primary source from which cracks originate (Swanson et al., 1987). The adopted life prediction approach addresses this complexity by separating the coating and single crystal crack initiation regimes. This provides a flexible means for using different life model formulations for the coating and single crystal materials. At present, the overlay coating constitutive and life models and single crystal constitutive models are available in equation form (Halford et al., 1988). Diffusion aluminide coating constitutive and life models and the single crystal life model are currently being developed.

At the completion of this program, all constitutive and life model formulations will be available in equation form and as software. The software will use the MARC general purpose finite element code to drive the constitutive models and calculate life parameters.

*Work performed under NASA contract NAS3-23939; Gary R. Halford serves as NASA technical monitor.

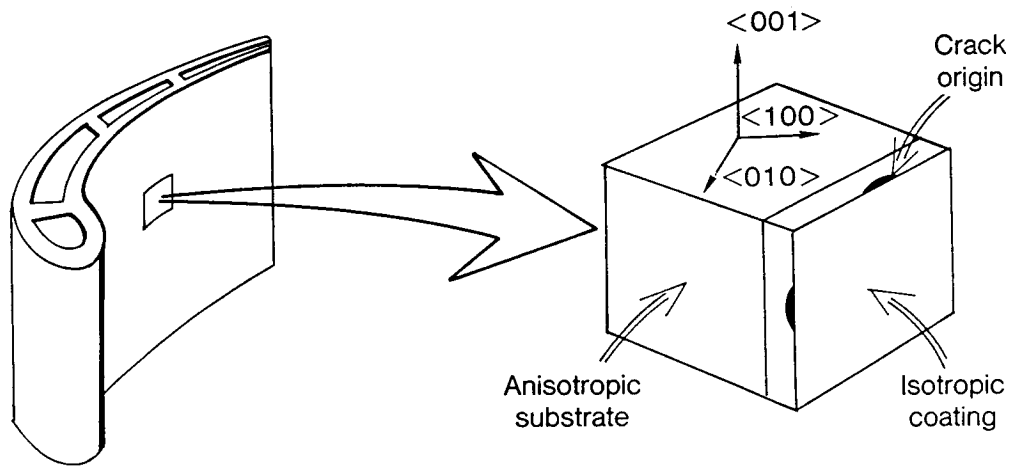
OVERVIEW

FATIGUE DAMAGE MODELING FOR COATED SINGLE CRYSTAL SUPERALLOYS

Cracking of coated single crystal airfoils is largely due to the severe thermal gradients introduced during engine transient operation. In general, oxidation/corrosion resistant coatings initiate cracks which eventually penetrate into the single crystal material thereby limiting the airfoil's useful fatigue life. This cracking behavior is modeled by considering the coating and substrate as a composite structure comprised of two materials with different constitutive and fatigue life behavior (Swanson et al., 1987; Halford et al., 1988). The effect of single crystal orientation on the constitutive and fatigue life behavior of the composite structure is included in the developed models.

NATURE OF PROBLEM

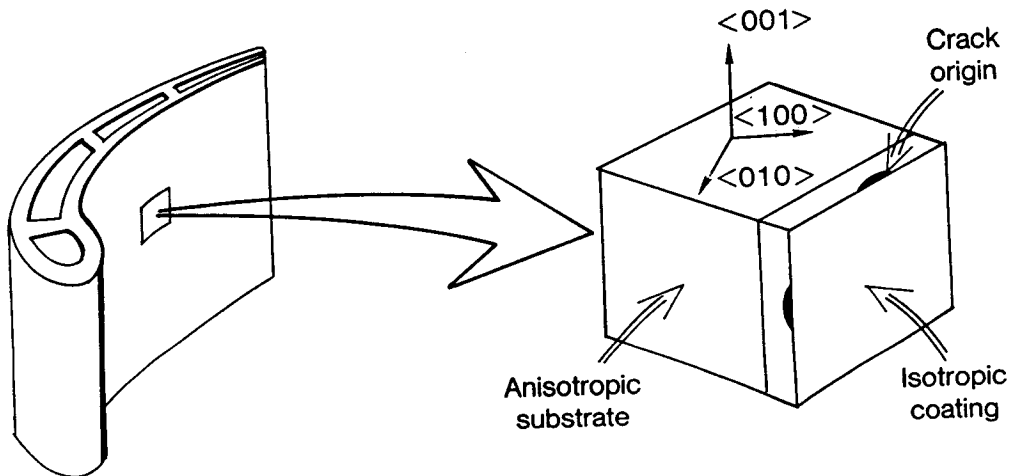
Cracking caused by thermal straining



POSTER PRESENTATION

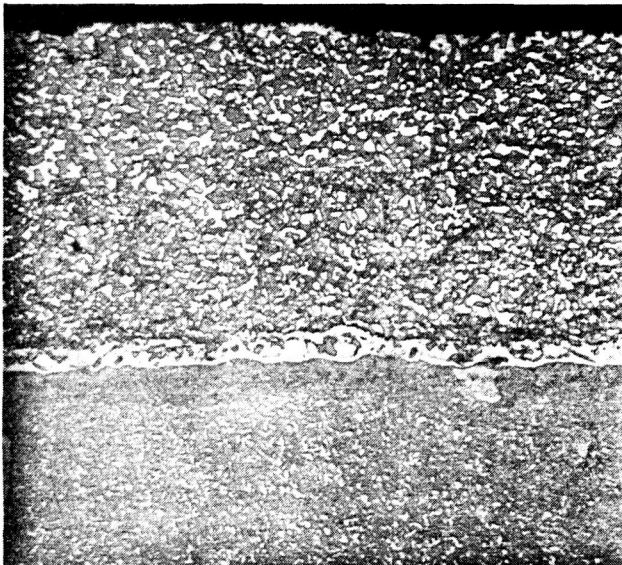
NATURE OF THE PROBLEM

This program addresses the complex cracking problem associated with coated nickel-base single crystal airfoils. It recognizes that cracking is not restricted to chordwise cracks (i.e., normal to centrifugal stress in blades), but may also occur in the spanwise direction. Since the coating is a primary crack initiation site, coating constitutive and life models must be developed as well as those for the single crystal material. Airfoil life prediction is further complicated by the fact that the fatigue life of single crystal material depends on its crystallographic orientation. All of these factors are investigated in this program.

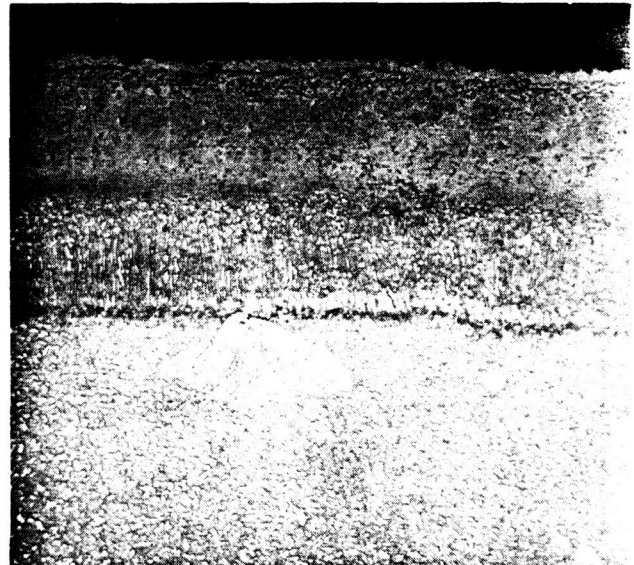


MICROSTRUCTURE OF OVERLAY AND ALUMINIDE COATINGS

Two generic coating types are being investigated: 1) PWA 286 overlay NiCoCrAlY and 2) PWA 273 aluminide. The overlay coating is applied by a low pressure plasma spray technique which produces a small diffusion zone layer and a distinct substrate/coating interface. By contrast, aluminide coatings produce a much larger diffusion zone and less distinct substrate/coating interface. The PWA 273 coating is applied by pack cementation. Both coating microstructures indicate that the coatings may be treated as isotropic for the purposes of constitutive modeling (Swanson et al., 1987). Overlay coating properties do not vary widely through the thickness so that tests of "stand-alone" coating material are useful for obtaining constitutive behavior. However, because aluminide coating properties are largely influenced by the substrate onto which it is applied, testing of a "stand-alone" aluminide coating is not possible. Unique tests useful for aluminide coating constitutive model development are described by Swanson et al. (1987).



Overlay coating,
PWA 286

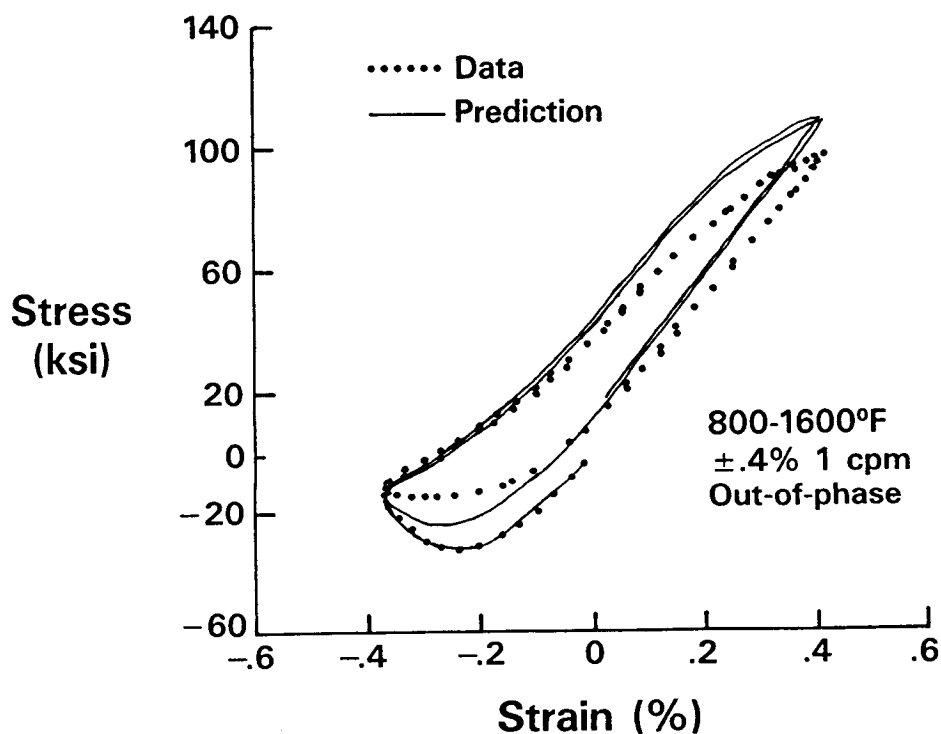


Pack aluminide diffusion
coating, PWA 273

ORIGINAL PAGE IS
OF POOR QUALITY

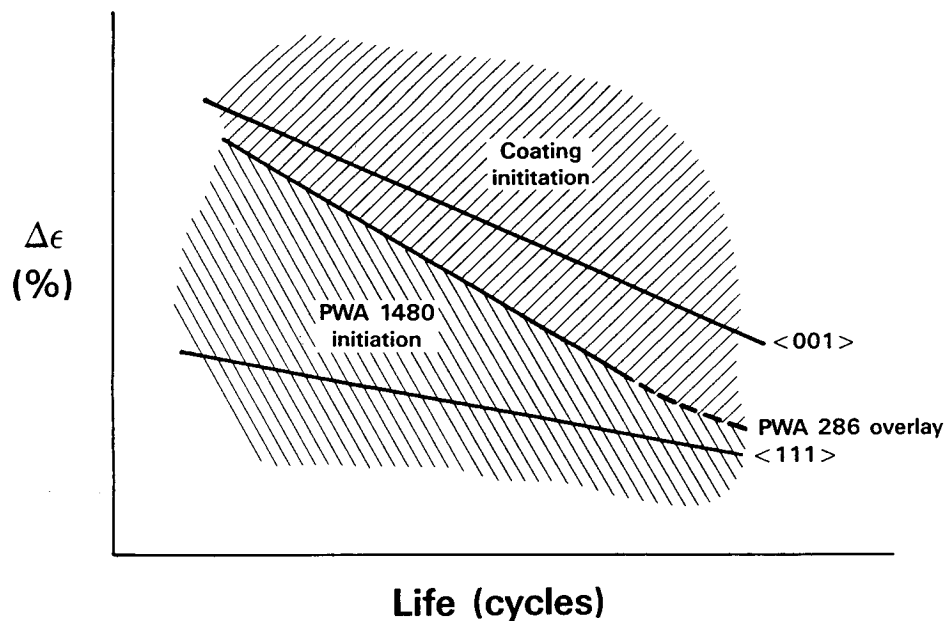
OVERLAY COATING LIFE MODEL COLLAPSES DATA WITHIN 2.5X

A modified tensile hysteretic energy life model was developed for the PWA 286 overlay coating and is reported by Halford et al. (1988). Model constants were determined from isothermal tests conducted at 427, 760, 927, and 1038C (800, 1400, 1700, and 1900F). Coating hysteresis loops were predicted using the PWA 286 overlay coating constitutive model incorporated into a two-bar mechanism. Preliminary results indicst that the model collapses a large body of isothermal and thermomechanical fatigue (TMF) life data within a factor of about 2.5. Generally, the worst predicted lives were limited to 1149C (2100F) max. temperature TMF tests. Prediction of these tests should improve when 1149C (2100F) isothermal tests are included in the data set used to determine model constants.



COMPLEX FAILURE MODES ARE OBSERVED FROM COATED SPECIMENS

The figure below schematically represents where coated PWA 1480 crack initiation occurs during isothermal fatigue. For the low elastic modulus orientation, $\langle 001 \rangle$, the coating typically cracks first, but for the high modulus orientations, in this case $\langle 111 \rangle$, the PWA 1480 may initiate cracks at defects, typically porosity. This represents the observed cracking at just one temperature. When the temperature is changed, the life lines tend to shift relative to one another. For example, only coating initiated cracks were observed during out-of-phase thermomechanical fatigue of both $\langle 001 \rangle$ and $\langle 111 \rangle$ orientations.



ADOPTED LIFE APPROACH REFLECTS OBSERVED CRACKING MODES

The observed specimen crack initiation modes dictated the life approach adopted for coated single crystal life prediction. The total life is considered as a sum of: 1) coating cracking, single crystal cracking (from coating cracks), and single crystal crack propagation, or 2) single crystal cracking due to discrete slip, oxidation effects, or defects (primarily porosity) and single crystal crack propagation. The obvious advantage in this approach is that life models can be individually tailored to the properties of each specific material (i.e., coating or substrate).

$$\left. \begin{array}{l} N_f = N_c + N_{sc} + N_{sp} \\ \text{or } N_f = N_{si} + N_{sp} \end{array} \right\} \text{whichever is smaller}$$

where: N_c = Cycles to initiate a crack through the coating.

N_{sc} = Cycles for coating crack to penetrate a small distance (.010") into the substrate.

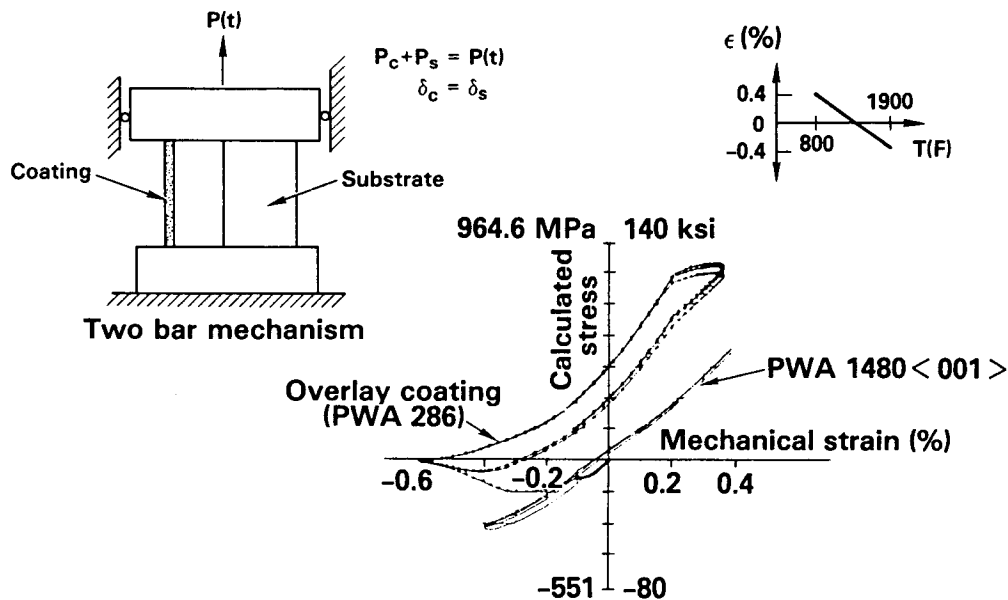
N_{si} = Cycles to initiate substrate crack.

N_{sp} = Cycles to propagate substrate crack to failure.

N_f = Total cycles to failure.

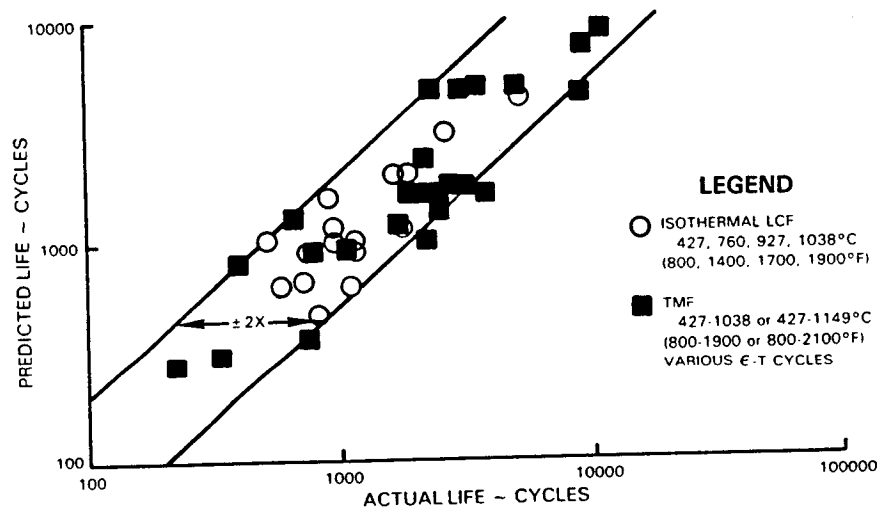
SIMPLE STRUCTURAL MODEL FOR PREDICTING COATING/SUBSTRATE BEHAVIOR

Since coating stress/strain behavior can not be measured during specimen tests, an analysis is used to obtain the non-linear coating response for life prediction. To facilitate this effort, a one-dimensional two-bar mechanism analysis is employed. As an example, the predicted response of overlay coated PWA 1480 <001> during an out-of-phase thermomechanical test is shown in the figure. The overlay coating response is highly non-linear relative to the single crystal PWA 1480 which remains nearly elastic. The coating mechanical strain range is higher than the PWA 1480 due to differences in the coefficient of thermal expansion between the two materials which is included in the two-bar model.



OVERLAY COATING CONSTITUTIVE MODEL PREDICTION OF TMF BEHAVIOR

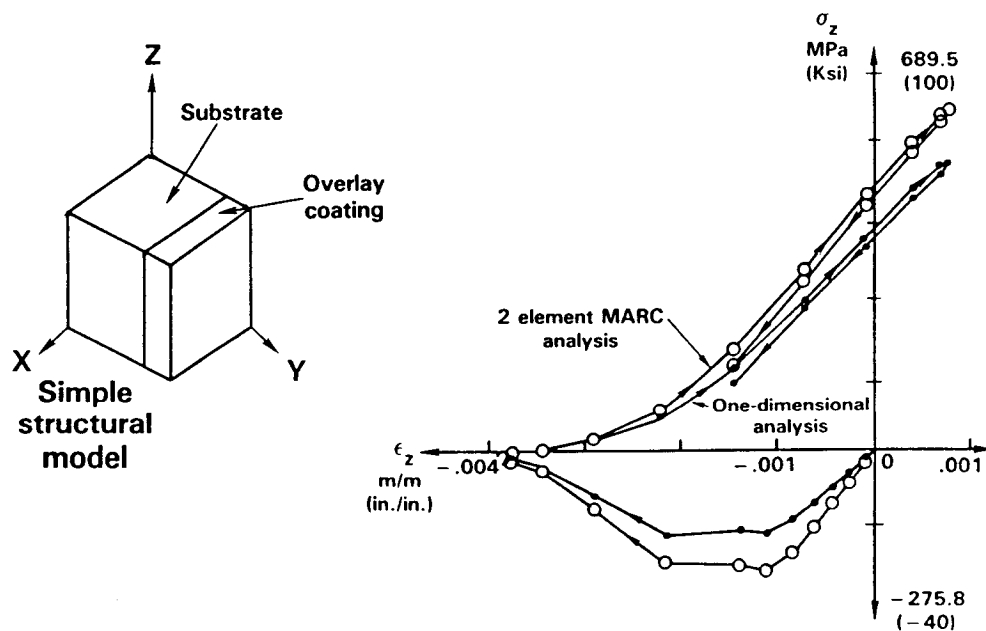
Walker's isotropic formulation (Walker, 1981) was chosen as the overlay coating constitutive model based on its ability to reproduce isothermal and thermomechanical hysteresis loop data. Shown in the figure is a comparison of the model prediction to an out-of-phase thermomechanical test cycle. The model captures the overall shape of the hysteresis loop, but overpredicts the maximum and minimum stresses. It is felt that the model predicts the coating behavior to the extent that current state-of-the-art viscoplastic models are capable. Baseline tests from which all model constants were determined consisted of cyclic stress relaxation tests which covered a temperature range from 427C to 1093C (800F to 2000F) (Swanson et al., 1987). MARC finite element user subroutine 'HYPELA' has been developed for the overlay coating to permit non-linear analysis of coated specimens and components.



- Overlay coating response calculated from 2-bar analysis

UNIAXIAL TMF INTRODUCES SIGNIFICANT BIAxIAL COATING LOADS

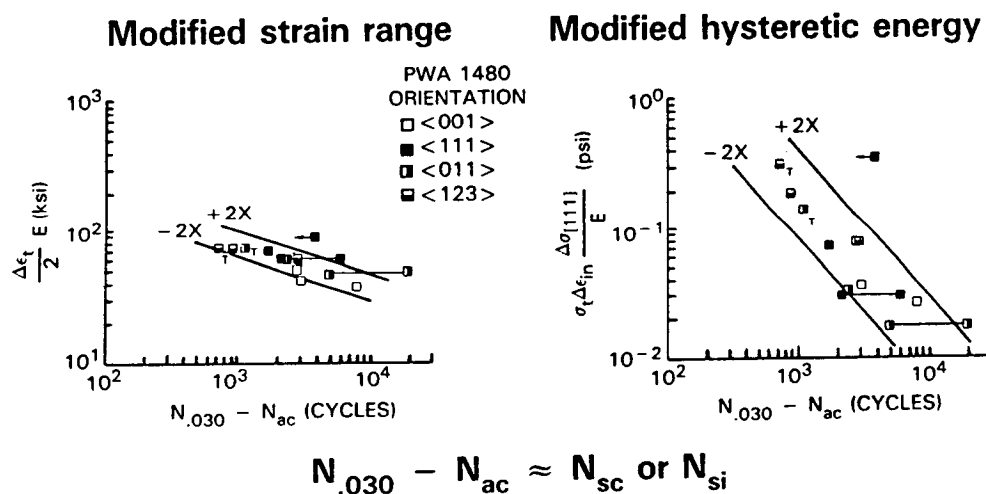
Ultimately, coated TMF life prediction must consider the biaxial coating loads introduced by the thermal growth mismatch between the coating and substrate. For example, MARC finite element analysis of a simple two element structure was performed to obtain the coating hysteretic response to a fully-reversed, uniaxial, out-of-phase TMF test conducted at 427-1038C (800-1900F), 1 cpm, and .3% mechanical strain range. Predicted hysteresis loops from the finite element and one-dimensional analyses are presented in the figure. The coating tensile hysteretic energy was obtained from the finite element analysis by the method proposed by Garud (1981). For this test condition, biaxial coating loads increased the tensile energy 70% which reduced the predicted life by a factor of about 1.5. Before the overlay coating life model is completed, all TMF test cycles must be analyzed in this manner.



PRELIMINARY PWA 1480 LIFE MODEL CORRELATIONS

Initial single crystal life correlations have been completed. The two models chosen for further development are: an elastic modulus modified strain range and the modified hysteretic energy approach developed by DeLuca and Cowles (1985). The strain range model is attractive because mechanical strains are readily available to the turbine airfoil designer. However, it does not currently have the capability to determine cyclic strain or strain-temperature history effects. For example, two tensile strain dwell cycles, which are denoted in the figure by the subscript "T", were incorrectly correlated to have identical life with that of a non-dwell cycle. This is a serious limitation since TMF lives are highly strain-temperature history dependent (Swanson et al., 1987). On the other hand, the modified hysteretic energy model includes parameters which enable correction for strain or strain-temperature effects. This model correctly correlated the two dwell cycles from the non-dwell cycle. Unfortunately, hysteretic energy models inherently use inelastic strain as one of their correlating parameters and, as noted previously, the single crystal TMF loops are virtually elastic in nature. Therefore, although both models have advantageous aspects, they require additional refinements for TMF life prediction.

Aluminide coated specimens at 927°C (1700°F)



REFERENCES

DeLuca, D. P. and Cowles B. A., 1985, "Fatigue and Fracture of Advanced Blade Materials," AFWAL-TR-84-4167.

Garud, Y. S., 1981, "A New Approach to the Evaluation of Fatigue Under Multiaxial Loadings," ASME J1. of Eng. Mat. and Tech., Vol. 103, pp. 118-125.

Halford et al., 1988 "Fatigue Life Prediction Modeling for Turbine Hot Section Materials, NASA Technical Memorandum 100291, Prepared for the 33rd Int'l. Gas Turbine and Aeroengine Congress and Exposition sponsored by ASME, Amsterdam, The Netherlands, June 5-9, 1988.

Swanson et al., 1987, "Life Prediction and Constitutive Models for Engine Hot Section Anisotropic Materials Program," Second Annual Report for NASA Contract NAS3-23939, NASA CR-179594.

Walker K. P., 1981, "Research and Development Program for Nonlinear Structural Modeling with Advanced Time-Temperature Dependent Constitutive Relationships," NASA CR-165533.

LIFE AND RELIABILITY OF ROTATING DISKS

Erwin V. Zaretsky, Todd E. Smith,* and Richard August*
Structures Division
NASA Lewis Research Center

INTRODUCTION

In aerospace applications, an engineer must be especially cognizant of size and weight constraints which affect design decisions. Although designing at or below the material fatigue limit may be desirable in most industrial applications, in aerospace applications it is almost mandatory to design certain components for a finite life at an acceptable probability of survival. Zaretsky (1987) outlined such a methodology based in part on the work of W. Weibull (1939, 1951) and G. Lundberg and A. Palmgren (1947a, 1947b, 1952). Zaretsky's method (1987) is similar in approach to that of Ioannides and Harris (1985).

Mahorter et al. (1985) discuss the accuracy of life prediction techniques for military turbine engine components such as compressor and turbine disks. The development of a 0.794 mm (0.03 in.) crack in any of the critical areas of a disk, such as bolt holes, bore, dovetail, etc., is considered the end of its low cycle fatigue (LCF) life. This is the life, $L_{0.1}$, at which the military requires a 99.9 percent probability of survival or a 0.1 percent failure rate. Disk retirement policy requires that the disks be removed from service or reworked at their $L_{0.1}$ life. The statistically predicted lives for bolt-hole cracks were shorter than the deterministically predicted values. These results imply that a deterministic approach to life prediction is not necessarily conservative, and that a probabilistic approach is viable in light of all the statistical variations in the design parameters.

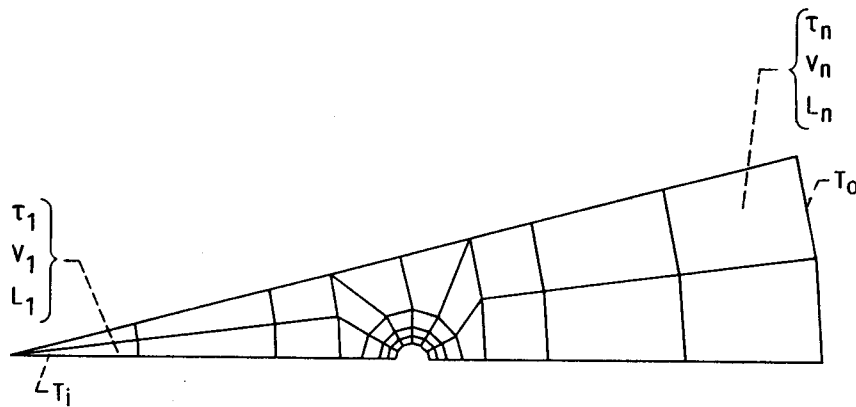
In view of the aforementioned, it is the objective of this work to (a) apply the method of Zaretsky (1987) to statistically predict the life of a generic solid disk with and without bolt holes, (b) determine the effect of disk design variables, thermal loads, and speed on relative life, and (c) develop a generalized equation for determining disk life by incorporating only these variables.

*Sverdrup Technology, Inc., Lewis Research Center Group. Work performed on-site at NASA Lewis under NASA Contract NAS3-24105.

OVERVIEW

FINITE ELEMENT MODEL

Parametric analytical studies were conducted to investigate the effect of varying physical dimensions and speed on the relative lives of a generic solid disk. The physical model of the solid disk requires that the structure be divided into a series of components (elements). This is most easily done by considering the disk as a collection of concentric rings. The disk was modeled with 10 rings of equal radial increment for the parametric values of disk diameter studied.



$$L_n = L_1 \left(\frac{\tau_1}{\tau_n} \right)^c \left(\frac{v_1}{v_n} \right)^{1/e}$$

$$\left(\frac{1}{L_s} \right)^e = \sum_{i=1}^n \left(\frac{1}{L_i} \right)^e$$

CD-88-32846

GOVERNING EQUATIONS

The following equation for the 10-percent life of a uniform solid rotating disk is obtained:

$$L_{10} = A \left[\left(\frac{K_D}{D} \right)^{20} \left(\frac{K_t}{t} \right) \left(\frac{K_N}{N} \right)^{14.3} \left(\frac{g}{c} \right)^{0.606} \left(\frac{K_T}{\Delta T} \right)^{0.52} \right] \exp(K_L \tau_L)$$

Introducing the concept of a Dynamic Speed Capacity N_o , which is defined by Zaretsky (1987) as the speed that would produce a theoretical life of one million stress cycles,

$$N_o = A \times 10^{-6} \left[\left(\frac{K_D}{D} \right)^{20} \left(\frac{K_t}{t} \right) K_N^{14.3} \left(\frac{g}{c} \right)^{0.606} \left(\frac{K_T}{\Delta T} \right)^{0.52} \right] \exp(K_L \tau_L)^{1/14.3}$$

and for any speed N for a given disk geometry.

$$L_{10} = \left(\frac{N_o}{N} \right)^{14.3} \times 10^6$$

SYMBOLS

A	material constant, stress cycles
c	stress-life exponent
D	disk diameter, m (in.)
E	material Young's modulus, N/m^2 (psi)
e	Weibull slope or modules
K_D	proportionality constant, m (in.)
K_L	proportionality constant, m^2/N (psi^{-1})
K_N	proportionality constant, rpm
K_T	proportionality constant, K ($^{\circ}F$)
K_t	proportionality constant, m (in.)
L	life, stress cycles
L_s	system life, stress cycles
L_{10}	ten-percent life, life at which 90 percent of a population survive, stress cycles
N	speed, rpm
N_o	dynamic speed capacity, rpm
T	temperature, K ($^{\circ}F$)
t	disk thickness, m (in.)
V	stress volume, m^3 (in. ³)
ΔT	temperature difference, K ($^{\circ}F$)
τ	shear stress, N/m^2 (psi)
τ_L	fatigue endurance limit, N/m^2 (psi)

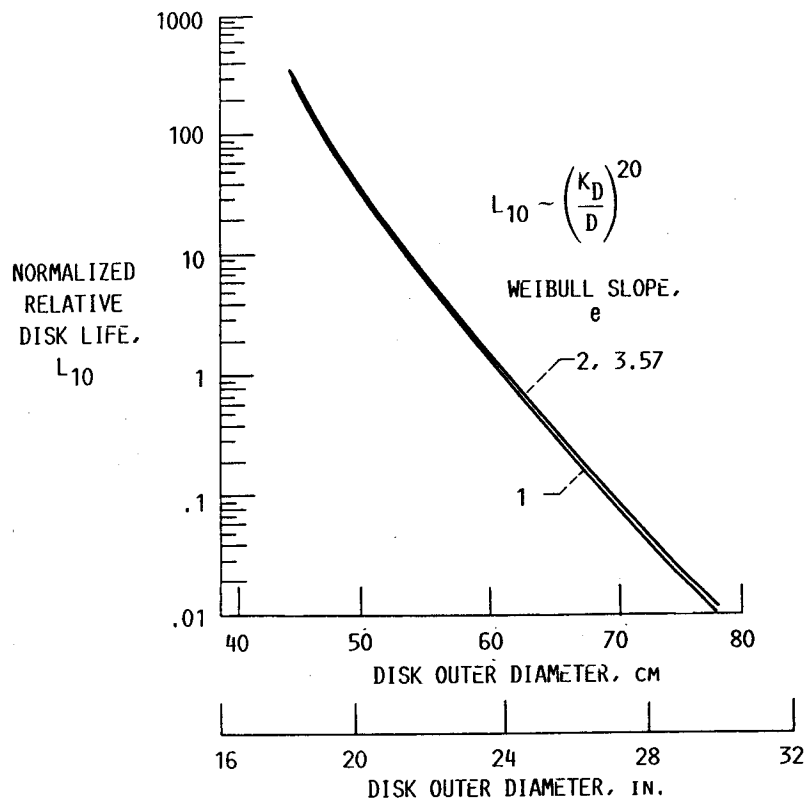
Subscripts:

i	<u>i</u> th component, and denotes inner disk radius
o	reference point, and denotes outer disk radius

POSTER PRESENTATION:

EFFECT OF DISK DIAMETER

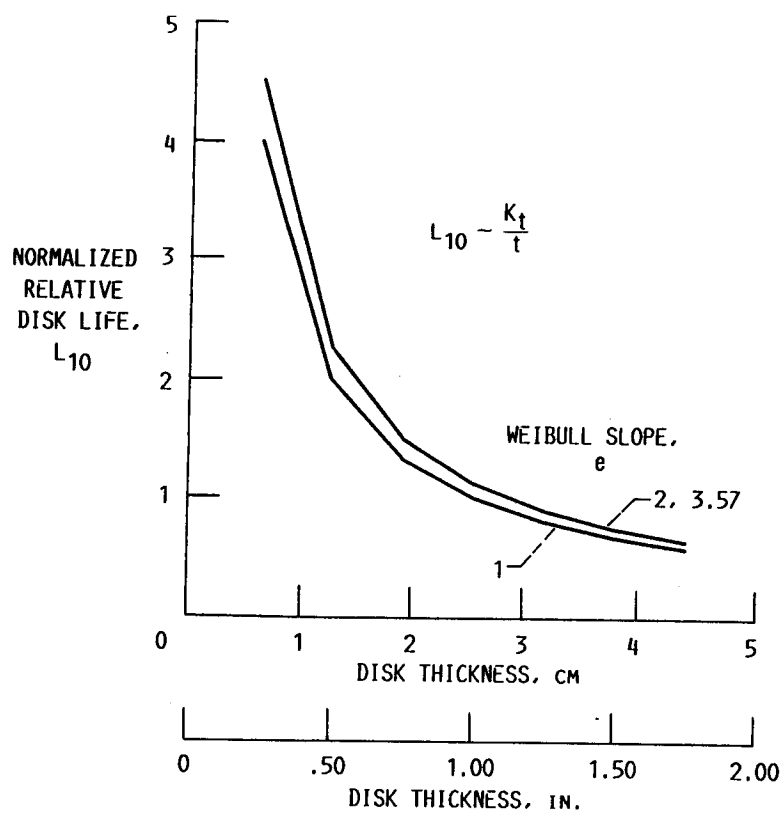
The effect of disk diameter on life for a speed of 9000 rpm and a stress-life exponent, c , of 9 is shown. As the disk diameter is increased, both the stress and the stress volume increase and life will decrease. The effect of Weibull slope is negligible. D is the disk diameter, K_D is a constant equal to 0.61 m (24.0 in.), and L_{10} is the life at a 90-percent probability of survival (or the life where 10 percent of the disks have failed).



CD-88-32848

EFFECT OF DISK THICKNESS

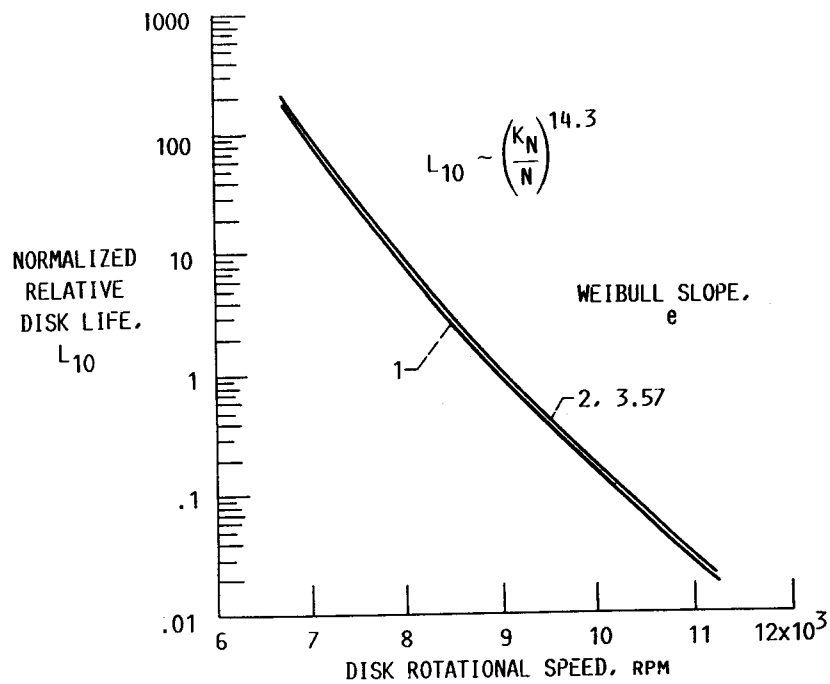
The effect of disk thickness on the L_{10} life is shown. Because the stressed volume is increased, life will decrease. The effect of Weibull slope is negligible. t is the disk thickness, and K_t is a constant equal to 0.0254 m (1.0 in.).



CD-88-32849

EFFECT OF SPEED

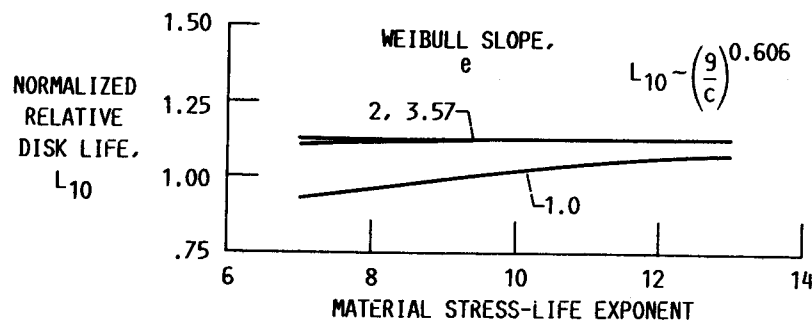
As disk speed is increased, stresses within the disk will increase. These stress increases will cause a decrease in life. The effect of disk rotational speed on L_{10} life is shown. N is the disk speed and K_N is a speed constant equal to 9000 rpm.



CD-88-32850

EFFECT OF STRESS-LIFE EXPONENT

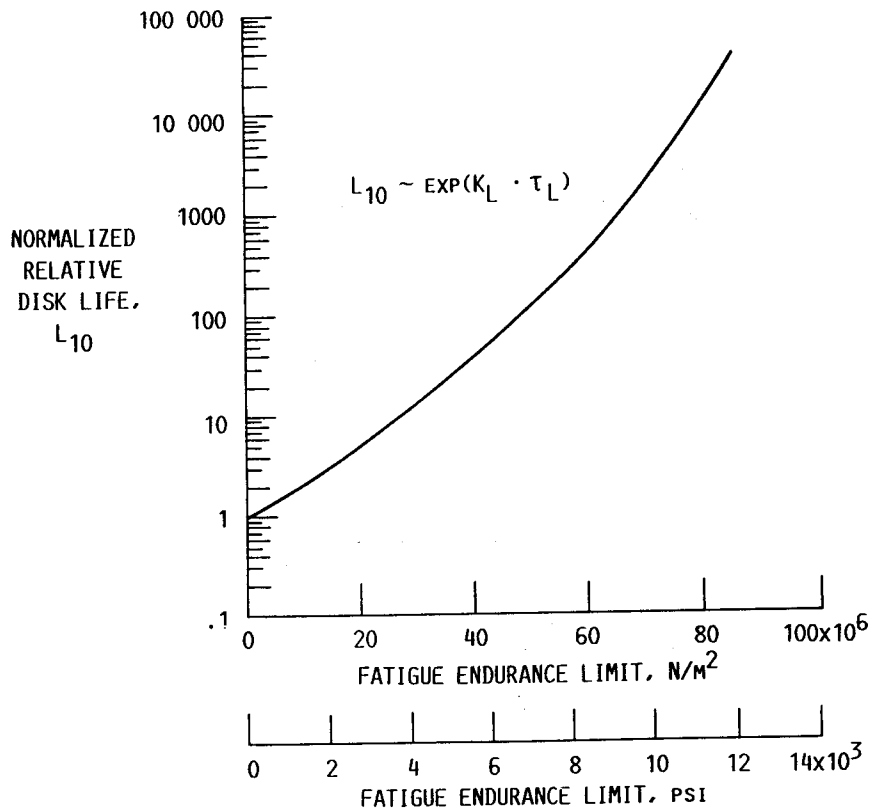
For each stressed elemental volume within the body of the disk, the life was determined by using an inverse stress-life relation. Not all materials will exhibit the same stress-life relation. The stress-life exponent is generally determined experimentally. For the previous calculations, a stress-life exponent of 9 was assumed. Using varying values of c with a reference disk, the effect of the stress-life exponent on the L_{10} life of the disk was determined. These results are shown.



CD-88-32851

EFFECT OF ENDURANCE LIMIT

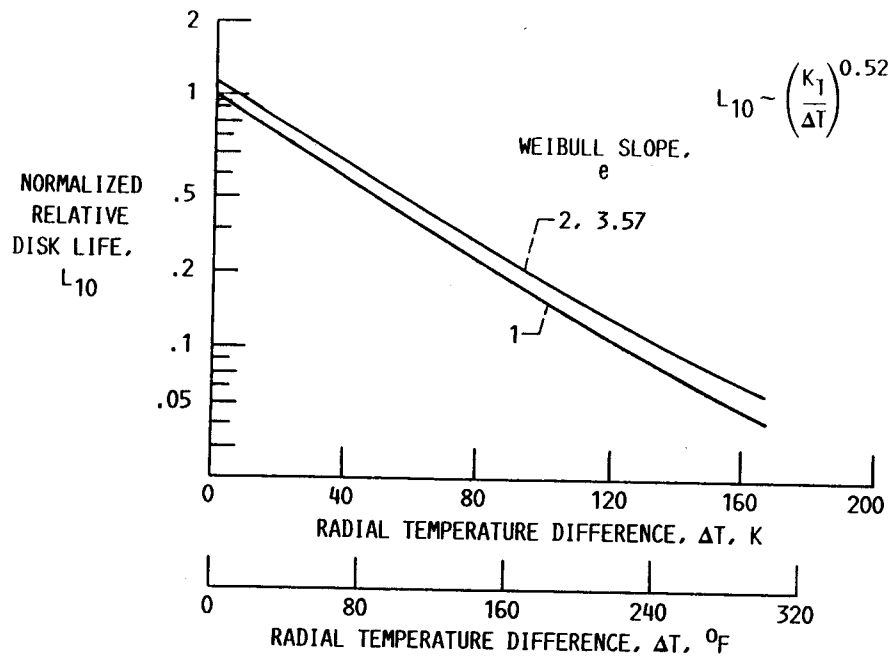
A concept first espoused by Ioannides and Harris (1985) was the application of a fatigue limit in the determination of the lives of the elemental stressed volumes. Basically, the concept is that where the shearing stress is equal to or less than the value determined or assumed for the fatigue limit, the probability of survival for that elemental stressed volume is 100 percent. The results of assuming varying values of a fatigue limit for the shearing stress is shown where τ_L is the fatigue endurance limit at or below which stress no failure is expected to occur and K_L is equal to $4.02 \times 10^{-8} \text{ m}^2/\text{N}$ ($2.77 \times 10^{-4} \text{ psi}^{-1}$).



CD-88-32852

EFFECT OF TEMPERATURE GRADIENTS

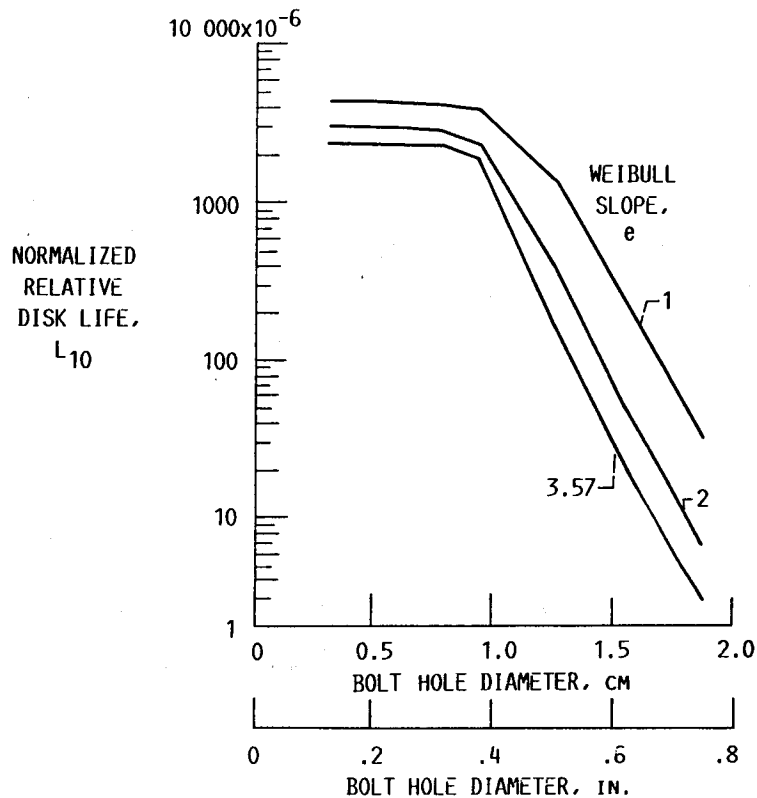
The effect of a radial temperature difference upon the overall disk relative life was determined by considering the thermal stresses superimposed upon the centrifugal disk stresses due to disk rotation. A steady-state radial temperature distribution was applied to a disk with a very small central hole. A disk with a small central hole was considered because this configuration relieved a mathematical singularity which occurs for isothermal boundary conditions upon a solid disk. The effect of various uniform radial linear temperature gradients on disk relative life is shown. ΔT is the total radial temperature difference and K_T is a constant equal to 0.56 K when ΔT is in Kelvin or 1F when ΔT is in Fahrenheit, and where ΔT is equal to or greater than K_T .



CD-88-32857

EFFECT OF HOLE SIZE

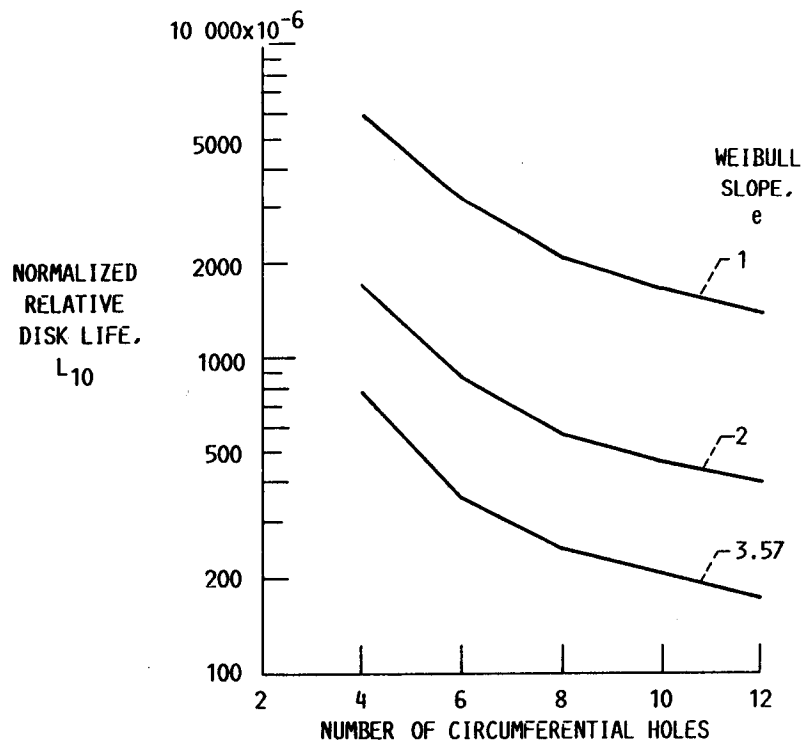
As discussed by Mahorter et al. (1985), tie-bolt holes will be the critical location for failure in a disk. Using the finite element model, the effect on disk life of bolt-hole size, location, and number was determined. The effect of bolt diameter on disk fatigue life is shown. It would appear that at bolt holes having a diameter of less than 10.2 mm (0.4 in.), the effect of hole size is nominal. At bolt holes larger in diameter, the effect is most significant. This analysis would suggest that the bolt holes in a disk should be smaller but more numerous.



CD-88-32854

EFFECT OF HOLE NUMBER

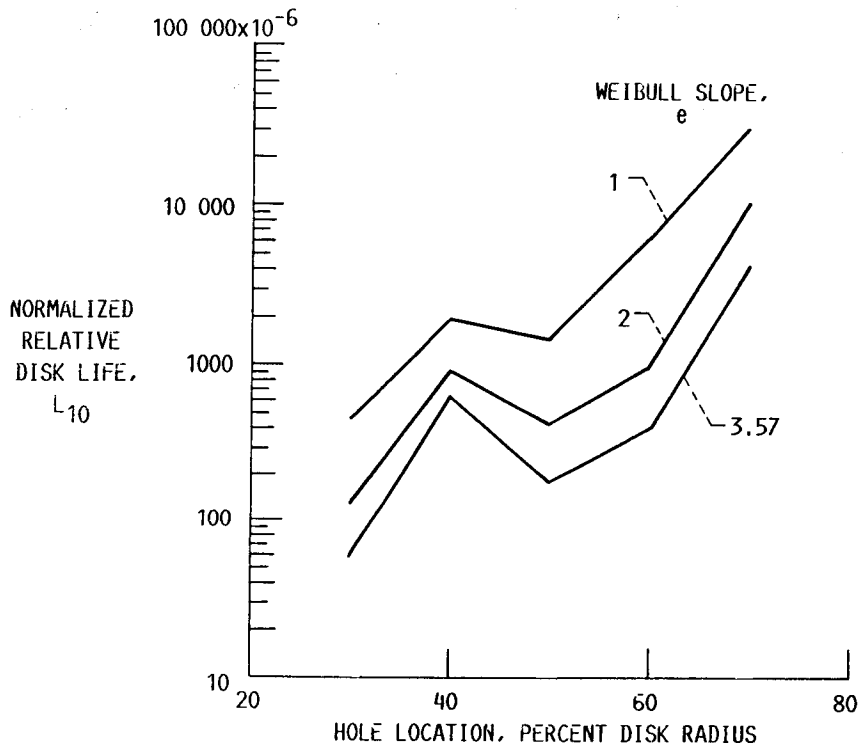
The effect of increasing the number of bolt holes is shown. Increasing the number of holes and keeping the hole diameter less than 10.2 mm (0.4 in.) appear to have less of an effect on life than having fewer holes with a larger diameter.



CD-88-32855

EFFECT OF HOLE LOCATION

The effect of hole location in the disk is shown as a percent of the disk radius measured from the axis of rotation. The results indicate a general trend of increasing life as the holes are moved radially outward. This would not be unexpected because stresses decrease with increasing distance from the center. The trend is not totally convincing, however, since there is an inversion of the trend at a location between 40 and 50 percent of the disk radius; that is, life decreases and then begins to increase again. It cannot be determined with reasonable certainty that this is correct or whether the finite element mesh size was properly selected for these calculations. Further analysis is required. However, it can be reasonably concluded that the bolt holes should be placed as far from the center of the disk as is practical.



CD-88-32856

REFERENCES

- Ioannides, E., and Harris, T.A., 1985, "A New Fatigue Life Model for Rolling Bearings," Journal of Tribology, Vol. 107, No. 3, pp. 367-378.
- Lundberg, G., and Palmgren, A., 1947a, "Dynamic Capacity of Rolling Bearings," Ingeniors Vetanskaps Akadmien-Handler, No. 196.
- Lundberg, G., and Palmgren, A., 1947b, "Dynamic Capacity of Rolling Bearings," Acta Polytechnica, Mechanical Engineering Series, Vol. 1, No. 3, pp. 1-50.
- Lundberg, G., and Palmgren, A., 1952, "Dynamic Capacity of Rolling Bearings," Acta Polytechnica, Mechanical Engineering Series, Vol. 2, No. 4.
- Mahort, R., London, G., Fowler, S., and Salvino, J., 1985, "Life Prediction Methodology for Aircraft Gas Turbine Engine Disks," AIAA Paper 85-1141.
- Weibull, W., 1939, "The Phenomenon of Rupture in Solids," Ingeniors Vetanskaps Akademien-Handler, No. 153.
- Weibull, W., 1951, "A Statistical Distribution Function of Wide Applicability," Journal of Applied Mechanics, Vol. 18, No. 3, pp. 293-297.
- Zaretsky, E.V., 1987, "Fatigue Criterion to System Design, Life and Reliability," Journal of Propulsion and Power, Vol. 3, No. 1, pp. 76-83.

LARGE-SCALE WIND TURBINE STRUCTURES

David A. Spera
Advanced Concepts and Applications Branch
NASA Lewis Research Center

INTRODUCTION

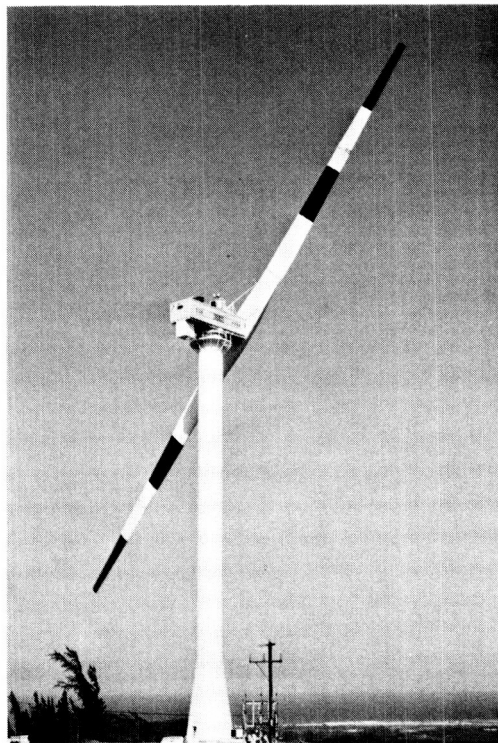
The purpose of this presentation is to show how structural technology has been applied in the design of modern wind turbines, which have recently been brought to an advanced stage of development as sources of renewable power. Wind turbine structures present many difficult problems because they are (1) relatively slender and flexible (2) subject to vibration and aeroelastic instabilities (3) acted upon by loads which are often nondeterministic (4) operated continuously with little maintenance in all weather, and (5) dominated by life-cycle cost considerations. Progress in horizontal-axis wind turbine (HAWT) development has been paced by progress in our understanding of structural loads, modeling of structural dynamic responses, and designing of innovative structural elements.

During the past 15 years, the NASA Lewis Research Center has developed a series of large HAWT's under the sponsorship of the U. S. Department of Energy and the Department of the Interior. This work has resulted in the design, construction, and testing of 13 HAWT's, with supporting research in aerodynamics, structural dynamics, electrical generating systems, and automatic controls. This has culminated in the recent completion of the world's largest operating wind turbine, the 3.2-MW Mod-5B power plant installed on the island of Oahu, Hawaii.

Some of the applications of structures technology to wind turbines will be illustrated by referring to the Mod-5B design. First, a video overview will be presented to provide familiarization with the Mod-5B project and the important components of the wind turbine system. Next, the structural requirements for large-scale wind turbines will be discussed, emphasizing the difficult fatigue-life requirements. Finally, the procedures used to design the structure will be presented, including the use of the fracture-mechanics approach for determining allowable fatigue stresses.

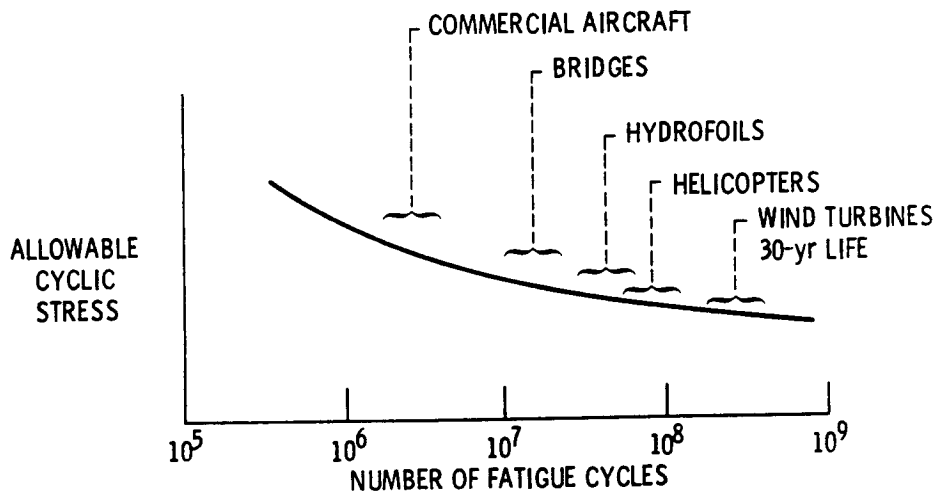
MOD-5B 3.2-MW WIND TURBINE

The Mod-5B is a third-generation horizontal-axis wind turbine that has evolved from a succession of federally-sponsored wind turbine research projects. This wind turbine, located in Hawaii on the northern tip of the island of Oahu, is the largest operating wind turbine in the world. Its design is based on technology developed during 15 years of intensive work at the Lewis Research Center, which managed the project. With a rated power of 3.2 megawatts, the Mod-5B has a rotor that spans 320 ft tip to tip, weighs 319,000 lb, and drives a power train inside a closed nacelle atop a 200-ft tower. In addition to an upwind teetered rotor, compact planetary gearbox, and pitchable tip control, the Mod-5B employs a variable-speed electrical induction generator/control system. While providing increased efficiency, variable-speed operation smooths out drivetrain and rotor tip vibrations and reduces fatigue loading because the rotor tips do not have to cycle constantly in gusting winds.



WIND TURBINE FATIGUE REQUIREMENTS ARE SEVERE COMPARED WITH OTHER STRUCTURES

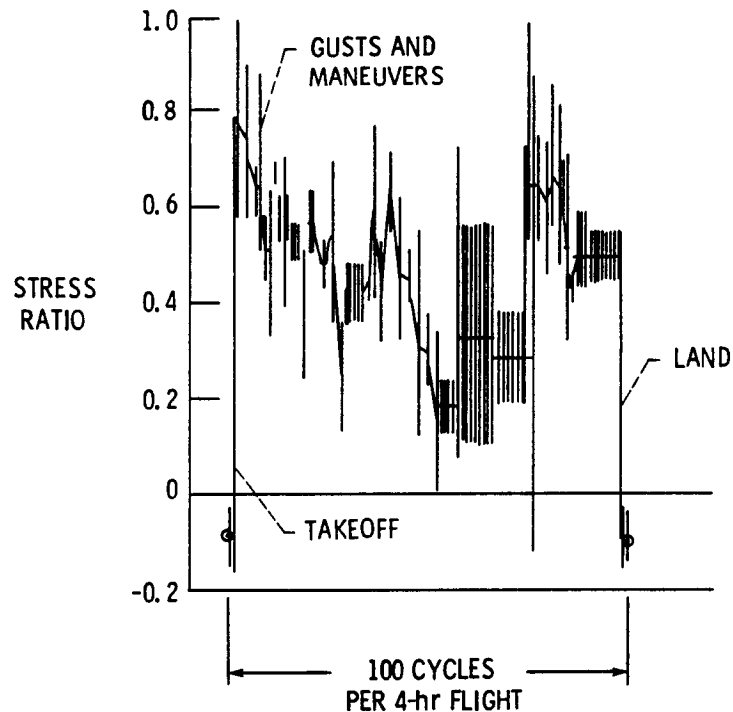
Fatigue is a design driver for at least one-half of the primary structure of a large HAWT. In order to be cost-effective, wind turbines must achieve fatigue lives longer than structures such as airplanes, bridges, and helicopters, often by more than an order of magnitude. Almost alone among engineering structures, wind turbine blades are subject to repeated, full reversals of dead load, which occur once each rotor revolution. Thus, a large HAWT rotor such as that of the Mod-5B (which rotates at speeds from 14 to 17.8 rpm) will experience about 150 million reversals of dead weight in its 30-yr design life. This number of cycles increases inversely with rotor size.



CD-88-33046

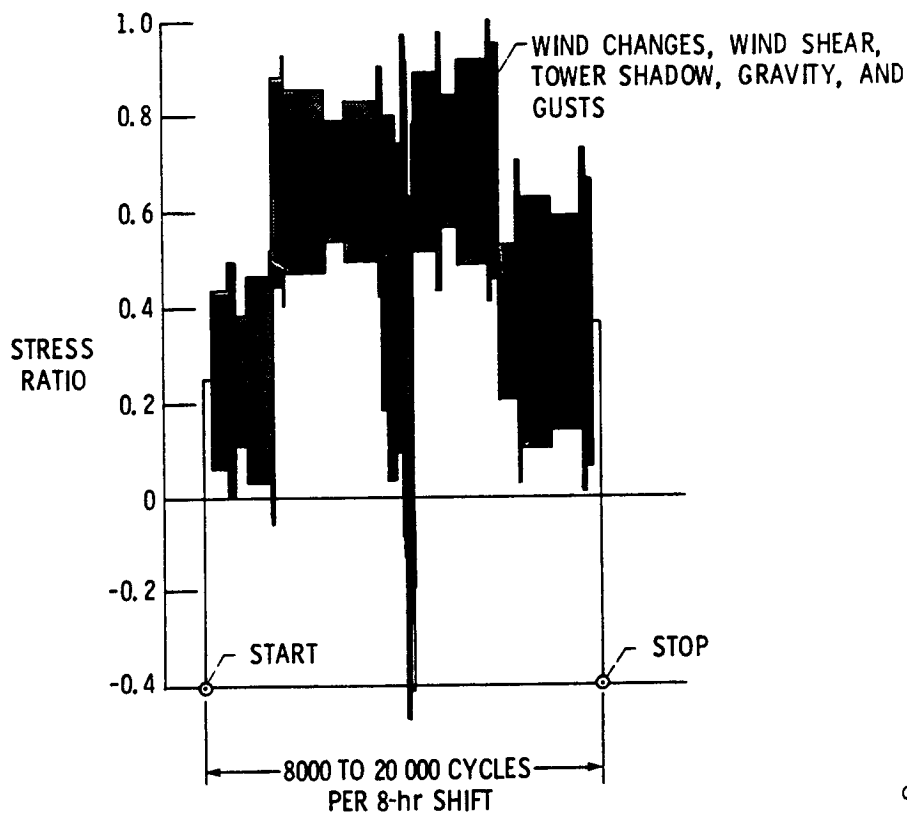
BOMBER WING STRESS SPECTRUM

As an example of a conventional structure subject to fatigue loading, consider a typical bomber aircraft wing. In a 4-hr flight, the wing may experience 100 measurable, significant cycles of fatigue loading, or 0.4 cpm, compared with a minimum of 14 cpm for a wind turbine blade. Even more important is the fact that a partial reversal of gravity loads occurs only once per flight, namely, during the so-called "ground-air-ground" cycle. The amplitudes of intermediate load cycles are generally limited to small fractions of the G-A-G cycle.



WIND TURBINE BLADE STRESS SPECTRUM

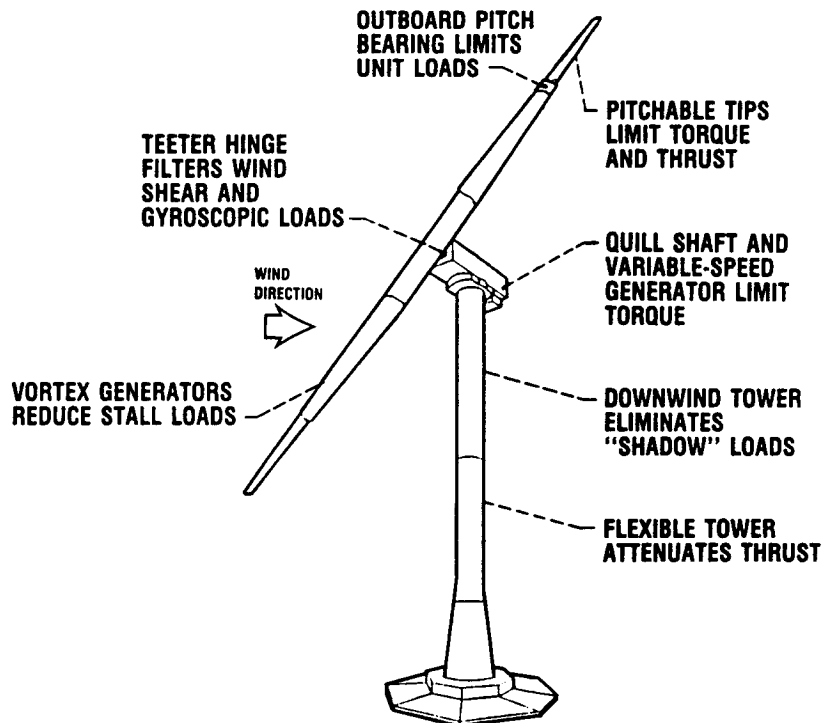
Wind turbine blades also experience a major "ground-air-ground" cycle during each period of operation. In addition, blades are subjected to two other types of load cycles which must be considered by the designer. The first type of load cycle occurs at least once per rotor revolution and is caused by gravity, wind shear (vertical gradient of wind speed near the ground), inflow distortions (tower blockage of the wind), and small-scale turbulence (smaller than the rotor diameter). The second type of load cycle is caused by longer-term changes in wind speed and large-scale turbulence.



CD-88-33048

THE MOD-5B AERO-STRUCTURAL-MECHANICAL CONFIGURATION REDUCES FATIGUE LOADS

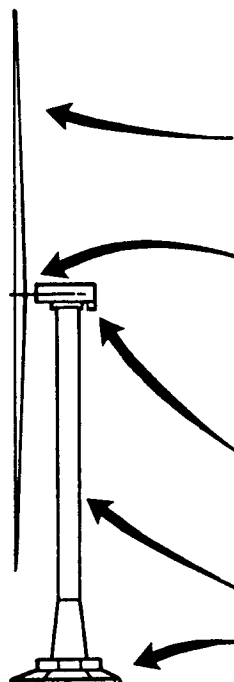
The configuration of the Mod-5B wind turbine is a result of a design development process which has incorporated active and passive load reduction into each major subsystem. Small tabs, called vortex generators, are located along the upwind leading edges of the blades, for the purpose of increasing the stall angle and reducing unsteady stall loads. The entire rotor is hinged at the hub to permit a teetering action, automatically balancing tip loads and largely eliminating gyroscopic loads during yawing. Pitching only the outboard $\frac{1}{4}$ of the blade, to control torque and thrust, reduces unit loads on the pitch bearings. A flexible quill shaft and variable-speed generator work together to reduce torque cycles. The flexible tower has a natural frequency of 1.3 per revolution to attenuate thrust and side loads from gusts. Its downwind location eliminates pulse loads on the blades caused by tower shadow.



CD-88-33049

STRUCTURAL DESIGN DRIVERS

While fatigue resistance is a critical design consideration for wind turbines, the design of large portions of the structure is governed by limit loads and by stiffness requirements for proper natural frequency placement. Some components, such as the quill shaft (the torque tube leading from the rotor to the gearbox) must meet both limit and stiffness requirements. Similarly, the tower must meet both fatigue and stiffness criteria. The geometric parameters available to the designer, such as diameter, wall thickness, and length, are sometimes not sufficient to meet all requirements. When this happens, fracture mechanics analysis is used to determine a combination of design allowable stress and inspection criteria that will lead to an acceptable design.



COMPONENT	DESIGN DRIVERS		
	FATIGUE	LIMIT	STIFFNESS
ROTOR			
UPWIND SIDE	✓	---	---
TEETER STOPS	✓	✓	---
DOWNWIND SIDE	---	✓	---
DRIVETRAIN			
ROTOR CAP	✓	---	---
LOW-SPEED SHAFT	✓	---	✓
GEARBOX	✓	---	---
QUILL SHAFT	---	✓	✓
HIGH-SPEED SHAFT	---	✓	---
NACELLE			
TRUSS	✓	✓	✓
YAW DRIVE	---	✓	---
YAW BRAKES	---	✓	---
TOWER	✓	---	✓
FOUNDATION	---	✓	---

CD-88-33050

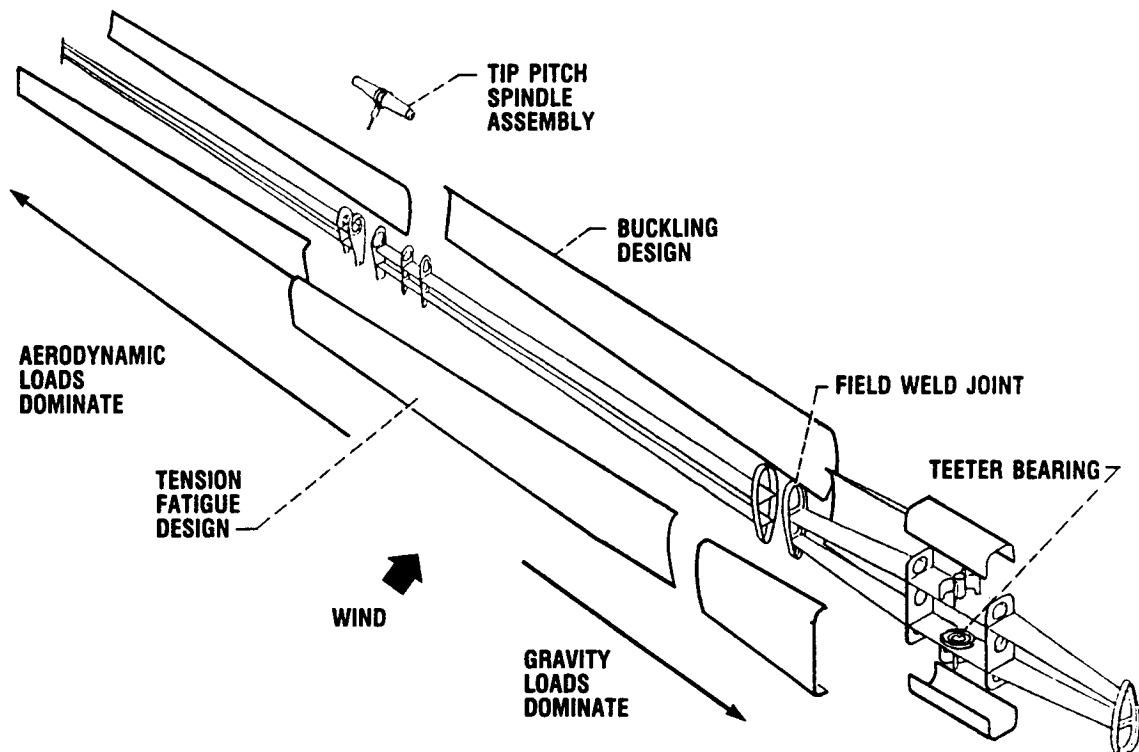
WELDED STEEL ROTOR TECHNOLOGY

Reducing the high cost of the rotor while maintaining its aerodynamic efficiency, ultimate strength, fatigue resistance, and stiffness has been the major technical challenge of wind turbine development. Welded steel was recognized as an ideal production material for large rotors, but technical risk was high because of severe fatigue requirements. A successful design, based on fracture mechanics technology, has been achieved. It tailors elements and joints to reduce stresses, and maintains strict quality assurance of materials, welds, and distortions.

Mod-5B Rotor Technical Data

Material Welded ASTM-A633
Diameter, ft 320
Total Weight, lb 318,000
Pitchable Tip Length, percent .. 34
Hub/Tip Chord, ft 13.7/4.1

Tip Speed, mph 147 to 198
Airfoil NACA 23010 to 23028
Appendages ... Vortex Gen., TE Tabs
Solidity 0.03
Twist, deg 7



CD-88-33051

FATIGUE DESIGN PROCEDURE

As an example of the fatigue design procedure, consider a cross-section weld joint in the rotor blade. Once the spectrum of fatigue loads acting on this cross section has been defined (including the probability of occurrence of mean and cyclic components of load), stress spectra can be calculated for points around the section. Using appropriate design flaws and a crack propagation model, a fatigue design life is calculated for each point. The stress spectrum at each critical point (a point with relatively short life) is then scaled up or down until a fatigue design life of 30 years is obtained. The 99.9th percentile stress in this scaled spectrum is then defined as the "design allowable stress" for that point and the selected inspection criteria.

Next, the dimensions of the elements in the section are changed in an iterative fashion until, considering all applicable factors of safety, the design margin at the most critical point is positive and approximately zero. Margins at other points around the section are calculated, and inspection criteria may be adjusted to optimize the trade-off between weight and cost.

- GIVEN: INTERFACE LOADS VS WIND SPEED VS PROBABILITY OF OCCURRENCE
- GIVEN: INITIAL DIMENSIONS, ASSUMED INITIAL CRACK SIZE AND CRACK GROWTH MODEL
- CALCULATE ANNUAL FATIGUE LOAD SPECTRUM (MEAN AND CYCLIC) AT CROSS-SECTION
- CALCULATE ANNUAL STRESS SPECTRUM AND FATIGUE LIFE AT POINTS IN SECTION
- SCALE STRESS SPECTRUM AT EACH CRITICAL POINT UNTIL LIFE EQUALS 30 YEARS
- "DESIGN ALLOWABLE STRESS" AT POINT IS 99.9TH PERCENTILE STRESS IN SCALED SPECTRUM
- APPLY SAFETY FACTORS AND ITERATE ELEMENT DIMENSIONS UNTIL DESIGN MARGIN AT MOST CRITICAL POINT IS ZERO
- CALCULATE MARGINS AT OTHER POINTS AND ADJUST INSPECTION CRITERIA FOR COST-EFFECTIVENESS

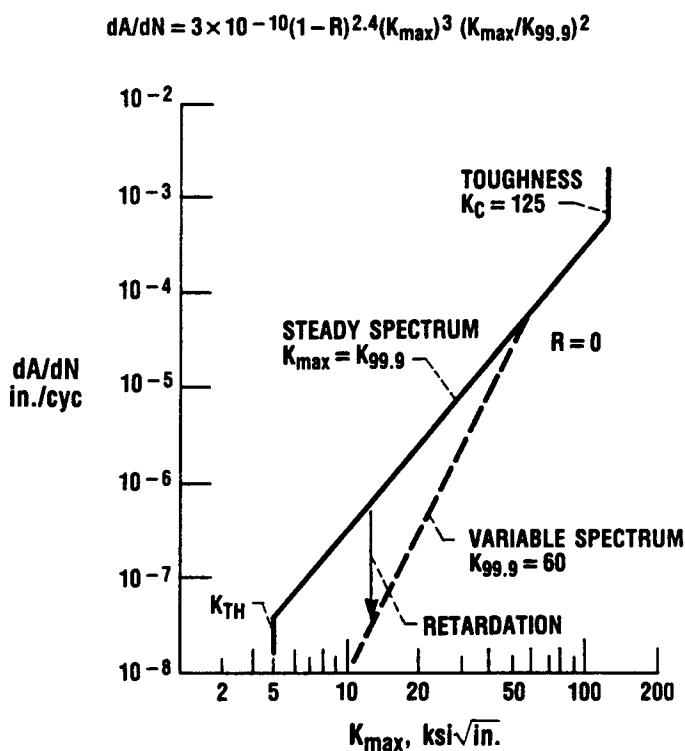
CD-88-33052

CRACK GROWTH RATE MODEL

An empirical crack growth rate model for the A-grade steels used in the Mod-5B wind turbine was developed on the basis of laboratory fatigue tests of pre-cracked specimens. These specimens were subjected to load spectra which simulated the highly variable stress cycles characteristic of wind turbine components. As is usual in such models, the amount by which the crack grows during a given cycle depends on the maximum and minimum stress intensities in the cycle, which, in turn, are dependent on the instantaneous crack size.

The crack growth rate model which best fit the test data was found to have the following characteristics:

- o A threshold stress intensity below which the growth rate is assumed to be zero. This threshold increases with increasing "R" ratio (i.e., ratio of minimum to maximum stress in the cycle).
- o A retardation factor which, for the same stress intensities, significantly reduces the growth rate under variable-spectrum loading compared with steady fatigue loading.
- o No effect of welding on crack growth rates in stress-relieved specimens.



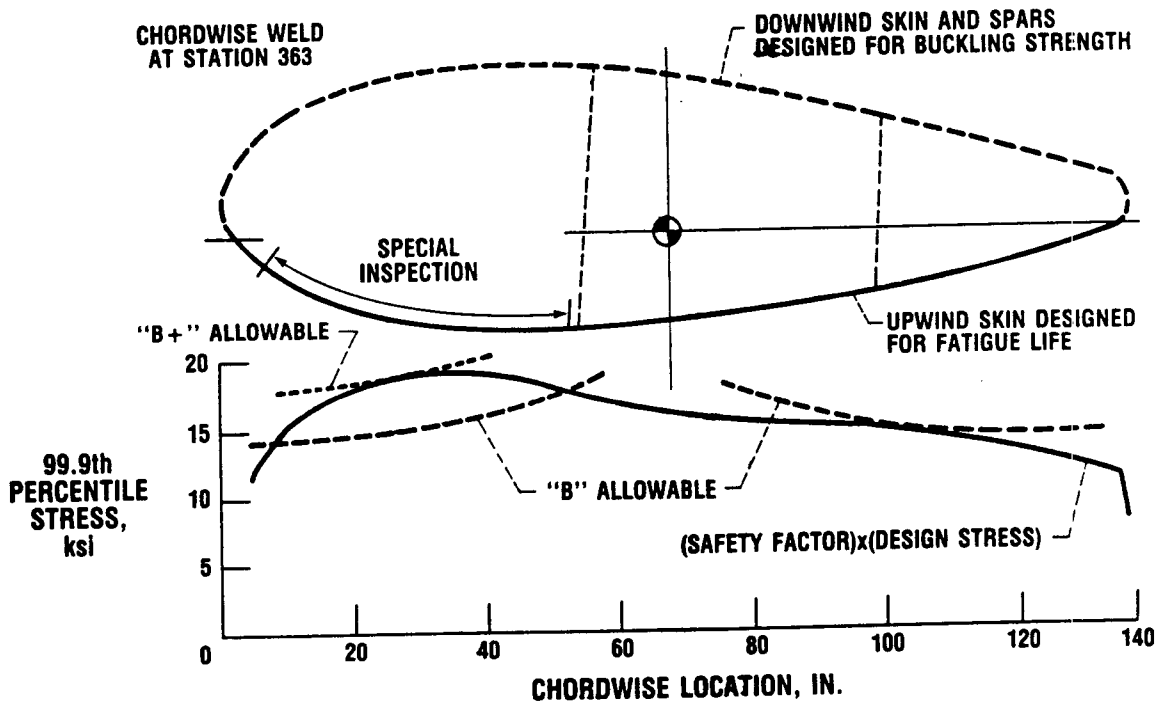
CD-88-33052

TYPICAL ROTOR DESIGN STRESS ALLOWABLES

A typical result of the Mod-5B fatigue design process is shown by this cross-section weld in the rotor blade at a station 363 in. from the shaft centerline (19 percent of span). The upwind skin, in which aerodynamic thrust produces tension loads, is designed for fatigue life requirements, while the downwind skin, which is generally in compression, is designed for buckling strength.

The inspection criteria for most of this weld is "B", with design allowable stresses in the range of 13,500 to 18,000 psi, depending on the "R" ratio which dominates the local stress spectrum. A "B" weld characteristically joins plates of equal thickness and is ground flush parallel to the stress direction.

However, a special "B+" inspection procedure has been specified for a small forward area. This special inspection detects smaller flaws and thus permits the design allowable stress to be about 25 percent higher than that for the "B" inspection. It is cost-effective to use extra inspection in this small but critical area.

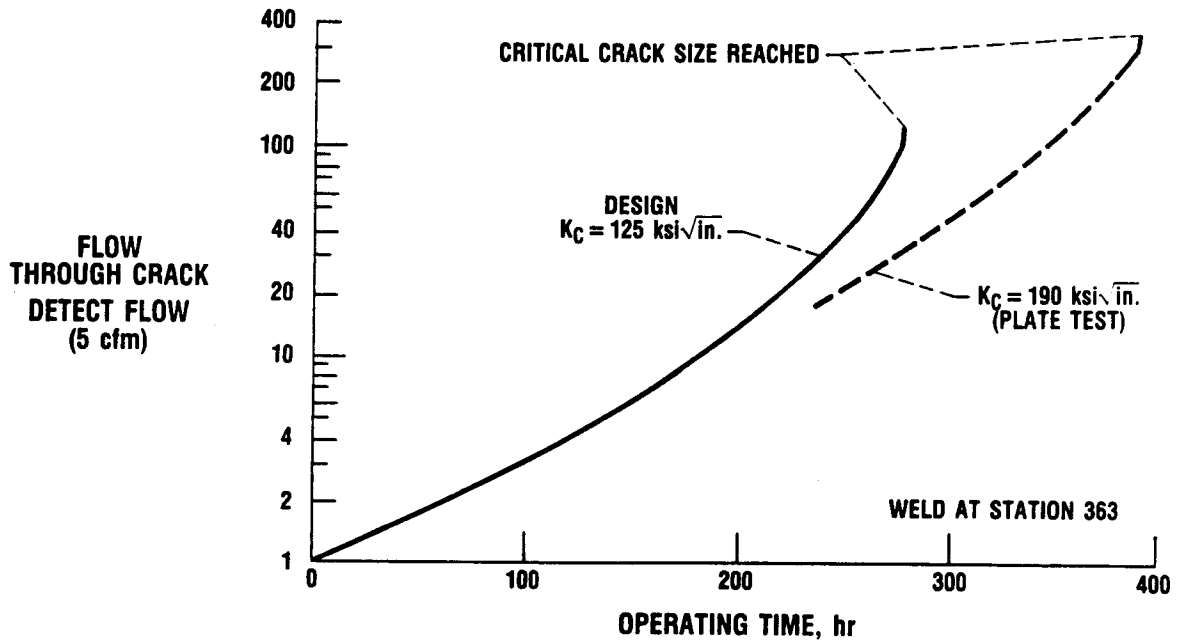


CD-88-33054

BLADE CRACK DETECTION SYSTEM

The Mod-5B rotor contains an air-pressure system for detecting a crack through the blade skin. Dried air is pumped into each blade independently and vented through calibrated exhaust ports. Air flow rates to the two blades are constantly compared, and a differential flow above an allowable level causes the automatic control system to shut down the turbine and signal the possible presence of a crack.

Fracture mechanics theory was used to calculate crack-opening displacements as a function of crack size and level of applied stress, in order to determine if there would be sufficient flow early enough to provide adequate warning. It was found that the toughness of the A-grade steel in the rotor was great enough that large cracks with detectable air flows were still stable. Tests were run to verify these flow calculations, using large plates containing 24-in. long through cracks and stressed to about 18 000 psi. Measured and predicted crack-opening displacements and air flows were found to agree.



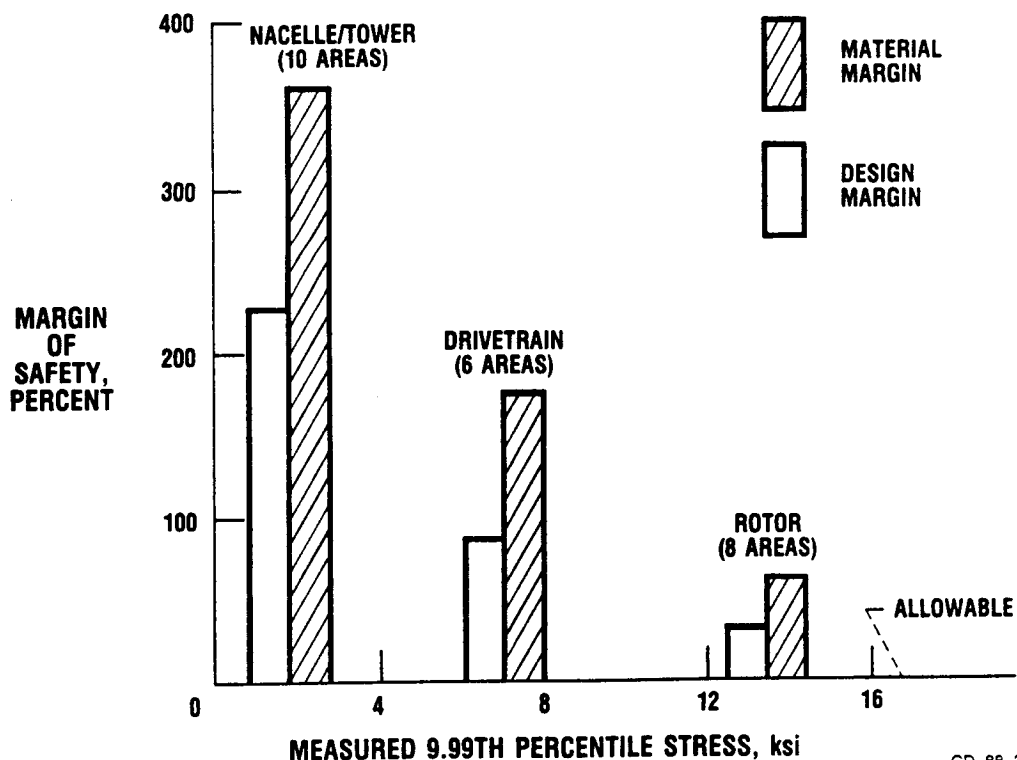
CD-88-33055

ASSESSMENT OF MOD-5B STRUCTURAL INTEGRITY

As part of a six-month series of acceptance tests, the structural integrity of the Mod-5B wind turbine was evaluated by measuring fatigue loads and local stresses during operation. Local stresses were monitored at 24 critical locations throughout the rotor, drivetrain, nacelle, and tower structures. Cumulative test time of over 25 hr represented in proportion the operating conditions which the turbine will experience in its lifetime. The continuously recorded dynamic stress data were analyzed statistically to determine the 99.9th percentile level for each critical location, and this level was then compared with the predicted design stress and the material allowable stress for that location.

The following conclusions were drawn from this assessment:

- o Stress and load levels were at or below design predictions and well below material allowables.
- o The assumptions on which the 30-yr design life of the structure was based have been verified, and meeting this design goal still appears feasible.
- o Steel rotor technology, including the fracture mechanics approach to fatigue-resistant design, has been verified.
- o Technical risk in building and operating steel wind turbines with diameters up to 320 ft is now commercially acceptable.



CD-88-33056

**AIRCRAFT ENGINE HOT SECTION TECHNOLOGY -
AN OVERVIEW OF THE HOST PROJECT**

Daniel E. Sokolowski*
Solar Dynamic Power and Propulsion Office
NASA Lewis Research Center

ABSTRACT

NASA sponsored the Turbine Engine Hot Section Technology (HOST) Project to address the need for improved durability in advanced aircraft engine combustors and turbines. Analytical and experimental activities aimed at more accurate prediction of the aerothermal environment, the thermomechanical loads, the material behavior and structural responses to loads, and life predictions for cyclic high-temperature operation were conducted from 1980 to 1987. The project involved representatives from six engineering disciplines who are spread across three work sectors - industry, academia, and NASA. The HOST Project not only initiated and sponsored 70 major activities, but also was the keystone in joining the multiple disciplines and work sectors to focus on critical research needs.

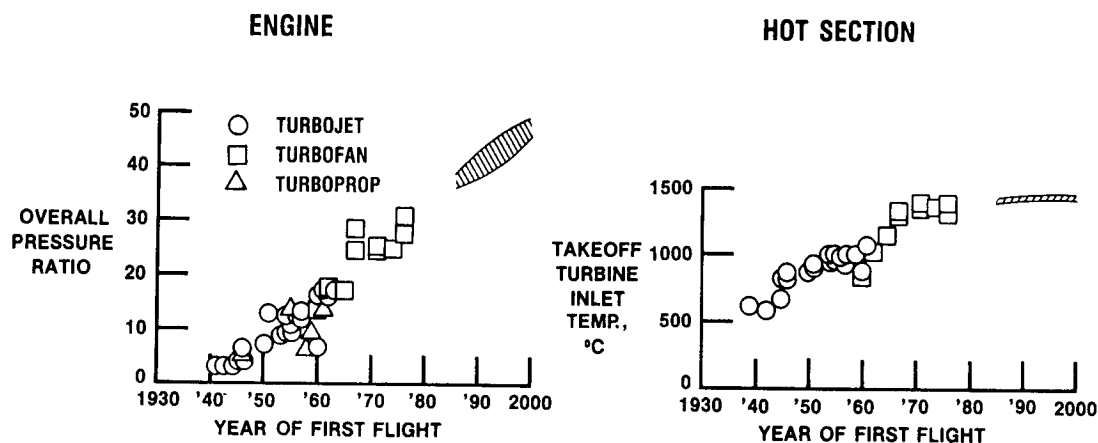
The project was managed from within the Structures Division at the NASA Lewis Research Center. Accordingly, research results from the HOST disciplines of structural analysis and fatigue and fracture are reported throughout this conference publication. The three papers that follow this one summarize the project's research results in the disciplines of advanced high-temperature instrumentation, combustion, and turbine heat transfer. Research in surface protection, such as thermal barrier coatings, is not reported in this conference publication. This paper provides a broad overview of the HOST Project, a summary of major accomplishments, and initial indications of the project's impact.

Numerous publications provide further details about research results from the HOST Project. Six annual workshops were conducted with conference proceedings being provided for each one (Turbine Engine Hot Section Technology, 1982 to 1987). Each of the proceedings generally covers research results for the preceding year. The last two proceedings also include a bibliography of definitive research reports. A comprehensive bibliography of the HOST Project is being prepared and is scheduled for publication later this year (Sokolowski, 1988a). Finally, a comprehensive final review of the HOST Project's research accomplishments and their impact has been prepared and also will be published later this year (Sokolowski, 1988b).

*Formerly Manager, HOST Project.

TRENDS IN TURBINE ENGINE OPERATING REQUIREMENTS

Since the introduction of the gas turbine engine to aircraft propulsion, the quest for greater performance has resulted in a continuing upward trend in overall pressure ratio for the engine core. Associated with this trend are increasing temperatures of gases flowing from the compressor and combustor and through the turbine. For commercial aircraft engines in the foreseeable future, compressor discharge temperature will exceed 1200 °F, while turbine inlet temperature will be approximately 2700 °F. Military aircraft engines will significantly exceed these values.

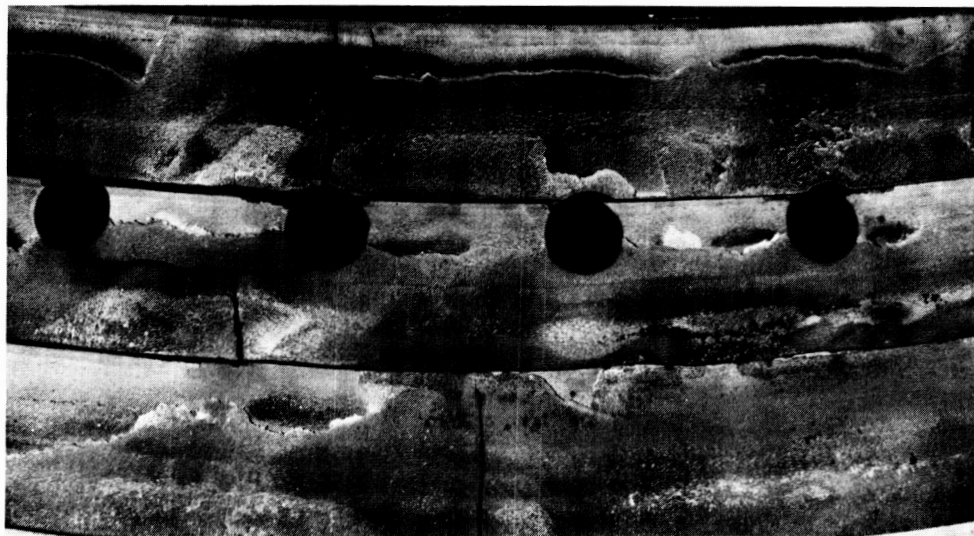


CD-88-32725

EFFECT OF MORE SEVERE OPERATING CONDITIONS ON COMBUSTOR LINERS

Since 1973 increasing fuel prices have created the demand for energy conservation and more fuel efficient aircraft engines. In response to this demand engine manufacturers continually increased the performance of current generation gas turbine engines. Soon afterward, the airline industry began to experience a notable decrease in the durability or useful life of critical parts in the engine hot section - the combustor and turbine. This was due primarily to cracking in the combustor liners, turbine vanes, and turbine blades. Spalling of the thermal barrier coatings that protect combustor liners also occurred.

**ORIGINAL PAGE IS
OF POOR QUALITY**



- AXIAL AND CIRCUMFERENTIAL CRACKS
- EXTENSIVE SPALLING OF THERMAL BARRIER COATING

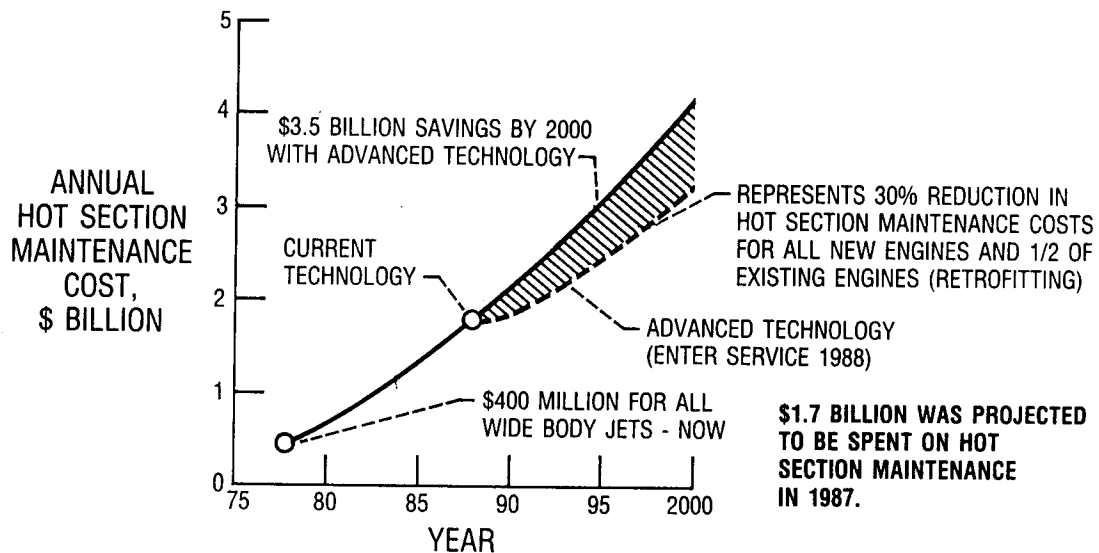
CD-88-32726

EFFECT OF MORE SEVERE OPERATING CONDITIONS ON ENGINE MAINTENANCE

For the airlines, reduced durability for in-service engines was measured by a dramatic increase in maintenance costs, primarily for high bypass ratio engines. Higher maintenance costs were especially evident in the hot section. Hot section maintenance costs account for almost 60 percent of the engine total, as reported by Dennis and Cruse, 1979.

"HOT SECTION PARTS ACCOUNT FOR 60 PERCENT OF ENGINE MAINTENANCE COSTS. IN 1978, APPROXIMATELY \$400 MILLION WAS SPENT..."

A.J. DENNIS, PRATT & WHITNEY (AIAA 79-1154)



CD-88-32727

EFFECT OF MORE SEVERE OPERATING CONDITIONS ON FLIGHT SAFETY

Besides having an effect on maintenance costs, failure of hot section parts can affect flight safety. An example is a Boeing 737 accident in Manchester, England, in August 1985, with the loss of 55 lives. The accident was a direct result of failure due to cracking in a combustor liner and subsequent puncture of a wing fuel tank.

ORIGINAL PAGE IS
OF POOR QUALITY



CD-88-32728

APPROACHES TO IMPROVING HOT SECTION DURABILITY

Durability can be improved in hot section components by using any combination of four approaches described below.

(1) High-temperature materials - High-temperature metallic materials currently include nickel- and cobalt-based superalloys. Certain elements of these alloys, such as cobalt, are in short supply and are expensive. Recently, Stephans (1982) completed a study of ways to reduce their usage. Advanced high-temperature superalloy components also include directionally solidified, single-crystal, and oxide-dispersion-strengthened materials. For such materials, the development time is lengthy, fabrication is sometimes difficult, and again, costs are high. Thus, successful use of these materials requires a balance among design requirements, fabrication possibilities, and total costs.

(2) More effective cooling techniques - Current cooling techniques tend to be sophisticated; fabrication is moderately difficult. In higher performance engines, cooling capability may be improved by increasing the amount of coolant. But the penalty for doing this is a reduction of thermodynamic cycle performance of the engine system. In addition, the coolant temperature of such advanced engines is higher than that for current in-service engines. Consequently, more effective cooling techniques are being investigated. Generally, they are more complex in design, demand new fabrication methods, and may require a multitude of small cooling holes, each of which introduces potential life-limiting high stress concentrations. Acceptable use of the advanced cooling techniques will require accurate models for design analysis.

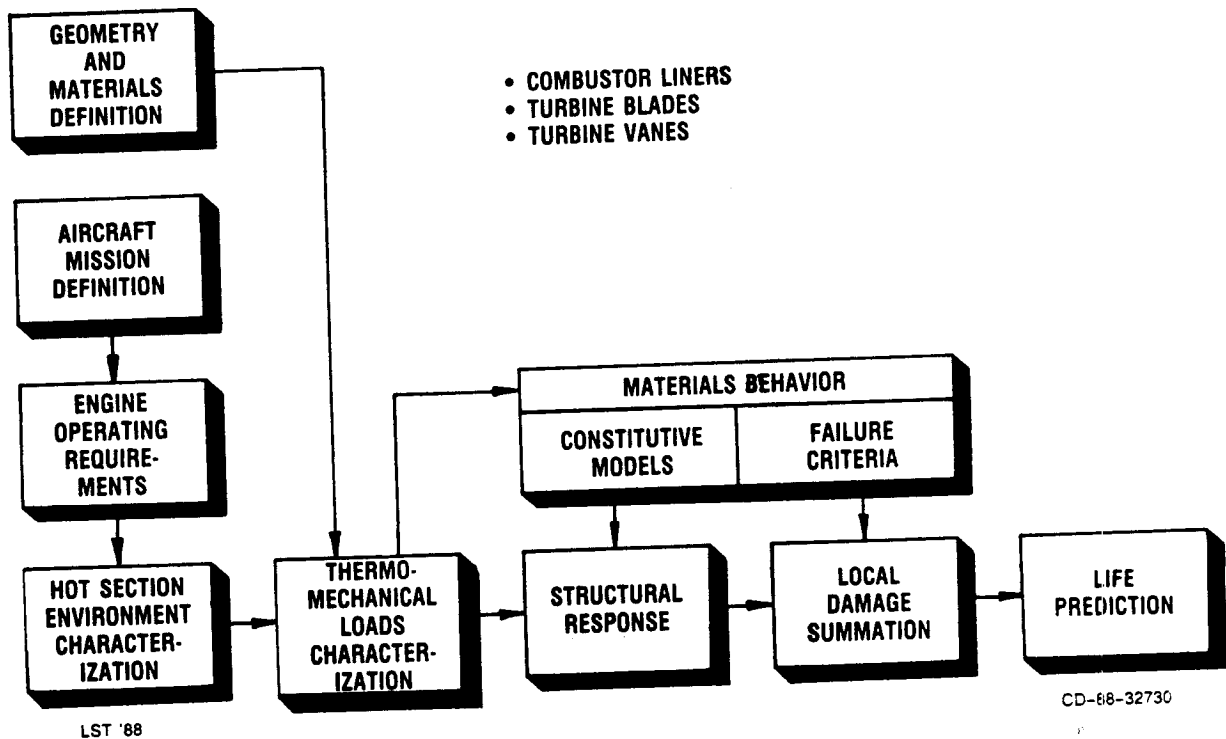
(3) Advanced structural design concepts - The introduction of advanced structural design concepts usually begins with a preliminary concept that then must be proven, must be developed, and most critically must be far superior to entrenched standard designs. Acceptance certainly is time consuming, and benefits must be significant. For improved durability in high-performance combustors, an excellent example of an advanced structural design concept is the segmented liner (Tanrikut, et al., 1981). The life-limiting problems associated with high hoop stresses were eliminated by dividing the standard full-hoop liners into segments. At the same time, designers realized increased flexibility in the choice of advanced cooling techniques and materials, including ceramic composites.

(4) More accurate design analysis tools - Finally, the design analysis of hot section component parts, such as the combustor liners or turbine vanes and blades, involves the use of analytical or empirical models. Such models often involve computer codes for analyzing the aerothermal environment, the thermo-mechanical loads, heat transfer, and material and structural responses to such loading. When the parts are exposed to high-temperature cyclic operation as in a turbine engine, the repetitive straining of the materials invariably leads to crack initiation and propagation until failure or break-away occurs. The useful life of a part is usually defined as the number of mission cycles that can be accumulated before initiation of significant cracks. Thus, designers need to predict useful life accurately so they can design a part to meet requirements.

FRAMEWORK FOR THE HOST PROJECT

Efforts to predict the life of a part generally follow the flow of analytical models shown in the figure below. Thus, designing a part such as a turbine blade to meet a specified life goal may require several iterations through the life prediction system, varying the blade geometry, material, or cooling effectiveness in each pass, until a satisfactory life goal is predicted.

INTEGRATION OF ANALYSES LEADS TO LIFE PREDICTION



THE HOST PROJECT

To meet the needs for improved analytical design and life prediction tools, especially those used for high-temperature cyclic operation in advanced combustors and turbines, NASA has sponsored the Turbine Engine Hot Section Technology (HOST) Project. The project was conducted from fiscal year 1981 through 1987.

The HOST Project has developed improved analytical models for the aerothermal environment, the thermomechanical loads, material behavior, structural response, and life prediction, along with more sophisticated computer codes, that can be used in design analyses of critical parts in advanced turbine engine combustors and turbines. Use of these more accurate analytical tools during the design process will ensure improved durability of future hot section engines components.

The complex durability problem in high-temperature, cyclically operated turbine engine components requires the involvement of numerous research disciplines. This involvement must include not only focused research but also interdisciplinary and integrated efforts. The disciplines included in HOST were instrumentation, combustion, turbine heat transfer, structural analysis, fatigue and fracture, and surface protection.

Most disciplines in the HOST Project followed a common approach. First, phenomena related to durability were investigated, often using benchmark quality experiments. With known boundary conditions and proper instrumentation, these experiments resulted in a better characterization and understanding of such phenomena as the aerothermal environment, the material and structural behavior during thermomechanical loading, and crack initiation and propagation. Second, state-of-the-art analytical models were identified, evaluated, and then improved upon through use of more inclusive physical considerations and/or more advanced computer code development. When no state-of-the-art models existed, researchers developed new models. Finally, predictions using the improved analytical tools were validated by comparison with experimental results, especially the benchmark data.

OBJECTIVE

- PROVIDE MORE ACCURATE DESIGN ANALYSIS TOOLS WHICH WILL BETTER ENSURE, DURING THE DESIGN PROCESS, IMPROVED DURABILITY OF HOT SECTION COMPONENTS.

APPROACH

- FOCUS MULTIDISCIPLINARY RESEARCH TOWARD
 - BENCHMARK QUALITY EXPERIMENTS
 - ADVANCED ANALYTICAL MODELS
 - IMPROVED COMPUTER CODES

HOST PROJECT ACTIVITIES

ORIGINAL PAGE IS
OF POOR QUALITY

The HOST Project initiated and sponsored 70 major research activities across six technical disciplines. Research results from many of these activities are reported throughout this publication.

TABLE 1. - HOST Project Activities

	Contract (C), Grant (G), or NASA Organization (N) Number
Instrumentation	
Hot Section Viewing System	C NAS3-23156
Dynamic Gas Temperature Measurement System - A	C NAS3-23154
Dynamic Gas Temperature Measurement System - B	C NAS3-24228
Turbine Static Strain Gage - A	C NAS3-23169
Turbine Static Strain Gage - B	C NAS3-23722
Turbine Heat Flux Sensors	C NAS3-23529
Laser Speckle Strain Measurement	C NAS3-26615
High Temperature Strain Gage Materials	G NAG3-501
Hot Section Sensors	N 2510
Laser Anemometry for Hot Section Applications	N 2520/2530
HOST Instrument Applications	N 2510
Combustion	
Assessment of Combustor Aerothermal Models - I	C NAS3-23523
Assessment of Combustor Aerothermal Models - II	C NAS3-23524
Assessment of Combustor Aerothermal Models - III	C NAS3-23525
Improved Numerical Methods - I	C NAS3-24351
Improved Numerical Methods - II	C NAS3-24350
Improved Numerical Methods - III	G NAG3-596
Flow Interaction Experiment	C NAS3-24350
Fuel Swirl Characterization - I	C NAS3-24350
Fuel Swirl Characterization - II	C NAS3-24352
Mass and Momenta Transfer	C NAS3-22771
Diffuser/Combustor Interaction	C F33615-84-C-2427
Dilution Jet Mixing Studies	C NAS3-22110
Lateral Jet Injection into Typical Combustor Flowfields	G NAG3-549
Flame Radiation Studies	N 2650
Turbine Heat Transfer	
Mainstream Turbulence Influence on Flow in a Turning Duct - A	C NAS3-23278
Mainstream Turbulence Influence on Flow in a Turning Duct - B	G NAG3-617
2-D Heat Transfer without Film Cooling	C NAS3-22761
2-D Heat Transfer with Leading Edge Film Cooling	C NAS3-23695
2-D Heat Transfer with Downstream Film Cooling	C NAS3-24616
Measurement of Blade and Vane Heat Transfer Coefficient in a Turbine Rotor	C NAS3-23717
Assessment of 3-D Boundary Layer Code	C NAS3-23716
Coolant Side Heat Transfer with Rotation	C NAS3-23691
Analytic Flow and Heat Transfer	C NAS3-24358
Effects of Turbulence on Heat Transfer	G NAG3-522
Tip Region Heat Transfer	G NAG3-623
Impingement Cooling	G NSG3-075
Computation of Turbine Blade Heat Transfer	G NAG3-579
Advanced Instrumentation Development	N 2640
Warm Turbine Flow Mapping with Laser Anemometry	N 2620
Real Engine-Type Turbine Aerothermal Testing	N 2640
Structural Analysis	
Thermal/Structural Load Transfer Code	C NAS3-23272
3-D Inelastic Analysis Methods - I	C NAS3-23697
3-D Inelastic Analysis Methods - II	C NAS3-23658
Component Specific Modeling	C NAS3-23687
Liner Cyclic Life Determination	N 5210
Structural Components Response Program	N 5210
High Temperature Structures Research Laboratory	N 5210
Constitutive Model Development	N 5210
Constitutive Modeling for Isotropic Materials - I	C NAS3-23925
Constitutive Modeling for Isotropic Materials - II	C NAS3-23927
Theoretical Constitutive Models for Single Crystal Alloys	G NAG3-511
Biaxial Constitutive Equation Development for Single Crystals and Directionally Solidified Alloys	G NAG3-512
Fatigue and Fracture	
Creep-Fatigue Life Prediction for Isotropic Materials	C NAS3-23288
Elevated Temperature Crack Propagation	C NAS3-23940
Life Prediction and Material Constitutive Behavior for Anisotropic Materials	C NAS3-23939
Analysis of Fatigue Crack Growth Mechanism	G NAG3-348
Vitalization of High Temperature Fatigue and Structures Laboratory	N 5220
Surface Protection	
Effects of Surface Chemistry on Hot Corrosion	C NAS3-23926
Thermal Barrier Coating Life Prediction - I	C NAS3-23943
Thermal Barrier Coating Life Prediction - II	C NAS3-23944
Thermal Barrier Coating Life Prediction - III	C NAS3-23945
Airfoil Deposition Model	G NAG3-201
Mechanical Behavior of Thermal Barrier Coatings	G NCC3-27
Coating Oxidation/Diffusion Prediction	N 5160
Deposition Model Verification	N 5160
Dual Cycle Attack	N 5160
Rig/Engine Correlation	N 5160
Burner Rig Modernization	N 5160
Notes: A, B Activities in series I, II, III Activities in parallel	

MAJOR ACCOMPLISHMENTS

The HOST Project produced numerous accomplishments through 70 activities that were initiated and conducted in the project's six disciplines. Major accomplishments categorized by discipline follow. Background for the work as well as results obtained are included.

INSTRUMENTATION

The instrumentation work entailed five programs, covering a combustor viewing system, a dynamic gas temperature system, laser anemometry, heat flux sensors, and high-temperature strain measurement.

Combustor Viewing System

To allow visual diagnoses of abnormal operation of combustors, fuel injectors, liners, and nozzle guide vanes, HOST researchers developed a combustor viewing system that provides qualitative images during component operation. The viewing system consists of a water-cooled optical probe, a probe actuator, an optical interface unit that couples the probe to cameras and to an illumination source, and system controls. This system has been used in both combustor component and full-scale engine tests, for combustor liner durability studies, and for flowpath diagnostics. It has been used to examine light-off and blowout characteristics and appears to have considerable potential for other time-dependent phenomena and for flame radiometry.

Dynamic Gas Temperature System

Prior to HOST, researchers had no techniques to accurately measure fluctuating hot gas temperatures at frequencies above 10 Hz. Through HOST we developed a dynamic gas temperature measurement system and tested it in a F-100 engine facility and a high-pressure component test facility. Accurate gas temperature measurements are now possible up to 1-KHz and 3000 °F peaks. This helps with modeling combustor flows and better defines the environment imposed on turbine airfoils.

Laser Anemometry

The laser anemometer (LA) has become a valuable tool for nonintrusive gas velocity measurements in turbine engine work. Under HOST, we developed technology needed to apply LA to high-temperature turbines. Specific work areas included seeding, data acquisition, system optimization, and optical design.

Seeding. - Seed materials and high-volume seed generators were evaluated in a small combustor facility. We examined various refractory materials dispersed with a fluidized bed and titanium dioxide seed produced by the chemical reaction of titanium tetrachloride and water vapor.

Data acquisition. - Efficient data acquisition requires minimum operator intervention during test runs. To accomplish this, we developed a computer-controlled signal preprocessor for counterprocessors. This preprocessor controls filter settings, photomultiplier tube (PMT) voltage, and radio-frequency gain, as well as monitoring the PMT current.

System optimization. - A computer model was developed to determine optimal designs for fringe-type LA's. Prediction analysis methods were used to determine optical designs that provide minimum measurement uncertainties for given particle size, proximity to surfaces, and signal processor parameters. Experiments were conducted to measure surface reflectance properties - data needed for system optimization. A study of filter-induced errors was conducted to determine the best filter designs for use with counterprocessors.

Optical design. - The conventional fringe-type LA is not necessarily optimal for measurements within turbomachines. It has the required large acceptance angle, but its relatively large probe volume precludes accurate measurements close to flow passage walls. Under HOST, a unique four-spot time-of-flight LA was developed and tested. The four-spot LA has both a large acceptance angle and the capability to measure close to walls. In testing, we obtained successful measurements as close as 75 μm from a surface normal to the viewing direction. Another optical design project conducted under HOST was the development of an optical corrector for use with the cylindrical windows used in turbine facilities. This corrector eliminates the aberrations caused by the window.

Heat Flux Sensors

Heat flux sensors were developed and tested in both combustor liner and turbine airfoil applications. Tests in combustor liners provided useful heat flux data. However, the sensors proved to be too sensitive to transverse temperature heat flux gradients for most applications to turbine airfoils. This was particularly true for the Gardon gage sensor because of its lack of symmetry. Sensor configurations with lower transverse sensitivity have been considered but not tested.

High-Temperature Strain Measurements

The program's goal was to improve the capability for static strain measurement from the pre-HOST temperature limits of roughly 700 to 1800 °F. This was the most ambitious research effort of HOST's instrumentation subproject. We used three approaches in this work: (1) To develop improved resistance strain gage alloys, (2) to learn how to use available strain gages more effectively, and (3) to evaluate alternative optical strain measuring systems.

Improved strain gage alloys. - Improved strain gage alloys in the FeCrAl and PdCr systems were developed, but neither has been demonstrated as a successful high-temperature strain gage. Work continues on developing wire and thin film strain gages of PdCr.

More effective use of available strain gages. - Evaluation tests of strain gages mainly from the FeCrAl system (including wire gages from China) have provided a better understanding of FeCrAl gage characteristics. As a result, an experiment to measure combustor liner strain in which strain gage cooling rates were carefully controlled to match those used in pre- and post-test calibrations provided useful strain data at temperatures up to 1250 °F.

Alternative strain measuring systems. - Optical systems appear to have potential for high-temperature noncontact strain measurements. One such system, a laser speckle photogrammetric system, was tested and shown to be capable of measuring thermal expansion of a Hastelloy-X plate at temperatures up to 1600 °F. However, problems related to index refraction gradients in the gas within the viewing path must be solved (or at least controlled) to permit this technology to be applied widely.

Thin Film Sensors

In addition to the work described above, we have been working on technology to put thin film sensors on turbine engine hot section components. Thin film thermocouple technology has been developed and such sensors are in use in engine testing. Current work in this area is focused on three goals: Basic improvements in sensor processing technology, extension to other sensors such as strain gages and heat flux sensors, and accommodating changes in substrate materials. This work was partially supported by the HOST Project.

COMBUSTION

The HOST Project combustion work emphasized aerothermal modeling. The original plan called for three work phases. During phase 1, researchers assessed existing gas turbine combustion models. They then made suggestions for improving existing models, particularly for numerical accuracy. In phase 2 they improved models for interacting but nonreacting fluid flows. Phase 3 was to improve models for interacting and reacting fluid flows. Phase 3 work was not performed (because HOST Project funding was curtailed), but it is still important work that substantially affects our understanding and the predictive accuracy of combustion fluid flow models.

A separate work element involved dilution jet mixing. This work started before the HOST Project, but after the initiation of the HOST Project it was funded by HOST. While the dilution jet mixing work had an independent existence, it became an integral part of the HOST research environment. This work was less ambitious in scope than the three-phase aerothermal modeling task, but it contributed significantly to the aerothermal phase 1 modeling assessment.

Assess Combustor Aerothermal Modeling - Phase 1

Gas turbine combustor models include submodels of turbulence, chemical kinetics, turbulence/chemistry interaction, spray dynamics, evaporation/combustion radiation, and soot formation/oxidation. During phase 1 model assessment work, three HOST contractors made extensive assessments of numerics, physical submodels, and the suitability of available data. They tested several models:

K-E turbulence, algebraic stress and its modifications, scalar transport, and turbulence/chemistry interaction. Their major conclusion was that available computational fluid dynamics codes provided a useful combustor design tool, but the codes were only qualitatively accurate. Further study was needed to improve the numerical scheme and specified experimental data before various emerging physical submodels could be properly assessed.

The assessment identified a serious deficiency in numerical accuracy for data on flows, particularly where the false diffusion is of the same order of magnitude as the turbulent diffusion. This masked differences between turbulence models such that very different models gave essentially the same result and sometimes caused undeservedly good agreement between data and predictions.

Improved Spatial Property Variations and Quantitative Accuracy - Phase 2

During the second phase of the aerothermal modeling work, HOST researchers undertook three tasks: Improved numerical methods, a flow interaction experiment, and fuel injector/air swirl characterization. We improved the resolution of spatial property variations and quantitative accuracy of aerothermal codes through three-dimensional numerical schemes, improved turbulence and chemistry models, and relevant benchmark quality data. We concentrated on nonreacting single- and two-phase swirling and nonswirling flows.

Improved numerical methods. - Here we found CONDIF and fluxspline useful; for improved computational efficiency, modifications such as SIMPLER and PISO have proven beneficial.

Flow interaction experiments. - Here researchers (1) studied the interactions between the combustor and diffuser systems and (2) obtained comprehensive mean and turbulence measurements for velocity and species concentration in a three-dimensional flow model of the primary zone of combustion chambers. These experiments were conducted with both air and water multiple-swirler rigs, as well as single swirler and swirling jet rigs. A key feature of this program provided a comparison of model calculations against data obtained, to ensure that data are complete and consistent and that they satisfy the boundary condition input requirements of current three-dimensional codes.

Fuel injector/air swirl characterization. - Here we sought to obtain fully specified mean and turbulence measurements of both gas and droplet phases downstream from a fuel injector and air swirler typical of those used in gas turbine combustion chambers. The flowfield of interest is an axisymmetric particle-laden jet flow with and without confinement and coannular swirling air flow. The comprehensive experimental data generated in these programs will be used to validate advanced models for turbulence, flow, stress, and spray.

Interacting-Reacting Flows - Phase 3

Just as important as phase 2 Aerothermal Modeling programs that have led to significant improvements in our technical ability to predict nonreacting gas turbine combustor flow fields is work planned for phase 3 but not performed during the HOST Project. This phase 3 work would have collected fully specified reacting flow data, similar to that being gathered for nonreacting flows.

Work should continue on the models for reacting sprays and multidimensional heat transfer.

Dilution Jet Mixing

This recently completed NASA work involves our ability to predict combustor exit temperature profiles (limited previously to jet trajectory analyses). The program provided a broad database and developed an empirical model for mixing diluting air jets with combustion gases. It also let us predict combustor exit temperatures accurately within the database's range.

The dilution jet mixing effort identified key flow parameters, collected data on the effect of varying these characteristics, and developed an empirical flow field model.

Conducted jointly by NASA Lewis and Garrett, this work concentrated on mixing of single-sided and opposed rows of jets in a confined duct flow to include effects of noncircular orifices and double rows of jets. The database was extended to include realistic effects of combustion chamber flow area convergence, nonisothermal mainstream flow, opposed (two-sided) in-line and staggered injection, and orifice geometry. Analysis of the mean temperature data obtained in this investigation showed that the effects of orifice shape and double rows are most significant in the region close to the injection plane.

This dilution jet mixing database is also being used to guide development of three-dimensional numerical codes so they provide broader and more accurate predictive capability. The dilution jet mixing work folded in with aerothermal modeling programs because (1) data was used in aerothermal modeling assessment and (2) the empirical model provides an alternative to numerical modeling for flows within the range of the dilution jet mixing experiments.

TURBINE HEAT TRANSFER

The major goal for the heat transfer program was to improve our basic understanding of the physics of aerothermodynamic phenomena in turbine components. Toward this end researchers gathered data for broad databases and, thus, prepared for future research. The development work was of two types: Experimental databases and analytical tools. The experimental databases covered both stationary and rotational work. The experimental work is discussed first.

Local Gas-to-Airfoil Heat Transfer Rates

HOST researchers obtained broad databases and modified the STAN5 code to accurately predict heat transfer coefficients, especially at the transition point, for film- and non-film-cooled airfoils.

Allison researchers did initial work on the stator airfoil heat transfer. They checked the effects of several factors such as Reynolds number, turbulence level, and Mach number on heat transfer coefficients for various airfoil geometries at simulated engine conditions. This research was conducted for non-film-cooled airfoils, showerhead film-cooled designs, and showerhead/

gill-region film cooling concepts. They obtained an extensive dataset that systematically shows the important effects of film cooling schemes on modern airfoils. The dataset went beyond the traditional effectiveness correlations to provide actual heat transfer data. It should provide a valuable baseline for emerging analysis codes.

Stanford University conducted a systematic study of the physical phenomena affecting heat transfer in turbine airfoil passages. Experimental research dealt with high free-stream turbulence intensity and large turbulence scale that might be representative of combustor exit phenomena. Their results show that heat transfer augmentation can be as high as 5X at a high value of free-stream turbulence intensity, but only 3X if the length scale is changed. These results suggest that the designer must know a great deal more about the aerodynamic behavior of the flow field in order to predict successfully the thermal performance of the turbine components.

The rotation work divided into concentrations on the gas-side airfoil and the coolant effect within passages.

Airfoil Rotation Effects on Heat Transfer

Scientists at United Technologies Research Center worked on determining the effects of airfoil rotation on heat transfer for the blade. This effort produced single-stage turbine data for both high- and low-inlet turbulence, one and one-half stage turbine data (focusing on the second vane row), and aerodynamic quantities such as interrow time averaged and rms value of velocity, flow angle, inlet turbulence, and surface pressure distributions. The results varied depending on location and surface. Work in this area indicates that pressure surface heat transfer still requires more study to explain high heat transfer.

Work in the blade's tip region was done at Arizona State University. The group at ASU experimentally modeled a blade tip cavity region and determined heat transfer rates by a mass transfer analogy with naphthalene. The dataset produced an important new addition to a traditionally neglected area and shows that with carefully designed datasets and analyses researchers can obtain an optimal design for tip cavities.

Coolant Rotation in Smooth-Wall Passages

Pratt & Whitney performed heat transfer experiments in a square passage with two 180° flow turns, with and without turbulators, and with and without rotation. Results for the smooth surface configuration show a strong rotational effect. Pratt also modified the three-dimensional Navier-Stokes TEACH code to predict flow and heat transfer in internal passages and rotation. It is adequate for simple geometric cases; however, it requires revision before application to more complex cases. Results for the turbulated passages also show strong rotational effects and significant differences in augmentation between leading and trailing surfaces.

The other half of the heat transfer subproject concentrated on developing analytical tools for boundary layer analysis and viscous flow analysis.

Three-Dimensional Boundary Layer

In this area HOST work concentrated on improving prediction accuracy for three-dimensional effects on heat transfer. This involved assessing three-dimensional boundary layer codes that were not designed for heat transfer work to determine what revisions were needed to make the code useful in heat transfer efforts.

Contracts were let for two efforts. United Technologies Research Center assessed the applicability of its three-dimensional boundary layer code to calculate heat transfer, total pressure loss, and streamline flow patterns in turbine passages. The results indicate a strong three-dimensional effect on a turbine blade, and they agree qualitatively with experimental data. The same code was modified for use as a two-dimensional unsteady code to analyze the rotor-stator interaction phenomena.

The other boundary layer study at the University of Minnesota addressed numerical turbulence modeling, particularly for turbine airfoils. This work extended modeling to apply to transitional flows for both free-stream turbulence and pressure gradients. There was a reasonable improvement in predictive ability. This effort is a good start in establishing a methodology for moving away from heavy dependence on empirical constants.

Analytic Flow and Heat Transfer Modeling

Scientific Research Associates (SRA) worked on a fully elliptic, three-dimensional Navier-Stokes code. This group modified the code to handle turbine applications. Comparisons of predictions with analytical experimental data are good when researchers can specify location for the boundary layer transition. Ideally, the code would allow researchers to handle various locations. In this respect, work still remains on improving turbulence and transition modeling.

STRUCTURAL ANALYSIS

Under this heading, there are six major thrusts, involving an interface code between heat transfer and structural analysis, three-dimensional inelastic codes, constitutive models, component-specific modeling, liner cyclic life testing, and substantiated design analysis methods and codes.

Heat Transfer/Structural Analysis Interface Code

With HOST support, General Electric researchers developed an interface code, called TRANSITS, that transfers up to three-dimensional thermal information automatically from heat transfer codes (that generally use coarse finite element grids) to structural analysis codes (that use finer grids). Key features include independent heat transfer and stress model meshes, accurate transfer of thermal data, computationally efficient transfer, steady-state and

transient data, user friendly program, flexible system, internal coordinate transformations, automated exterior surfacing techniques, and geometrical and temporal windowing.

Three-Dimensional Inelastic Codes

HOST provided development of three-dimensional inelastic structural analysis codes, involving two contractors, for nonlinear behavior at high thermo-mechanical loads. At Pratt & Whitney, three developed codes covered different approaches and degrees of complexity: MOMM, MHOST, and BEST3D. These codes provide a tenfold increase in computational efficiency - with improved accuracy. They embody a progression of mathematical models for increasingly comprehensive representation of the geometrical features, loading conditions, and forms of nonlinear material response. MOMM, a mechanics of materials model, is a stiffness method finite element code that uses one-, two-, and three-dimensional arrays of beam elements to simulate hot section component behavior. MHOST employs both shell and solid (brick) elements in a mixed method framework to provide comprehensive capabilities for investigating local (stress/strain) and global (vibration, buckling) behavior of hot section components. BEST3D is a general purpose, three-dimensional, structural analysis program using the boundary element method.

General Electric, the second contractor on the inelastic work, also developed a code that performs three-dimensional, inelastic structural analysis. The objective of this program was to develop analytical methods for evaluating the cyclic time-dependent inelasticity that arises in hot section engine components. Because of the large excursions in temperature associated with hot section engine components, the techniques developed must be able to accommodate large variations in material behavior including plasticity and creep. To meet this objective, General Electric developed a matrix consisting of three constitutive models and three element formulations. A separate program for each combination of constitutive model/element model was written, making a total of nine programs. Each program can stand alone in performing cyclic nonlinear analysis.

The three constitutive models assume distinct forms: A simplified theory (simple model), a classical theory, and a unified theory. The three element formulations used an 8-node isoparametric shell element, a 9-node shell element, and a 20-node isoparametric solid element.

For linear structural analysis, the nine codes use a blocked-column skyline, out-of-core equation solver. To analyze structures with nonlinear material behavior, the codes use an initial stress interactive scheme. This code contains a major advance in our ability to handle a dynamic time incrementing strategy.

Constitutive Models

Before HOST, there was no capability to perform combined elastic-plastic creep structural analyses. There were limited high-temperature databases for constitutive model formulations and verifications. Through the HOST Project, researchers developed viscoplastic constitutive models for both isotropic and

anisotropic materials, broadened the database capability, and verified models for a range of test conditions. These efforts led to a 30-percent improvement in high-temperature stress-strain prediction. These factors combined to make Lewis an internationally recognized leader in constitutive model development.

Isotropic material modeling. - In efforts aimed at isotropic material modeling, theorists from three organizations provided new models. The first organization, Southwest Research Institute, developed two existing models (Walker and Bodner-Partom) of the unified type for application to isotropic, cast, nickel-base alloys used for air-cooled turbine blades and vanes. Both models demonstrated good correlation with experimental results for two PWA alloys, B1900+Hf and MAR-M247. The program also demonstrated rather conclusively that the unified constitutive model concept is a powerful tool for predicting material response in hot section components under complex, time-varying thermomechanical loadings. At General Electric, researchers evaluated several viscoplastic constitutive theories against a large uniaxial and multi-axial database on René 80 material, which is a cast nickel-base alloy used in turbine blade and vane applications. No available approach for modeling the high-temperature, time-dependent behavior of René 80 was satisfactory, so GE developed a new theory that predicts with good accuracy the 90° out-of-phase tension-torsion experimental results at elevated temperatures. Finally, at a third organization, the University of Akron, researchers developed a time-dependent description potential function based on constitutive theory with stress dependence on J2 and J3 integrals that reduces to a J2 theory as a special case.

Anisotropic material modeling. - Modeling of anisotropic material also had three groups involved, all universities. Turbine manufacturers have been developing nickel-base monocrystal superalloys for years. University of Connecticut theorists successfully modeled the deformation behavior of these materials using both a macroscopic constitutive model and a micromechanical formulation based on crystallographic slip theory. The University of Cincinnati developed a model for nickel-base single-crystal alloy René N4 using a crystallographic approach. The current equations modified a previous model proposed by Dame and Stouffer, where a Bodner-Partom equation with only the drag stress was used to account for the local inelastic response in each slip system. The University of Akron developed a continuum theory for representing the high-temperature, time-dependent, hereditary deformation behavior of metal composites that can be idealized as pseudohomogeneous continua with locally definable directional characterizations.

Component-Specific Modeling

HOST allowed us to develop a modular code for nonlinear structural analyses that predicts temperatures, deformation, and stress and strain histories. It also gave us an automatic solution strategy for liners, with similar strategies underway for blades and vanes. The package contains five modular elements that are linked by an executive module. The Thermodynamic Engine Model (TDEM) translates a list of mission flight points and time differences into time profiles of major engine performance parameters. The Thermodynamic Loads Model (TDLM) works with the output of the TDEM to produce the mission cycle loading on the individual hot section components. The Component Specific

Structural Modeling Module provides a generic geometry pattern for each component. General Electric also created a software recipe that contains default values for point coordinates, lengths, thicknesses, angles, and radii. Users may modify specific values, but the software has saved them the effort of identifying basic geometry and parameters. Once a researcher defines specific values, the software develops a finite-element model of this geometry consisting of 20-noded isoparametric elements. The fourth subsystem performs incremental nonlinear finite element analysis on complex three-dimensional structures under cyclic thermomechanical loading with temperature-dependent material properties and material response behavior. A major advance in the ability to perform time-dependent analyses is a dynamic time incrementing strategy incorporated in this software. The fifth element, COSMO, is an executive module that controls the whole system.

Liner Cyclic Life Testing

Through a cooperative effort, Pratt & Whitney and NASA Lewis Research Center developed a unique vehicle to obtain cyclic thermal and mechanical test data under realistic but controlled test conditions using annular combustor hardware. Pratt & Whitney provided the test rig, while Lewis supplied the test facility, integrated the rig into the facility, conducted tests, and analyzed the data. The program initially tested a conventional liner of sheet metal, seam-welded louver construction from Hastelloy-X material; later, the program tested an advanced segmented liner made from materials developed by Pratt & Whitney. The tests radiantly heated segments (cylindrical sections) of turbine engine combustor liners. Quartz lamps provided cyclical heating of the test liners. This caused axial and circumferential temperature variations as well as through-the-wall temperature gradients in the test liner. The thermally induced stresses and strains were similar to those of in-service liners. A typical engine mission cycle (i.e., take-off, cruise, landing, and taxi) of 3 to 4 hr was simulated in 2 to 3 min. Based on nonlinear structural analyses of the two liners, researchers determined that the critical stress-strain location in the conventional liner was at the seam weld. For the advanced liner, it was at the retention loop. For the same heat flux, the advanced liner will have a much longer life than the conventional liner, because it has a lower operational temperature (440 °F) and has no structural or hoop constraint in the circumferential direction. The predicted life is greater than one million cycles. There is good agreement between predicted life and measured life.

Substantiated Design Analysis Methods and Codes

An important goal in the structural analysis discipline was concerned with developing user confidence in the models and codes discussed above. Confidence comes with experimental validation. HOST allowed scientists to validate many technologies: Time-varying thermomechanical load models, component-specific automated geometric modeling and solution strategy capabilities, advanced inelastic analysis methods, inelastic constitutive models, high-temperature experimental techniques and experiments, and nonlinear structural analysis codes. Under HOST, test facilities were upgraded, and codes in two major areas were developed. We also conducted experiments to calibrate and validate the codes. Unique high-temperature cyclic thermomechanical tests on tubular and solid bar specimens were conducted in upgraded structures test laboratories at

the Lewis Research Center. Categories for validation activities included: (1) New types of multiaxial viscoplastic constitutive models for high-temperature isotropic and anisotropic superalloys and metal matrix composites; (2) nonlinear structural analysis methods and codes; and (3) uniaxial and multiaxial thermomechanical databases for René N4, René 80, Hastelloy-X, MAR-M247, B1900+Hf, PWA 1480, and Haynes 188.

FATIGUE AND FRACTURE

Prior to HOST work in fatigue and fracture, we had no confidence in life predictions involving complex loading conditions, multiaxial stress states, or thermomechanical loading conditions until components had service experience. Now we have far more confidence in constitutive equations and life models for advanced configurations and materials under complex, multiaxial, and thermomechanical loading circumstances. Five major accomplishments are summarized below.

Crack Initiation Life-Prediction Methods

This is the first major fatigue-fracture work element. Two new crack-initiation, life-prediction methods have been developed for application to complex creep-fatigue loading of nominally isotropic superalloys at high temperatures (at Pratt & Whitney and at Lewis). The Pratt work led to a new method, called Cyclic Damage Accumulation (CDA), for predicting high-temperature fatigue life. Under the Lewis program, the Strainrange Partitioning (SRP) method was advanced to allow researchers to express the approach in terms of total strain range versus cyclic life.

Cyclic Constitutive Models - Protective Coatings and Single-Crystal Alloys

HOST efforts in this second fatigue-fracture concern developed and verified cyclic constitutive models for oxidation protective coatings and for highly anisotropic single-crystal turbine blade alloys. Pratt & Whitney formulated a viscoplastic constitutive model for two fundamentally different coating types: A plasma-sprayed NiCoCrAlY overlay coating and a pack-cementation-applied NiAl diffusion coating. Pratt & Whitney also developed a unified constitutive model for PWA 1480 single-crystal material; it is in the final development stages.

Pratt & Whitney is also the contractor proposing a model for a preliminary cyclic crack initiation life-prediction model. It is being evaluated. The model utilizes tensile hysteretic energy and frequency as primary variables.

Two High-Temperature, Cyclic Crack-Growth Life-Prediction Models

Two models have been proposed for the fourth fatigue and fracture work element. Micromechanistic and phenomenological engineering approaches have been taken. The micromechanistic approach, being developed by University of Syracuse scientists, is based on oxidation interactions with mechanical deformation at the crack tip. The engineering approach, at General Electric, has its origins

in the Path-Independent Integrals approach, which describes the necessary fracture mechanics parameters.

High-Temperature Fatigue and Structures Laboratory

Lewis Research Center created an advanced high-temperature fatigue and structures research laboratory. Test facilities have been significantly upgraded to allow uniaxial, high cycle/low cycle, and axial torsional fatigue research. Additionally, the laboratory contains a powerful computer facility that is among the best in the world for this kind of effort.

The uniaxial test facility now includes twelve load frame systems. The original eight frames are rated for $\pm 20\,000$ lb. Lewis added two more frames rated at $\pm 20\,000$ lb and two at $\pm 50\,000$ lb. Commercially available servocontrollers control each test system. The test facility provides both diametral and axial extensometers. Computer enhancements have had a major impact on the lab's uniaxial capabilities because each uniaxial system has its own minicomputer for experimental control and data acquisition. To further aid in simulating operating conditions, two machines allow tests to be conducted under two closely controlled environmental conditions, high temperature and vacuum.

To improve our understanding of cumulative cyclic loadings, Lewis bolstered its facility in this area as well. A new system produces arbitrary load or deformation histories corresponding to fatigue lives up to 10 million in less than 10 hr, using state-of-the-art servohydraulic materials test systems.

The third type of test enhancement relates to multiaxial stress. The load frames for each test system are rated for loads of $\pm 50\,000$ lb axial and $\pm 25\,000$ in.-lb torsional. These systems allow tests involving rapid thermal transients. A number of experimental projects are currently underway. Thus far the testing has been biaxial; eventually it will be triaxial.

The high-temperature fatigue and structures lab computer offers a versatile system, with a Data General Eclipse MV/4000 connected with 14 satellite computers in a multiprocessor class of computing configuration. This configuration also introduced the first validated ADA-language compiler within NASA.

SURFACE PROTECTION

The surface protection subproject hosted two programs: Thermal barrier coating life prediction and an airfoil deposition process/deposition model. These programs are discussed below.

TBC Life Prediction

HOST provided pioneering research on thermal barrier coatings (TBC) involving three approaches to TBC life-prediction modeling. Lewis Research Center, Pratt & Whitney, Garrett, and General Electric worked on this modeling effort. The state-of-the-art coating system consists of about 0.25 mm of zirconia-yttria ceramic over 0.13 mm of an MCrAlY alloy bond coat. Both layers are

applied by plasma spraying onto a structural base material. Benefits arise from thermal insulation of the structure that is provided by the ceramic layer.

Following an in-house model development program, Lewis awarded contracts (1) to determine thermomechanical properties, (2) to analyze coating stresses and strains, and (3) to develop life models for thermal barrier coatings.

Thermomechanical properties. - The effort to determine thermomechanical properties achieved general agreement that (1) these coatings fail primarily because of stresses induced by the thermal expansion mismatch between ceramic and metallic base layers and (2) that these stresses are greatly influenced by time-at-temperature processes - oxidation and possibly sintering.

Analyze coating stresses and strains. - Next researchers developed a laboratory model. This model represented a first step, but it was not in a form useful to engine designers.

Develop life models. - The model developed by Pratt & Whitney and its subcontractor, Southwest Research, is a fatigue-based coating life model. The model is accurate to plus or minus a factor of three, which is acceptable. The Garrett model considers bond coat oxidation, zirconia toughness reduction, and damage due to molten salt deposits. This model analyzes thermal data for specific elements in terms of mission. The General Electric model employs time-dependent, nonlinear, finite-element modeling of stresses and strains present in the thermal barrier coating system, followed by correlation of these stresses and strains with test lives. This model was the only one to check failure induced by edges and, hence, the only one to consider shear strain.

Airfoil Deposition Process/Model

This activity raised fundamental questions about hot corrosion of blades and about deposition of corrosive salts. Scientists needed to identify what corrosive species and deposits were accumulating, how deposits reached the blade, and then what effect they had on the surface protection. Through HOST, researchers identified the corrosive as sodium sulfate, but they also learned from process studies that prior to reaching the blade it was not yet sodium sulfate (it was sodium carriers, sulfate carriers, etc.). People had been performing static studies, but research results in this area indicated that dynamic studies were needed. The reason was that in real-life situations the sodium sulfate supply continually accumulates and then, because of heat, becomes molten, creating a film that flows on the blade surface. The result is that salt deposition and flow rates are variable, prompting the need for a deposition model.

The deposition model that Lewis researchers developed assumes that the sodium-sulfate dissolution rate correlates with corrosion rate. This was the first attempt to correlate the process - initial corrosive species diffusing, moving, depositing, forming, filming, dissolving metal, and starting the corrosive effect. Researchers completed the model; however, funding limitations prevented validation experiments. This model is a significant step toward reality - modeling a real-life, dynamic environment.

BROAD IMPACT OF HOST PROJECT

The HOST Project met all the objectives in the NASA long-range aeronautics plan, including

(1) Recognition of the importance of NASA Aeronautics to both civil and military aviation. Ivan Bush stated before his recent retirement from the AFAPL, "The Air Force looks to the HOST Project for the technology required in advanced fighters."

(2) Providing the U.S. with improved capability for research and technology. State-of-the-art test facilities have been built at Lewis and at certain universities. Lewis has established an international leadership in constitutive modeling of materials behavior under complex thermomechanical loading.

(3) Restoring a balanced aeropropulsion program between performance improvement and durability (e.g., EEE, ATP, QCSEE Programs versus HOST).

(4) Strengthening the NASA-university partnership in aeronautics research and technology. The HOST Project initiated 13 direct grants and approximately 26 indirect grants through industry. Also, Robert Henderson from the AFAPL stated "HOST improved the relationship between the government (NASA and the Air Force) and universities."

(5) Strengthening user interfaces to promote technology transfer. The HOST Project was responsible for 250 technical publications including six NASA Conference Publications, six major workshops and numerous miniworkshops, and dedicated HOST sessions at AIAA and ASME society meetings.

The HOST Project spearheaded a change from the traditional "build 'em and bust 'em" approach to turbine engine development to analytical predictions made before building hardware. These predictions were based on improved and more accurate mathematical models, computer codes, and broad experimental databases. Some results from this change in approach include

- (1) Improved durability in advanced hot sections
- (2) Reduced development time and costs
- (3) More accurate trade-off between performance and durability

Research supported and focused by HOST improved quantitative accuracy to predict physical behavior of hot section parts under complex cyclic loading. The project efforts

- (1) Developed better understanding and modeled more accurately basic physics of durability phenomena
- (2) Emphasized local as well as global conditions and responses
- (3) Accommodated nonlinear and inelastic behavior
- (4) Expanded some models from two to three dimensions

REFERENCES

- Dennis, A.J., Cruse, T.A., 1979, "Cost Benefits from Improved Hot Section Life Prediction Technology," AIAA Paper 79-1154.
- Sokolowski, D.E., 1988a, "Comprehensive Bibliography of the Turbine Engine Hot Section Technology (HOST) Project," NASA TM-100275 (to be published).
- Sokolowski, D.E., 1988b, "Toward Improved Durability in Advanced Aircraft Engine Hot Sections," NASA TM-100817 (to be published).
- Stephans, J.R., 1982, "COSAM Program Overview," COSAM (Conservation of Strategic Aerospace Materials), Program Overview, NASA TM-83006, pp. 1-11.
- Tanrikut, S., Marshall, R.L., and Sokolowski, D.E., 1981, "Improved Combustor Durability - Segmented Approach With Advanced Cooling Techniques," AIAA Paper 81-1354.
- Turbine Engine Hot Section Technology - 1982, NASA TM-83022.
- Turbine Engine Hot Section Technology - 1983, NASA CP-2289.
- Turbine Engine Hot Section Technology - 1984, NASA CP-2339.
- Turbine Engine Hot Section Technology - 1985, NASA CP-2405.
- Turbine Engine Hot Section Technology - 1986, NASA CP-2444.
- Turbine Engine Hot Section Technology - 1987, NASA CP-2493.

RESEARCH SENSORS

David R. Englund
Instrumentation and Control Technology Office
NASA Lewis Research Center

ABSTRACT

The work described here is part of a program (Englund and Seasholtz, 1988) to develop sensors and sensing techniques for research applications on aircraft turbine engines. In general, the sensors are used to measure the environment at a given location within a turbine engine or to measure the response of an engine component to the imposed environment. Locations of concern are generally in the gas path and, for the most part, are within the hot section. Specific parameters of concern are dynamic gas temperature, heat flux, airfoil surface temperature, and strain on airfoils and combustor liners. To minimize the intrusiveness of surface-mounted sensors, a considerable effort has been expended to develop thin-film sensors for surface temperature, strain, and heat flux measurements. In addition, an optical system for viewing the interior of an operating combustor has been developed. Most of the work described is sufficiently advanced that sensors have been used and useful data have been obtained. The notable exception is the work to develop a high-temperature static strain measuring capability; this work is still in progress. The work described here has been done at NASA Lewis Research Center and at other institutions, under various contracts and grants.

HIGH-TEMPERATURE INSTRUMENTATION FOR HOT SECTION APPLICATIONS

The work described here is part of a program to develop instrumentation for research applications on aircraft turbine engines. In general, the instrumentation is used to either measure the environment at a given location within a turbine engine or to measure the response of an engine component to the imposed environment. Locations of concern are generally within the gas path and, for the most part, are within the hot section of the engine. Since this instrumentation is used for research testing as opposed to operational use, a sensor lifetime of the order of 50 hr is considered sufficient. The work described here was done at NASA Research Center and at various other institutions, under various contracts and grants.

INSTRUMENTATION FOR RESEARCH MEASUREMENTS ON AEROPROPULSION SYSTEMS:

- **DYNAMIC GAS TEMPERATURE MEASURING SYSTEMS**
- **COMBUSTOR VIEWING SYSTEM**
- **HEAT FLUX SENSORS**
- **THIN-FILM SENSORS**
- **HIGH-TEMPERATURE STRAIN MEASURING SYSTEMS**

DYNAMIC GAS TEMPERATURE MEASURING SYSTEM

One of the most important environmental parameters in a turbine engine hot section is gas temperature. Normally only time-average temperature is measured. Fluctuations in gas temperature are, however, of great concern for hot section durability and combustor modeling activities. In this measuring system (Elmore et al., 1983, 1984, 1986a, and 1986b; and Stocks and Elmore, 1986), a probe with two wire thermocouples of different diameters provides dynamic signals with limited frequency response. Comparing these signals over a range of frequencies makes it possible to generate a compensation spectrum sufficient to provide compensated temperature data at frequencies up to 1000 Hz.

- MEASURES GAS TEMPERATURE FLUCTUATIONS AT THE EXIT OF A TURBINE ENGINE COMBUSTOR
- A TWO-ELEMENT PROBE PROVIDES DATA TO PERMIT ACCURATE FREQUENCY COMPENSATION



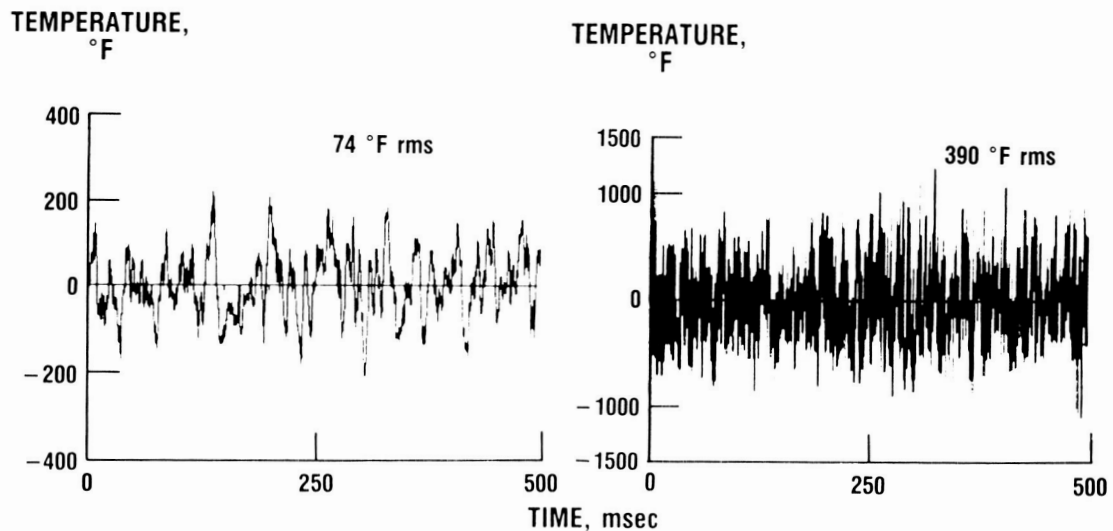
ORIGINAL PAGE IS
OF POOR QUALITY

CD-87-29397

DYNAMIC GAS TEMPERATURE MEASUREMENT

This figure shows dynamic gas temperature data obtained from a probe at the turbine inlet of a PWA F-100 engine operating at an intermediate power setting with an average turbine inlet gas temperature of 1700 °F. The plot on the left is the dynamic signal from a 0.003-in.-diameter wire thermocouple with no frequency compensation. The rms value of the temperature fluctuation is 74 °F. The plot on the right is the compensated signal from the same thermocouple. The rms value of the temperature fluctuation is 390 °F and the peak-to-peak fluctuation is ± 900 °F. Such a large temperature fluctuation implies that there are filaments of primary combustion gas and dilution gas within the combustor exhaust stream.

TEMPERATURE AT TURBINE INLET

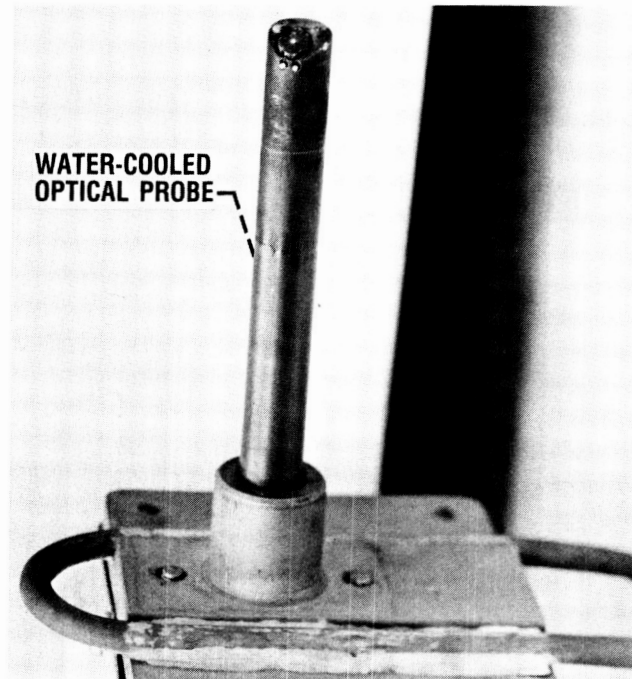


CD-88-32747

COMBUSTOR VIEWING SYSTEM

ORIGINAL PAGE IS
OF POOR QUALITY

The Combustor Viewing System (Morey, 1984 and 1985) was designed to provide recorded images of the interior of a combustor during operation; the objective was to produce a visual record of some of the causes of premature hot section failure. The system consists of a water-cooled optical probe (shown below), a probe actuator, an optical interface unit that couples the probe to cameras and to an illumination source, and system controls. The probe is 0.5 in. in diameter, small enough to fit into an igniter port. The actuator provides $\pm 180^\circ$ of rotation and radial insertion of up to 3 in. Both wide and narrow fields of view and different viewing axes are provided from two different probes. The probes are water cooled and gas purged and can operate within the primary combustion zone of a combustor.

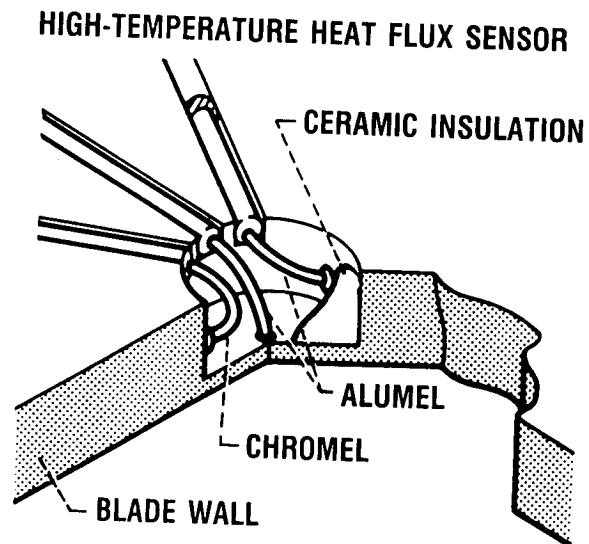


CD-88-32748

HEAT FLUX SENSORS

An environmental parameter of interest for hot section durability is heat flux. We have developed miniature heat flux sensors which can be welded into combustor liners (Atkinson and Strange, 1982; and Atkinson et al., 1983) and built into cooled turbine airfoils (Atkinson et al., 1984). This figure shows one sensor configuration based on the Gardon gage design. An innovation in these sensors is the use of the burner liner or airfoil material as part of a differential thermocouple circuit. Calibration tests (Atkinson and Strange, 1982; and Holanda, 1984) on these materials showed that this technique could provide acceptable signals. The differential thermocouple simplifies construction and permits a direct measurement of the differential temperature proportional to heat flux. These miniature heat flux sensors must be calibrated over the temperature range in which they will be used.

- MEASURE HEAT FLUX ON BURNER LINERS AND TURBINE AIRFOILS
- MINIATURE WIRE THERMOCOUPLE SENSOR:
 - WELD INTO BURNER LINERS
 - BUILD INTO AIRFOILS
- SENSOR BODY PART OF THERMOCOUPLE CIRCUIT
- CALIBRATION SYSTEM REQUIRED

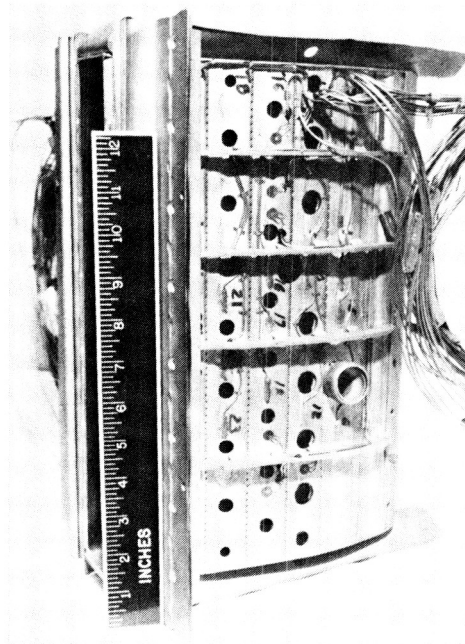


CD-88-32749

COMBUSTOR SEGMENT INSTRUMENTED WITH HEAT FLUX SENSORS

This photograph shows a segment of a combustor liner which has been instrumented with six heat flux sensors. The sensors are 0.3-in.-diameter disks with thermocouple leads radiating from the edge of the disk. The actual sensor part of the unit is at the center of the disk and is only 0.06 in. in diameter. The sensors are individually calibrated and then welded into holes cut in the liner. Tests on combustors such as this one have produced useful heat flux data over a range of combustor operating conditions (Atkinson et al., 1985a). Similar sensors built into turbine airfoils have been less successful because of the sensitivity of these sensors to temperature or heat flux gradients, which are more prevalent in turbine airfoils (Atkinson et al., 1985b). Sensor designs that are less sensitive to gradients have been examined but have not yet been put into use.

ORIGINAL PAGE IS
OF POOR QUALITY.

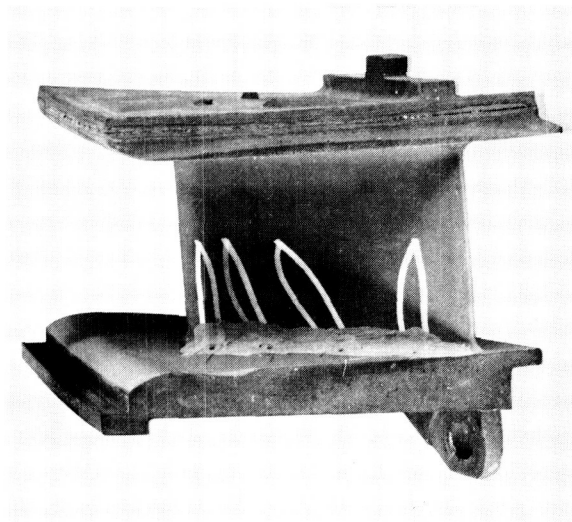


CD-88-32750

THIN-FILM THERMOCOUPLES

Lewis has been the major advocate and sponsor for development of thin-film sensors for turbine engine applications. Sensors applicable to turbine engines include temperature sensors, strain gages, and heat flux sensors. Thin-film thermocouples for measuring the surface temperature of a cooled turbine airfoil are shown here. The surface of the vane is covered with Al_2O_3 thermally grown from an anticorrosion coating and augmented with sputtered Al_2O_3 . Platinum and Pt-Rh films are sputter deposited with thermocouple junctions formed by overlapping the two films at the desired spot. The films extend to the base of the vane where leadwires are connected. The sensor is less than 0.001 in. thick. The advantage of this technique over the previous technology, which required swaged thermocouple wires to be buried into grooves cut into the surface, should be obvious. This technology has been developed (Grant and Przybyszewski, 1980, and Grant et al., 1981 and 1982) for turbine airfoil temperature measurement. Further work has been directed at other sensor types, other sensor and substrate materials, and maturing the technology (Grant et al., 1983; Kreider et al., 1984; Kreider and Semancik, 1985; Prakash et al., 1985; and Budhani et al., 1986a and 1986b).

- MEASURE SURFACE TEMPERATURE OF COOLED TURBINE AIRFOILS
- FABRICATION: SPUTTER ALLOY FILM LEADS OVER INSULATING COATING ON AIRFOIL SURFACE
- SENSOR THICKNESS, < 0.001 in.



CD-88-32751

ORIGINAL PAGE IS
OF POOR QUALITY

HIGH-TEMPERATURE STRAIN MEASURING SYSTEMS

The most ambitious goal of the research sensor program is development of high-temperature (1800 °F) strain measuring systems. Approaches being followed in this work include both wire and thin-film resistance strain gages and remote measuring systems. Our resistance strain gage work has included work on new strain gage materials (Hulse et al., 1985 and 1987a; and Lei, 1987) and testing of available strain gages, including the Chinese 700 °C gages (Hobart, 1985; Stetson, 1984; and Hulse et al., 1987b). Work on remote strain measuring systems has involved three different system concepts based on laser speckle patterns (Stetson, 1983; and Lant and Qaqish, 1987a and 1987b).

- **GOAL:**

MEASURE STATIC STRAIN ON TEST SAMPLES AND TURBINE ENGINE COMPONENTS AT TEMPERATURES UP TO 1800 °F

- **APPROACHES:**

RESISTANCE STRAIN GAGES—

WIRE GAGES

THIN-FILM GAGES

REMOTE STRAIN MEASURING SYSTEM—

LASER SPECKLE BASED SYSTEM

FUTURE THRUSTS IN RESEARCH SENSORS

Future work in research sensors will be strongly influenced by new materials being developed for turbine engine components. These materials are expected to be in the forms of metal and ceramic matrix composites. Both the nature of the materials and the significantly higher hot section temperatures that these materials are expected to make possible will influence our sensor work. If thin-film sensors are to be applied to these materials, methods for producing suitable insulating films must be developed. As surface temperatures rise, the temperature limits of available sensor materials will force more emphasis on remote, noncontact sensing techniques. In addition, we will continue to search for new sensor materials with higher temperature capabilities. Work has already started in these directions relative to surface temperature, strain, and heat flux measurements on ceramic and ceramic matrix composite materials.

MAJOR DRIVER:

- **PROGRAM TO DEVELOP MATERIALS TO OPERATE AT SIGNIFICANTLY HIGHER HOT SECTION TEMPERATURES—METAL- AND CERAMIC-MATRIX COMPOSITES**

EFFECT ON SENSOR PROGRAMS:

- **DEVELOP TECHNOLOGY FOR THIN-FILM SENSORS ON NEW SUBSTRATE MATERIALS**
- **DEVELOP SENSOR MATERIALS FOR HIGHER TEMPERATURE RANGES**
- **IMPROVE REMOTE SENSING TECHNIQUES**

REFERENCES

- Atkinson, W.H., and Strange, R.R., 1982, "Development of Advanced High-Temperature Heat Flux Sensors," NASA CR-165618.
- Atkinson, W.H., Hobart, H.F., and Strange, R.R., 1983, "Advanced High Temperature Heat Flux Sensors," Proceedings of the 38th Instrument Society of America Conference, Advances in Instrumentation, Vol. 38, Part 2, Instrument Society of America, pp. 1457-1479.
- Atkinson, W.H., Cyr, M.A., and Strange, R.R., 1984, "Turbine Blade and Vane Heat Flux Sensor Development, Phase I - Final Report," NASA CR-168297.
- Atkinson, W.H., Cyr, M.A., and Strange, R.R., 1985a, "Development of High-Temperature Heat Flux Sensors, Phase II - Verification Testing," NASA CR-174973.
- Atkinson, W.H., Cyr, M.A., and Strange, R.R., 1985b, "Turbine Blade and Vane Heat Flux Sensor Development, Phase II - Final Report," NASA CR-174995.
- Budhani, R.C., Prakash, S., and Bunshah, R.F., 1986a, "Thin Film Temperature Sensors for Gas Turbine Engines: Problems and Prospects," J. Vacuum Sci. and Tech. A, Vol. 4, No. 6, pp. 2609-2617.
- Budhani, R.C., et al., 1986b, "Oxygen Enhanced Adhesion of Platinum Films Deposited on Thermally Grown Alumina Surfaces," J. Vacuum Sci. and Tech. A, Vol. 4, No. 6,, pp. 2023-3024.
- Elmore, D.L., Robinson, W.W., and Watkins, W.B., 1983, "Dynamic Gas Temperature Measurement System Final Report, Volume I - Technical Efforts," (NASA Contract NAS3-23154) NASA CR-168267.
- Elmore, D.L., Robinson, W.W., and Watkins, W.B., 1984, "Dynamic Gas Temperature Measurement System," Proceedings of the 30th International Instrumentation Symposium, Instrumentation in the Aerospace Industry - Volume 30, Advances in Test Measurements - Volume 21, (NASA Contract NAS3-23154) Instrument Society of America, pp. 289-302.
- Elmore, D.L., Robinson, W.W., and Watkins, W.B., 1986a, "Further Development of the Dynamic Gas Temperature Measurement System," Volume I - Technical Efforts." NASA CR-179513.
- Elmore, D.L., Robinson, W.W., and Watkins, W.B., 1986b, "Further Development of the Dynamic Gas Temperature Measurement System," AIAA Paper 86-1648.
- Englund, D.R., and Seasholtz, R.G., 1988, "Recent Advances in High Temperature Instrumentation for Hot Section Applications," NASA TM-100282.
- Grant, H.P., and Przybyszewski, J.S., 1980, "Thin Film Temperature Sensor," NASA CR-159782.
- Grant, H.P., Przybyszewski, J.S., and Claing, R.G., 1981, "Turbine Blade Temperature Measurements Using Thin Film Temperature Sensors," NASA CR-165201.

- Grant, H.P., et al., 1982, "Thin Film Temperature Sensors, Phase III," NASA CR-165476.
- Grant, H.P., et al., 1983, "Thin Film Strain Gage Development Program Final Report," NASA CR-174707.
- Hobart, H.F., 1985, "Evaluation Results of the 700 °C Chinese Strain Gages," NASA TM-86973.
- Holanda, R., 1984, "Analysis of Thermoelectric Properties of High Temperature Complex Alloys of Nickel-base, Iron-base, and Cobalt-base Groups," NASA TP-2278.
- Hulse, C.O., Bailey, R.S., and Lemkey, F.D., 1985, "High Temperature Static Strain Gage Alloy Development Program," NASA CR-174833.
- Hulse, C.O., et al., 1987a, "Advanced High Temperature Static Strain Sensor Development Program," NASA CR-179520.
- Hulse, C.O., et al., 1987b, "High Temperature Static Strain Gage Development Contract," NASA CR-180811.
- Kreider, K.G., Semancik, S., and Olson, C., 1984, "Advanced Thin Film Thermocouples," National Bureau of Standards NBSIR 84-2949.
- Kreider, K.G., and Semancik, S., 1985, "Thermal and Sputtered Aluminum Oxide Coatings for High Temperature Electrical Insulation," J. Vacuum Sci. and Tech. A, Vol. 3, No. 6, pp 2582-2556.
- Lant, C.T., and Qaqish, W., 1987a, "Optical Strain Measurement System Development - Phase I," NASA CR-179619.
- Lant, C.T., and Qaqish, W., 1987b, "Optical Strain Measurement System Development," NASA CR-179646.
- Lei, J.F., 1987, "Electrical Properties of Materials for Elevated Temperature Resistance Strain Gage Applications," Ph.D. Thesis, Northwestern University.
- Morey, W.W., 1984, "Hot Section Viewing System," NASA CR-174773.
- Morey, W.W., 1985, "Jet Engine Combustor Viewing System," Conference on Lasers and Electro-Optics, IEEE, NY, pp. 298.
- Prakash, S., et al., 1985, "Pretreatment Effects on the Morphology and Properties of Aluminum Oxide Thermally Grown on NiCoCrAlY," J. Vacuum Sci. and Tech. A, Vol. 3, No. 6, pp. 2551-2556.
- Stetson, K.A., 1983, "The Use of Heterodyne Speckle Photogrammetry to Measure High-Temperature Strain Distributions," Holographic Data Nondestructive Testing, Vukicevic, D., ed., Proc. SPIE-370, SPIE, pp. 46-55.

Stetson, K.A., 1984, "Demonstration Test of Burner Liner Strain Measuring System," NASA CR-174743.

Stocks, D.R., and Elmore, D.L., 1986, "Further Development of the Dynamic Gas Temperature Measurement System," Vol. II, Computer Program User's Manual, NASA CR-179513.

HOST COMBUSTION R&T OVERVIEW

Raymond E. Gaugler and James D. Holdeman
Internal Fluid Mechanics Division
NASA Lewis Research Center

ABSTRACT

The overall objective of the Turbine Engine Hot Section Technology Combustion Project was to develop and verify improved and more accurate numerical models of the internal combustor flow field and liner heat transfer as a means to shorten combustor development time and increase turbine engine hot section life.

The objective was approached from two directions: computational and experimental. On the computational side, a contracted effort was initiated during fiscal year 1982 to assess and evaluate existing combustor aerothermal analysis models. This effort has quantified the strengths and deficiencies of existing models. Next, phase II contracts were let in fiscal 1984 to develop new and improved numerical methods for analyzing turbulent viscous recirculating flows, with the prime objectives being improved accuracy and speed of convergence.

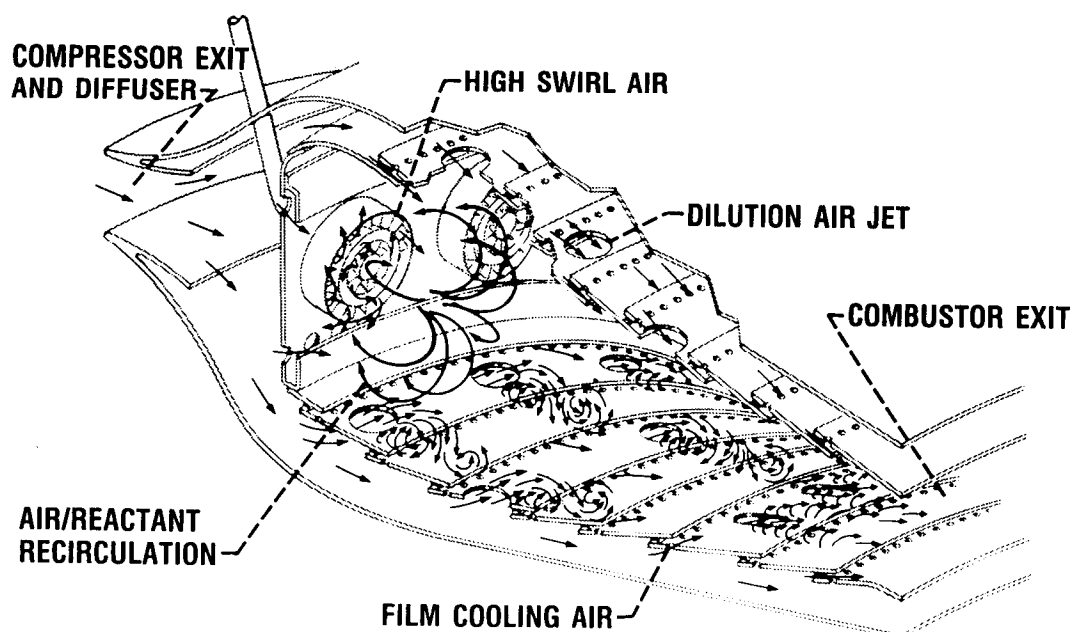
On the experimental side, three types of experiments can be identified: first, fundamental experiments directed toward an improved understanding of the flow physics and chemistry; second, experiments run to provide data for the empirical modeling of complex phenomena; and third, benchmark experiments for computer code validation.

Four experimental efforts have been completed and three are nearing completion. The completed experimental programs were aimed primarily at obtaining a basic understanding of the flows and improving the empirical models. Two programs that concentrated on the interaction of dilution jets and the main stream flow field have added substantially to the understanding of such flows. A third experimental program examined in detail the mass and momentum transport in swirling and nonswirling coaxial jets. The fourth effort was an investigation of the radiative heat loading in an advanced, high-pressure gas turbine combustor. The three experimental programs in progress concentrate on generating benchmark quality data for use in validating new computer codes and models.

PRECEDING PAGE BLANK NOT FILMED

COMBUSTOR FLOW PHENOMENA

The goal of gas turbine combustion system design and development was to obtain an acceptable solution to the conflicting design trade-offs between combustion efficiency, gaseous emissions, smoke, ignition, restart, lean blowout, burner exit temperature quality, structural durability, and life cycle cost. For many years, these combustor design trade-offs have been carried out with the help of fundamental reasoning and extensive component and bench testing, backed by empirical and experience correlations. The ultimate goal has been to develop a reliable combustor design system that can provide quantitatively accurate predictions of the complex combustion flow-field characteristics in order to achieve an optimum combustion system design within reasonable cost and schedule constraints.



- FULLY 3-DIMENSIONAL FLOW
- HIGH TURBULENCE LEVELS
- CHEMICAL REACTION/HEAT RELEASE
- 2 PHASE WITH VAPORIZATION

CD-88-32293

HOT SECTION TECHNOLOGY (HOST) COMBUSTION SUBPROJECT

The overall objective of the HOST Combustion Project was to develop and verify advanced analytical methods to improve the capability of designing combustion systems for advanced aircraft gas turbine engines. This objective was approached both computationally and experimentally.

Computationally, HOST first sponsored studies to assess and evaluate the capabilities of existing aerothermal models (circa 1982). Based on the results of these assessments and other studies in the literature, HOST supported several studies to develop new and improved numerical methods for the analysis of turbulent viscous recirculating flows, with emphasis on accuracy and speed of solution.

The objectives of HOST-sponsored experimental studies were to improve understanding of the flow physics and chemistry in constituent flows, and to obtain fully specified, benchmark-quality experimental data suitable for the assessment of the capabilities of advanced computational codes.

APPROACH

COMPUTATIONAL

- ASSESS EXISTING AEROTHERMAL CODES AND NUMERICAL METHODS
- DEVELOP NEW AND IMPROVED NUMERICAL METHODS
- INCORPORATE IMPROVED PHYSICAL MODELS INTO CODES

EXPERIMENTAL

- FUNDAMENTAL TESTS TO IMPROVE UNDERSTANDING OF FLOW PHYSICS
- EMPIRICAL MODELING OF COMPLEX PHENOMENA
- BENCHMARK TESTS FOR CODE VERIFICATION

AEROTHERMAL MODELING PHASE I

Gas turbine combustion models include submodels of turbulence, chemical kinetics, turbulence/chemistry interaction, spray dynamics, evaporation/combustion, radiation, and soot formation and oxidation. An extensive assessment of numerical, physical submodels, and the suitability of the available data was made by three contractors under Phase I of the HOST Aerothermal Modeling program (Kenworthy et al., 1983; Sturgess, 1983; Srinivasan et al., (1983a, 1983b)). These investigations surveyed and assessed current models and identified model deficiencies through comparison between calculated and measured quantities. Results of the assessment by Srinivasan et al. (1983a, 1983b) are summarized by Mongia et al. (1986). The constituent flows examined included: (1) simple flows with no streamline curvature (2) complex flows without swirl, and (3) complex flows with swirl.

The major conclusion in the HOST Aerothermal Modeling Phase I assessment studies by Kenworthy et al. (1983), Sturgess (1983), and Srinivasan et al. (1983a, 1983b) was that the available computational fluid dynamics (CFD) codes provided a useful combustor design tool. Although significant advances have been made in the development and validation of multidimensional gas turbine combustion calculation procedures, the codes assessed were only qualitatively accurate, especially for complex three-dimensional flows. Further work was clearly needed. It was concluded that both a significantly improved numerical scheme and fully specified experimental data (i.e. both mean and turbulence flow-field quantities, with measured boundary conditions) for complex non-reacting and reacting constituent flows were needed before various emerging physical submodels of turbulence, chemistry, sprays, turbulence/chemistry interactions, soot formation/oxidation, radiation, and heat transfer could be properly assessed.

OBJECTIVE:

- **ASSESS PREDICTIVE ACCURACY OF AND DEFICIENCIES IN CURRENT COMBUSTOR AEROTHERMAL MODELS**
- **RECOMMEND MODEL IMPROVEMENTS**

RESULTS:

- **CURRENT CALCULATIONS ARE OF QUALITATIVE ACCURACY ONLY**
- **GOOD BENCHMARK EXPERIMENTS ARE LACKING**

RECOMMENDATIONS:

- **IMPROVE 3-D NUMERICAL SCHEMES**
 - **GRIDS**
 - **ACCURACY**
 - **SPEED**
- **IMPROVE MODELS**
 - **TURBULENCE**
 - **CHEMISTRY**
- **GENERATE RELEVANT BENCHMARK DATA**

AEROTHERMAL MODELING PHASE II

Based on the recommendations of the Phase I assessment studies, activities in Phase II of the HOST Aerothermal Modeling program concentrated on developing improved numerical schemes, and collecting completely specified data for nonreacting single and two-phase swirling and nonswirling flows.

The hybrid finite differencing scheme employed in generally available combustor codes gives excessive numerical diffusion errors that preclude accurate quantitative calculations. In response to this deficiency, HOST supported three programs with the primary objective being to identify, assess, and implement improved solution algorithms applicable to analysis of turbulent viscous recirculating flows. Both solution accuracy and solution efficiency were addressed (Turbine Engine Hot Section Technology, 1985, 1986, 1987; Turan and VanDoormal, 1987).

One scheme, named CONDIF (Controlled Numerical Diffusion with Internal Feedback) (Runchal et al., 1987) has unconditionally positive coefficients and still maintains the essential features of central differencing and its second-order accuracy.

Another advanced numerical scheme, called flux spline (Patankar et al., 1987) is based on a linear variation of total flux (convection + diffusion between two grid points). This is an improvement over the assumption of uniform flux used in hybrid schemes, and leads to reduced numerical diffusion.

Other advanced schemes (Turbine Engine Hot Section Technology, 1985, 1986, 1987; Vanka, 1987), such as block correction techniques and direct solution of the coupled equations, have been proposed. Calculations with the latter, coupled with the flux spline technique, have shown a speed increase by a factor of 15 for a calculation of turbulent flow over a backward-facing step (Mongia, 1987).

OBJECTIVE:

- **IMPROVE ACCURACY AND CONVERGENCE SPEED OF COMBUSTOR FLOW COMPUTER CODES**

APPROACH:

- **EVALUATE NEW TECHNIQUES**
 - FLUX SPLINE
 - DIRECT SOLUTION
 - CONTROLLED NUMERICAL DIFFUSION WITH INTERNAL FEEDBACK (CONDIF)
 - COMPACT IMPLICIT METHODS
 - COUPLED MOMENTUM AND CONTINUITY EQUATIONS

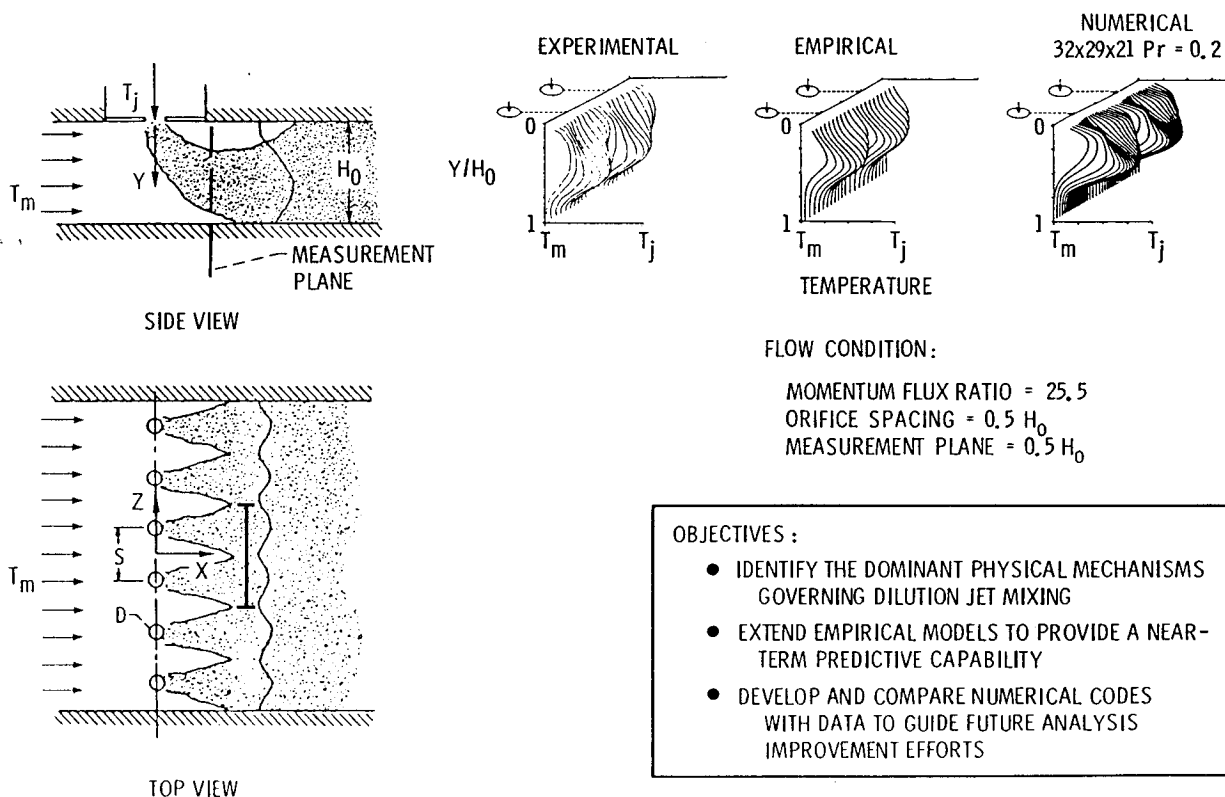
RESULTS:

- **RESULTS INDICATE POTENTIALLY SIGNIFICANT IMPROVEMENTS IN ACCURACY AND SPEED COMPARED WITH PREVIOUS METHODS**

EXPERIMENTS AND MODELING OF DILUTION JET FLOW FIELDS

Considerations in designing or tailoring temperature patterns at the exit of gas-turbine combustion chambers, necessary to maximize engine power and life, have motivated several studies of the thermal mixing characteristics of multiple jets injected into a confined crossflow (Holdeman et al., 1984, Holdeman and Srinivasan, 1986, Holdeman et al., 1987a, Holdeman et al., 1987b).

The objectives of these studies were to (1) identify the dominant physical mechanisms governing the mixing (2) develop and extend empirical models for use as a near-term combustor design tool, and (3) provide a data base for the assessment and verification of three-dimensional numerical codes.

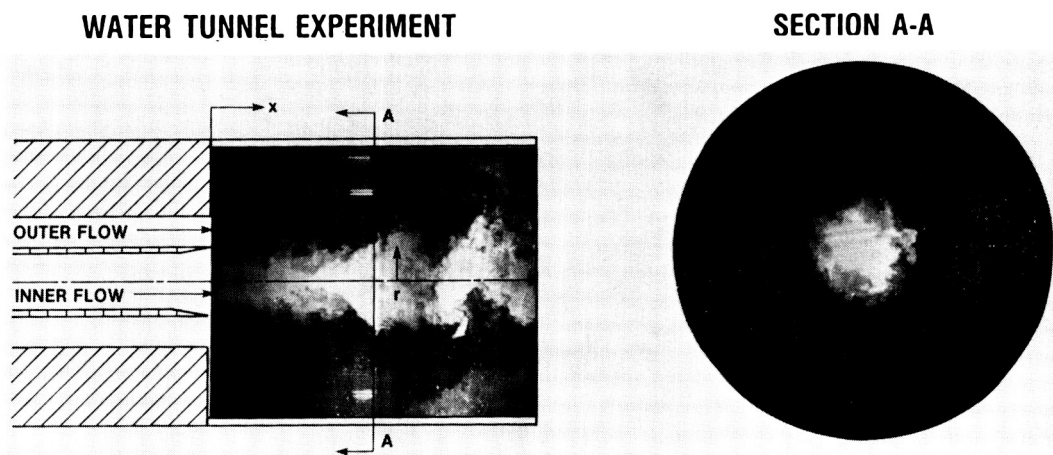


CD-88-32297

MASS AND MOMENTUM TRANSPORT EXPERIMENTS

The objective of this work was to obtain data for the evaluation and improvement of turbulent transport models for axial and swirling coaxial jets. Laser velocimeter and laser-induced fluorescence techniques were used to measure mass and momentum transport.

Extensive data were generated for mean and fluctuating axial velocities, turbulence dissipation rate, and integral- and micro-turbulence length scales.



OBJECTIVE

OBTAIN DETAILED DATA FOR ASSESSING CURRENT TURBULENCE MODELING CAPABILITY AND PROVIDE INFORMATION FOR ADVANCED CONCEPTS IN EDDY MASS & MOMENTUM TRANSFER

APPROACH

EXPERIMENTALLY INVESTIGATE TURBULENT MIXING IN CONFINED COAXIAL JET USING LASER-INDUCED FLUORESCENCE AND LASER DOPPLER VELOCIMETER DIAGNOSTICS

LST '88

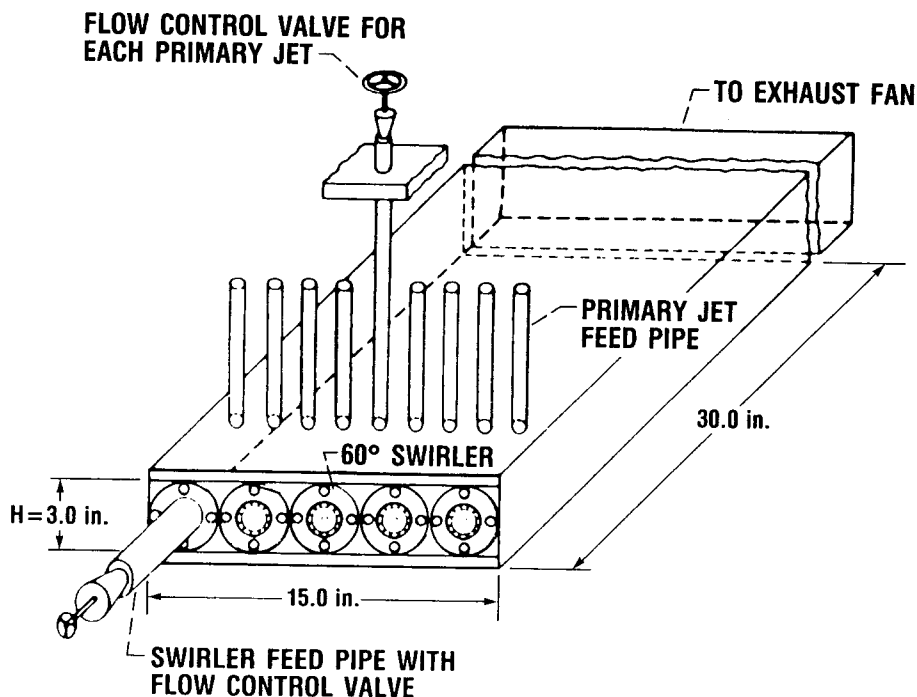
CD-88-32298

FLOW INTERACTION EXPERIMENT

Another study in progress will obtain comprehensive mean and turbulence measurements of velocity and species concentration in a three-dimensional flow model of the primary zone of gas turbine combustion chambers (Turbine Engine Hot Section Technology, 1985, 1986, 1987). The flow field of interest is the interaction between swirling flow and lateral jets in a rectangular channel. The mainstream flow enters through 5 swirlers with the transverse jets injected from both the top and bottom duct walls with either 2 or 4 jets per swirler at $1/2$ or 1 channel height downstream from the swirler.

These experiments are being conducted on both air and water multiple-swirler rigs, as well as single-swirler and swirling-jet rigs. Fifteen cases (combinations of swirl, jet strength and location) are under test using laser sheet light and dye water flow visualization. Detailed velocity and scalar mean and turbulence LDV measurements are being made in the air rig.

A key feature of this program is the comparison of model calculations with the data obtained to ensure that the data are complete and consistent, and that they satisfy the boundary condition input requirements of current three-dimensional codes. Before the experiments were begun, calculations were performed using a three-dimensional code (Srivatsa, 1980) for all test cases. As the data are obtained, they are compared with both previous and advanced model calculations.



CD-88-32299

FUEL-INJECTOR/AIR-SWIRL CHARACTERIZATION

The objective of this study is to obtain fully specified mean and turbulence measurements of both gas and droplet phases downstream of a fuel injector and air swirler that are typical of those used in gas turbine combustion chambers.

The flow field of interest is an axisymmetric particle-laden jet flow with and without confinement and co-annular swirling airflow. Approximately 30 cases are under test with both glass-bead, particle-laden jets and liquid sprays, with various combinations of swirl strengths and confinement (Turbine Engine Hot Section Technology, 1985, 1986, 1987). Measurements of mean and turbulence quantities for both gas and solid phases are being made using a 2-component Phase/Doppler LDV particle analyzer (McDonnell et al., 1987).

The comprehensive experimental data generated in these programs will be used to validate advanced models of turbulence, scalar, and spray transport, including two-equation turbulence models, algebraic and differential Reynolds stress models, scalar and scalar-velocity transport models, and Eulerian and Lagrangian deterministic and stochastic spray models.

OBJECTIVE:

- **BENCHMARK DATA ON FUEL SPRAY—SWIRLING FLOW INTERACTIONS**
- **VALIDATE CURRENT & ADVANCED 2-PHASE MODELS**

APPROACH:

- **DESIGN 2-PHASE, ISOTHERMAL EXPERIMENT WITH GUIDANCE FROM CURRENT COMPUTATIONAL TOOLS**
- **MAP FLOW USING 2-COMPONENT PHASE/DOPPLER SYSTEM**
- **VALIDATE NEWEST MODELS**

CD- 88-32300

REFERENCES

- Holdeman, J.D., Reynolds, R., and White, C., 1987, "A Numerical Study of the Effects of Curvature and Convergence on Dilution Jet Mixing," AIAA Paper 87-1953.
- Holdeman, J.D., and Srinivasan, R., 1986, "Modeling Dilution Jet Flowfields," Journal of Propulsion and Power, Vol. 2, No. 1, pp. 4-10.
- Holdeman, J.D., Srinivasan, R., Coleman, E.B., Meyers, G.D., and White, C.D., 1987, "Effects of Multiple Rows and Noncircular Orifices on Dilution Jet Mixing," Journal of Propulsion and Power, Vol. 3, No. 3, pp. 219-226.
- Holdeman, J.D., Srinivasan, R., and Berenfeld, A., 1984, "Experiments in Dilution Jet Mixing," AIAA Journal, Vol. 22, No. 10, pp. 1436-1443.
- Kenworthy, M.J., Correa, S.M., and Burrus, D.L., 1983, "Aerothermal Modeling: Phase I Final Report - Volume I Model Assessment," NASA CR-168296.
- McDonell, V.G., Cameron, C.D., and Samuelson, G.S., 1987, "Symmetry Assessment of a Gas Turbine Air-Blast Atomizer," AIAA Paper 87-2136.
- Mongia, H.C., 1987, "A Status Report on Gas Turbine Combustor Modeling," presented at the AGARD Combustion and Fuels in Gas Turbine Engines Meeting, Crete, Oct. 12-16.
- Mongia, H.C., Reynolds, R.S., and Srinivasan, R., 1986, "Multidimensional Gas Turbine Combustion Modeling: Applications and Limitations," AIAA Journal, Vol. 24, No. 6, pp. 890-904.
- Patankar, S.W., Karki, K.C., and Mongia, H.C., 1987, "Development and Evaluation of Improved Numerical Schemes for Recirculating Flows," AIAA Paper 87-0061.
- Runchal, A.K., Anand, M.S., and Mongia, H.C., 1987, "An Unconditionally-Stable Central Differencing Scheme for High Reynolds Number Flows," AIAA Paper 87-0060.
- Srinivasan, R., Reynolds, R., Ball, I., Berry, R., Johnson, K., and Mongia, H.C., 1983, "Aerothermal Modeling Program: Phase I Final Report - Volume I," NASA CR-168243.
- Srinivasan, R., Reynolds, R., Ball, I., Berry, R., Johnson, K., and Mongia, H.C., 1983, "Aerothermal Modeling Program: Phase I Final Report - Volume II," NASA CR-168243.
- Srivatsa, S.K., 1982, "Computations of Soot and NO_x Emissions from Gas Turbine Combustors," NASA CR-165196.
- Sturgess, G.J., 1983, "Aerothermal Modeling: Phase I Final Report," NASA CR-168202.
- Turan, A., and VanDoormaal, J.P., 1987, "Improved Numerical Methods for Turbulent Viscous Recirculating Flows," NASA CR-180852.

Turbine Engine Hot Section Technology 1985, NASA CP-2405.

Turbine Engine Hot Section Technology 1986, NASA CP-2444 (FEDD until Oct. 1988).

Turbine Engine Hot Section Technology 1987, NASA CP-2493 (FEDD until Oct. 1989).

Vanka, S.P., 1987, "Block-Implicit Computation of Viscous Internal Flows - Recent Results," AIAA Paper 87-0058.

REVIEW AND ASSESSMENT OF THE HOST TURBINE HEAT TRANSFER PROGRAM

Herbert J. Gladden
Internal Fluid Mechanics Division
NASA Lewis Research Center

ABSTRACT

The objectives of the HOST Turbine Heat Transfer subproject were to obtain a better understanding of the physics of the aerothermodynamic phenomena occurring in high-performance gas turbine engines and to assess and improve the analytical methods used to predict the fluid dynamics and heat transfer phenomena. At the time the HOST project was initiated, an across-the-board improvement in turbine design technology was needed. Therefore, a building-block approach was utilized, with research ranging from the study of fundamental phenomena and analytical modeling to experiments in simulated real-engine environments. Experimental research accounted for 75 percent of the project, and analytical efforts accounted for approximately 25 percent. Extensive experimental datasets were created depicting the three-dimensional flow field, high free-stream turbulence, boundary-layer transition, blade tip region heat transfer, film cooling effects in a simulated engine environment, rough-wall cooling enhancement in a rotating passage, and rotor-stator interaction effects. In addition, analytical modeling of these phenomena was initiated using boundary-layer assumptions as well as Navier-Stokes solutions.

PRECEDING PAGE BLANK NOT FILMED

TURBINE HEAT TRANSFER PROGRAM

In the multidisciplinary HOST Project each participating discipline selected its own objective based on the greatest need in that particular area, rather than some common interdisciplinary goal. In Turbine Heat Transfer it was decided, based on evaluations of the type performed by Stepka (1980), that an across-the-board improvement in turbine heat transfer technology was needed. A ratcheting up of the overall technology, a moving from a correlation base to a more analytical base, was identified as the Turbine Heat Transfer Subproject goal. It was also identified that the existing data base was insufficient to support this movement and that increasing both the size and quality of the data base was essential. It was further recognized that HOST alone could not achieve this goal. It was hoped that HOST could be a sufficient catalyst and provide a sufficient forum to make this goal one that all of the partners - government, industry, and universities - would find obtainable and worth pursuing.

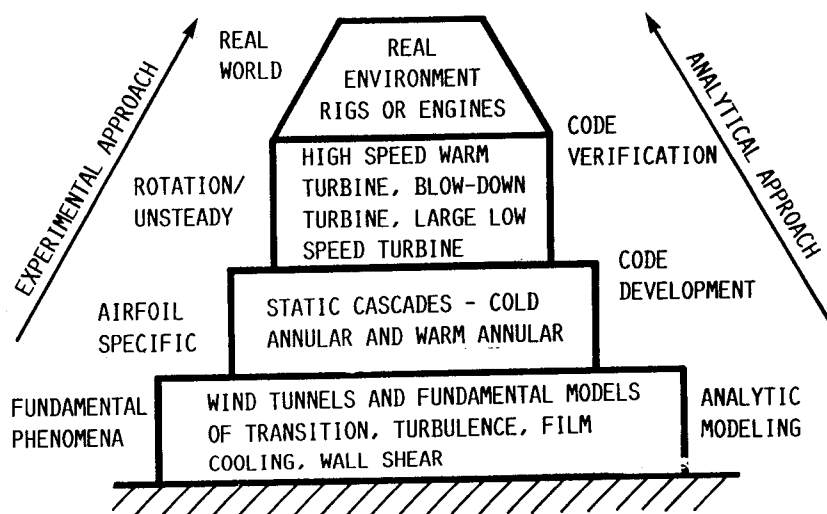
Objectives

- **OBTAIN A BETTER UNDERSTANDING OF THE PHYSICS OF THE AEROTHERMODYNAMIC PHENOMENA OCCURRING IN HIGH-PERFORMANCE TURBINES**
- **ASSESS AND IMPROVE THE ANALYTICAL METHODS USED TO PREDICT THE FLOW AND HEAT TRANSFER IN HIGH-PERFORMANCE TURBINES**

CD-88-32349

RESEARCH APPROACH

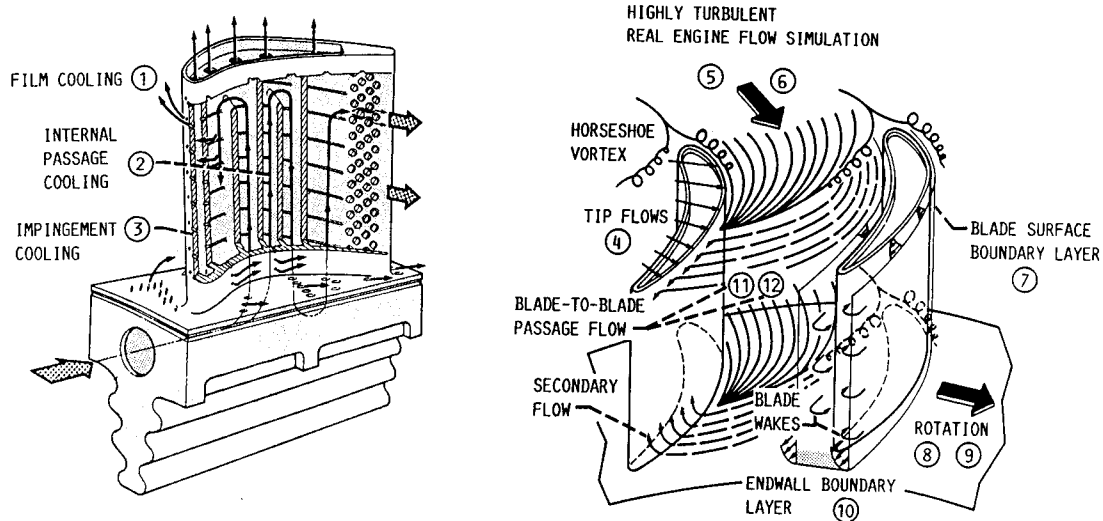
The research program of the Turbine Heat Transfer Subproject was based on the idea that an across-the-board improvement in turbine design was needed. It was also based on an overall philosophy at NASA Lewis Research Center of taking a building block approach to turbine heat transfer. The research for this program ranged from the study of fundamental phenomena and analytical modeling to experiments in real engine environments. Both experimental and analytical research were conducted.



CD-86-32350

PHYSICAL PHENOMENA INVESTIGATED

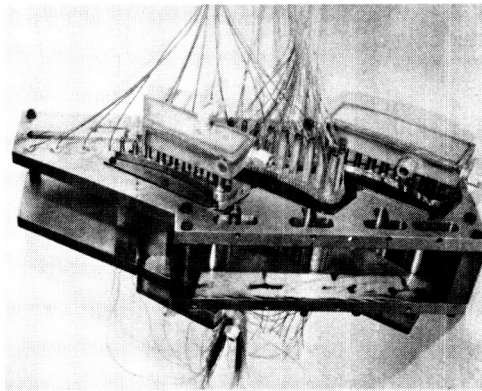
The range of phenomena addressed in the Turbine Heat Transfer Subproject are identified by numbers and arrows on the following figure. One can see from this figure that the Turbine Heat Transfer Subproject covered most of the key heat transfer points on the turbine airfoil: film-cooled airfoils, passage curvature, endwall flows, transitioning blade boundary layers, tip regions, and free-stream turbulence on the external surfaces. The subproject included impingement and turbulated serpentine passages on the internal surfaces. In addition, the program broke some new ground. An experiment was conducted which obtained heat transfer data on the surfaces of the airfoils in a large, low-speed one and one-half stage rotating turbine. Another experiment acquired data on the internal turbulated serpentine passages subject to rotation at engine condition levels. Finally, vane heat transfer data were acquired in a real engine type environment behind an actual operating combustor.



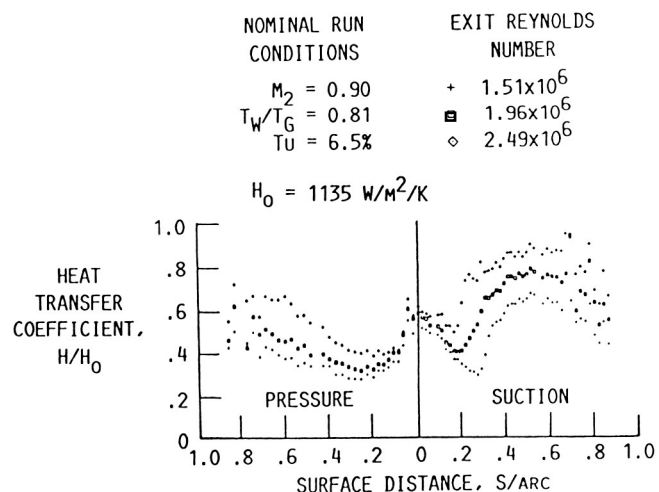
CD-88-32351

One of the initial research efforts was the stator-airfoil heat transfer program performed at the Allison Gas Turbine Division (Nealy et al., 1983; Hylton et al., 1983; Hylton et al., 1988; Nealy et al., 1984; Turner et al., 1985; Yang et al., 1985). This research consisted of determining the effects of Reynolds number, turbulence level, Mach number, temperature ratio, acceleration, and boundary-layer transition on heat transfer coefficients for various airfoil geometries at simulated engine conditions. This research was conducted for non-film-cooled airfoils, showerhead film-cooled designs and showerhead "gill-region" film cooling concepts. Typical results of this research are shown in the following figure. A typical cascade configuration is shown in the photograph (fig. (a)). Two-dimensional midspan heat transfer coefficients and static pressure distributions were measured on the central airfoil of the three-vane cascade. Non-film-cooled data are shown in figure (b), where the boundary-layer transition is clearly identified as a function of Reynolds number on the suction surface. Figure (c) shows the effect on heat transfer in the downstream recovery region to the addition of showerhead film cooling. Data are presented as Stanton number reductions. A detrimental effect is noted in the boundary-layer transition region of the suction surface to the addition mass at the leading edge. Figure (d) shows a strong dependence on "gill-region" film cooling, which is consistent with experience. However, when combining showerhead with "gill-region" film cooling, more mass addition is not always better as indicated by the Stanton number reduction data on the pressure surface. This is a very extensive dataset which systematically shows the important effects of modern film cooling schemes on modern airfoils. It went beyond the traditional effectiveness correlations to provide actual heat transfer data. It should provide a valuable baseline for emerging analysis codes.

(A) THREE-VANE CASCADE

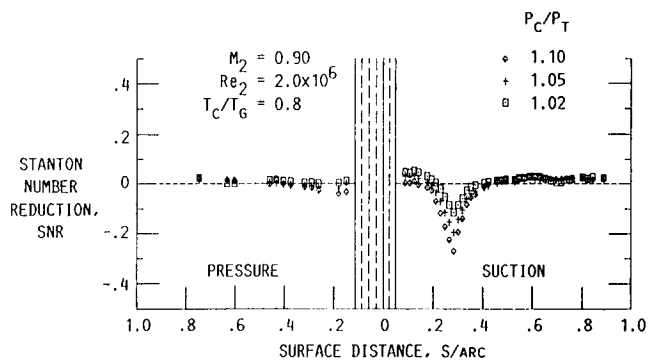


(B) NONFILM-COOLED AIRFOIL HEAT TRANSFER COEFFICIENTS



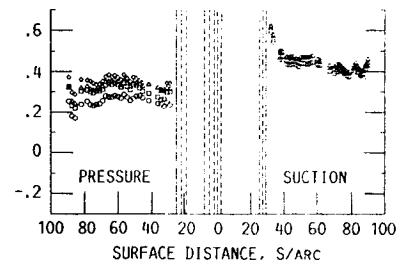
CD-88-32353

(C) INFLUENCE OF LEADING EDGE FILM-COOLING ON HEAT TRANSFER



(D) COMBINED LEADING EDGE AND DOWN-STREAM FILM-COOLING

DATA	M_2	Re_2	$P_{C,DS}/P_T$	$P_{C,LE}/P_T$	T_w/T_G
BASE	0.75	2.00E6			
\circ	.75	2.05E6	1.10	1.10	0.67
\triangle	.74	2.00E6	1.10	1.05	.65
\diamond	.75	2.01E6	1.10	1.02	.65
\square	.75	2.00E6	1.10	1.00	.66

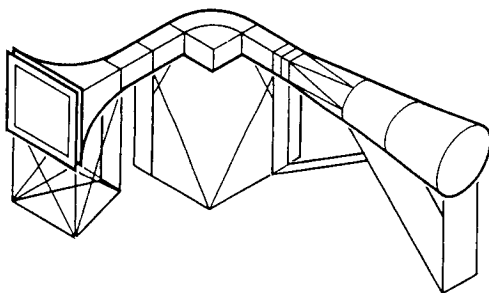


CD-88-32352

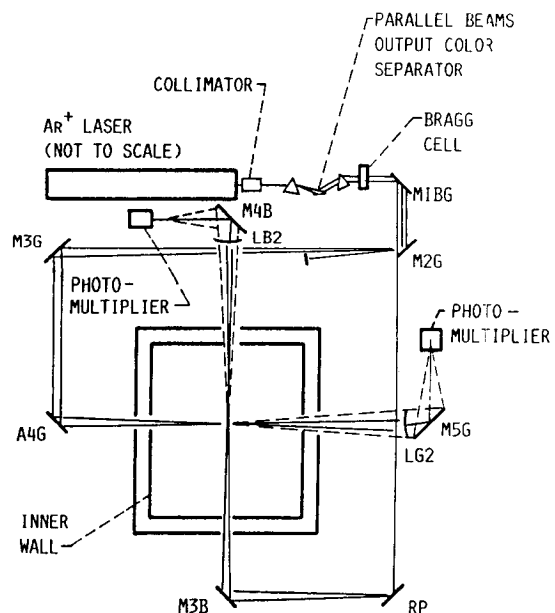
THREE-DIMENSIONAL FLOW FIELD IN CURVED PASSAGES

An investigation of secondary flow phenomena in a 90° curved duct was conducted at the University of Tennessee Space Institute (Crawford et al., 1985). The curved duct was used to represent airfoil passage curvature without the complexity of the horseshoe vortex. These data consist of simultaneous three-dimensional mean value and fluctuating components of velocity through the duct, and they compliment similar data in the literature. A schematic of the test facility and the three-dimensional laser velocimeter are shown in the following figure. The first phase of the research examined flows with a relatively thin inlet boundary layer and low free-stream turbulence. The second phase studied a thicker inlet boundary layer and higher free-stream turbulence. Typical experimental results of this research are also shown in this figure. The vector plot of cross-flow velocities clearly shows the development of a vortex in the duct corner near the low pressure surface. The University of Tennessee Space Institute also developed a three-dimensional viscous flow analysis capability for the curved duct experiment utilizing the P.D. Thomas code (Thomas, 1979) as a base. Some analytical results from this code are shown where a vector plot of the cross-flow velocities is compared with the experiment. In addition, a stream sheet is shown as it propagates through the duct and is twisted and stretched. Additional comparisons of analysis and experiment show that the thin turbulent boundary-layer results of this experiment are difficult to calculate with current turbulence models.

CURVED-DUCT FACILITY



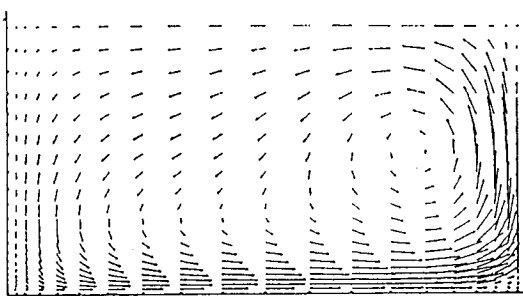
3-D LV OPTICAL SYSTEM



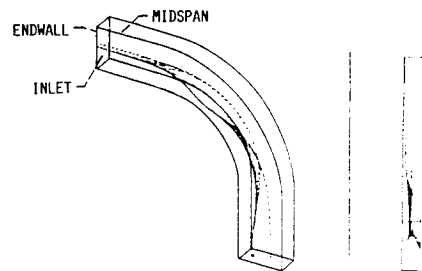
CD-88-32354

ANALYTICAL RESULTS

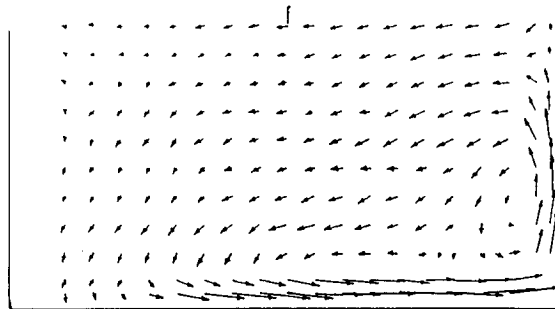
DUCT CROSS-FLOW PLOT P.D. THOMAS CODE



STREAM SHEET VELOCITY PATTERN THROUGH DUCT



EXPERIMENTAL RESULTS LOW REYNOLDS NUMBER DATA

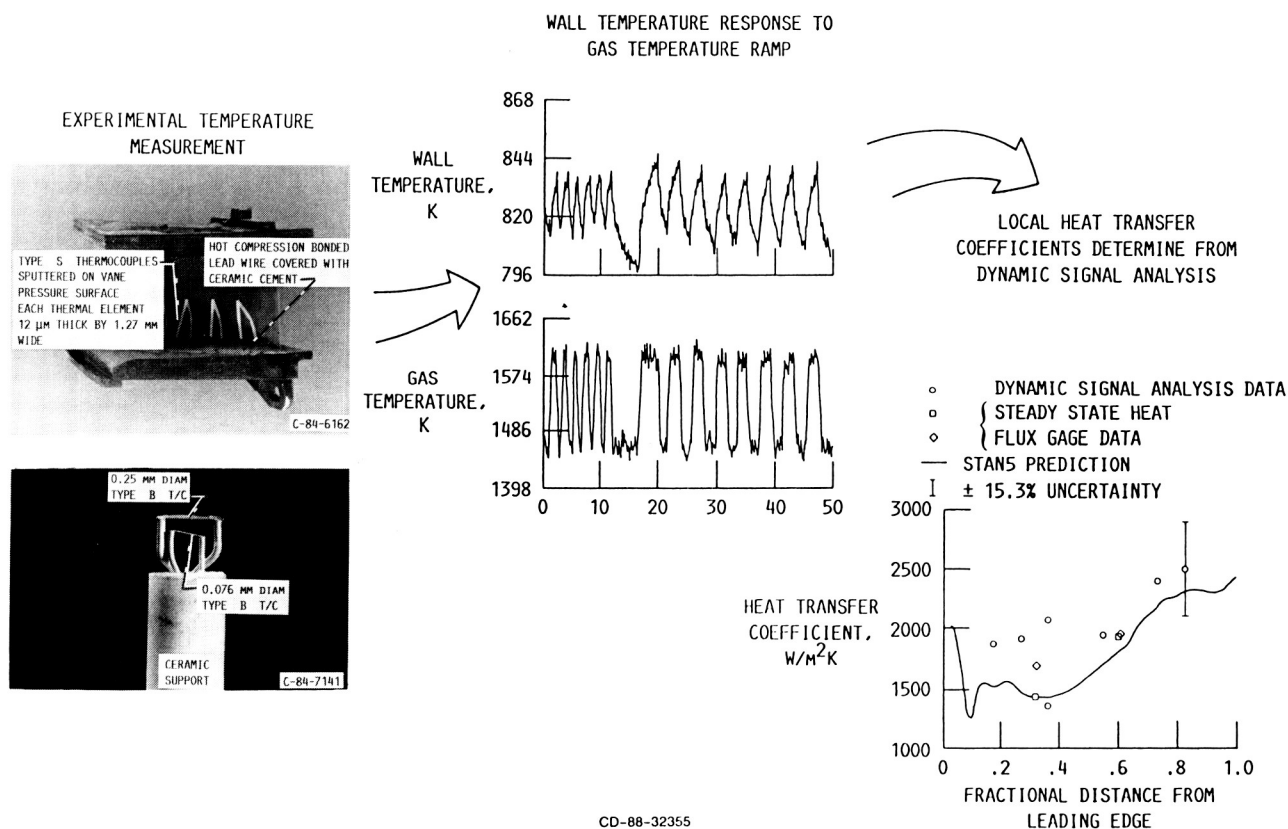


CD-88-32398

HEAT TRANSFER COEFFICIENTS IN REAL-ENGINE ENVIRONMENT

Two experiments were also conducted at NASA Lewis in the high-pressure facility (Gladden et al., 1985; Gladden and Proctor, 1985; Gladden et al., 1987; Hippensteele et al., 1985). This facility was capable of testing a full-sized single-stage turbine at simulated real-engine conditions. The tests, however, were limited to combined combustor-stator experiments. One experiment examined full-coverage film-cooled stator airfoils, whereas the second experiment utilized some of the advanced instrumentation developed under the instrumentation subproject. A comparison of experimental airfoil temperatures with temperatures obtained from a typical design system showed substantial differences for the full-coverage, film-cooled airfoils and suggests that models derived from low-temperature experiments are inadequate for real-engine conditions. The advanced instrumentation tests demonstrated the capability and the challenges of measuring heat flux and time-resolved gas temperature fluctuation in a real-engine environment.

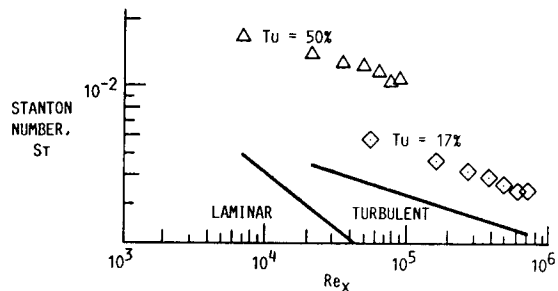
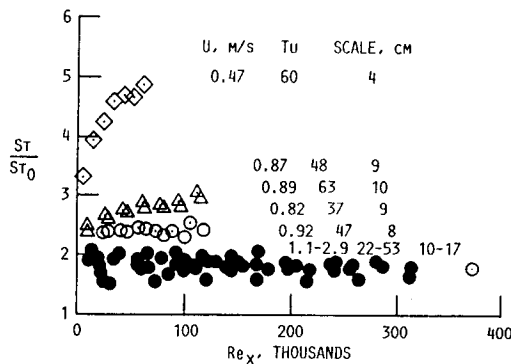
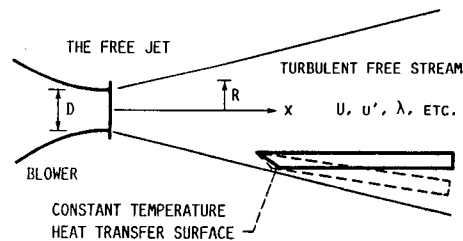
Typical results are shown in the following figure for thin film thermocouples. The dynamic gas temperature probe tested a simulated real-engine condition. A comparison is made between steady state heat flux measurements and those determined from dynamic signal analysis techniques.



CD-88-32355

HIGH FREE-STREAM TURBULENCE EFFECTS

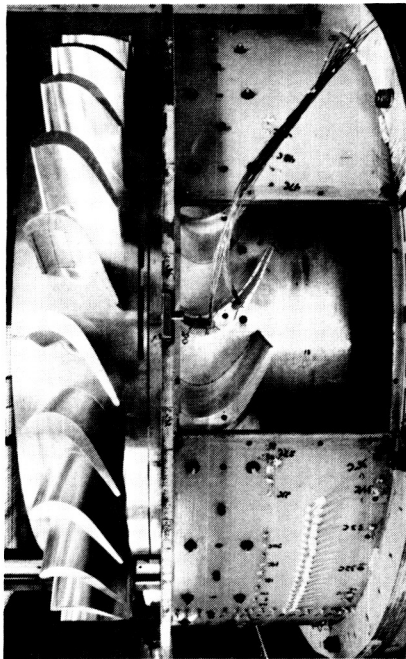
Stanford University has conducted a systematic study of the physical phenomena that affect heat transfer in turbine airfoil passages. Their recent experimental research has been concerned with high free-stream turbulence intensity and a large turbulence scale that might be representative of combustor exit phenomena. A schematic of their free jet test facility and typical results are shown in this figure. Data are measured on a constant temperature flat plate located at a specified radial and axial distance from the jet exit centerline. These data, presented as Stanton number ratios, indicate that heat transfer augmentation can be as high as 5X at a high value of free-stream turbulence intensity but only 3X if the length scale is changed. These results suggest that the designer must know a great deal more about the aerodynamic behavior of the flow field in order to successfully predict the thermal performance of the turbine components.



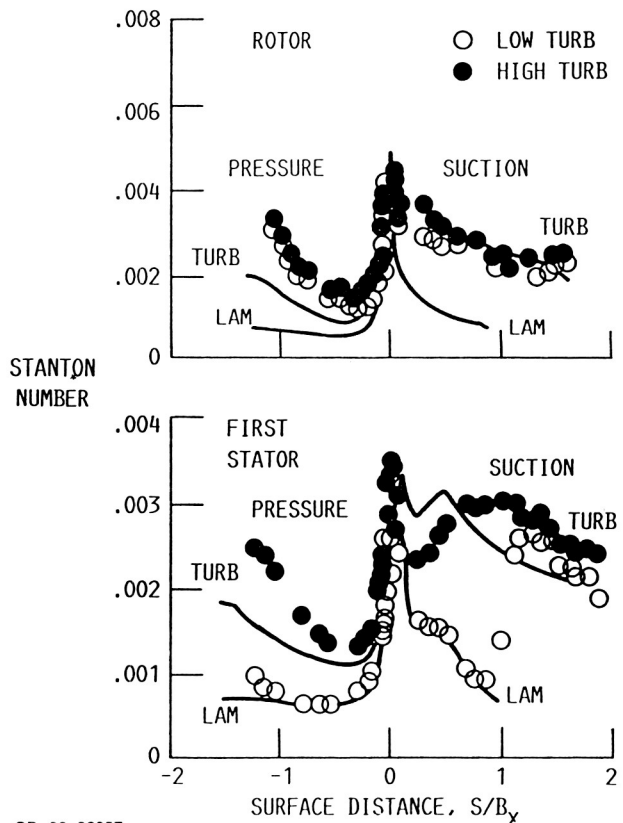
CD-88-32356

In the rotating reference frame, experimental aerodynamic and heat transfer measurements were made in the large, low-speed turbine at the United Technologies Research Center (Dring et al., 1986a; Dring et al., 1986b; Dring et al., 1986c; Dring et al., 1987; Blair et al., 1988a; Blair et al., 1988b). Single-stage data with both high and low-inlet turbulence were taken in phase I. The second phase examined a one and one-half stage turbine and focused on the second vane row. Under phase III, aerodynamic quantities such as interrow time-averaged and rms values of velocity, flow angle, inlet turbulence, and surface pressure distributions were measured. A photograph of the test facility is shown in the following figure. Typical heat transfer data for both the first stator and rotor are also shown. These data show that an increase of inlet turbulence has a substantial impact on the first stator heat transfer. However, the impact on the rotor heat transfer is minimal. These data are also compared with Stanton numbers calculated by a boundary-layer code and the assumption that the boundary layer was either laminar (LAM) or fully turbulent (TURB). These assumptions generally bracketed the data on the suction surface of both the stator and the rotor. However, the heat transfer on the pressure surface, especially for the high-turbulence case, was generally above even fully turbulent levels on both airfoils. Pressure surfaces have traditionally received less attention than suction surfaces. The high heat transfer on the pressure surface is not readily explainable and calls for additional research, especially modeling, on pressure surfaces.

LARGE-SCALE ROTATING RIG 1-1/2 STAGE
TURBINE CONFIGURATION FIRST VANE AND
ROTOR CASE REMOVED



HIGH REYNOLD'S NUMBER: 65-PERCENT GAP

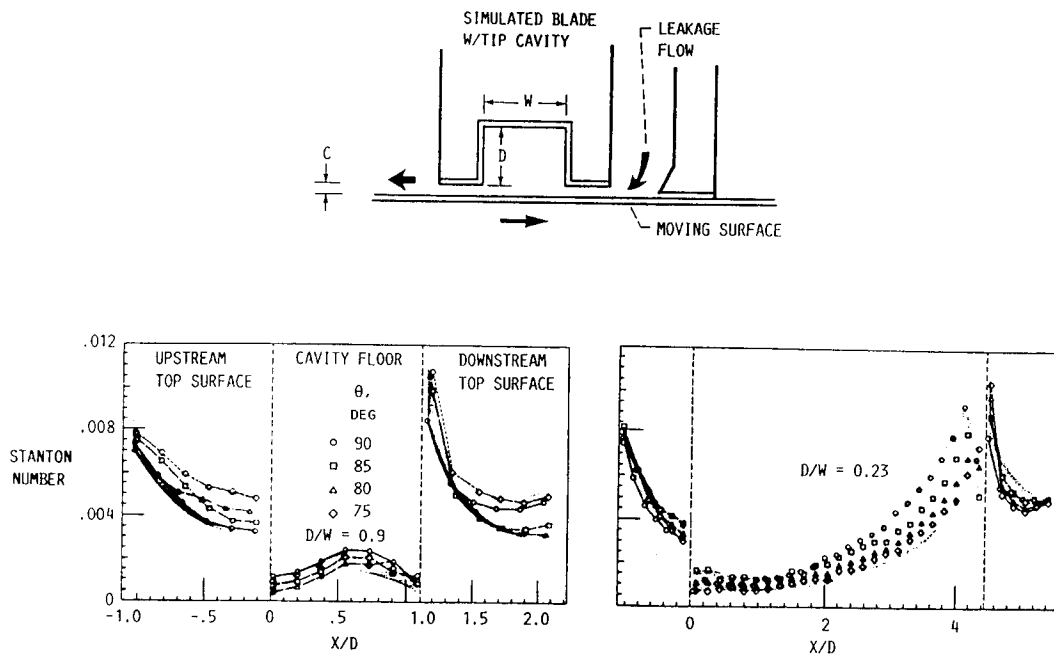


CD-88-32357

TIP REGION HEAT TRANSFER

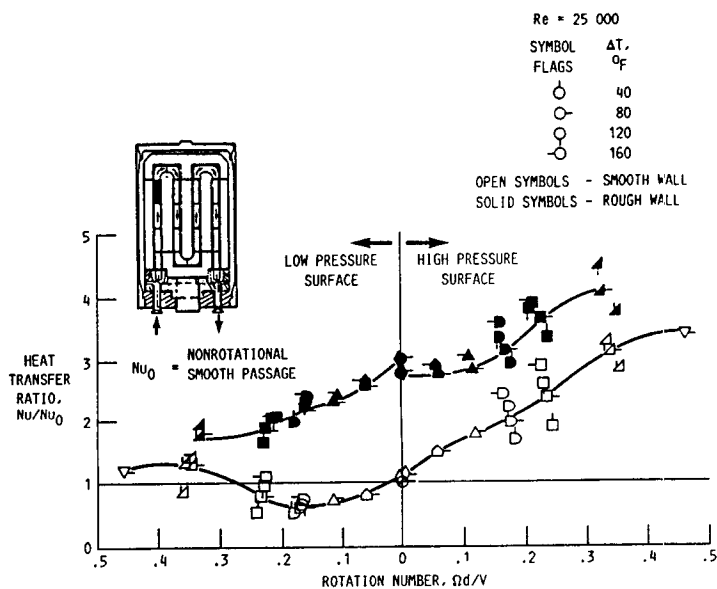
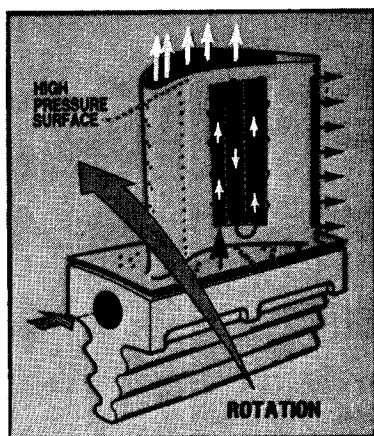
The tip region of rotor blades is often a critical region and an area that suffers substantial damage from the high-temperature environment. Arizona State University has experimentally modeled the blade tip cavity region and determined heat transfer rates by a mass transfer analogy with naphthylene (Chyu et al., 1987). A schematic of the test is shown in the following figure.

The blade tip cavity is a stationary model and the relative velocity of the shroud is represented by a moving surface at a specified gap spacing from the blade. Stanton number results for two different cavity aspect ratios are also shown. The heat transfer on the surfaces next to the shroud are little changed by the aspect ratio, which is not surprising. However, the heat transfer to the floor of the cavity is increased significantly on the downstream portion at the lower aspect ratio. Also shown in the figures is the flow angle effect on heat transfer. Because the airfoil turns at the tip, the cavity will be at different angles of attack to the mean crossflow direction. The data shows a minimal effect at an aspect ratio of 0.9 and a substantial effect at an aspect ratio of 0.23. This dataset is really quite a new addition to a traditionally neglected area and shows that with careful datasets and analyses one can obtain an optimal design for tip cavities.



CD-88-32358

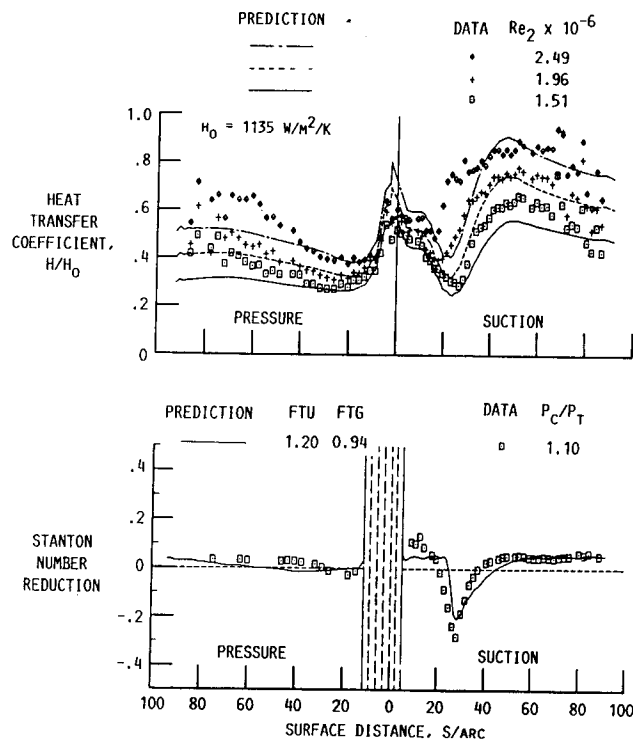
Coolant passage heat-transfer and flow measurements in a rotating reference frame were also obtained at Pratt & Whitney Aircraft/United Technologies Research Center (Kopper, 1984; Sturgess and Datta, 1987; Lord et al., 1987). Experimental data were obtained for smooth-wall serpentine passages and for serpentine passages with skewed and normal turbulators. The flow and rotation conditions were typical of those found in actual engines. This was a very realistic experiment. Data for both the smooth-wall and skewed turbulator passages are shown in this figure for radial outflow, representing only a tiny fraction of the total data involved in this very complex flow. Both datasets are shown correlated with the rotation number except for high rotation numbers on the high pressure surface. This is an area that requires additional research to understand and model the physical phenomena occurring in these passages.



CD-88-32359

BOUNDARY-LAYER ANALYSIS

The STAN5 boundary-layer code (Crawford and Kay, 1976) (which was developed on NASA contract at Stanford University in the mid-1970's) was modified by Allison Gas Turbine Division to define starting points and transition length of turbulent flow to accommodate their data, with and without film cooling, as well as data in the literature. Specific recommendations were made to improve turbine airfoil heat transfer modeling used in the boundary-layer analysis. These recommendations address the boundary conditions, the initial condition specification, including both velocity and thermal profiles, and modifications of conventional zero-order turbulence models. The results of these improvements are shown in the following figure, where the start of transition and its extent on the suction surface are reasonably well characterized. For the case of shower-head film cooling, two empirical coefficients were used to modify the free-stream turbulence intensity and the gas stream enthalpy boundary conditions and to permit a representative prediction of the Stanton number reduction in the recovery region. Boundary-layer methods can be used for midspan analysis; however they require a realistic data base to provide the coefficients needed for proper reference.



CD-88-32360

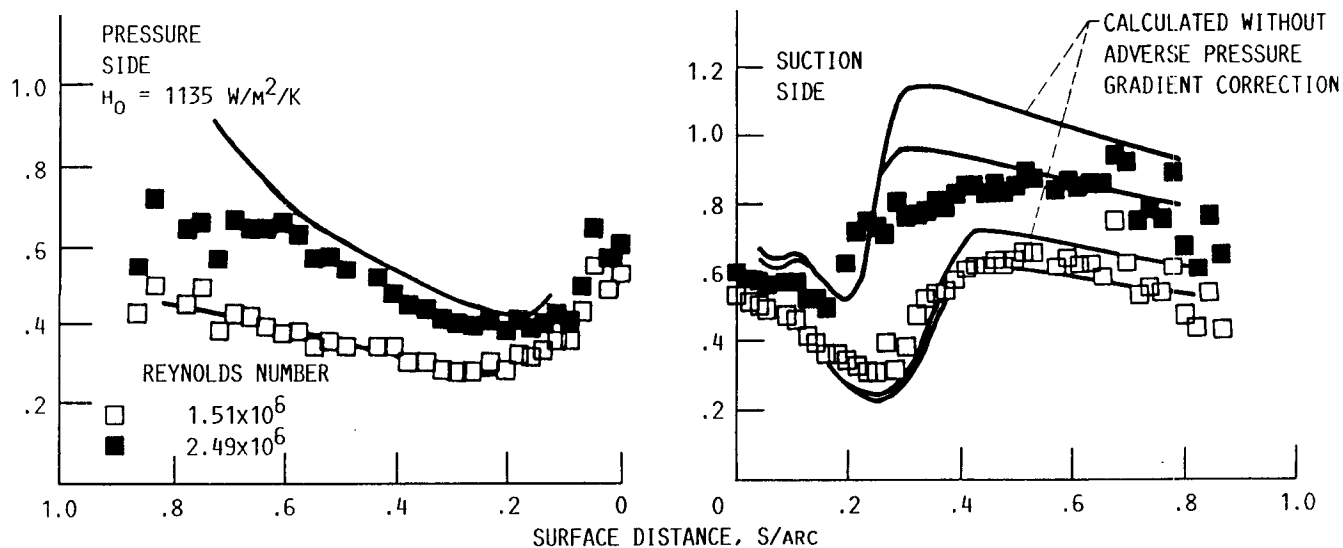
TURBULENCE MODELING

A fundamental study on numerical turbulence modeling, directed specifically at the airfoil in the turbine environment, was conducted at the University of Minnesota. A modified form of the Lam-Bremhorst low-Reynolds-number k - ϵ turbulence model was developed to predict transitional boundary-layer flows under conditions characteristic of gas turbine blades (Schmidt and Patankar, 1987) including both free-stream turbulence and pressure gradients.

The purpose was to extend previous work on turbulence modeling to apply the model to transitional flows with both free-stream turbulence and pressure gradients. The results of the effort are compared with the experimental data of Allison Gas Turbine Division. The augmentation of heat transfer on the pressure surface over the fully turbulent value is predicted reasonably well. In addition, when an adverse pressure gradient correction is used, the suction surface heat transfer data is also predicted reasonably well.

This research established a methodology for moving away from the heavy dependence on empirical constants. Although boundary-layer methods will never solve the whole problem, they will always remain important analytic tools.

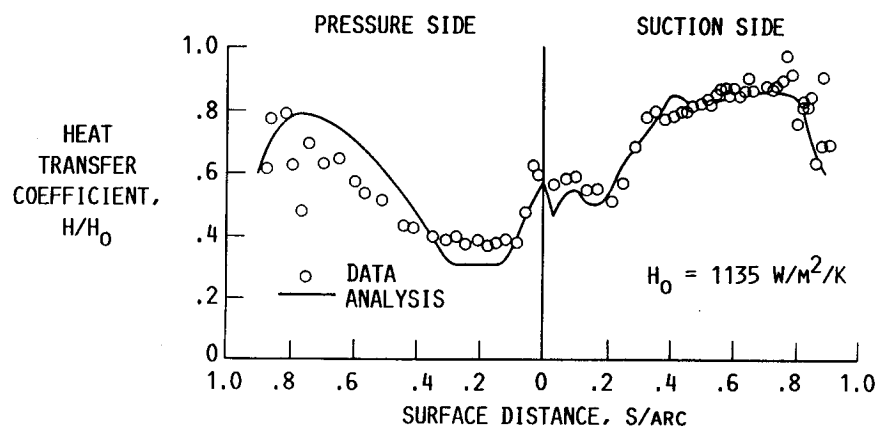
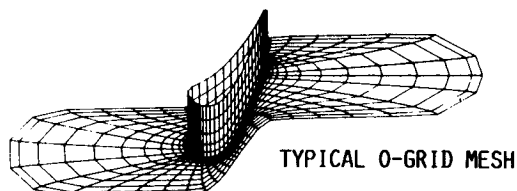
TURBULENCE = 6.5 PERCENT; EXIT MACH NUMBER = 0.90



CD-88-3236

VISCOUS FLOW ANALYSIS

A fully elliptic, three-dimensional Navier-Stokes code has been under development at Scientific Research Associates (SRA) for many years. This code was primarily directed at inlets and nozzles. SRA, Inc., has modified the code for turbine applications (Weinberg et al., 1985). This includes grid work for turbine airfoils, adding an energy equation and turbulence modeling, and improved user friendliness. The heat transfer predictions from the MINT code are shown compared to the data from the Allison Gas Turbine research. The analytical-experimental data comparison is good, however, the location of boundary-layer transition was specified for the analytical solution.



CD-88-32362

LOOK TO THE FUTURE

Many recent studies have been made to assess aeropropulsion technology requirements into the 21st century. The consensus seems to suggest that significant technology advances are required to meet the goals of the future. Whether the goals are high-speed sustained flight vehicle, single-stage-to-orbit transport, or subsonic transport, the issues for the designer are improved fuel efficiency, high thrust-to-weight ratio vehicle, improved component performance while maintaining component durability, and reduced operating and maintenance costs. These issues will only serve to increase the opportunities available to the researcher in aerothermal loads and structures analysis. The verifiable predictions of unsteady flowfields with significant secondary flow phenomena and coupled thermal-velocity profiles is a fertile research area. Very little progress has been made to date in applying CFD techniques to the intricate and complex coolant channels required in the hot-section components. With the expected advances in high-temperature materials, the components with significant aerothermal loads problems will expand beyond the airfoils and combustor liners to shrouds, rims, seals, bearings, compressor blading, ducting, nozzles, and other turbine components. The issues to be addressed and the technology advances required to provide the aeropropulsion systems of the 21st century are quite challenging.

REFERENCES

- Blair, M.F., Dring, R.P., and Joslyn, H.D., 1988a, "The Effects of Turbulence and Stator/Rotor Interactions on Turbine Heat Transfer, Part II - Effects of Reynolds Number and Incidence," ASME Paper 88-GT-5, 33rd ASME Gas Turbine Conference, The Netherlands.
- Blair, M.F., Dring, R.P., and Joslyn, H.D., 1988b, "The Effects of Turbulence and Stator/Rotor Interactions on Turbine Heat Transfer, Part I - Design Operating Conditions," ASME Paper 88-GT-125, 33rd ASME Gas Turbine Conference, The Netherlands.
- Chyu, M.K., Metzger, D.E., and Hwan, C.L., 1987, "Heat Transfer in Shrouded Rectangular Cavities," Journal of Thermophysics and Heat Transfer, Vol. 1, No. 2, pp. 247-252.
- Crawford, M.E. and Kay, W.M., 1976, "STAN5 - A Program for Numerical Computation of Two-Dimensional Internal and External Boundary Layer Flows," NASA CR-2742.
- Crawford, R.A. et al., 1985, "Mean Velocity and Turbulence Measurements in a 90° Curved Duct With Thin Inlet Boundary Layer," NASA CR-174811.
- Dring, R.P., Blair, M.F., and Joslyn, H.D., 1986a, "The Effects of Inlet Turbulence and Rotor Stator Interactions on the Aerodynamics and Heat Transfer of a Large-Scale Rotating Turbine Model. Vol. III, Heat Transfer Data Tabulation. 65% Axial Spacing," NASA CR-179468.
- Dring, R.P., Blair, M.F., and Joslyn, H.D., 1986b, "The Effects of Inlet Turbulence and Rotor/Stator Interactions on the Aerodynamics and Heat Transfer of a Large-Scale Rotating Turbine Model. Vol. IV, Aerodynamic Data Tabulation," NASA CR-179469.
- Dring, R.P., Blair, M.F., and Joslyn, H.D., 1986c, "The Effects of Inlet Turbulence and Rotor Stator Interactions on the Aerodynamics and Heat Transfer of a Large-Scale Rotating Turbine Model. Vol. II, Heat Transfer Data Tabulation. 15% Axial Spacing," NASA CR-179467.
- Dring, R.P. et al., 1987, "The Effects of Inlet Turbulence and Rotor/Stator Interactions on the Aerodynamics and Heat Transfer of a Large-Scale Rotating Turbine Model, Vol. I," NASA CR-4079.
- Gladden, H.J., Yeh, F.C., and Fronek, D.L., 1985, "Heat Transfer Results and Operational Characteristics of the NASA Lewis Research Center Hot Section Cascade Test Facility," ASME Paper 85-GT-82. (NASA TM-86890).
- Gladden, H.J. and Proctor, M.P., 1985, "Transient Technique for Measuring Heat Transfer Coefficients on Stator Airfoils in a Jet Engine Environment," AIAA Paper 85-1471. (NASA TM-87005).
- Gladden, H.J., Yeh, F.C., and Austin, P.J., Jr., 1987, "Computation of Full-Coverage, Film-Cooled Airfoil Temperatures by Two Methods and Comparison With High Heat Flux Data," ASME Paper 87-GT-213. (NASA TM-88931).

- Hippensteele, S.A., Russell, L.M., and Torres, F.J., 1985, "Local Heat-Transfer Measurements on a Large Scale-Model Turbine Blade Airfoil Using a Composite of a Heat Element and Liquid Crystals," ASME Paper 85-GT-59. (NASA TM-86900).
- Hylton, L.D. et al., 1988, "The Effects of Leading Edge and Downstream Film Cooling on Turbine Vane Heat Transfer," NASA CR-182133.
- Hylton, L.D. et al., 1983, "Analytical and Experimental Evaluation of the Heat Transfer Distribution Over the Surfaces of Turbine Vanes," NASA CR-168015.
- Kopper, F.C., 1984, "Coolant Passage Heat Transfer With Rotation," Turbine Engine Hot Section Technology, NASA CP-2339, pp. 401-409.
- Lord, W.K. et al., 1987, "Application of CFD Codes to the Design and Development of Propulsion Systems," Supercomputing in Aerospace, NASA CP-2454, P. Kutler and H. Yee, eds., NASA, Washington, D.C., pp. 139-148.
- Nealy, D.A. et al., 1983, "Measurement of Heat Transfer Distribution Over the Surfaces of Highly Loaded Turbine Nozzle Guide Vanes," ASME Paper 83-GT-53.
- Nealy, D.A. et al., 1984, "Measurements of Heat Transfer Distribution Over the Surfaces of Highly Loaded Turbine Nozzle Guide Vanes," Journal of Engineering for Gas Turbines and Power, Vol. 106, No. 1, pp. 149-158.
- Schmidt, R.C. and Patankar, S.V., 1987, "Prediction of Transition on a Flat Plate Under the Influence of Free-Stream Turbulence Using Low-Reynolds-Number Two-Equation Turbulence Models," ASME Paper 87-HT-32.
- Stepka, F.S., 1980, "Analysis of Uncertainties in Turbine Metal Temperature Predictions," NASA TP-1593.
- Sturgess, G.J. and Datta, P., 1987, "Calculation of Flow Development in Rotating Passages for Cooled Gas Turbine Blades," Computers in Engineering - 1987, Vol. 3, ASME, New York, pp. 149-158.
- Thomas, P.D., 1979, "Numerical Method for Predicting Flow Characteristics and Performance of Nonaxisymmetric Nozzles Theory," NASA CR-3147.
- Turner, E.R. et al., 1985, "Turbine Vane External Heat Transfer, Vol. I - Analytical and Experimental Evaluation of Surface Heat Transfer Distributions With Leading Edge Showerhead Film Cooling," NASA CR-174827.
- Weinberg, B.C. et al., 1985, "Calculations of Two- and Three-Dimensional Transonic Cascade Flow Fields Using the Navier-Stokes Equations," ASME Paper 85-GT-66.
- Yang, R.J. et al., 1985, "Turbine Vane External Heat Transfer, Vol. II - Numerical Solutions of the Navier-Stokes Equations for Two- and Three-Dimensional Turbine Cascades With Heat Transfer," NASA CR-174828.

APPENDIX
CONTENTS TO VOLUMES 1 AND 2

PRECEDING PAGE BLANK NOT FILMED

CONTENTS TO VOLUME 1

VIBRATION CONTROL

Session Overview	1-1
Louis J. Kiraly, NASA Lewis Research Center	
Survey of Impact Damper Performance	1-3
Gerald V. Brown, NASA Lewis Research Center	
Periodic Response of Nonlinear Systems	1-13
C. Nataraj, Trumpler Associates, Inc., and H.D. Nelson, Arizona State University	
Piezoelectric Pushers for Active Vibration Control of Rotating Machinery	1-29
Alan B. Palazzolo, Texas A&M University, and Albert F. Kascak, U.S. Army Aviation Research and Technology Activity - AVSCOM	
Active Control and System Identification of Rotordynamic Structures . .	1-47
M.L. Adams, Case Western Reserve University	
Electromagnetic Dampers for Cryogenic Applications	1-53
Gerald V. Brown and Eliseo DiRusso, NASA Lewis Research Center	

PARALLEL COMPUTING

Session Overview	1-65
Louis J. Kiraly, NASA Lewis Research Center	
Multigrid for Structures Analysis	1-67
Albert F. Kascak, U.S. Army Aviation Research and Technology Activity - AVSCOM	
Parallel Computer Methods for Eigenvalue Extraction	1-91
Fred Akl, Ohio University	
Adapting High-Level Language Programs for Parallel Processing Using Data Flow	1-103
Hilda M. Standley, University of Toledo	
Iterative Finite Element Solver on Transputer Networks	1-113
Albert Danial and James Watson, Sparta, Inc.	
Multiprocessor Graphics Computation and Display Using Transputers . . .	1-125
Graham K. Ellis, Institute for Computational Mechanics in Propulsion	

DYNAMIC SYSTEMS

Session Overview	1-141
Louis J. Kiraly, NASA Lewis Research Center	
Microgravity Mechanisms and Robotics Program	1-143
Douglas A. Rohn, NASA Lewis Research Center	
Base Reaction Optimization of Manipulators with Redundant Kinematics	1-157
C.L. Chung and S. Desa, Carnegie Mellon University	

Evaluation of a High-Torque Backlash-Free Roller Actuator	1-175
Bruce M. Steinetz, NASA Lewis Research Center	
Low-Cost Optical Data Acquisition System for Blade Vibration Measurement	1-191
Stephen J. Posta, NASA Lewis Research Center	
Roller Drive Materials Performance	1-203
Douglas A. Rohn, NASA Lewis Research Center	
Microgravity Manipulator Demonstration	1-217
Andrew S. Brush, Sverdrup Technology, Inc., Lewis Research Center Group	
Accurate Positioning of Long, Flexible ARM's	1-229
Michael J. Malachowski, CCE - Robotics	

AEROELASTICITY

Session Overview	1-245
Louis J. Kiraly, NASA Lewis Research Center	
Development of Aeroelastic Analysis Methods for Turborotors and Propfans - Including Mistuning	1-247
Krishna Rao V. Kaza, NASA Lewis Research Center	
2-D and 3-D Time Marching Transonic Potential Flow Method for Propfans	1-263
Marc H. Williams, Purdue University	
Propfan Model Wind Tunnel Aeroelastic Research Results	1-273
Oral Mehmed, NASA Lewis Research Center	
Aeroelastic Forced Response Analysis of Turbomachinery	1-287
Todd E. Smith, Sverdrup Technology, Inc., Lewis Research Center Group	
Reduced Order Models for Nonlinear Aerodynamics	1-299
Aparajit J. Mahajan, Earl H. Dowell, and Donald B. Bliss, Duke University	
Application of Navier-Stokes Analysis to Stall Flutter	1-309
J.C. Wu, R. Srivastava, and L.N. Sanker, Georgia Institute of Technology	

COMPUTATIONAL METHODS FOR DYNAMICS

Session Overview	1-321
Louis J. Kiraly, NASA Lewis Research Center	
A Computational Procedure for Automated Flutter Analysis	1-323
Durbha V. Murthy, University of Toledo	
Characterization of Structural Connections for Multicomponent Systems	1-337
Charles Lawrence, NASA Lewis Research Center, and Arthur A. Huckelbridge, Case Western Reserve University	
Mixed Finite Element Formulation Applied to Shape Optimization	1-353
Helder Rodrigues, John E. Taylor, and Noboru Kikuchi, The University of Michigan	
Modal Forced Response of Propfans in Yawed Flow	1-367
G.V. Narayanan, Sverdrup Technology, Inc., Lewis Research Center Group	

STRUCTURAL DYNAMICS CODE APPLICATIONS

Session Overview	1-377
Krishna Rao V. Kaza, NASA Lewis Research Center	
Vibration and Flutter Analysis of the SR-7L Large-Scale Propfan	1-379
Richard August, Sverdrup Technology, Inc., Lewis Research Center Group	
Supersonic Axial-Flow Fan Flutter	1-393
John K. Ramsey, NASA Lewis Research Center	
Stall Flutter Analysis of Propfans	1-405
T.S.R. Reddy, University of Toledo	
SSME Single-Crystal Turbine Blade Dynamics	1-421
Larry A. Moss, Sverdrup Technology, Inc., Lewis Research Center Group	
PARAFRASE Restructuring of FORTRAN Code for Parallel Processing	1-431
Atul Wadhwa, Sverdrup Technology, Inc., Lewis Research Center Group	
Analysis of Rotating Flexible Blades Using MSC/NASTRAN	1-449
Michael A. Ernst, NASA Lewis Research Center	

APPENDIX

Contents to Volume II	1-466
Contents to Volume III	1-468

CONTENTS TO VOLUME 2

CONSTITUTIVE MODELS AND EXPERIMENTAL CAPABILITIES

Session Overview	2-1
Robert L. Thompson, NASA Lewis Research Center	
High-Temperature Combustor Liner Tests in Structural Component Response Test Facility	2-5
Paul E. Moorhead, NASA Lewis Research Center	
Life Assessment of Combustor Liner Using Unified Constitutive Models	2-15
M.T. Tong, Sverdrup Technology, Inc., Lewis Research Center Group, and R.L. Thompson, NASA Lewis Research Center	
Experiments Investigating Advanced Materials Under Thermomechanical Loading	2-27
Paul A. Bartolotta, NASA Lewis Research Center	
Biaxial Experiments Supporting the Development of Constitutive Theories for Advanced High-Temperature Materials	2-37
J.R. Ellis, NASA Lewis Research Center	
Unified Constitutive Model Development for Metal Matrix Composites at High Temperature	2-49
D.N. Robinson, University of Akron	
Unified Constitutive Model for Single Crystal Deformation Behavior with Applications	2-57
K.P. Walker, Engineering Science Software, Inc., T.G. Meyer, Pratt & Whitney, and E.H. Jordan, University of Connecticut	
Finite Element (MARC) Solution Technologies for Viscoplastic Analyses	2-73
V.K. Arya, National Research Council, and Robert L. Thompson, NASA Lewis Research Center	

STRUCTURAL MECHANICS CODES

Session Overview	2-81
Christos C. Chamis, NASA Lewis Research Center	
The Composite Blade Structural Analyzer (COBSTRAN)	2-83
Robert A. Aiello, NASA Lewis Research Center	
Features and Applications of the Integrated Composites Analyzer (ICAN) Code	2-99
C.A. Ginty, NASA Lewis Research Center	
Three-Dimensional Inelastic Approximate Analysis Code (MOMM)	2-113
Jeffrey P. Meister, Sverdrup Technology, Inc., Lewis Research Center Group	
Specialty Three-Dimensional Finite Element Analysis Codes	2-123
Joseph J. Lackney, Sverdrup Technology, Inc., Lewis Research Center Group	

MHOST: An Efficient Finite Element Program for Inelastic Analysis of Solids and Structures	2-131
S. Nakazawa, MARC Analysis Research Corp.	
METCAN - the Metal Matrix Composite Analyzer	2-141
Dale A. Hopkins, NASA Lewis Research Center, and Pappu L.N. Murthy, Cleveland State University	
Computational Simulation Methods for Composite Fracture Mechanics . . .	2-157
Pappu L.N. Murthy, Cleveland State University	

STRUCTURAL OPTIMIZATION

Session Overview	2-171
Robert H. Johns, NASA Lewis Research Center	
Probabilistic Structural Analysis Computer Code (NESSUS)	2-173
Michael C. Shiao, Sverdrup Technology, Inc., Lewis Research Center Group	
Structural Tailoring of High-Speed Turbine Blades(SSME/STAEBL)	2-183
Robert Rubinstein, Sverdrup Technology, Inc., Lewis Research Center Group	
Computational Structural Mechanics for Engine Structures	2-189
Christos C. Chamis, NASA Lewis Research Center	
Structural Tailoring of Advanced Turboprops	2-205
K.W. Brown, Pratt & Whitney, and Dale A. Hopkins, NASA Lewis Research Center	
Advanced Probabilistic Methods for Quantifying the Effects of Various Uncertainties in Structural Response	2-219
Vinod K. Nagpal, Sverdrup Technology, Inc.	

STRUCTURAL MECHANICS CODE APPLICATIONS

Session Overview	2-233
Robert H. Johns, NASA Lewis Research Center	
Impact Damage in Composite Laminates	2-235
Joseph E. Grady, NASA Lewis Research Center	
Thermostructural Analysis of Simulated Cowl Lips	2-245
Matthew E. Melis, NASA Lewis Research Center	
Thermal-Structural Analyses of Space Shuttle Main Engine (SSME) Hot Section Components	2-255
Ali Abdul-Aziz, Sverdrup Technology, Inc., Lewis Research Center Group, and Robert L. Thompson, NASA Lewis Research Center	
Structural Analyses of Engine Wall Cooling Concepts and Materials . . .	2-265
Albert Kaufman, Sverdrup Technology, Inc., Lewis Research Center Group	
Structural Assessment of a Space Station Solar Dynamic Heat Receiver Thermal Energy Storage Canister	2-281
R.L. Thompson and T.W. Kerslake, NASA Lewis Research Center, and M.T. Tong, Sverdrup Technology, Inc., Lewis Research Center Group	
An Efficient Mindlin Finite Strip Plate Element Based on Assumed Strain Distribution	2-295
Abhisak Chulya, Institute for Computational Mechanics in Propulsion, and Robert L. Thompson, NASA Lewis Research Center	

1. Report No. NASA CP-3003		2. Government Accession No.		3. Recipient's Catalog No.	
4. Title and Subtitle Lewis Structures Technology - 1988				5. Report Date May 1988	
				6. Performing Organization Code	
7. Author(s)				8. Performing Organization Report No. E-3970	
				10. Work Unit No. 505-63-1B	
9. Performing Organization Name and Address National Aeronautics and Space Administration Lewis Research Center Cleveland, Ohio 44135-3191				11. Contract or Grant No.	
				13. Type of Report and Period Covered Technical Paper	
12. Sponsoring Agency Name and Address National Aeronautics and Space Administration Washington, D.C. 20546-0001				14. Sponsoring Agency Code	
15. Supplementary Notes					
16. Abstract A Symposium and Exposition entitled Lewis Structures Technology - 1988 (LST '88), sponsored by the Structures Division of the NASA Lewis Research Center, was held May 24 and 25, 1988, in Cleveland, Ohio. The charter of the Structures Division is to perform and disseminate results of research conducted in support of aerospace engine structures. These results have a wide range of applicability to practitioners of structural engineering mechanics beyond the aerospace arena. The specific purpose of the symposium was to familiarize the engineering structures community with the depth and range of research performed by the division and its academic and industrial partners. The more significant results of the division's research efforts were presented in 14 overviews and 83 technical presentations. The complete text of each presentation is included in this volume. Sessions covered vibration control, fracture mechanics, ceramic component reliability, parallel computing, nondestructive evaluation, constitutive models and experimental capabilities, dynamic systems, fatigue and damage, wind turbines, hot section technology (HOST), aeroelasticity, structural mechanics codes, computational methods for dynamics, structural optimization, and applications of structural dynamics, and structural mechanics computer codes.					
17. Key Words (Suggested by Author(s)) Engine structures, Structures mechanics, Structural dynamics, Structural optimization, Structural durability, Fatigue(metals), Fracture mechanics, Nondestructive evaluation, Aeroelasticity, Parallel computing, Cyclic constitutive models, Wind turbines, HOST				18. Distribution Statement Unclassified - Unlimited Subject Category 39	
19. Security Classif. (of this report) Unclassified		20. Security Classif. (of this page) Unclassified		21. No of pages	
				22. Price*	